B.3

General Motors Corporation
Legal Staff

Facsimile
(586) 492-2928

Telephone
(586) 947-9212

FEB 2 8 2002

L. Robert Shelton,
Executive Director
NATIONAL HIGHWAY TRAFFIC
SAFETY ADMINISTRATION
400 Seventh Street, S.W., Room 5220
Washington, DC 20590

Dear Mr. Shelton:

Re: **Settlement Agreement**
Section B. Fire Safety Research

Enclosed is a final report prepared by Jeffrey Santrock of General Motors Corporation, entitled, "Evaluation of Motor Vehicle Fire Initiation and Propagation/Part 7: Propagation of an Engine Fire in a 1997 Rear Wheel Drive Passenger Car."

This report relates to Project B.3 (Fire Initiation and Propagation Tests).

Yours truly,

D.K. Nowak-Vanderhoef

Deborah K. Nowak-Vanderhoef
Attorney

Enclosure

Mail Code: 480-210-225
Vehicle Engineering Center 30001 Van Dyke Avenue Warren, Michigan 48090-9020

Evaluation of Motor Vehicle Fire Initiation and Propagation Part 7: Propagation of an Engine Compartment Fire in a 1997 Rear Wheel Drive Passenger Car

Jeffrey Santrock
General Motors Corporation

ABSTRACT

This report describes a vehicle fire propagation test conducted pursuant to an agreement between GM and the United states Department of Transportation. This fire test was conducted on October 1, 1997. The test vehicle was a crash-tested 1997 Chevrolet Camaro. In the crash test, the test vehicle was towed into a fixed steel pole. No fire was observed during this crash test, nor was there evidence of fire present in the test vehicle detected during an inspection of the test vehicle after the crash test. An artificial means of starting a fire in the engine compartment of the test vehicle was used in the fire test described in this report. A propane torch was installed in the engine compartment of the test vehicle so that flames from the torch impinged on the upper and lower cases of the HVAC module just forward of the dash panel. Flames appear to have entered the passenger compartment through the HVAC module and through the windshield. Flame temperatures were recorded in the HVAC module rearward of the dash panel by 11 minutes post-ignition. A section of the forward edge on the right side of the instrument panel upper trim panel was burning by 5 minutes post-ignition. A section of the windshield fell inward about 11 minutes post-ignition. Flames were observed under the right side of the instrument panel at 13 minutes post-ignition. Fire suppression started approximately 16 minutes after ignition.

Table of Contents

Appendicies

List of Figures

Report

List of Figures

Appendicies

List of Tables

Report

List of Tables

Appendicies

1 Introduction and Test Summary

The work described in this report was conducted by General Motors (GM) pursuant to an agreement between GM and the United states Department of Transportation. According to this agreement, GM and the National Highway Traffic Safety Administration (NHTSA) jointly developed fifteen separate vehicle fire safety research projects. One of these projects, entitled "Fire Initiation and Propagation Tests", involves conducting 1) vehicle crash tests to investigate potential ignition events that occur in vehicle crashes, and 2) subsequent vehicle fire tests to characterize fire propagation in these crash-tested vehicles. The vehicle models to be tested, and the crash- and fire-test methods to be used for Project B.3 are described in another report [1]. The objectives of the fire tests are:

- To determine the principal fire paths and time-lines for flame propagation into the passenger compartment under the test conditions;
- To identify which components burn and to measure the thermal environments around those components associated with their ignition under the test conditions; and
- To measure air temperatures, heat fluxes, and combustion gas concentrations in the passenger compartment under the test conditions.

These tests were conducted under carefully designed test conditions noted throughout this and other reports. They cannot be relied upon to predict the specific nature and characteristics of actual post-collision fires in the field.

The test vehicle was a 1997 Chevrolet Camaro (VIN: 2G1FP22K5V2109780) with the following options: 3.8 liter 6-cylinder engine, a 4-speed automatic transmission, air conditioning, a six-way power drivers' seat, and 16-inch aluminum wheels.

The test vehicle was crash tested on May 14, 1997 at the General Motors Proving Ground in Milford, Michigan [2]. In the crash test, this vehicle was towed into a fixed steel pole (diameter = 356 mm). The mass of the test vehicle, including Anthropomorphic Test Devices and test instrumentation, was 1849 kg (4077 lbs.). The speed of the test vehicle at impact was 55.3 km/h. The point of initial contact between the test vehicle and the pole was on the front bumper fascia 305 mm to the right of the vehicle longitudinal centerline. The change in velocity measured along the longitudinal axis of the test vehicle was 62 kmh. The crash test did not result in a fire or a fuel system leak in the test vehicle. A detailed description of this test can be found in another report [2].

Figure 1 is a photograph of the test vehicle after the crash test. The maximum penetration of the pole into the test vehicle (dynamic crush) during the crash test was approximately 1255 mm and occurred at 118 milliseconds. The residual crush was not determined. The hood and right fender were crushed. The windshield and window in the right door were broken. The left side of the front bumper fascia was detached from the test vehicle.

Figure 1. Fire Test F971003. Photograph of the test vehicle after the crash test.

The engine and transmission were displaced rearward. Two of the bolts securing the transmission case to the rear of the engine punctured the dash panel in two places (Fig. 2). The upper and lower cases of the HVAC module were broken, and the heat exchanger and A/C evaporator were displaced rearward (Fig. 2). A section of the weld seam between the floor pan and inner rocker panel separated during the crash test (Fig. 2).

The fire test described in this report was conducted on October 2, 1997. The fire test was designed to study propagation of a fire artificially ignited in the engine compartment into the passenger compartment. Table 1 summarizes the timing of flame-spread into the passenger compartment along these pathways.

An artificial method of igniting a fire in the engine compartment was used in this test. A propane torch was installed in the engine compartment of the test vehicle so that flames from the torch impinged on the upper and lower cases of the HVAC module just forward of the dash panel[1]. This placed the torch at the rear of the right side of the engine compartment.

[1] In this report, the dash panel refers to the sheet metal panel that forms the separation between the engine compartment and the passenger compartment.

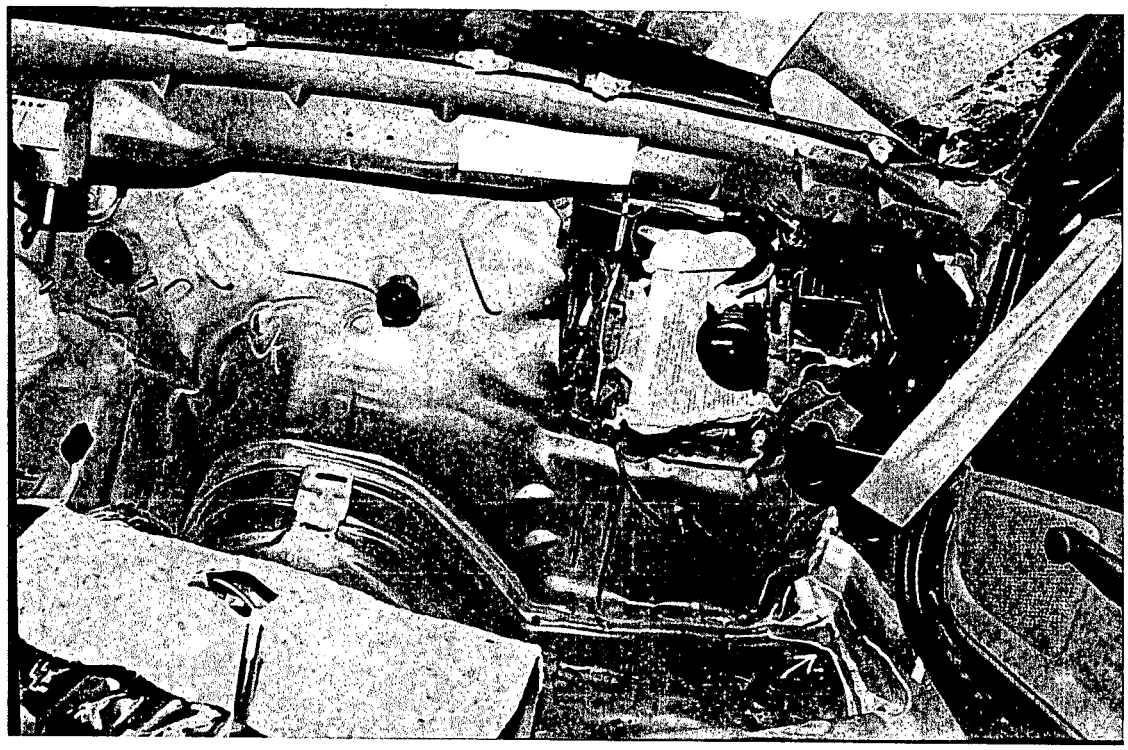

Figure 2. Fire Test F971003. Photograph of the interior of the dash panel of the test vehicle after the crash test. The instrument panel, interior section of the HVAC module, and dash sound absorber were removed for this photograph.

To start the test, the propane torch was ignited and allowed to burn for two minutes. Flames spread laterally and forward in the engine compartment from the point of ignition. Flames spread rearward into the passenger compartment through the HVAC module. The inner layer in the broken windshield melted and pieces of the broken windshield fell onto the instrument panel upper trim panel, the deployed passenger airbag, the front passenger's seat cushion, and the carpet in front of the passenger's seat. This test was stopped and the fire extinguished about 15 minutes after ignition.

Table 1

Summary of Fire Development during in Fire Test F971003

Time[1] (min)	Event
0	Ignition of the propane torch
2	Propane torch turned-off
2.25	Flames visible on the right air inlet screen
4 – 6	Flames spread laterally in the engine compartment
11.1	Sections of the windshield fall onto the instrument panel upper trim panel
8 – 9	A measurable pressure difference develops across dash panel
13 – 15	Deployed passenger airbag ignites and burns
14.92	Flames emerge through defroster outlet in instrument panel upper trim panel
15.83	Test ended

[1]Time after ignition of the propane torch.

2 Vehicle Condition and Test Protocol

The fire test described in this report was conducted at the Factory Mutual Test Center in West Glocester, Rhode Island. The crash-tested vehicle was prepared for the fire tests at the General Motors Research and Development Center (GM R&D Center) in Warren, Michigan, and shipped to the Factory Mutual Test Center. The test vehicle was returned to the GM R&D Center after the fire test, where it was systematically disassembled to permit closer inspection of the fire damage and identification of fire spread paths that were not obvious during the tests.

A description of the video cameras used in during this test is in **APPENDIX A**. A description of the infrared cameras used in this test is in **APPENDIX B**. A description of the thermocouples installed in the test vehicle and data from these thermocouples are in **APPENDIX C**. A description of the aspirated thermocouples used in this test and date from these aspirated thermocouples are in **APPENDIX D**. A description of the heat flux transducer/radiometer assemblies installed in the test vehicle and data from these devices are in **APPENDIX E**. A description of the pressure and airflow measurement equipment and analysis procedures, and data from these measurements are in **APPENDIX F**. A description of the experimental fire detectors installed in the test vehicle for this test and plots of the data recorded from these devices air in **APPENDIX G**. A description of the Fire Products Collector (FPC) at the Factory Mutual Global Test Center and analysis procedures, and data from this device are in **APPENDIX H**. Descriptions of the Fourier Transform Infrared Gas Analysis System used during this test and results from this device are in **APPENDIX I**. A description of the Gas Chromatography/Mass Spectrometry equipment and analysis procedures, and the results of these analyses are in **APPENDIX J**. A descriptions of the particulate sampling equipment and analysis procedures, and the results of these analyses are in **APPENDIX K**.

The vehicle was placed in a rectangular steel pan (length = 25 ft., width = 15 ft., height = 4 in.) to prevent spilled and leaking automotive fluids from spreading in the test facility. This fluid containment pan was fabricated from two sheets of carbon steel. Angle-braces were welded to the under-side of the pan to keep it from flexing under the weight of the vehicle. The corners of the support frame rested on load cells. Mass loss was determined from data acquired from the load cells during the test.

A layer of fiberglass-reinforced cement construction board (DuraRock, USG Corporation) was placed on bottom of the fluid containment pan. A thin layer of sand was used to level the concrete board so that the grade of the surface measured from the center to the edges along the major and minor axes was no greater than 1%. The joints between boards were sealed with latex caulking.

The test vehicle was placed in the center of the pan (Fig. 3). All doors were closed. The windshield and the glass in the right door were broken in the crash test, and were not replaced for the fire test. The glass in the left door was raised to its fully closed position. All components in the vehicle were at ambient temperature at the start of the fire test.

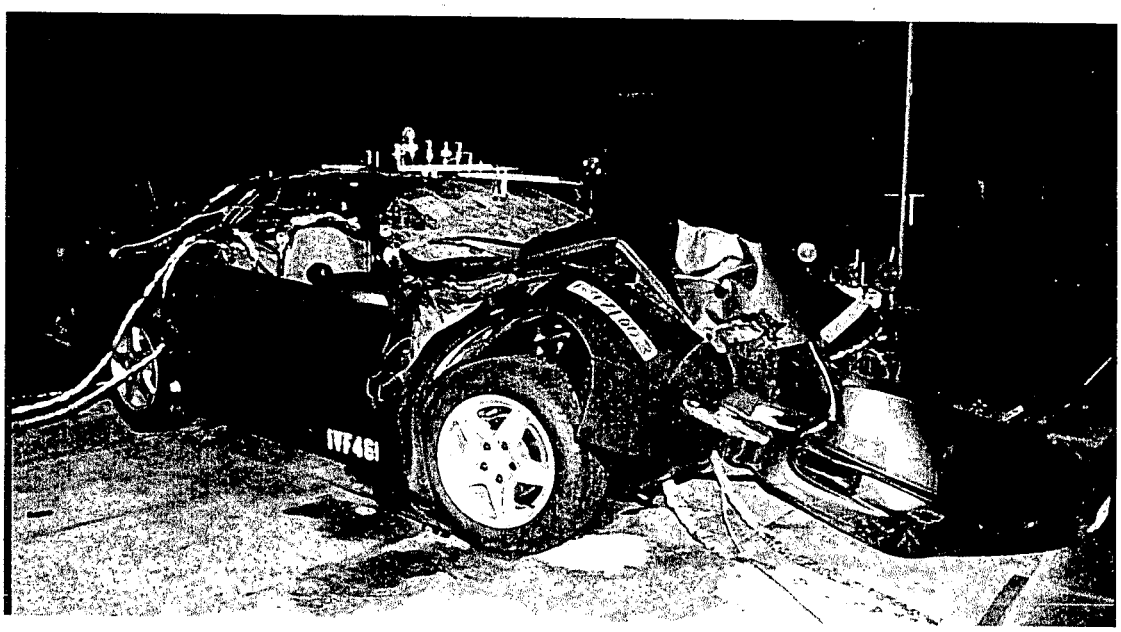

Figure 3. Fire Test F971003. Photograph of the test vehicle before this test. The supports on the broken windshield seen in this photograph were removed before the test was started.

A mixture of 3 quarts of automatic transmission fluid (Dexron III, Quaker State), 1 quart of SAE 10W-30 motor oil (Goodwrench, General Motors), and 1 quart of DOT 3 brake fluid (Delco Supreme II, General Motors) was heated to a temperature of approximately 150°C. This mixture of heated oils was poured onto the cement board surface under the engine compartment of the test vehicle just before the start of the test. About 2 L of a mixture of antifreeze and water (1:1) heated to approximately 80°C was sprayed onto the hood lining.

A circular propane torch was used to artificially start a fire in the engine compartment of the test vehicle (Fig. 4). This torch was constructed from stainless steel tubing (o.d. = 6.4 mm) and had a ring-shaped section (i.d. = 5.1 cm) with 12 holes (diameter = 1.3 mm) evenly spaced around the ring. The holes were pointed in toward the ring axis at a 45° angle.

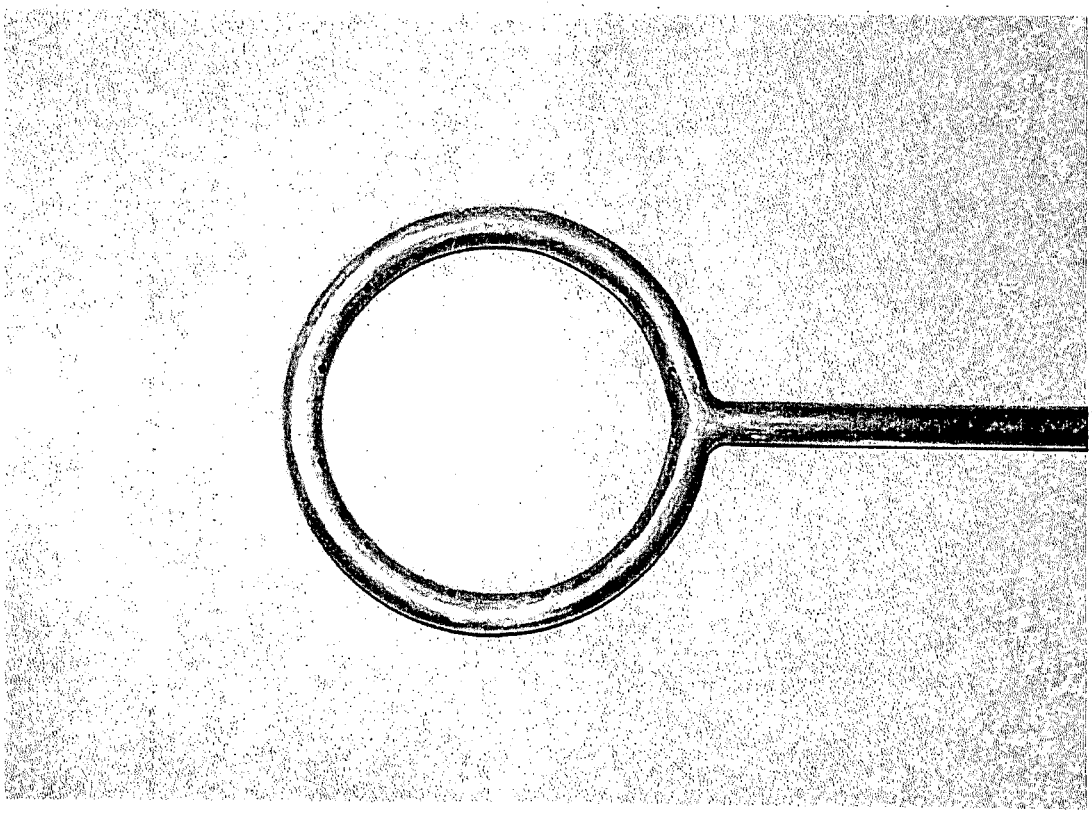

Figure 4. Fire Test F971003. Photograph of the propane torch used to artificially ignite a fire in the engine compartment of the test vehicle during this test.

The propane torch was installed in the right side of the engine compartment so that the flames from this torch impinged on the lower and upper cases of the HVAC module. Propane was supplied to the torch from an external propane tank. The flow rate of propane to the torch was controlled with a mass flow controller (Brooks Model 585E) that was calibrated for propane at the factory. A coiled Nichrome heating wire was installed just above the torch and used to ignite the propane gas.

Two experimental fire detectors, a linear fire detector and a pneumatic fire detector, were installed on the under-side of the deformed hood of the test vehicle after the crash test. Both experimental fire detectors were attached to the hood-lining panel, and were located along the crease in the deformed hood (see Fig.'s 1 and 3). These experimental fire detectors spanned the width of the engine compartment along the highest section of the crushed hood. The signals from these experimental fire detectors were recorded during this test.

An air horn was used to synchronize the data acquisition systems used in this test and was sounded to signal three events: (1) ignition of the circular propane torch installed in the engine

compartment, (2) cessation of propane flow to the torch, and (3) the end of the test. The air horn was used to synchronize the various data systems in this test. The air horn was audible on the videotapes and infrared imaging systems. One channel of the data acquisition system for vehicle instrumentation monitored a normally open switch, which was depressed at each sounding of the air horn. The real-time clock in the FTIR data system was synchronized to the real-time clock in the vehicle instrumentation data system.

A fine water mist was used to extinguish the fire in the test vehicle. After the signal to end the test was sounded, the water mist was directed into the passenger compartment through the right side window to extinguish flames in the interior of the vehicle first. The water mist was then directed toward the engine compartment to extinguish flames outside of the passenger compartment.

3 Ignition

To start this test, the valve on external propane tank was opened and the mass flow controller was adjusted for a flow rate of 3.0 NTP L/min of propane.[2] Electrical power was supplied to the coiled Nichrome wire using a variable tap transformer connected to 120 VAC. The Nichrome heating wire was preheated for approximately 30 seconds before propane flow was started. The time of ignition was determined by viewing a remote monitor connected to a CCD camera installed in the engine compartment of the test vehicle (Fig. 5). The flow of propane to the igniter was stopped 2 minutes after ignition.

Video stills from Camera 7 show that the flames from the propane torch had extinguished by 5 seconds after the flow of propane was turned-off (Fig. 6). Reflected light visible in the video still from Camera 7 at 125 seconds post-ignition indicates that material in the engine compartment was burning after the propane torch was turned-off. The oil filler tube blocked the view of the flames and it was not possible to determine what material or components were burning at this time.

Isothermal contours in the upper part of the engine compartment of the test vehicle were estimated from the data recorded by the E-Thermocouples.[3] Figure 7 shows a series of diagrams with the estimated isothermal contour plots in the upper engine compartment between - 0.25 and + 2.25 minutes post-ignition. Thermocouples in the area of the igniter were heated indirectly by the flame from the propane torch. Temperatures recorded from the E-Thermocouples were less than 600°C throughout this time period, indicating that flames from the propane torch igniter had not spread to components in the in the upper engine compartment by 2.5 minutes post-ignition. A small fire plume was visible at the rear of the engine compartment under the upper dash extension panel between 2 and 2.5 minutes post-ignition (Fig. 8). Flames had not emerged from around the hood at the time the propane torch was turned-off (Fig.'s 9 and 10).

---

[2] The estimated power output of this torch with a flow of 3.0 NTP L/min of propane was 4.2 kW. This estimate was obtained by calculating ΔH for oxidation of propane by molecular oxygen to carbon dioxide and water.

[3] Isothermal contours of the temperature in the upper engine compartment of the test vehicle were estimated from recorded temperature data using a three-dimensional interpolation algorithm available in SigmaPlot for Windows Version 4.00 [3]. This algorithm uses an inverse distance method to generated temperature values for points on a uniformly spaced Cartesian grid from input [x,y,t] triple data. Data recorded from thermocouples located in the upper engine compartment (Thermocouples E1 through E9, and E18) and below the air inlet screen (Thermocouples E10 through E17) were used in these calculations.

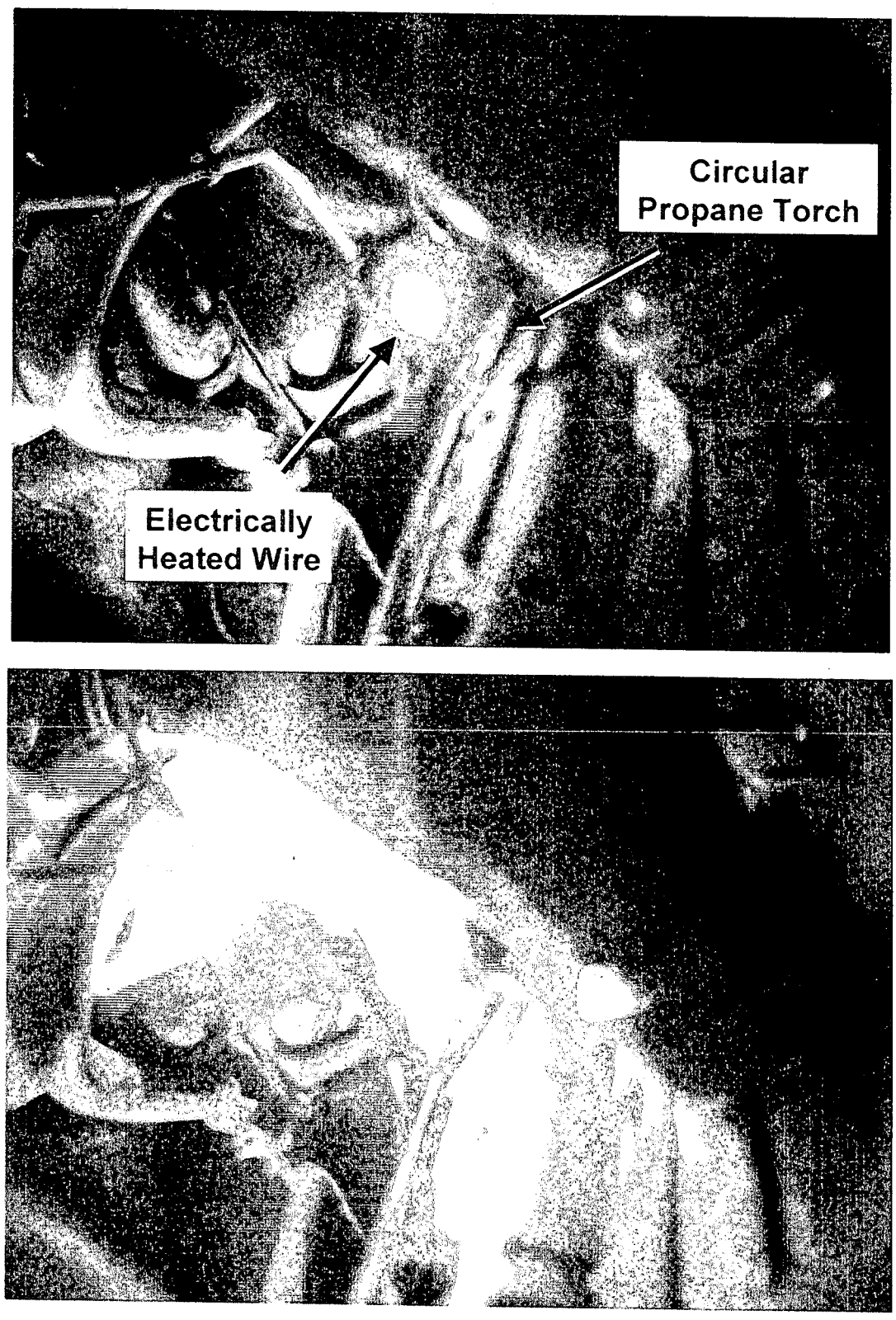

Figure 5. Fire Test F971003. Video stills from Camera 7 at 1 second before ignition (upper panel) and the time of ignition (lower panel).

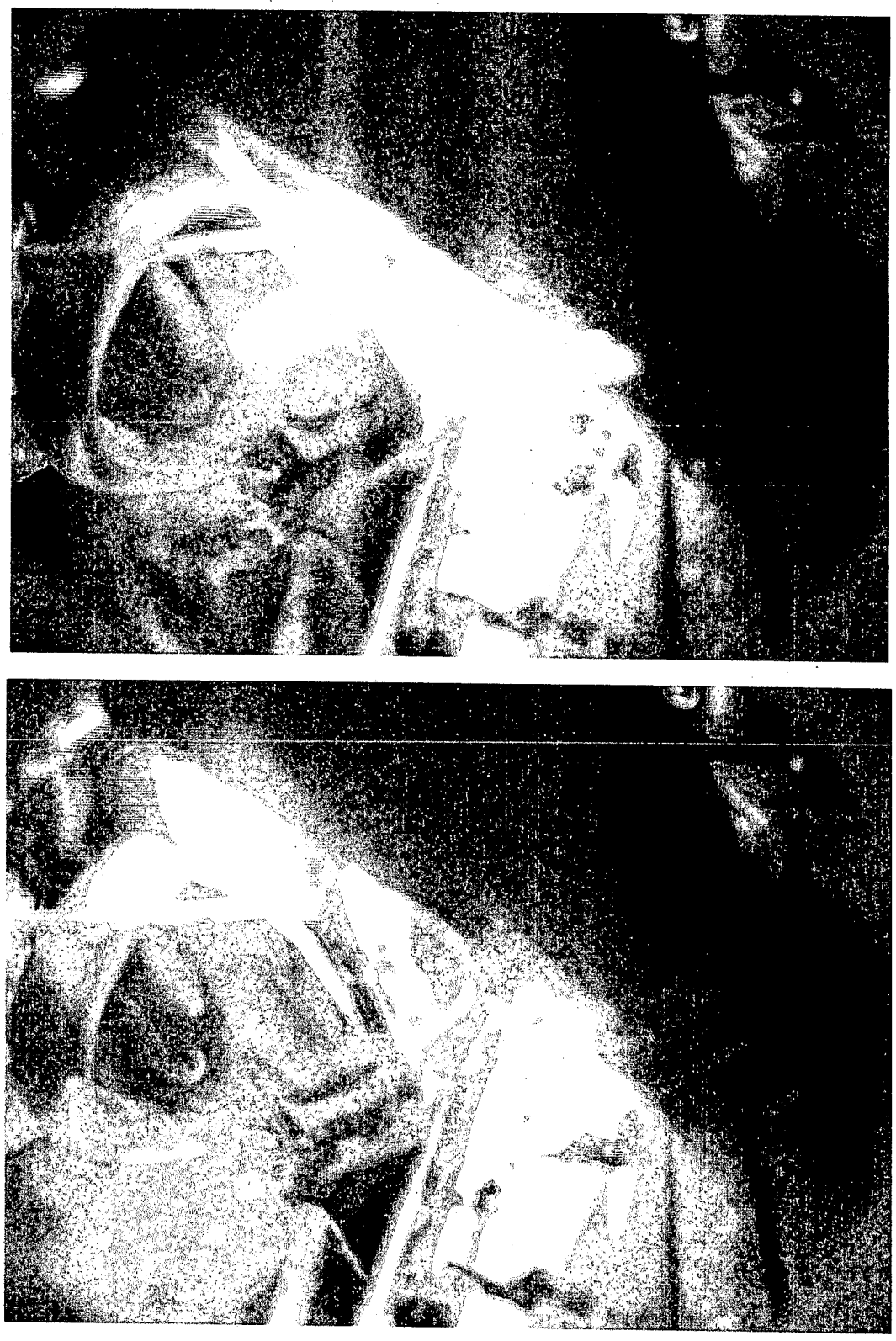

Figure 6. Fire Test F971003. Video stills from Camera 7 at 120 second post-ignition (upper panel) and at 125 seconds post-ignition (lower panel).

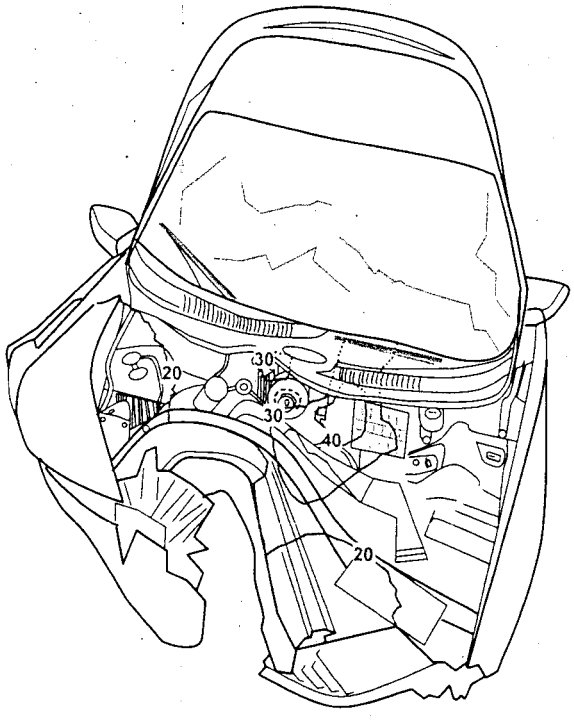

-0.25 minutes post-ignition

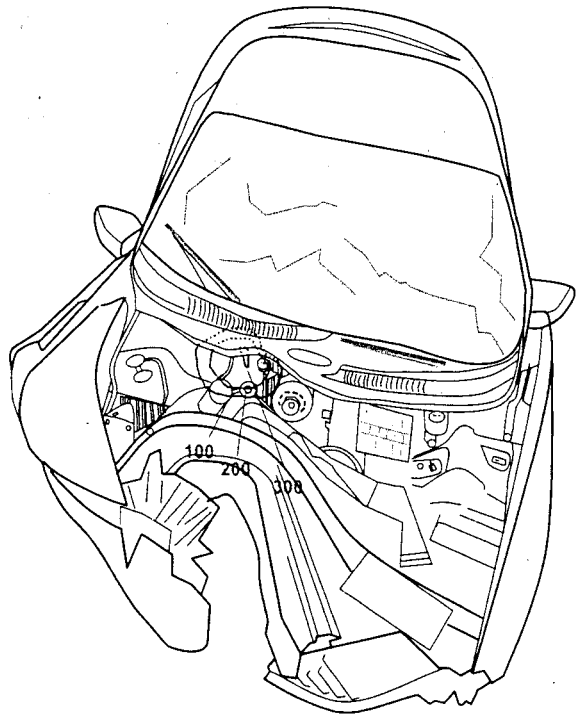

0.00 minutes post-ignition

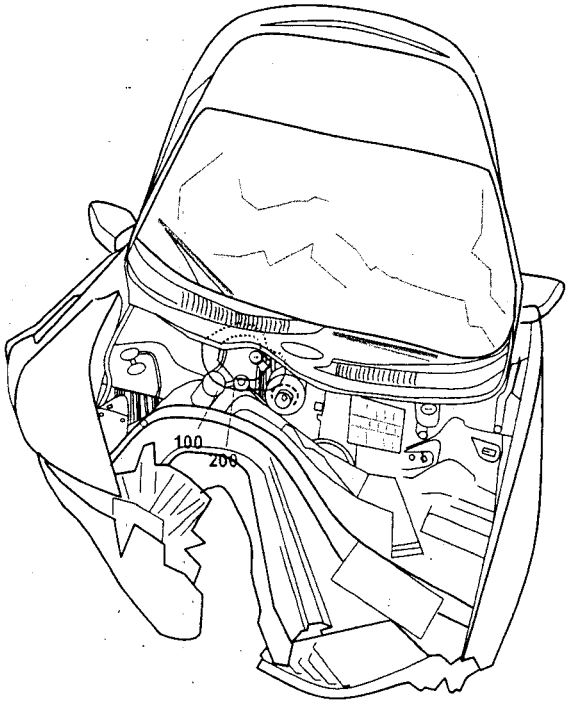

+0.25 minutes post-ignition

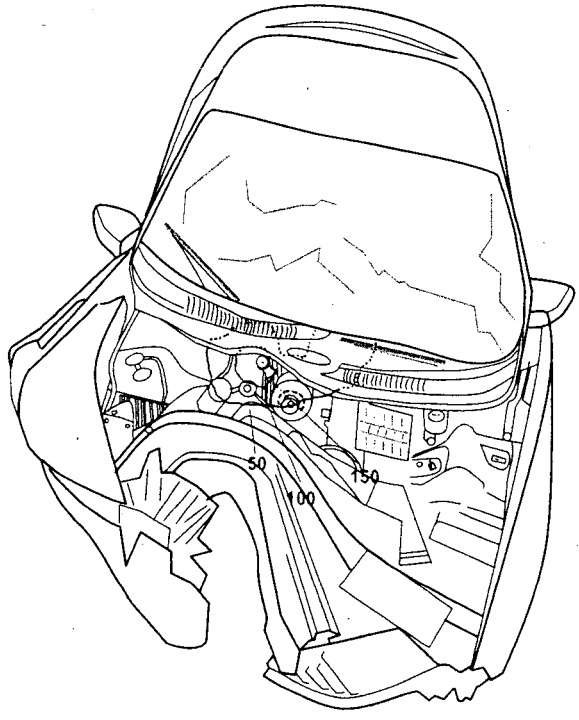

+0.50 minutes post-ignition

Figure 7. Fire Test F971003. Isothermal contour plots of estimated temperatures in the top of the engine compartment –0.25, 0, 0.25, 0.50, 0.75, 1.00, 1.25, 1.50, 1.75, 2.00, 2.25, and 2.50 minutes post-ignition.

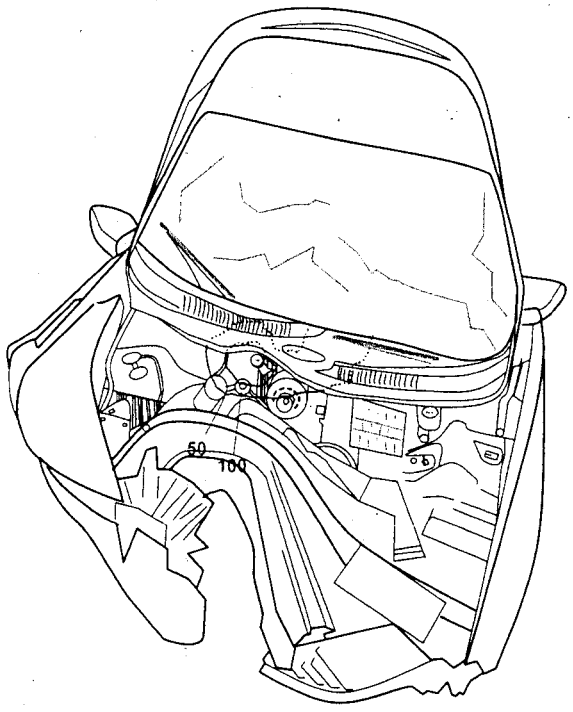

+0.75 minutes post-ignition

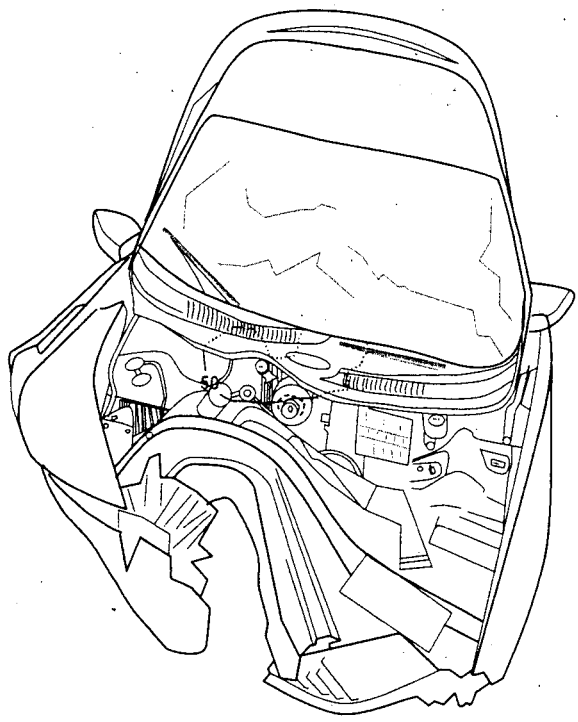

+1.00 minutes post-ignition

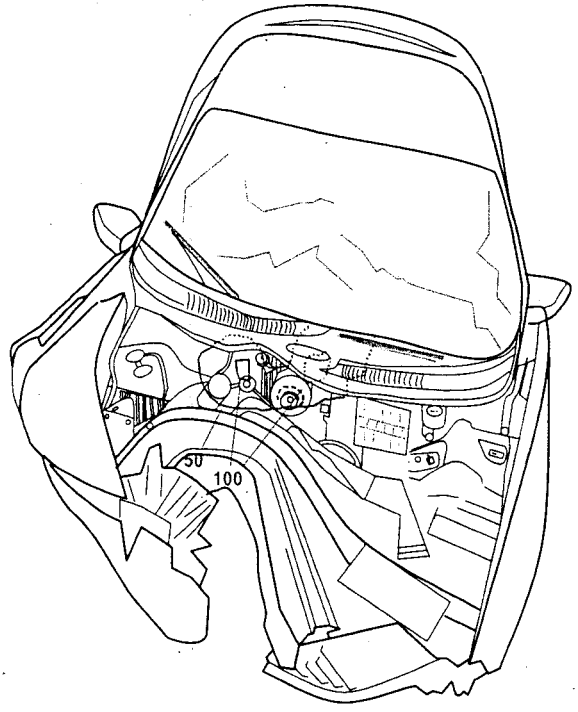

+1.25 minutes post-ignition

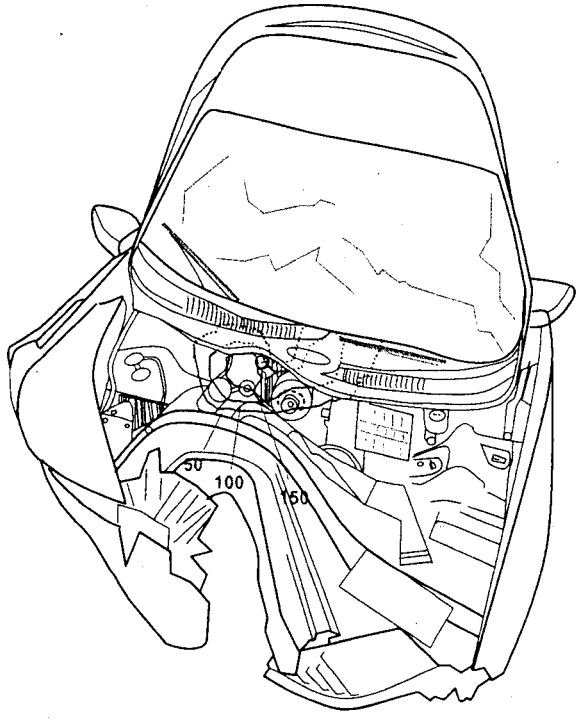

+1.50 minutes post-ignition

Figure 7, continued. Fire Test F971003. Isothermal contour plots of estimated temperatures in the top of the engine compartment –0.25, 0, 0.25, 0.50, 0.75, 1.00, 1.25, 1.50, 1.75, 2.00, 2.25, and 2.50 minutes post-ignition.

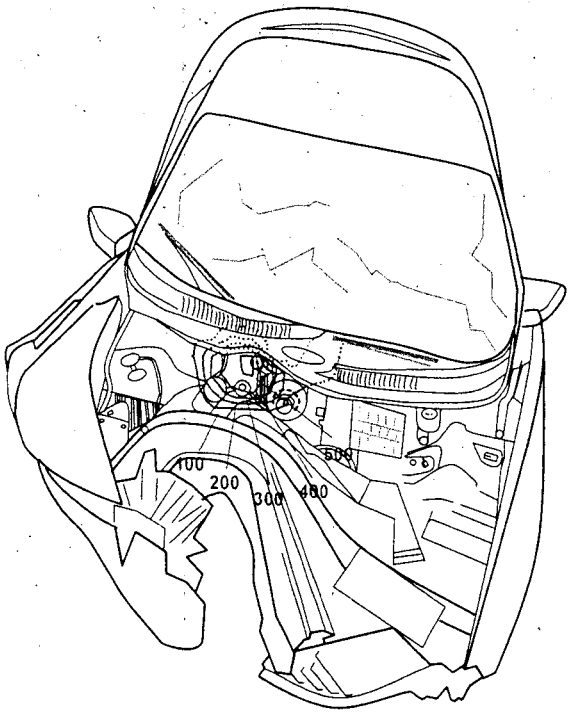

+1.75 minutes post-ignition

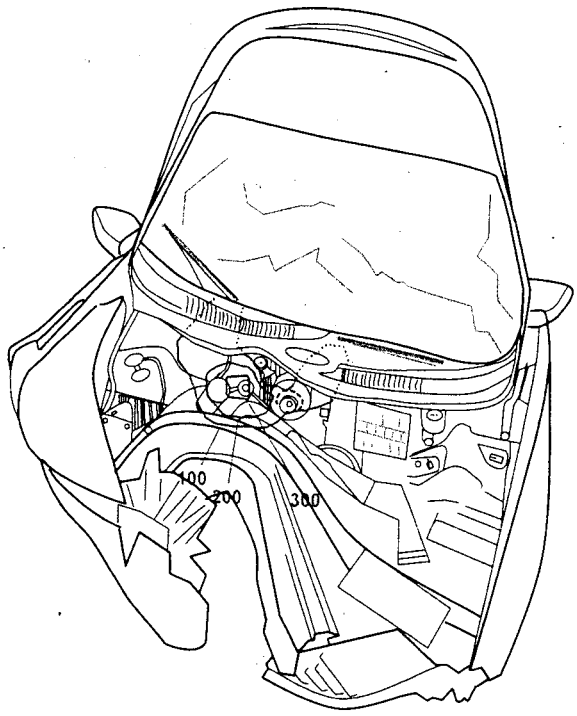

+2.00 minutes post-ignition

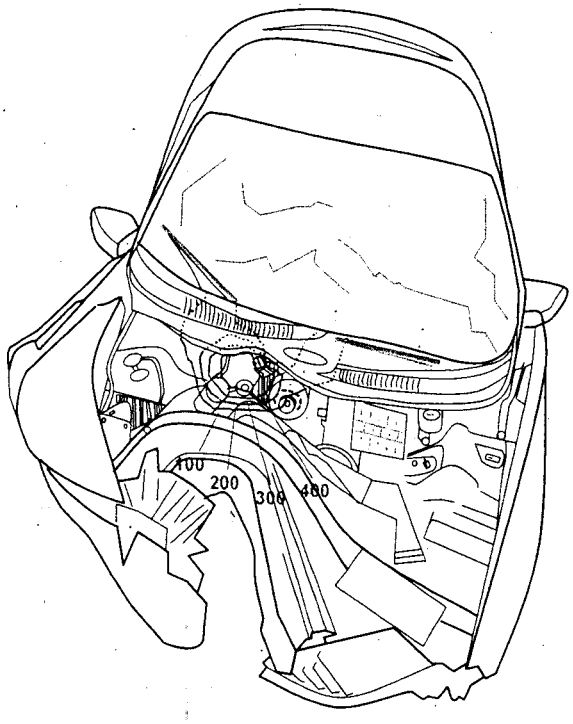

+2.25 minutes post-ignition

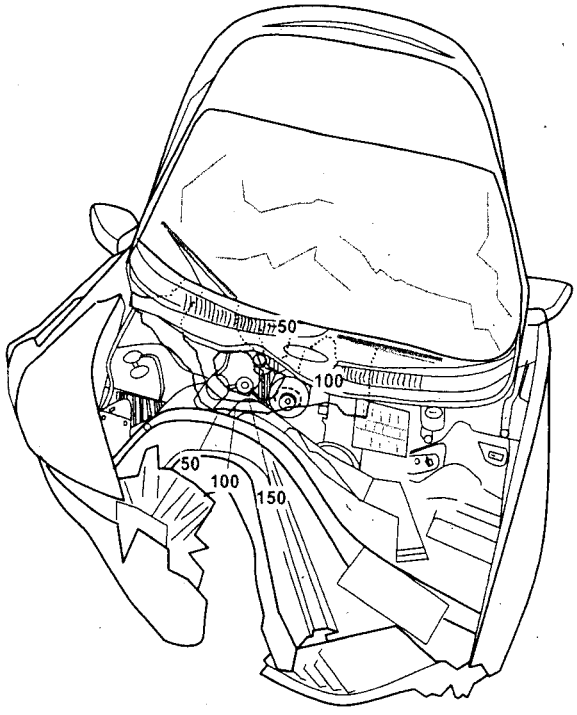

+2.50 minutes post-ignition

Figure 7, continued. Fire Test F971003. Isothermal contour plots of estimated temperatures in the top of the engine compartment –0.25, 0, 0.25, 0.50, 0.75, 1.00, 1.25, 1.50, 1.75, 2.00, 2.25 and 2.50 minutes post-ignition.

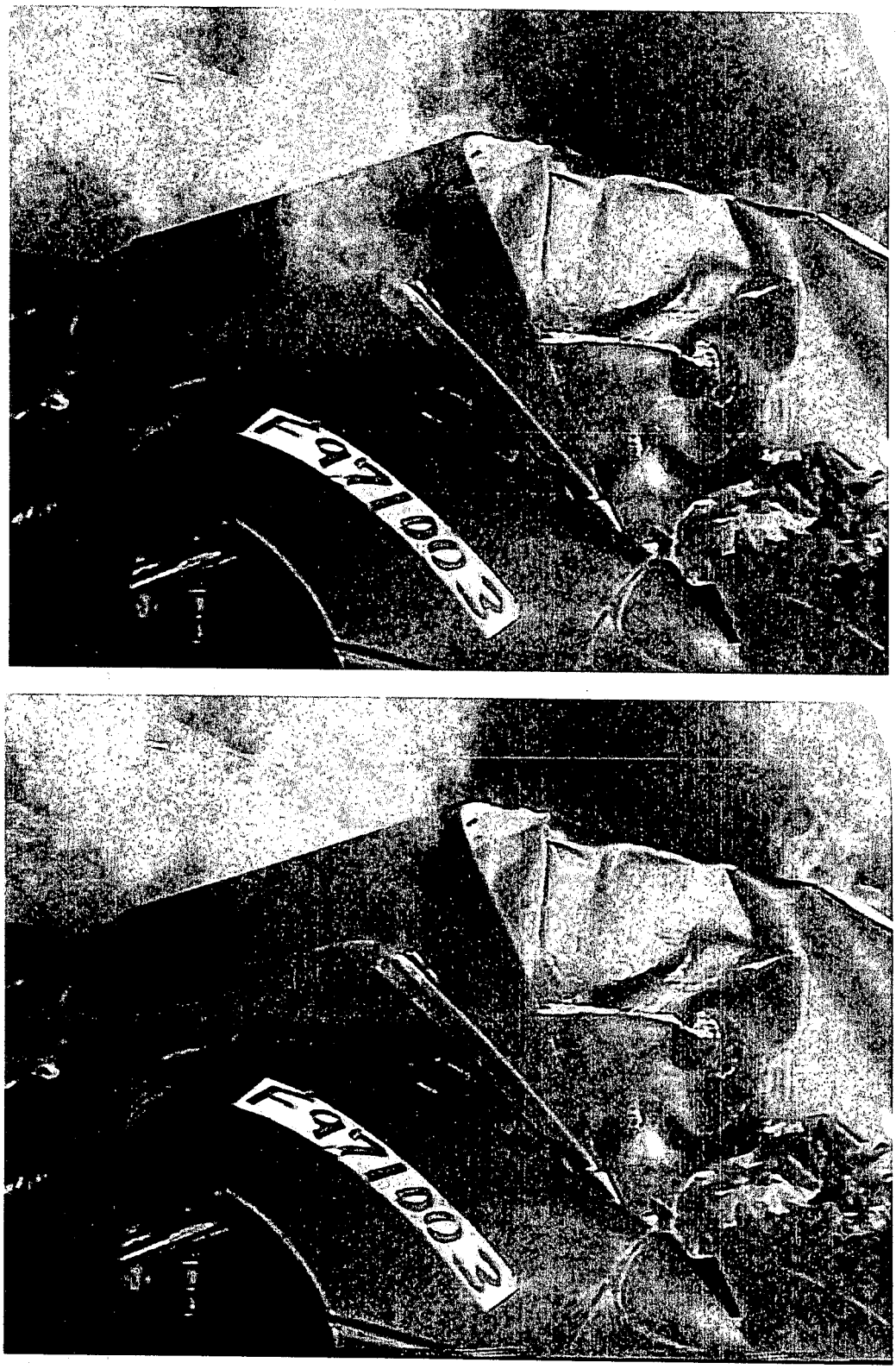

Figure 8. Fire Test F971003. Video stills from Camera 9 at 120 and 150 seconds post-ignition.

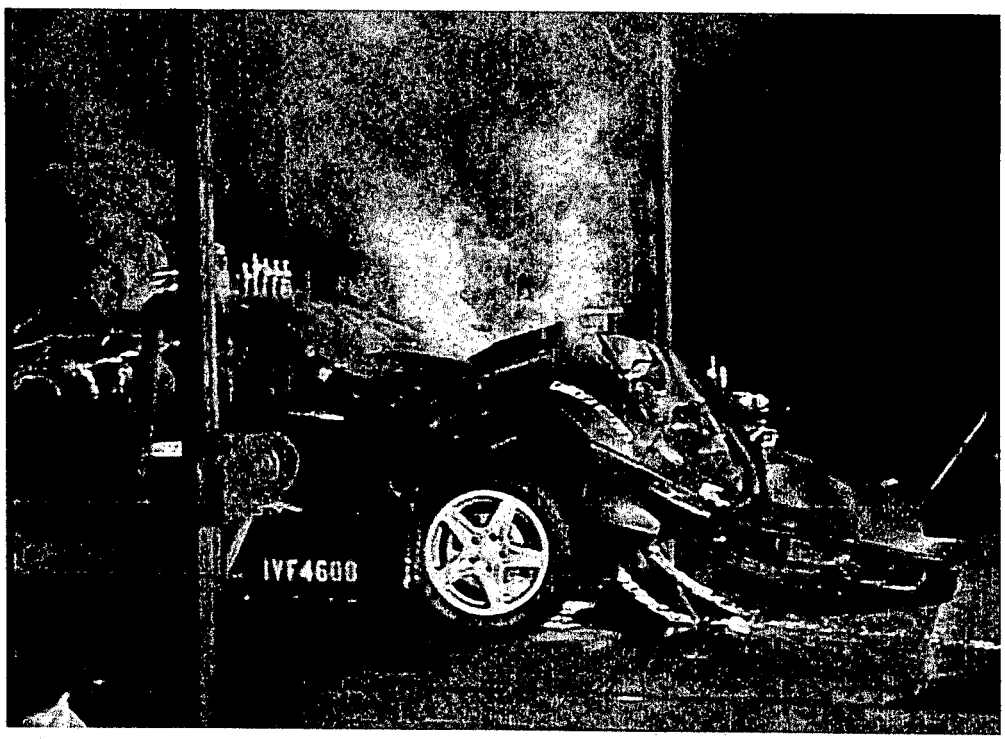

Figure 9. Fire Test F971003. Video still from Camera 2 at 2 minutes post-ignition.

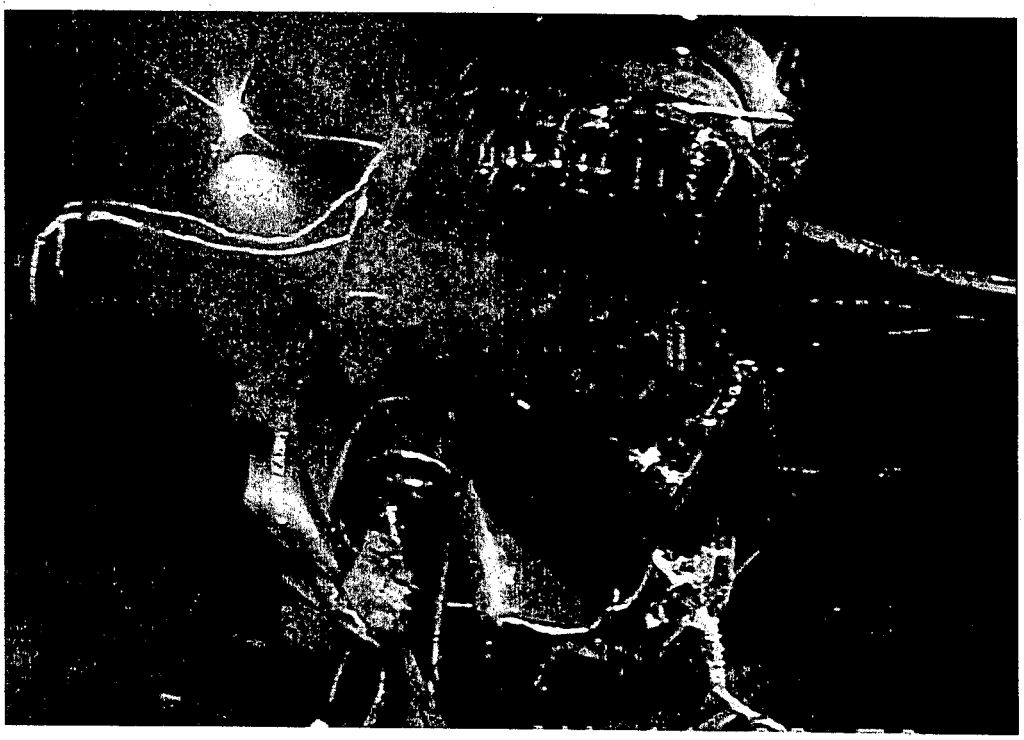

Figure 10. Fire Test F971003. Video still from Camera 4 at 2 minutes post-ignition.

4 Flame-Spread in the Engine Compartment

Illumination of objects in the field-of-view of Camera 7 from above after the propane torch was shut off indicated that flames from the torch ignited material above the igniter (Fig. 11). The sections of the HVAC upper or lower cases in the field-of-view of Camera 7 were not burning at 3 minutes post-ignition (Fig. 11). This burning material was under the dash upper extension panel and out of the field-of-view of both video cameras installed under-hood, so the objects that were burning could not be identified.[4]

Figure 11. Fire Test F971003. Video still from Cameras 7 at 2½ minutes post-ignition.

Flames were visible under the dash upper extension panel to the left of the engine at 3 minutes post-ignition (Fig. 12). This area was approximately 50 cm to the left of the igniter. The video from Camera 8 showed illumination in this area while the igniter was lit, but it was not possible to distinguish between flames and reflected light in this video, and it was therefore not possible to

[4] Components in this area included sections of the engine and transmission wiring harnesses, and hoses to the HVAC heater core.

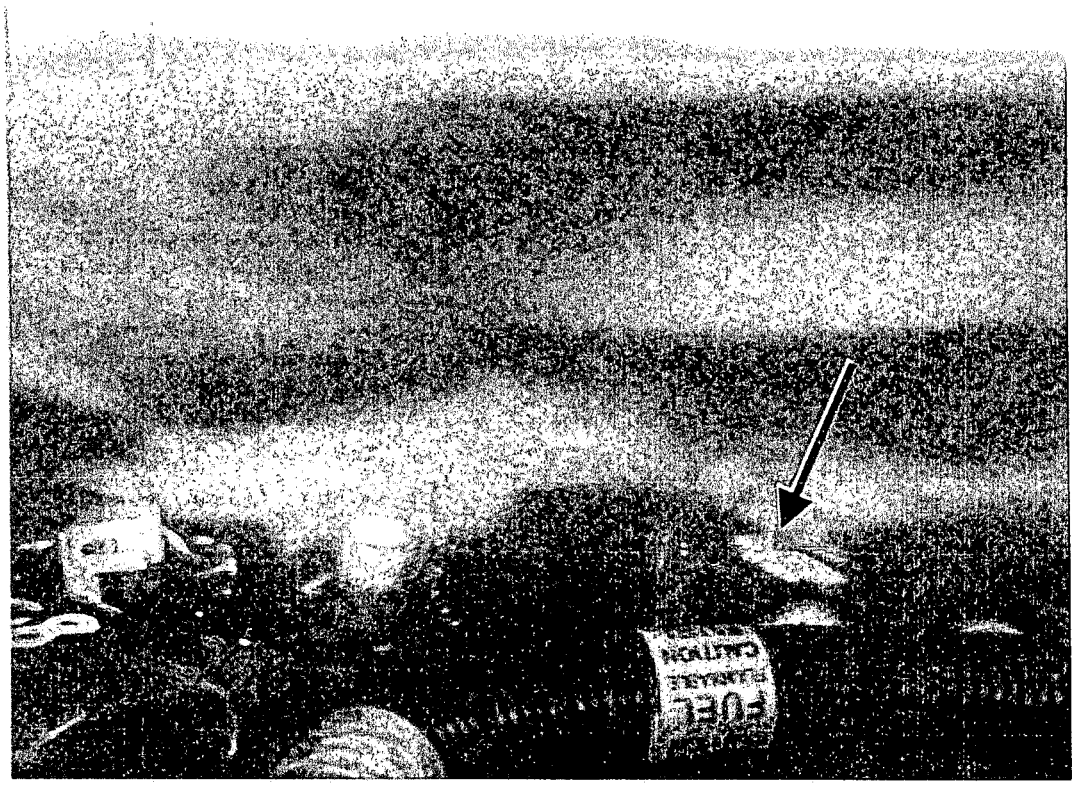

Figure 12. Fire Test F971003. Video still from Cameras 8 at 2½ minutes post-ignition.

determine the distance from the igniter that flames had spread laterally to the left under the dash upper extension panel.

4.1 Flame-Spread to the HVAC Upper Case in the Engine Compartment

Burning polymer melt was observed dripping periodically onto the inboard section of the HVAC upper case, right exhaust manifold heat shield, and right valve cover starting between 1½ and 3 minutes post-ignition. Initially, it was not possible to determine the source of this material as it appeared to originate from above and left, out of the field-of-view of Camera 7. By 3 minutes post-ignition, a section of the HVAC upper case[5] near one of the heater hoses was burning, and pools of burning polymer melt were observed on the right exhaust manifold heat shield (Fig.13). The burning polymer melt on the right exhaust manifold heat shield self-extinguished by 5 minutes post-ignition (Fig.'s 14 and 15). Flames spread lower on the HVAC module as burning polymer melt flowed downward on the upper case between 3 and 6 minutes post-ignition (Fig.'s 13 through 16).

[5] The HVAC upper case was 40% talc filled poly(propylene).

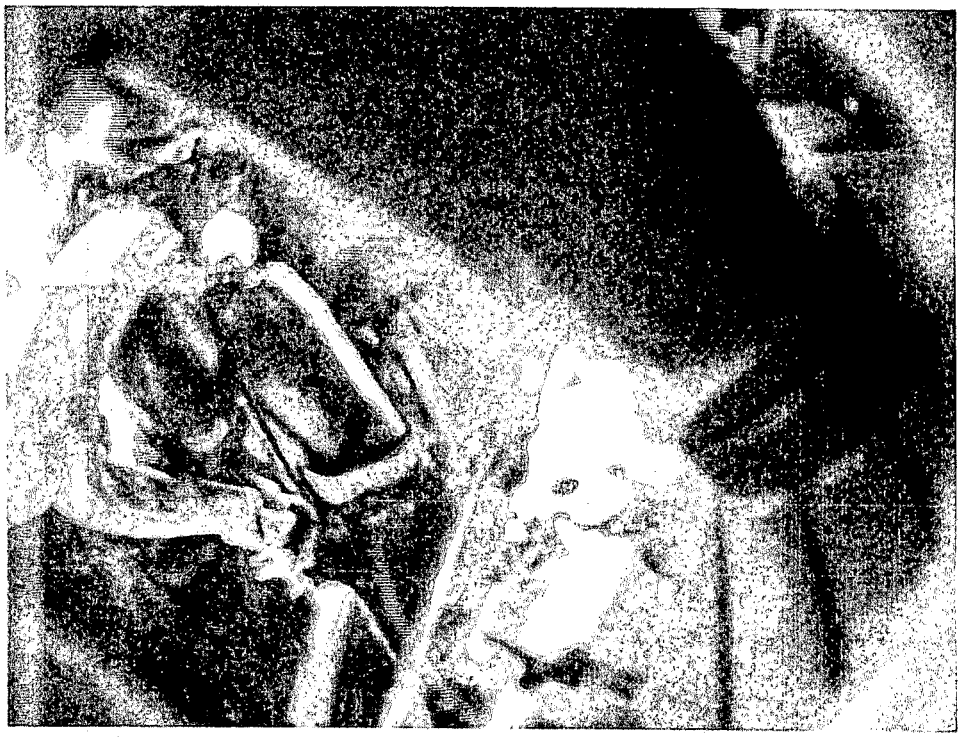

Figure 13. Fire Test F971003. Video still from Camera 7 at 3 minutes post-ignition.

Figure 14. Fire Test F971003. Video still from Camera 7 at 4 minutes post-ignition.

Figure 15. Fire Test F971003. Video still from Camera 7 at 5 minutes post-ignition.

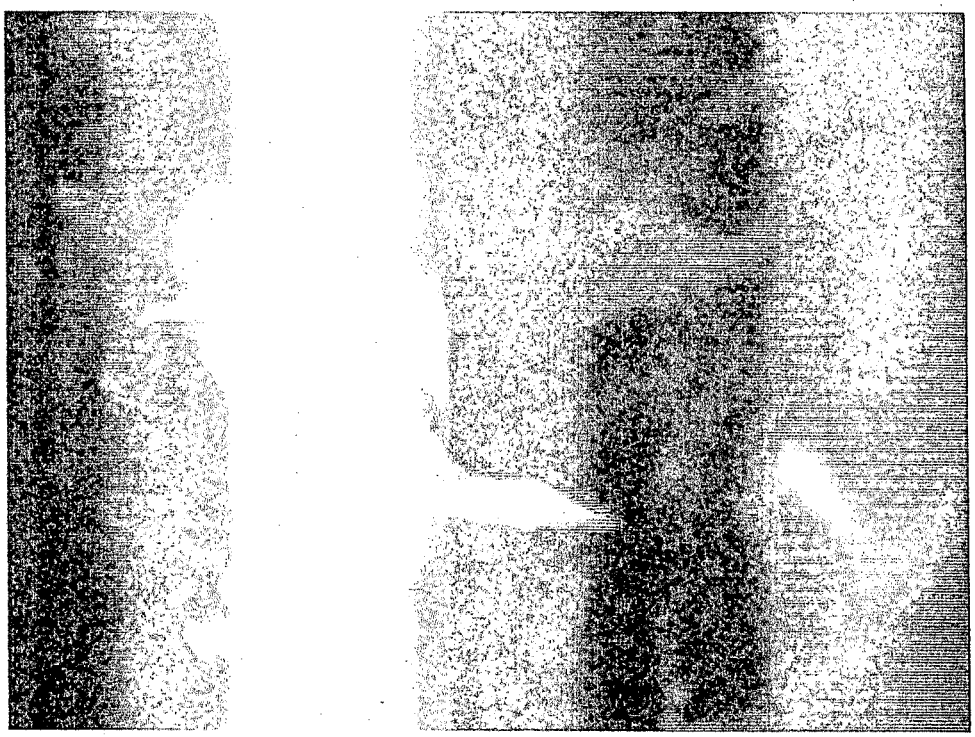

Figure 16. Fire Test F971003. Video still from Camera 7 at 6 minutes post-ignition.

4.2 Flame-Spread Laterally and Forward in the Engine Compartment

Video Cameras 2, 3, and 9 provided a limited view under the deformed hood of the test vehicle. Unambiguous determination of the location of the flame front and what objects were burning as flames spread laterally and forward in the engine compartment was not possible by analysis of these videos from these cameras. Temperature profiles in the top of the engine compartment were estimated from temperature data recorded from the E-Thermocouples.[2] The E-thermocouples were located on components in the upper section of the engine compartment and just under the HVAC air inlet screen. Isothermal contours estimated from this data indicate approximate temperatures along an imaginary surface in the upper part of the engine compartment with boundaries roughly defined by the upper radiator support member, the inside top edges of the front fenders, and the forward edge of the HVAC air inlet screen. These estimated isothermal contours provide no information about flame-spread downward in the engine compartment, or flame-spread outside of the engine compartment.

Figure 17 shows estimated isothermal contours in the upper part of the engine compartment of the test vehicle at 2, 3, 4, 5, 6, 7, 8, 9, 10, 11, 12, 13, 14, 15 and 16 minutes post-ignition. These estimated isothermal contour plots suggest that flames emerged from under the upper dash extension panel above the area where the propane torch was located between 3 and 4 minutes post-ignition[6] (Fig. 17). The video records from Cameras 4 and 9 show that flames reached the air inlet screen at the base of the windshield in the area above the propane torch about 3½ minutes post-ignition (Fig. 18). For example, a view into the engine compartment under the right side of the deformed hood shows a fire plume emerging from under the dash upper extension panel, extending under and in front of the right air inlet screen at this time (upper video still, Fig. 18). An overall view of the front of the test vehicle from above shows flames emerging from the front and rear around the right air inlet screen at this time (lower video still, Fig. 18). The timing of flame-spread to the right air inlet screen estimated from the isothermal contour plots (Fig. 17) is consistent with the timing of flame-spread to this area observed in the videos from Cameras 4 and 9 (Fig. 18).

The estimated isothermal contour plots suggest that flames spread laterally at the rear of the engine compartment along the air inlet screen and forward from the area where the propane torch was located between 4 and 8 minutes post-ignition (Fig. 17). The video record from Camera 8 showed that flames emerged from the forward edge of the left upper dash extension panel under

[6] As in previous reports, a value of 600°C was used in this report as the threshold to indicate the presence of flame. Using this criterion, the 600°C isothermal contour indicated the approximate boundary of the flame front in the engine compartment.

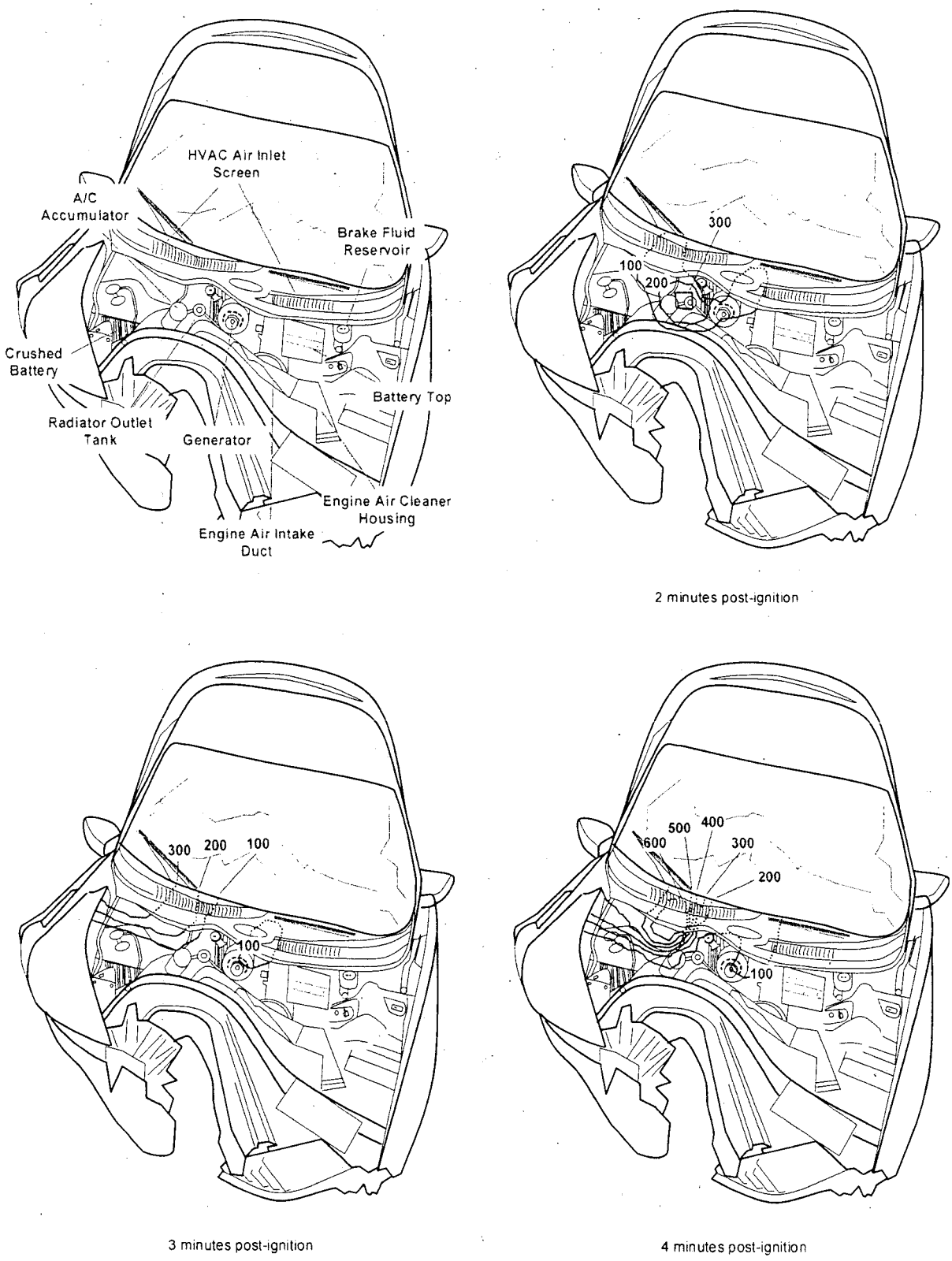

Figure 17. Fire Test F971003. Isothermal contour plots of estimated temperatures in the upper part of the engine compartment at 2, 3, 4, 5, 6, 7, 8, 9, 10, 11, 12, 13, 14, 15 and 16 minutes post-ignition.

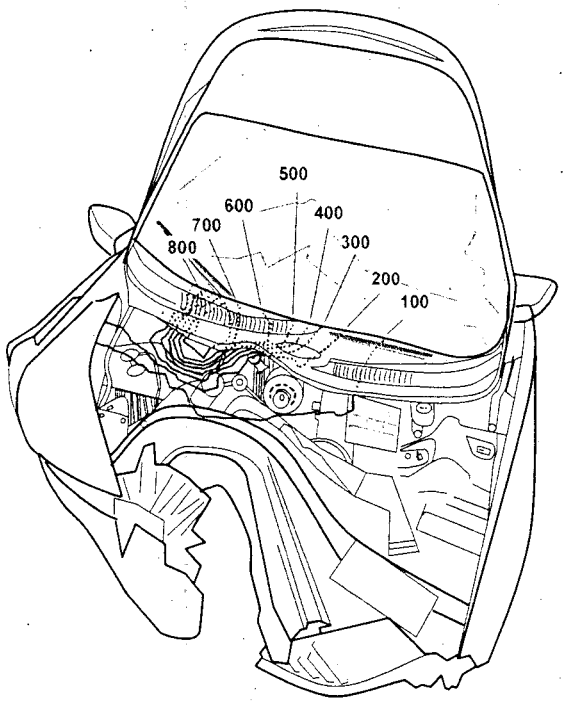

5 minutes post-ignition

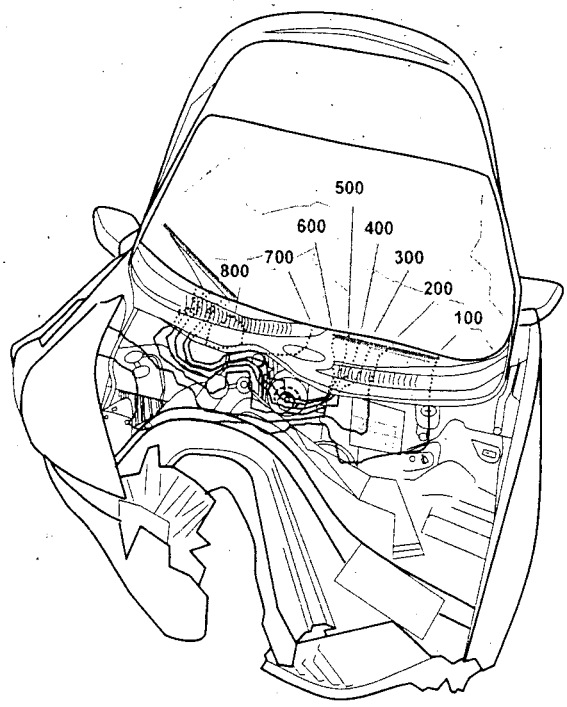

6 minutes post-ignition

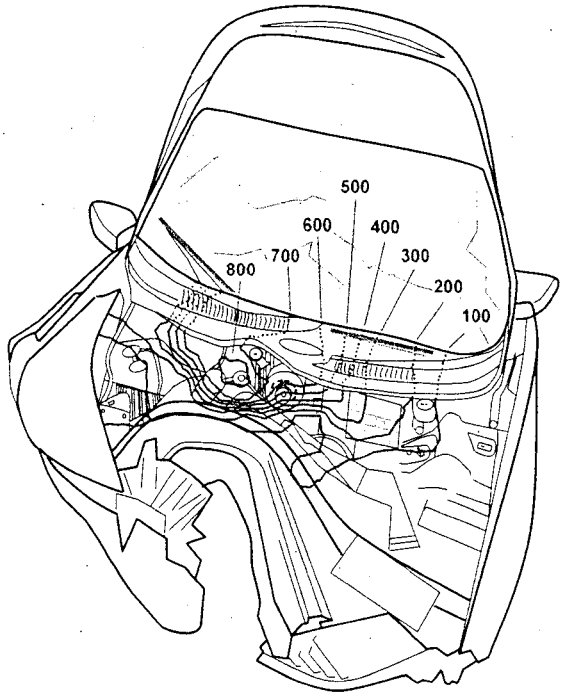

7 minutes post-ignition

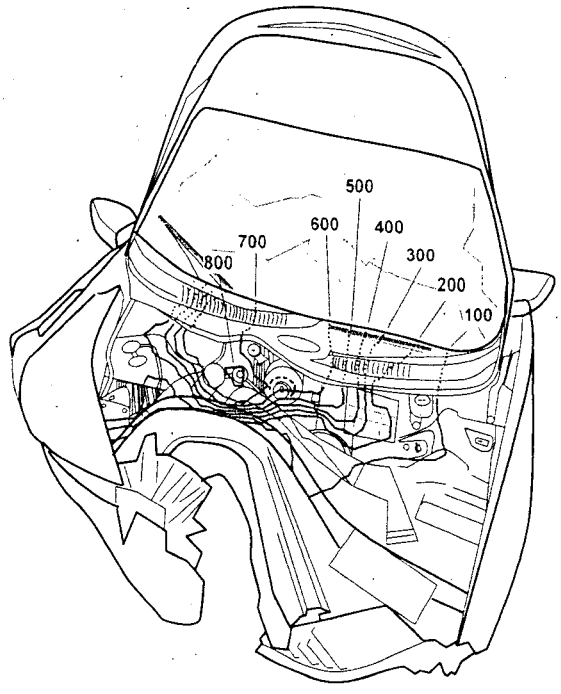

8 minutes post-ignition

Figure 17, continued. Fire Test F971003. Isothermal contour plots of estimated temperatures in the upper part of the engine compartment at 2, 3, 4, 5, 6, 7, 8, 9, 10, 11, 12, 13, 14, 15 and 16 minutes post-ignition.

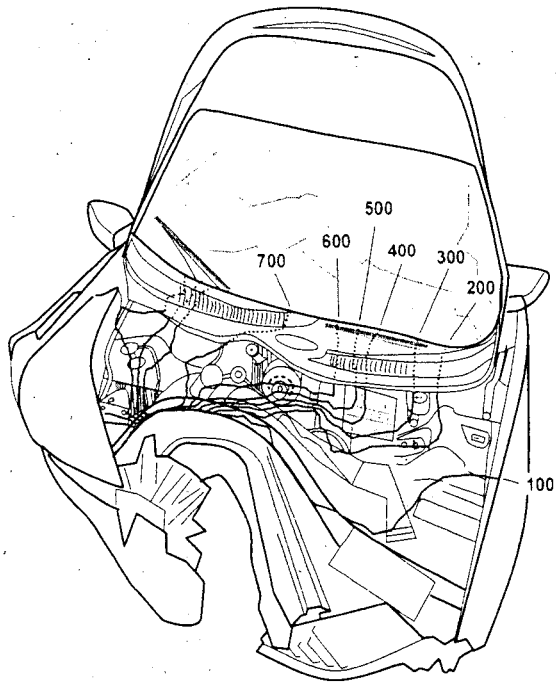

9 minutes post-ignition

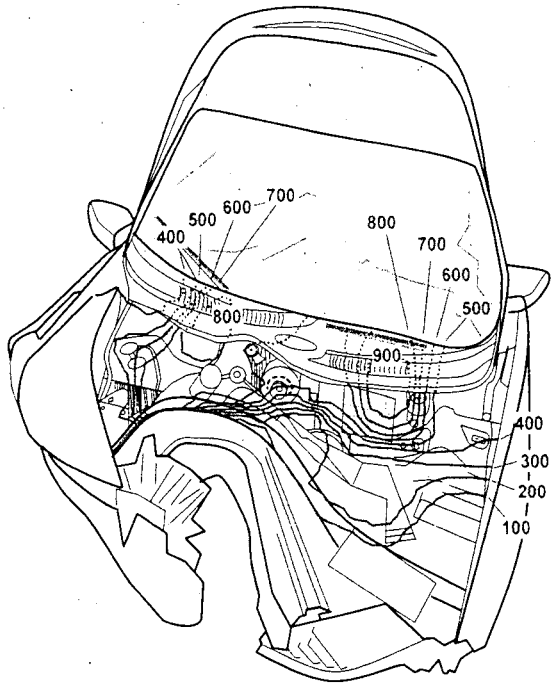

10 minutes post-ignition

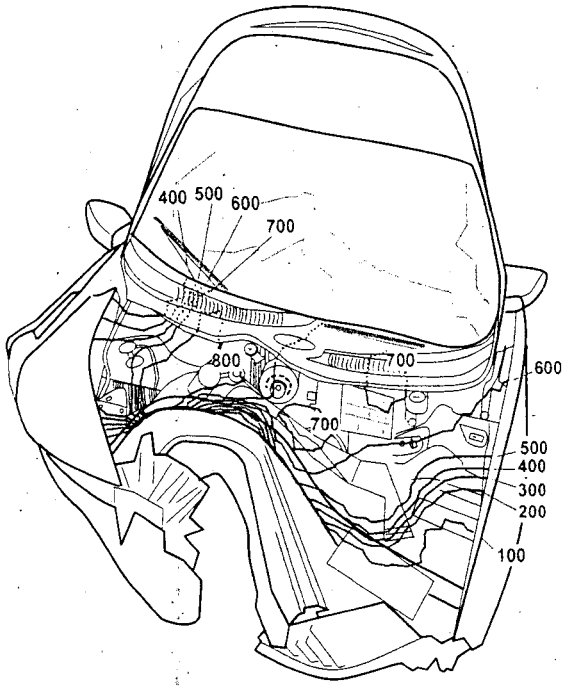

11 minutes post-ignition

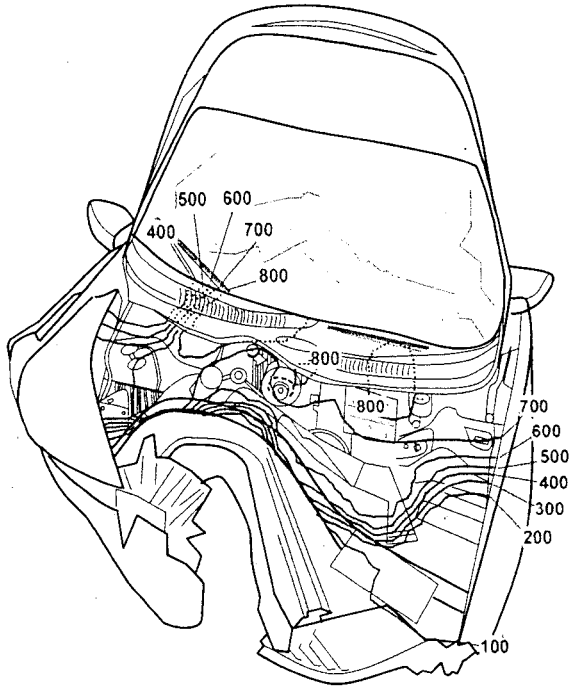

12 minutes post-ignition

Figure 17, continued. Fire Test F971003. Isothermal contour plots of estimated temperatures in the upper part of the engine compartment at 2, 3, 4, 5, 6, 7, 8, 9, 10, 11, 12, 13, 14, 15 and 16 minutes post-ignition.

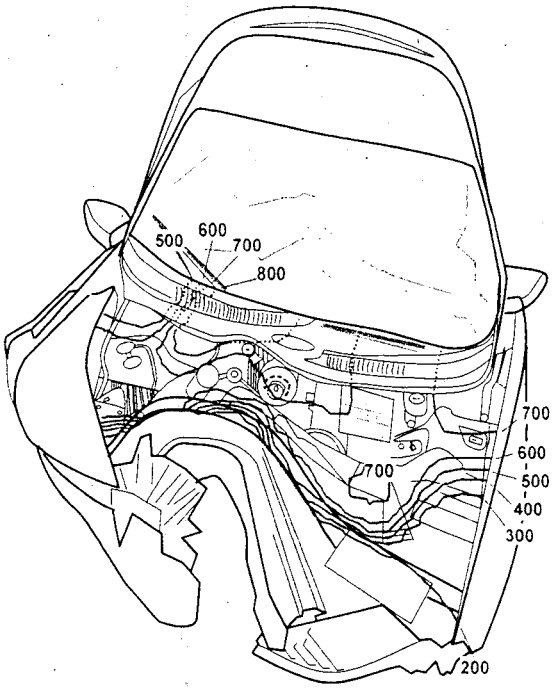

13 minutes post-ignition

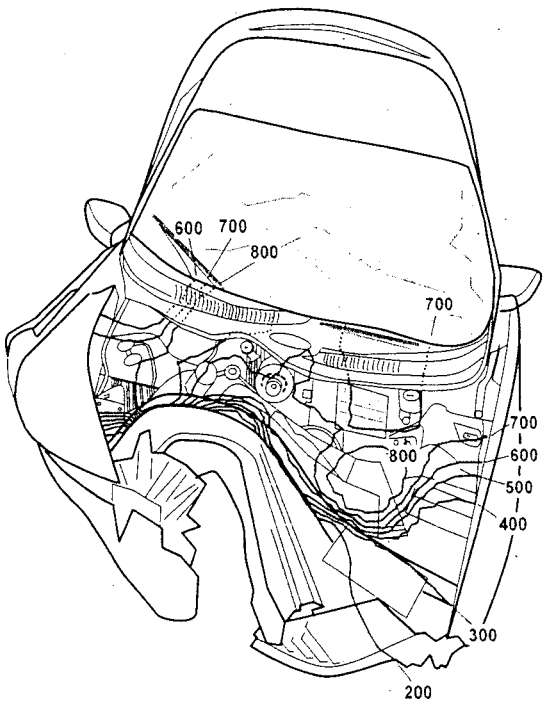

14 minutes post-ignition

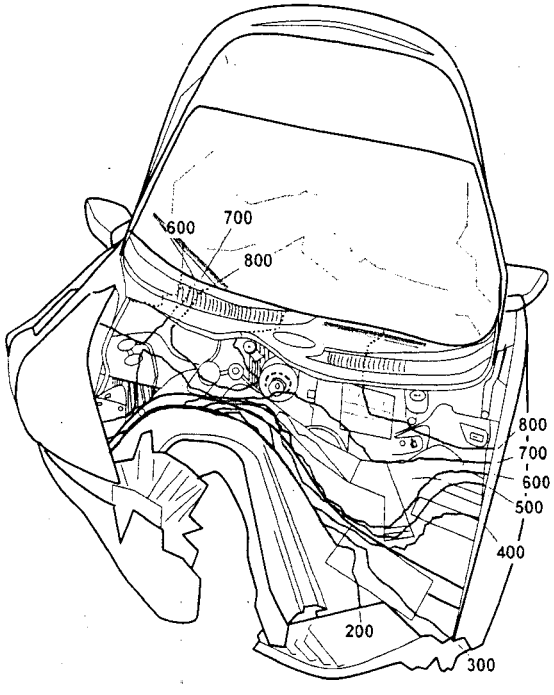

15 minutes post-ignition

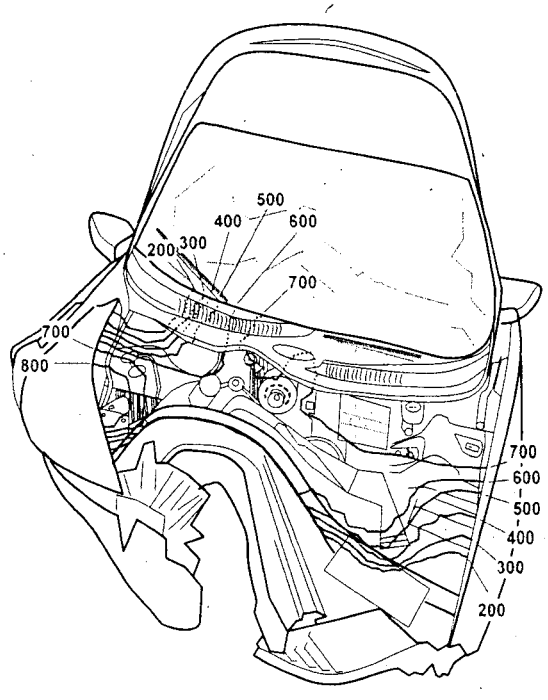

16 minutes post-ignition

Figure 17, continued. Fire Test F971003. Isothermal contour plots of estimated temperatures in the upper part of the engine compartment at 2, 3, 4, 5, 6, 7, 8, 9, 10, 11, 12, 13, 14, 15 and 16 minutes post-ignition.

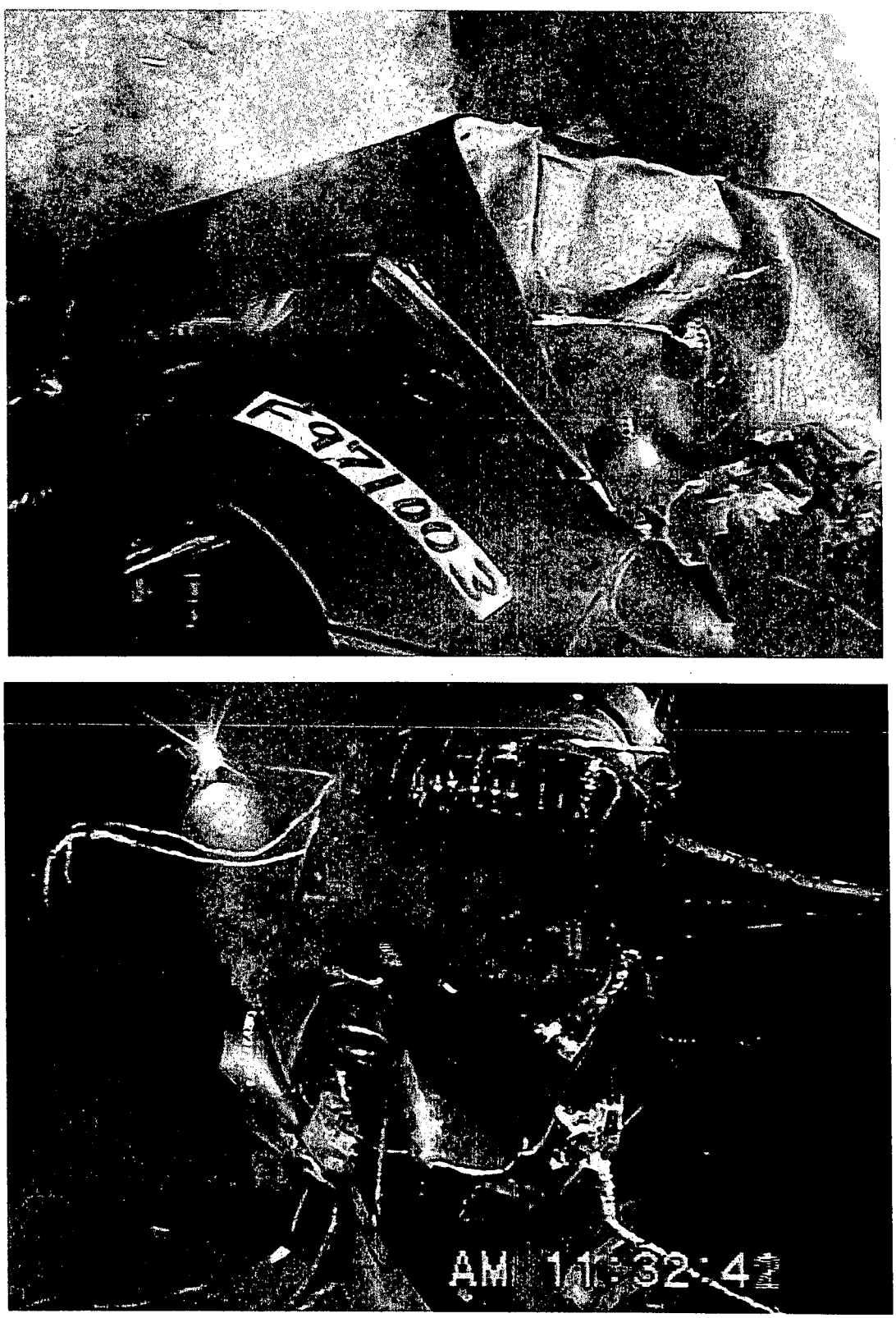

Figure 18. Fire Test F971003. Video still from Cameras 9 and 4 at 3½ minutes post-ignition.

the dislodged battery top between 8 and 8 ½ minutes post-ignition (Fig. 19). The isothermal contour plots show temperatures were greater than 600°C in this area at 10 minutes post-ignition (Fig. 17), suggesting that flames spread to the left air inlet screen above the dislodged battery top between 9 and 10 minutes post-ignition.

Flames spread laterally and forward in the right and left sides of the engine compartment between 10 and 16 minutes post-ignition. When the test was ended at about 16 minutes post-ignition, flames had spread laterally to the right upper side panel and forward on the right side of the engine compartment to the upper radiator support cross-member (Fig. 17). Flames had spread laterally to the left upper side panel in the rear of the engine compartment, and forward to the engine air cleaner housing in the right side of the engine compartment (Fig. 17).

The inner edge of the right front fender[7], which was broken during the crash test, ignited between 6 and 8 minutes post-ignition. It was not possible to distinguish between flames emerging from the right side of the deformed hood and flames attached to the right front fender from the data recorded during this test. Therefore, it was not possible to determine the exact time of ignition of the right front fender. The right front wheelhouse panel liner[8] ignited between 10 and 11 minutes post-ignition. Burning pieces of the right front fender fell off of the test vehicle and onto the test surface beginning at about 13½ minutes post-ignition (Fig.'s 20 and 21). The estimated isothermal contour plots and the video records indicate that flames did not spread forward of the deformed hood when the test was ended at about 16 minutes post-ignition (Fig.'s 17 and 21).

The pattern of fire damage to components in the engine compartment of the test vehicle after this test (Fig. 22) is consistent with the extent of flame-spread in the engine compartment inferred from the estimated isothermal contour plots of temperatures in the upper engine compartment at 16 minutes post-ignition (Fig. 17). For example, the air inlet screen at the rear of the engine compartment, and the engine air intake duct and engine air cleaner housing along the upper radiator support cross-member were in areas where the estimated temperature was at least 600°C (Fig. 17). Burned and charred residue from these components was present in the engine compartment after this test (Fig. 22). Components forward of the upper radiator support cross-member on the left side of the test vehicle such as the windshield washer fluid reservoir showed no evidence of melting or igniting (Fig. 22).

[7] The fenders were a styrene-cross-linked-polyester-glass-fiber composite (Sheet Molding Compound).
[8] The front wheelhouse panel liners were poly(propylene).

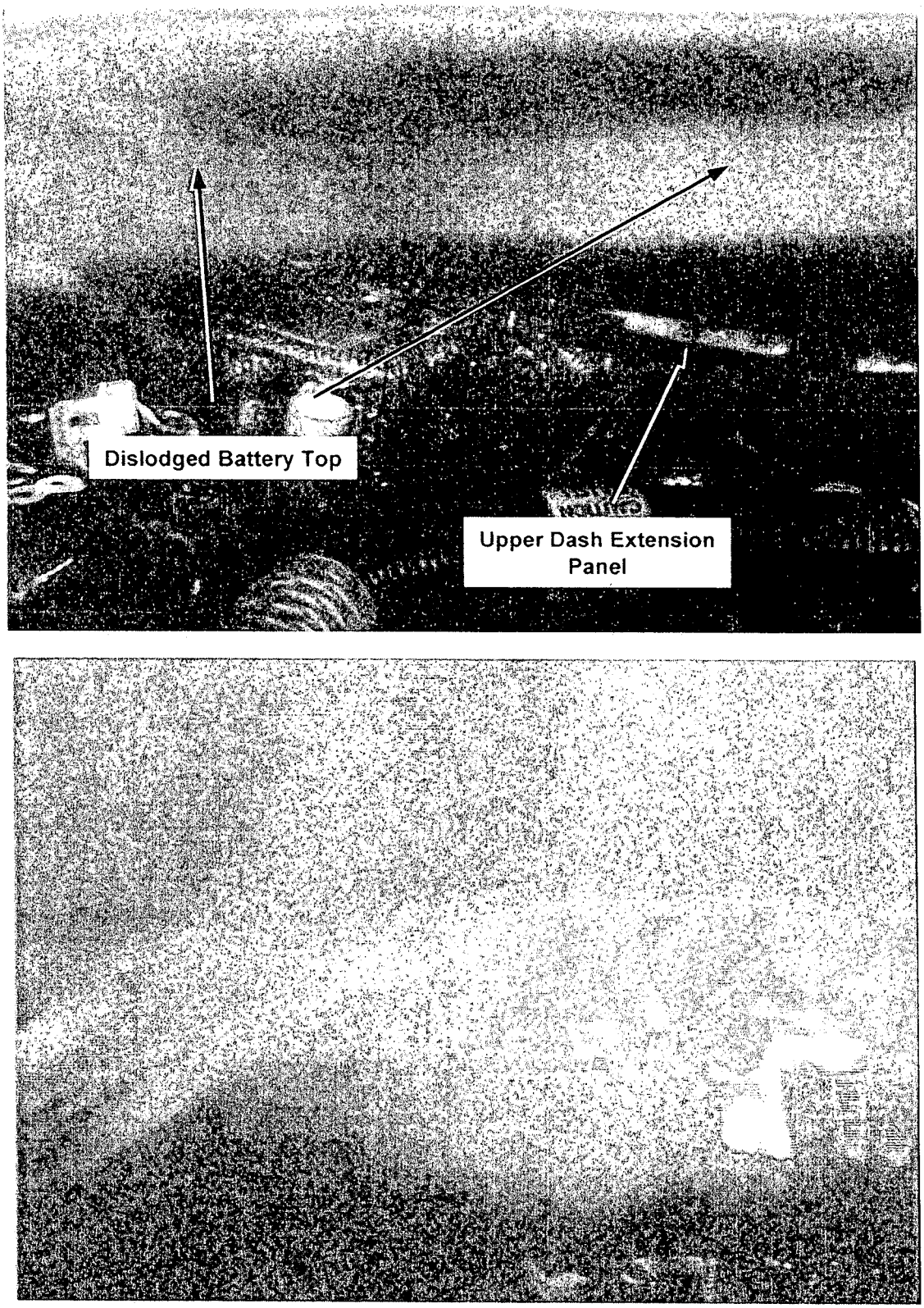

Figure 19. Fire Test F971003. Video stills from Camera 8 before ignition (upper video still) and at 8½ minutes post-ignition (lower video still).

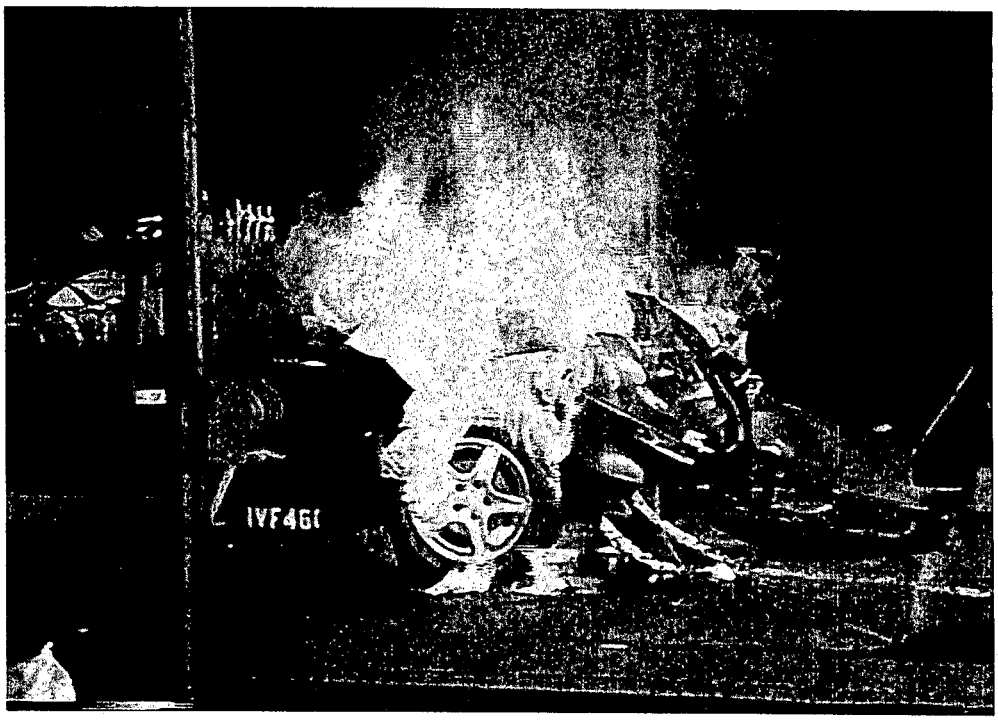

Figure 20. Fire Test F971003. Video still from Camera 2 at 14 minutes post-ignition.

Figure 21. Fire Test F971003. Video still from Camera 4 at 15½ minutes post-ignition.

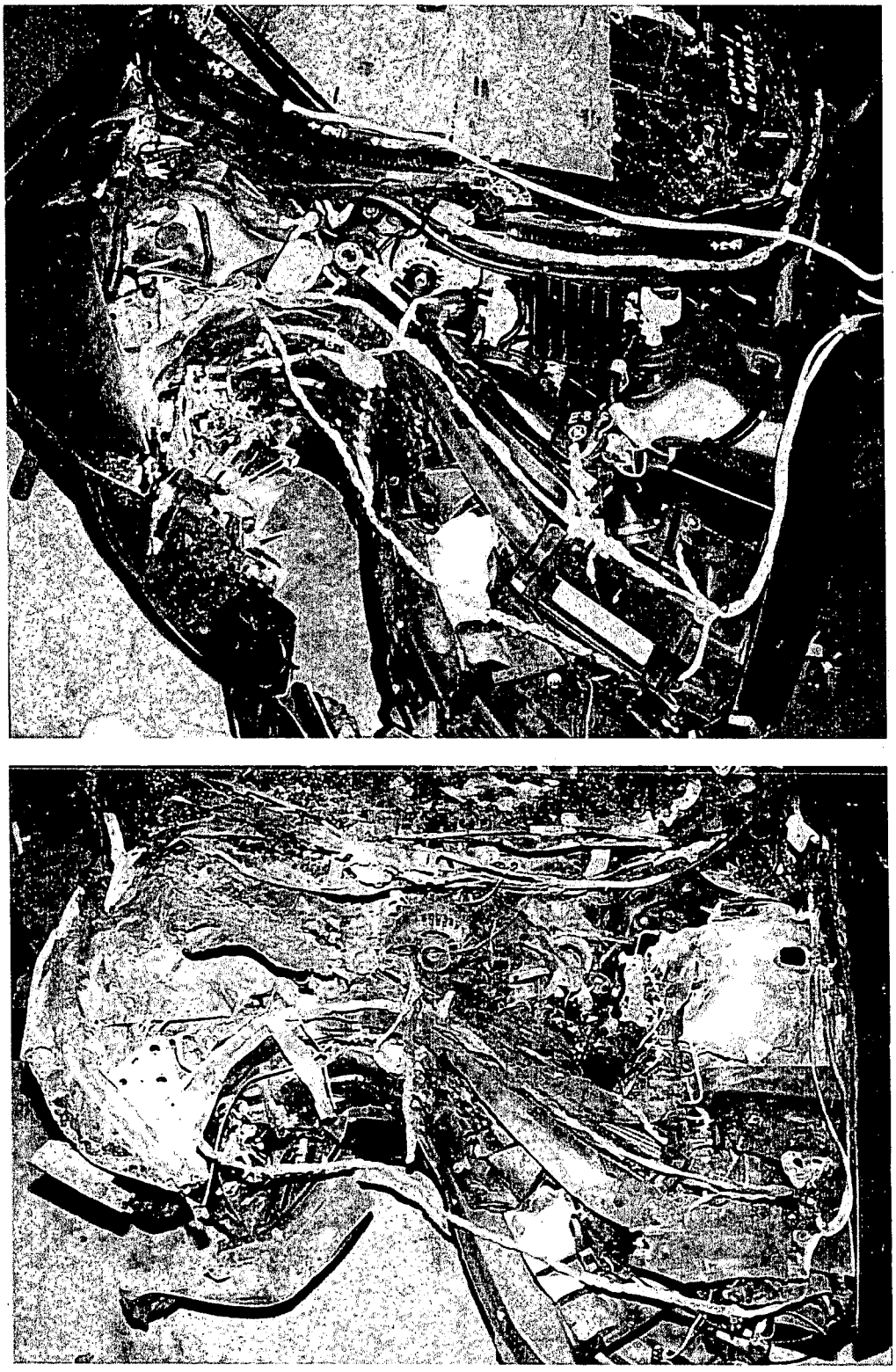

Figure 22. Fire Test F971003. Photographs of the front of the test vehicle before (upper) and after (lower) this test.

4.3 Flame-Spread to Fluids Under the Test Vehicle

Pieces of burning material started to fall into the mixture of petroleum oils, brake fluid, and engine coolant that was pooled under the engine compartment of the test vehicle at about 8½ minutes post-ignition. The state or condition of this material (e.g., solid of polymer melt) could not be determined unambiguously from the test data. Some of this burning material self-extinguished shortly after falling into this fluid pool under the engine compartment. Other pieces continued to burn until the test was ended and the fire was extinguished (Fig. 23). It could not be determined whether the fluid mixture ignited in the area around the pieces of plastic that continued to burn. At the time this test was ended, flames had not spread across the surface of the pooled fluids away from the burning material that fell from the vehicle (Fig. 23).

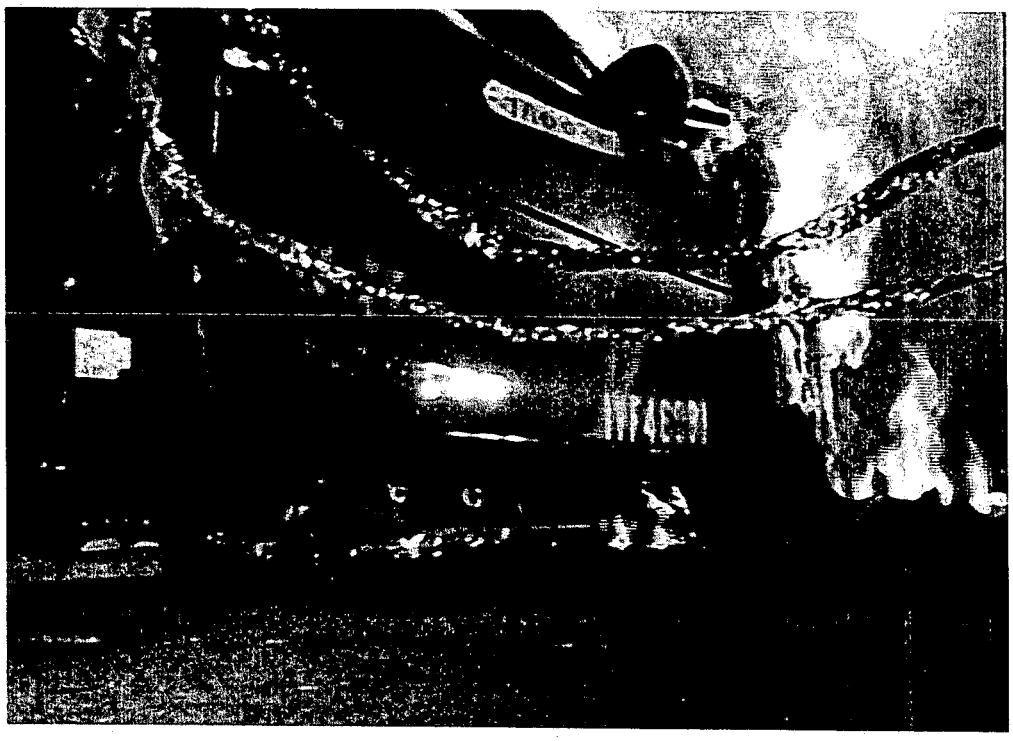

Figure 23. Fire Test F971003. Video still from Camera 5 at 15 minutes post-ignition.

5 Flame-Spread into the Passenger Compartment

The pattern of fire damage observed during inspection of the test vehicle after this test suggested that flame-spread into the passenger compartment progressed along two pathways simultaneously. These pathways include the windshield and the HVAC module in the dash panel, both of which were broken in the crash test.

The diagram below shows a top-view of the dash panel, windshield support panel, HVAC module, and defroster nozzle and air distributor assembly in the test vehicle after the crash test.

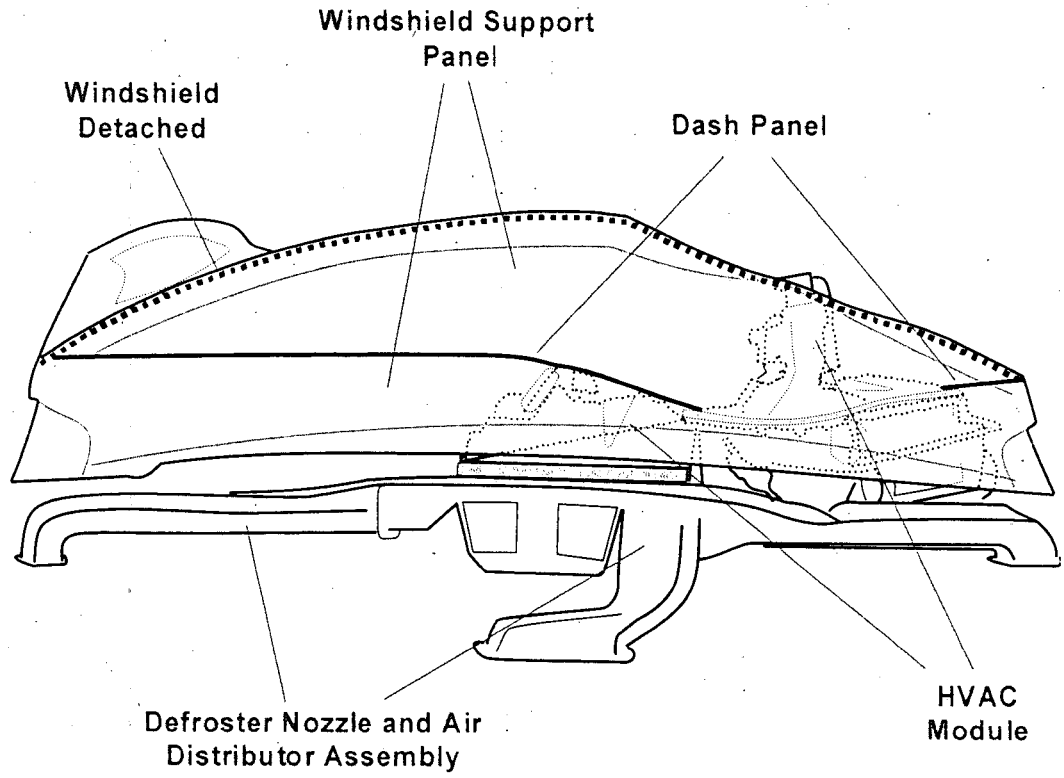

Both glass outer layers of the windshield[9] were shattered during the crash test. The right side of the dash panel was displaced rearward. The right sides of the upper dash extension panel and windshield support panel were deformed, and the bottom (forward) edge of the broken windshield had detached from the windshield support panel. The sides and top of the windshield remained

[9] Motor vehicle windshields generally are composite structures, consisting of two outer layers of annealed glass and an inner layer of a vinyl butyral/vinyl alcohol copolymer. The inner layer in the windshield of the test vehicle contained dihexyl adipate (plasticizer) and 2-(2H-benzotriazol-2-yl)-4-methylphenol (UV-inhibitor).

attached to the A-pillars and roof. The front section of the broken windshield sagged onto the instrument panel upper trim panel.

The dash panel in the test vehicle contained a number of crash-induced openings that could provide a path for flames to spread from the engine compartment into the passenger compartment. These potential fire paths included the broken HVAC module, two tears caused by transmission bolts loading the dash panel when the engine was displaced rearward, and a seam opening at the lower right corner of the dash panel. The diagram below shows a face-view of the dash panel in the test vehicle.

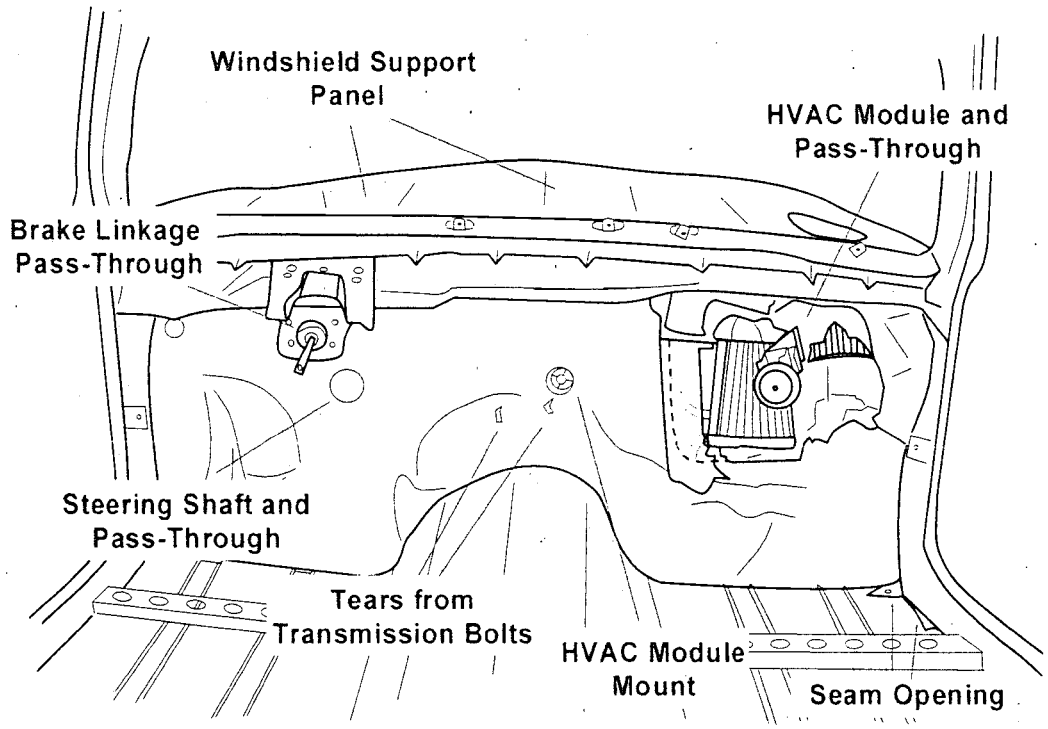

The HVAC module was broken and dislodged rearward from its mount in the center of the dash panel. Thermocouples were installed along the exterior of the windshield and around each of the potential fire paths in the dash panel to document where and when flame-spread into the passenger compartment occurred during this test. Flame-spread through the brake-linkage pass-through and the steering shaft pass-through was not anticipated because the master cylinder power booster covered the brake-linkage pass-through and the steering-column dash panel cover was intact after the crash test, and covered the steering shaft pass-through.

Flame-spread through the windshield was characterized by analyzing the video records from some of the exterior and interior cameras, the recorded thermocouple data, and the infrared

thermography data. The exterior of the dash panel was obscured by the engine and other components that were pushed to the rear of the engine compartment during the crash test. The interior of the dash panel was covered by the carpet and the instrument panel[10]. Thus, the video record was of limited utility in characterizing flame-spread through the dash. The recorded thermocouple data and the pattern of fire damage in the instrument panel and on the dash panel were used to characterize flame-spread through the dash.

5.1 Flame-Spread through the Windshield

Flames began to contact the windshield between 3 and 4 minutes post-ignition, when flames emerged from the engine compartment along the rear edge of the deformed hood (see Fig. 18). Figures 24 through 33 show a series of video stills from Cameras 4 and 6 at 4, 5, 6, 7, 8, 9, 10, 11, and 12 minutes post-ignition. The isothermal contour plots overlaid on the video stills from Camera 4 are estimated temperature profiles at the exterior surface of the windshield.[11] The thermocouples used to measure the temperature data used in the calculation of these isothermal contours were located approximately 5 mm away from (in front of) the exterior surface of the windshield or below the air inlet screen just above the leading edge of the windshield. These thermocouples were heated by convection and radiation from hot gases and flames venting from the engine compartment along the rear edge of the deformed hood. Thus, the estimated temperature profiles shown in Figures 24 through 33 indicate the approximate distribution of heated gases and flames along the exterior surface of the windshield. This analysis cannot be used to estimate the temperature of the exterior surface of the windshield because the thermocouples used to acquire the data for these calculations were not in contact with the windshield.

Temperatures along the exterior surface of the windshield in the area where flames emerged from the rear edge of the deformed hood increased from approximately 350°C at 3 minutes post-ignition to greater than 600°C at 4 minutes post-ignition (upper video stills, Fig.'s 24 and 25). The height and width of the fire plume along the rear edge of the deformed hood increased between 4 and 10 minutes post-ignition as flames spread laterally along the air inlet screen (Fig.'s 25 through 31).

---

[10] In this report, instrument panel refers to the component assembly in the passenger compartment that is attached to the interior side of the dash panel and usually contains the instrument cluster, the glove box, etc.

[11] The isothermal contour plots in Figures 24 through 32 were estimated from recorded temperature data using a three-dimensional interpolation algorithm available in SigmaPlot for Windows Version 4.00 [3]. This algorithm uses an inverse distance method to generated temperature values for points on a uniformly spaced Cartesian grid from input [x,y,t] triple data. Data recorded from thermocouples located in front of the exterior surface of the windshield (Thermocouples W1 through W10) and below the air inlet screen (Thermocouples E10 through E17) were used in these calculations.

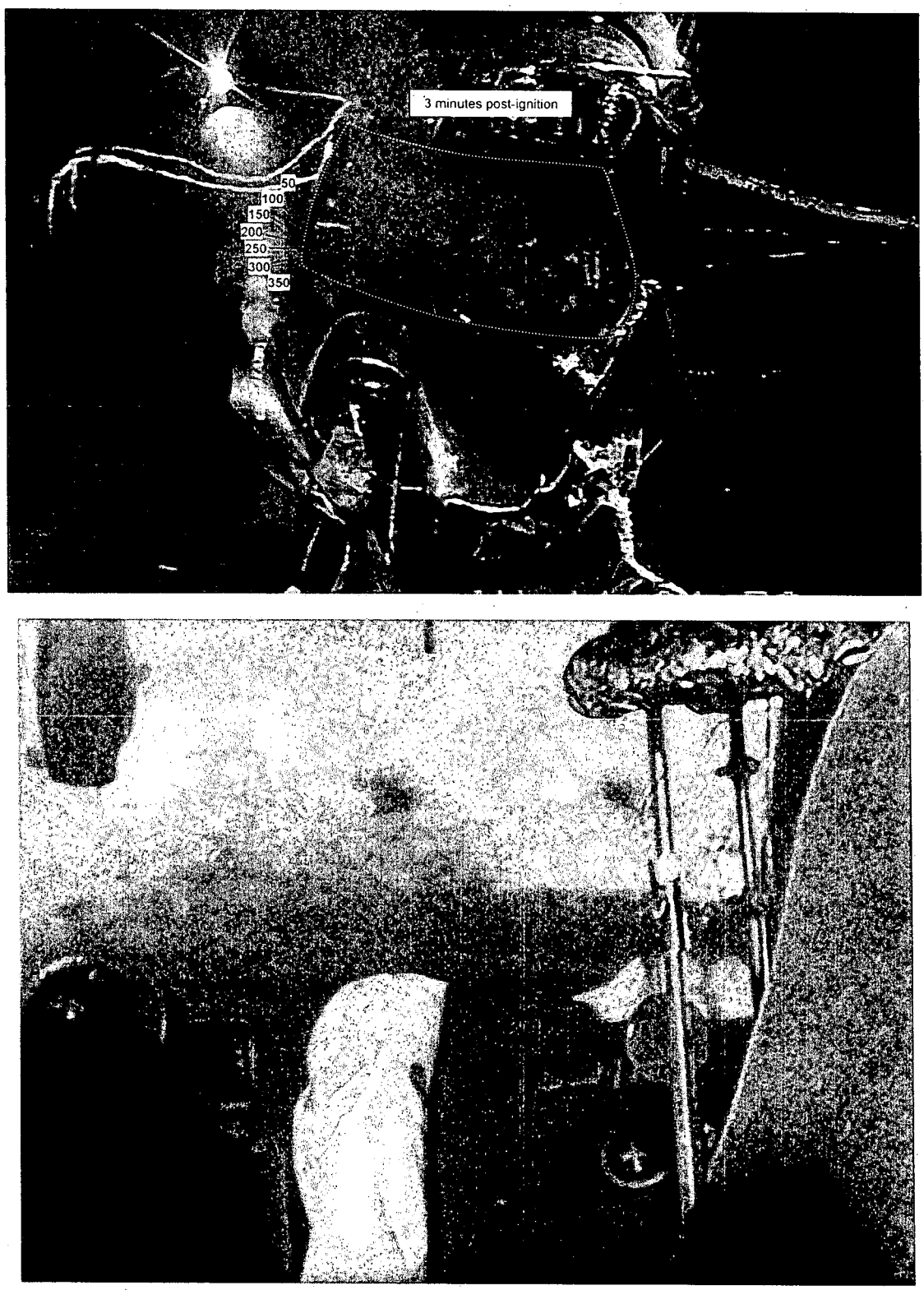

Figure 24. Fire Test F971003. Video Stills from Camera 4 with estimated isothermal contour plots of temperatures on the windshield and Camera 6 at 3 minutes post-ignition.

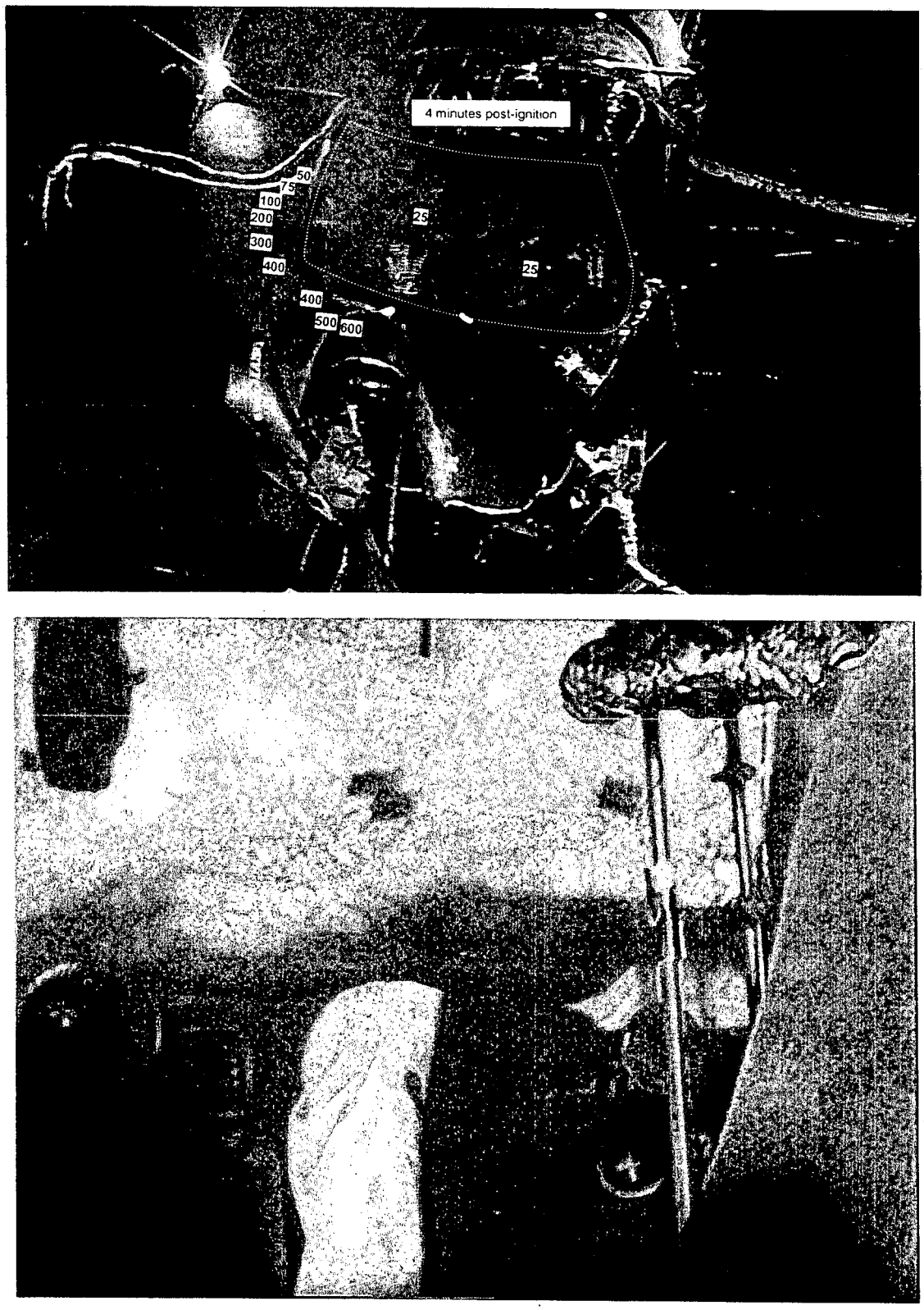

Figure 25. Fire Test F971003. Video Stills from Camera 4 with estimated isothermal contour plots of temperatures on the windshield and Camera 6 at 4 minutes post-ignition.

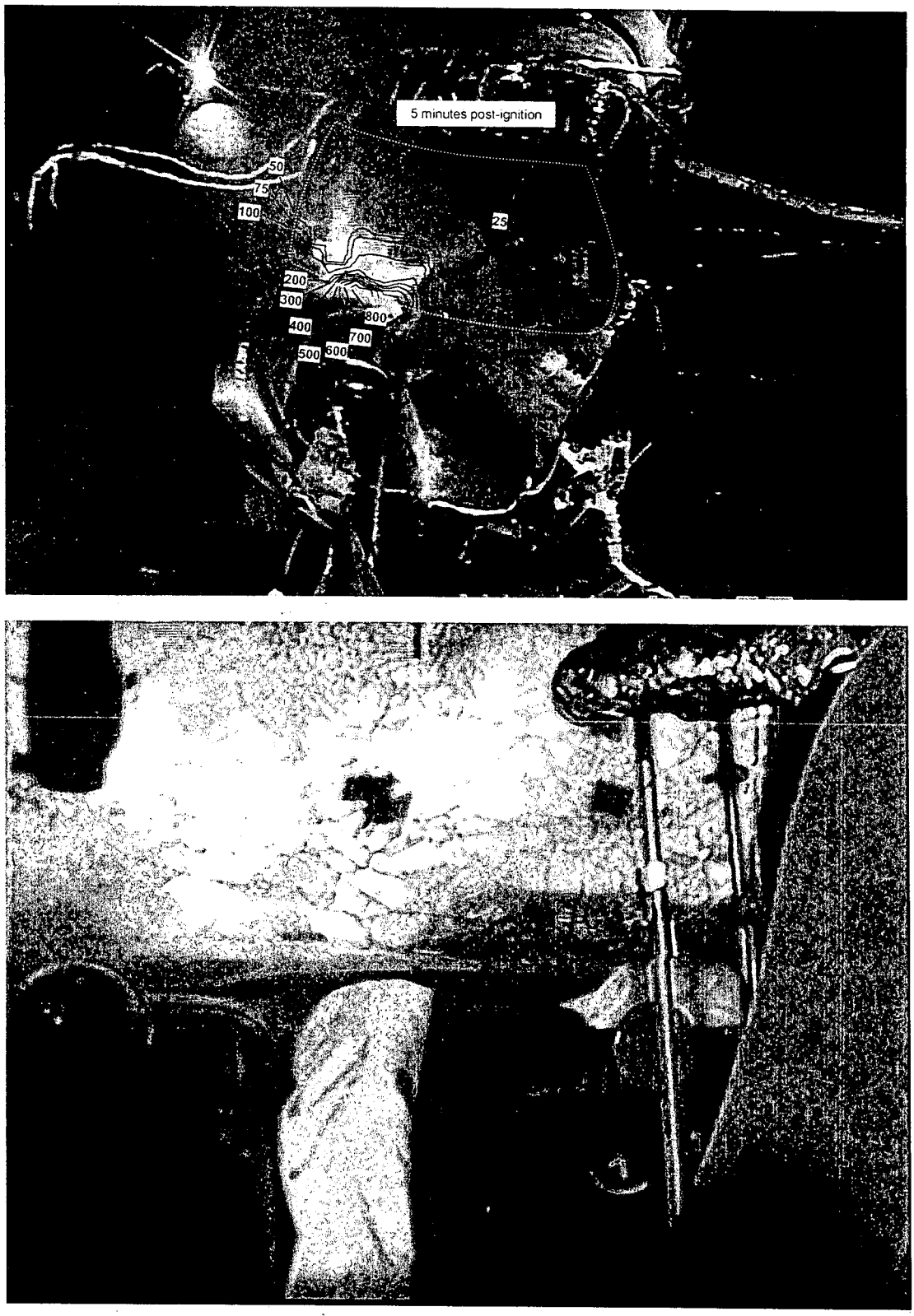

Figure 26. Fire Test F971003. Video Stills from Camera 4 with estimated isothermal contour plots of temperatures on the windshield and Camera 6 at 5 minutes post-ignition.

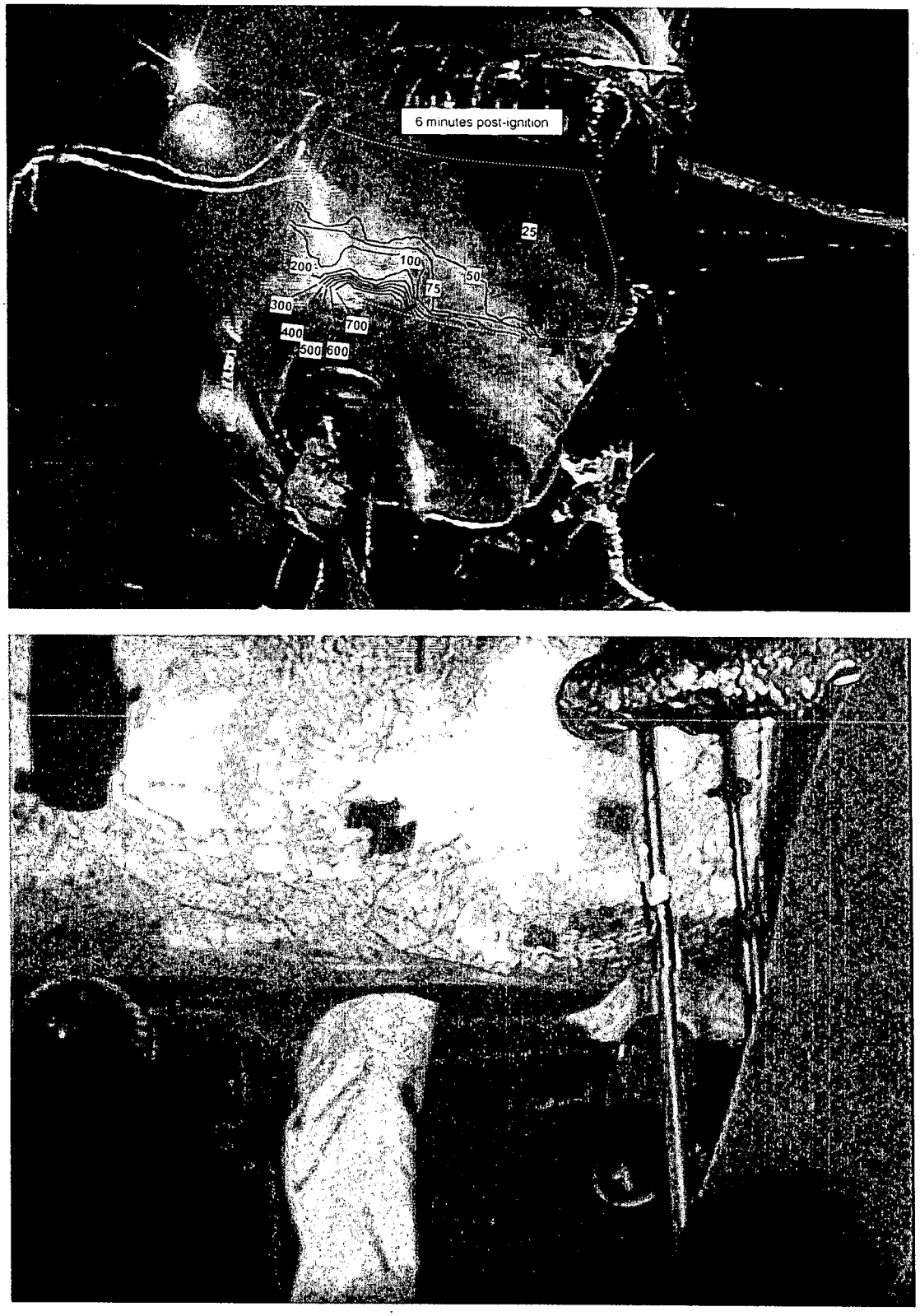

Figure 27. Fire Test F971003. Video Stills from Camera 4 with estimated isothermal contour plots of temperatures on the windshield and Camera 6 at 6 minutes post-ignition.

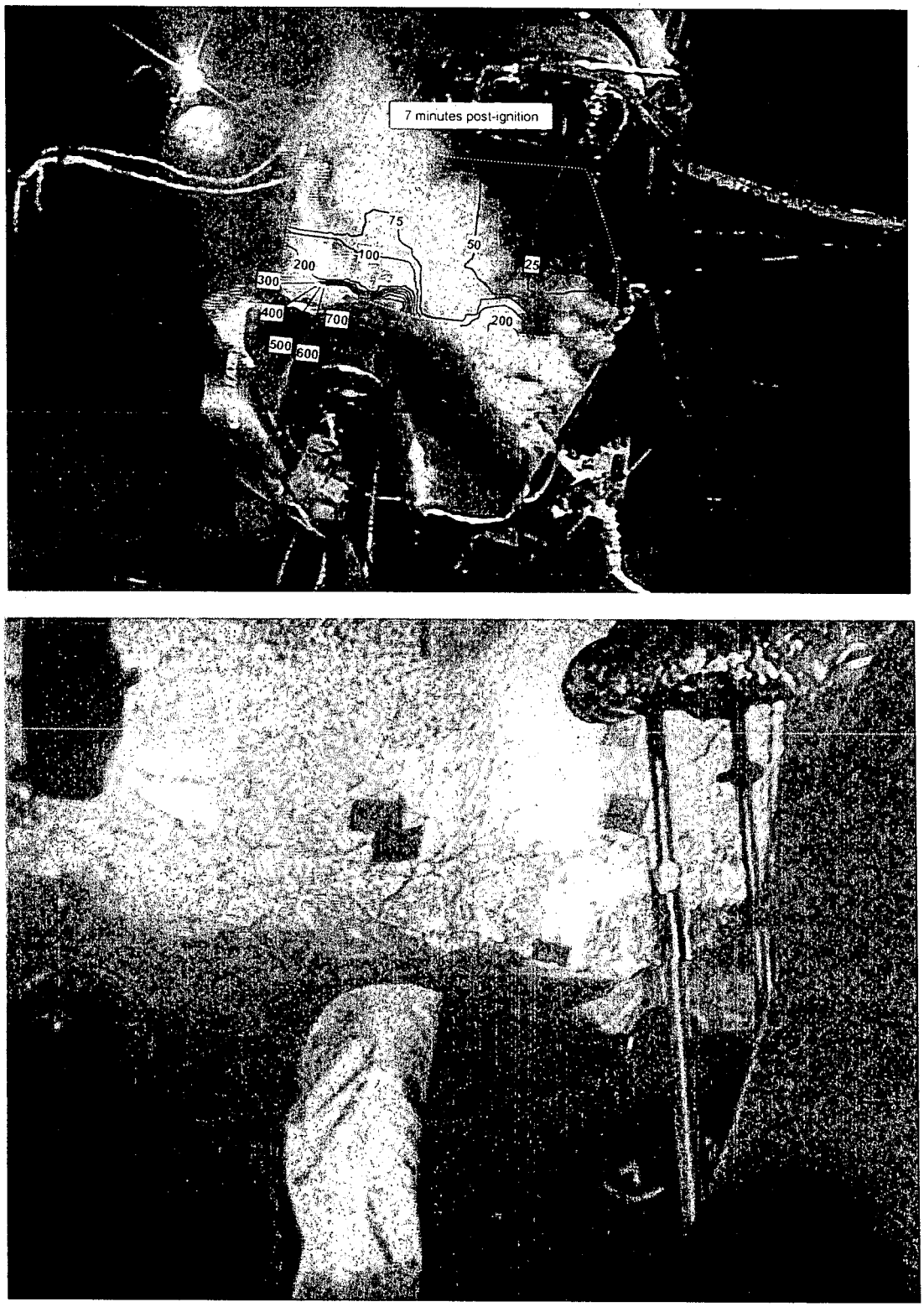

Figure 28. Fire Test F971003. Video Stills from Camera 4 with estimated isothermal contour plots of temperatures on the windshield and Camera 6 at 7 minutes post-ignition.

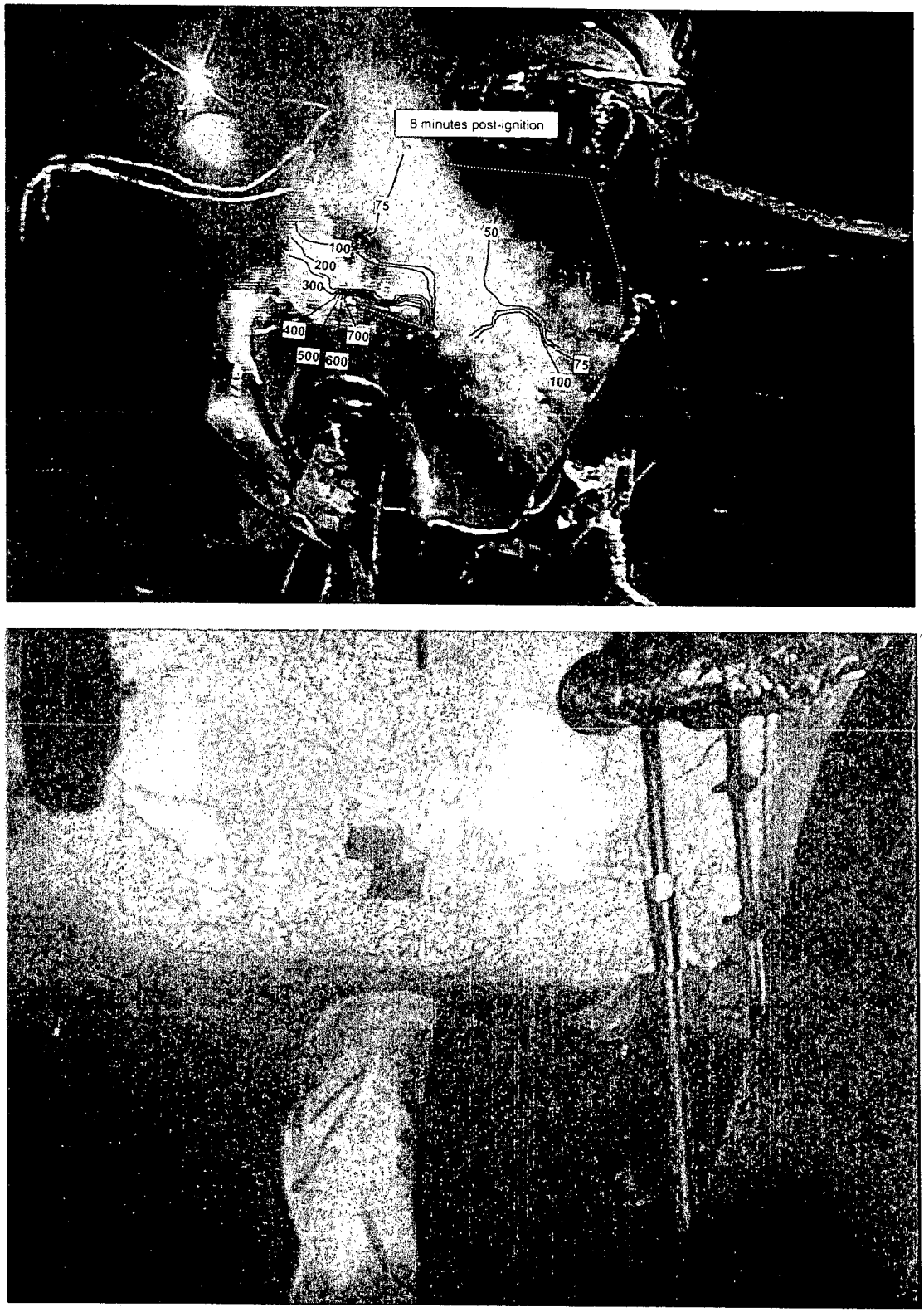

Figure 29. Fire Test F971003. Video Stills from Camera 4 with estimated isothermal contour plots of temperatures on the windshield and Camera 6 at 8 minutes post-ignition.

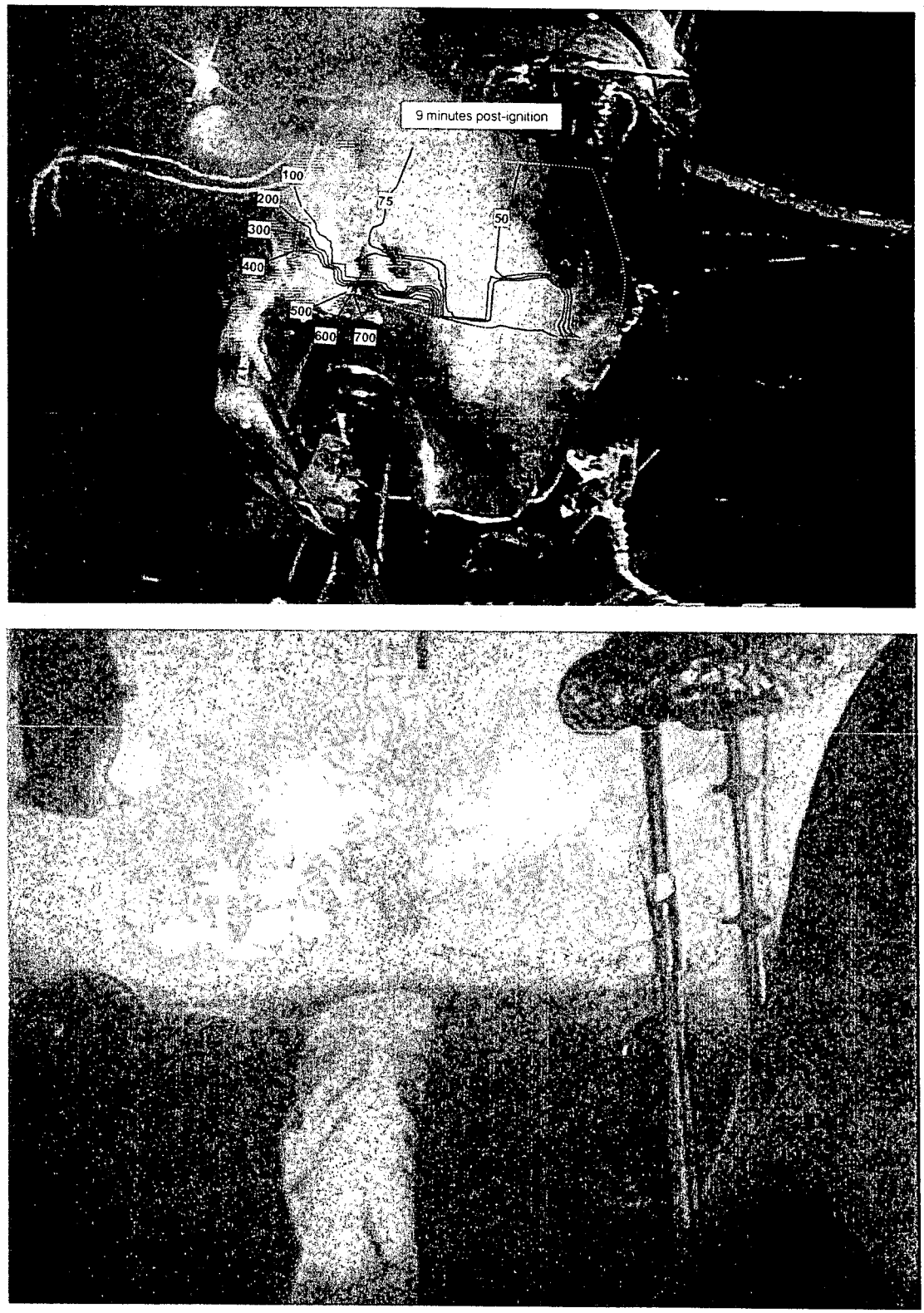

Figure 30. Fire Test F971003. Video Stills from Camera 4 with estimated isothermal contour plots of temperatures on the windshield and Camera 6 at 9 minutes post-ignition.

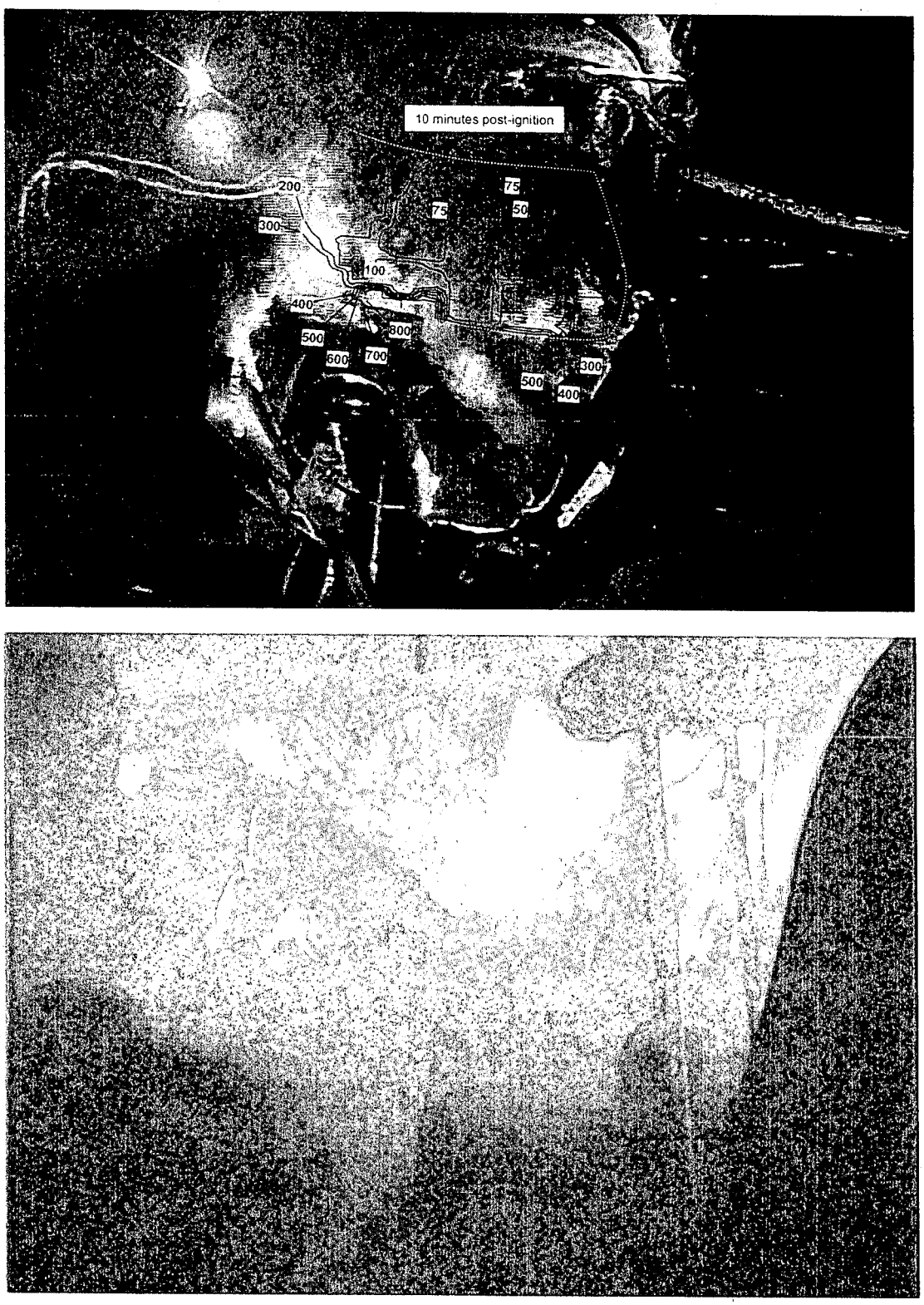

Figure 31. Fire Test F971003. Video Stills from Camera 4 with estimated isothermal contour plots of temperatures on the windshield and Camera 6 at 10 minutes post-ignition.

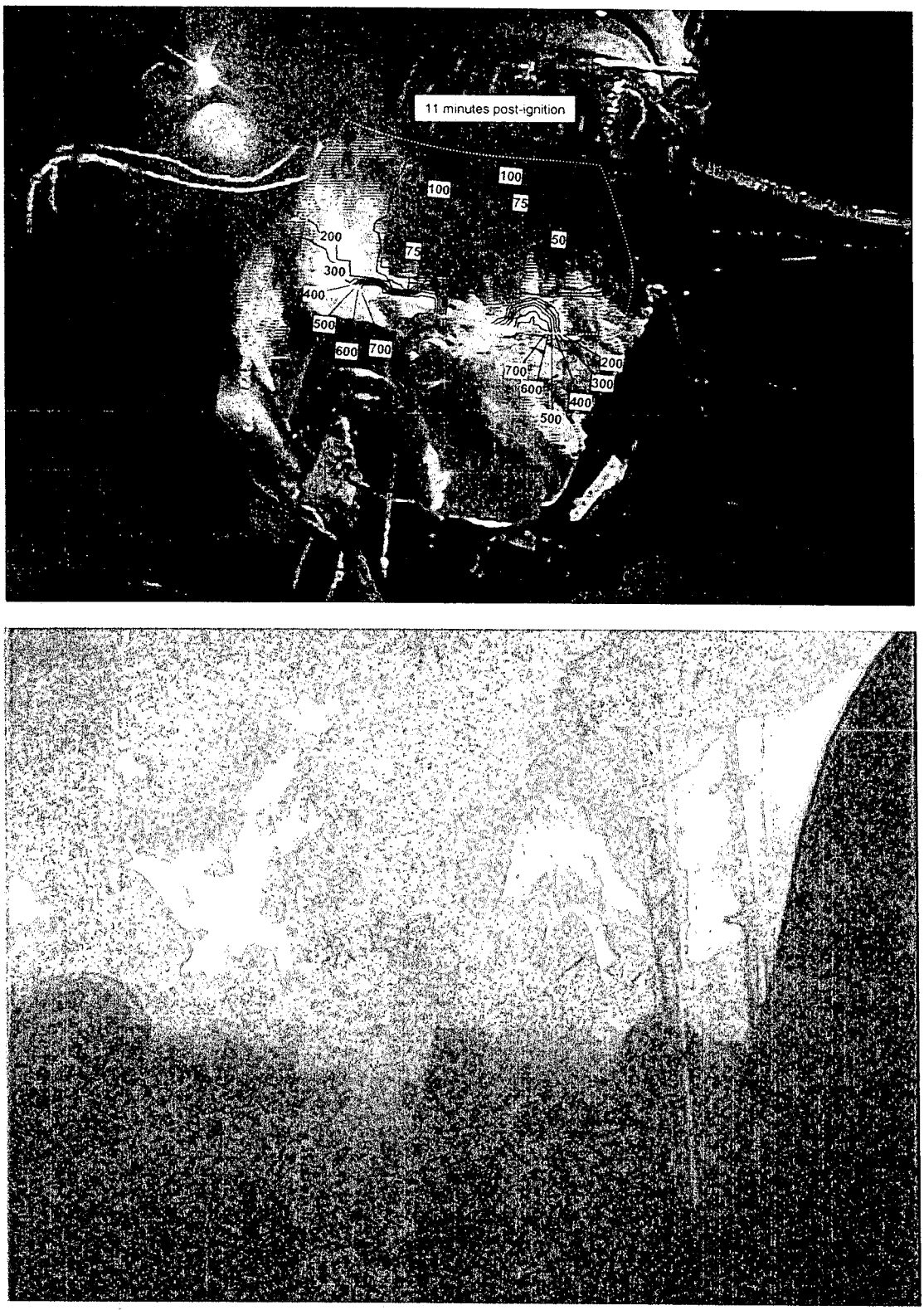

Figure 32. Fire Test F971003. Video Stills from Camera 4 with estimated isothermal contour plots of temperatures on the windshield and Camera 6 at 11 minutes post-ignition.

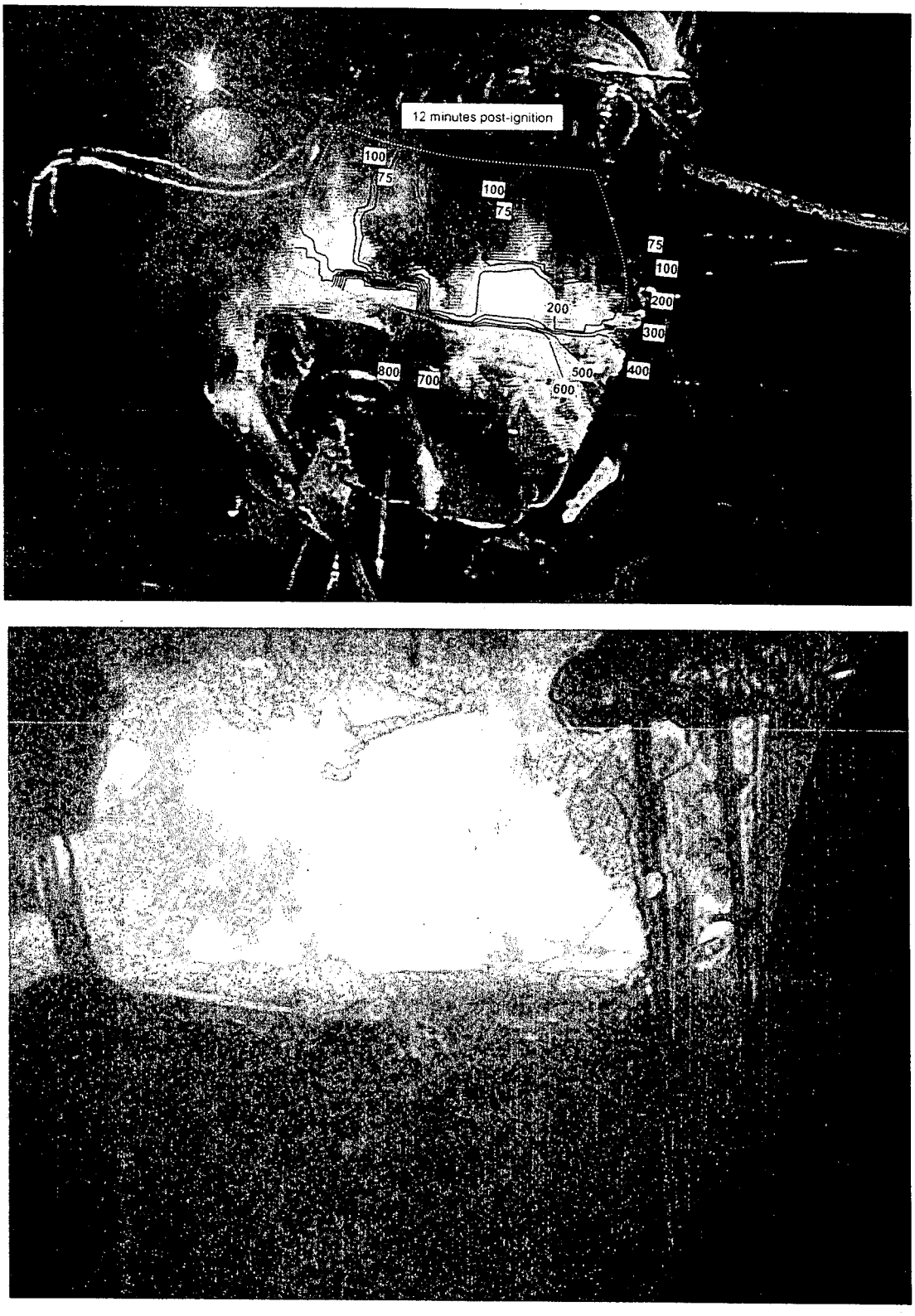

Figure 33. Fire Test F971003. Video Stills from Camera 4 with estimated isothermal contour plots of temperatures on the windshield and Camera 6 at 12 minutes post-ignition.

Temperatures at the exterior surface of the windshield increased during this time, causing the windshield inner layer to soften and stretch. The lower portion of the windshield sagged onto the instrument panel top cover.

The heat release-rate of the fire was approximately 240 kW at 10 minutes post-ignition (plot H1, **APPENDIX H**). The velocity of the vent flow along the rear of the engine compartment was insufficient to force the flames against the sagged windshield (Fig. 34). The natural buoyancy of the flames predominated, causing the fire plumes to rise almost straight up from the rear edge of the hood. Although these fire plumes did not contact the windshield, convection and radiation from flames along the rear edge of the hood heated the exterior glass outer layer causing the inner layer to soften and stretch (Fig.'s 24 through 32). The video stills from Camera 6 show that the windshield inner layer started to soften and stretch along the cracks in the glass outer layers of the attached glass between 8 and 9 minutes post-ignition (Fig.'s 29 and 30). A section of the windshield fell on top of the instrument panel between 11:05 and 11:10 minutes:seconds post-ignition (Fig. 35).

Figure 34. Fire Test F971003. Video still from Cameras 2 at 10 minutes post-ignition.

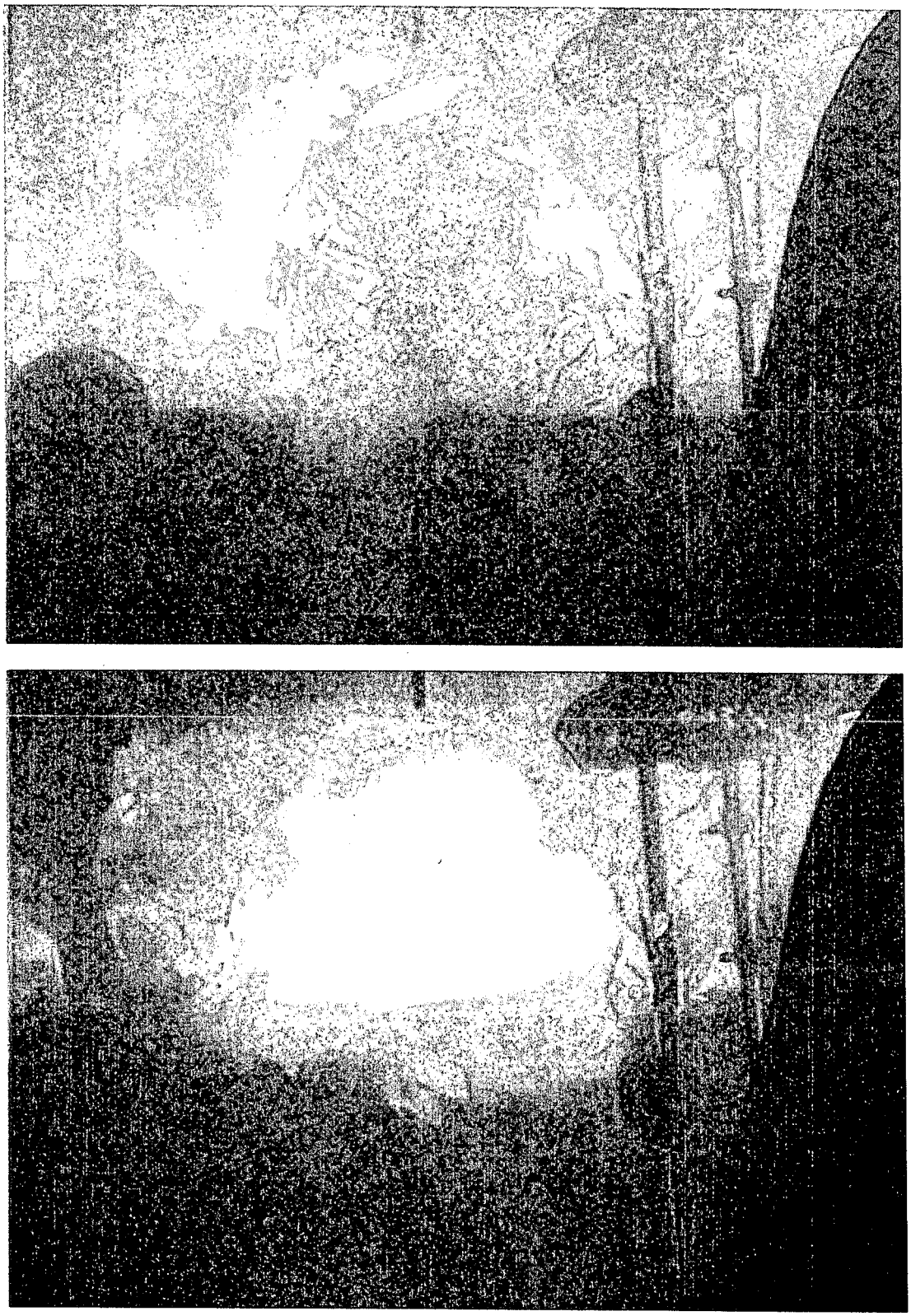

Figure 35. Fire Test F971003. Video Stills from Camera 6 at 665 and 670 seconds post-ignition.

The inner layer in the section of windshield that fell onto the instrument panel was not burning. An infrared thermogram from IR Camera 6 indicates that the temperature of the exposed inner layer was approximately 275°C at 11 minutes post-ignition (Fig. 36). The surface temperature of the interior glass outer layer of the windshield was between 100 and 140°C (Fig. 37).

Figure 36. Fire Test F971003. Infrared thermogram from IR06 at 11:00 minutes:seconds post-ignition.

The estimated temperature profiles in Figures 32 and 33 indicate that this section of the windshield was not exposed to flame when it fell inward. The video record shows that flames were not attached to the exposed inner layer around the hole in the center of the windshield or on the section of the windshield that fell on top of the instrument panel at this time (lower photograph, Fig. 35).

Pieces of the broken windshield continued to fall into the passenger compartment until the test was ended at about 16 minutes post-ignition. The instrument panel, the deployed passenger's airbag, and the front passenger's seat cushion were charred where pieces of the windshield fell onto these objects (Fig. 38). Fragments of the windshield were embedded in the residue from the

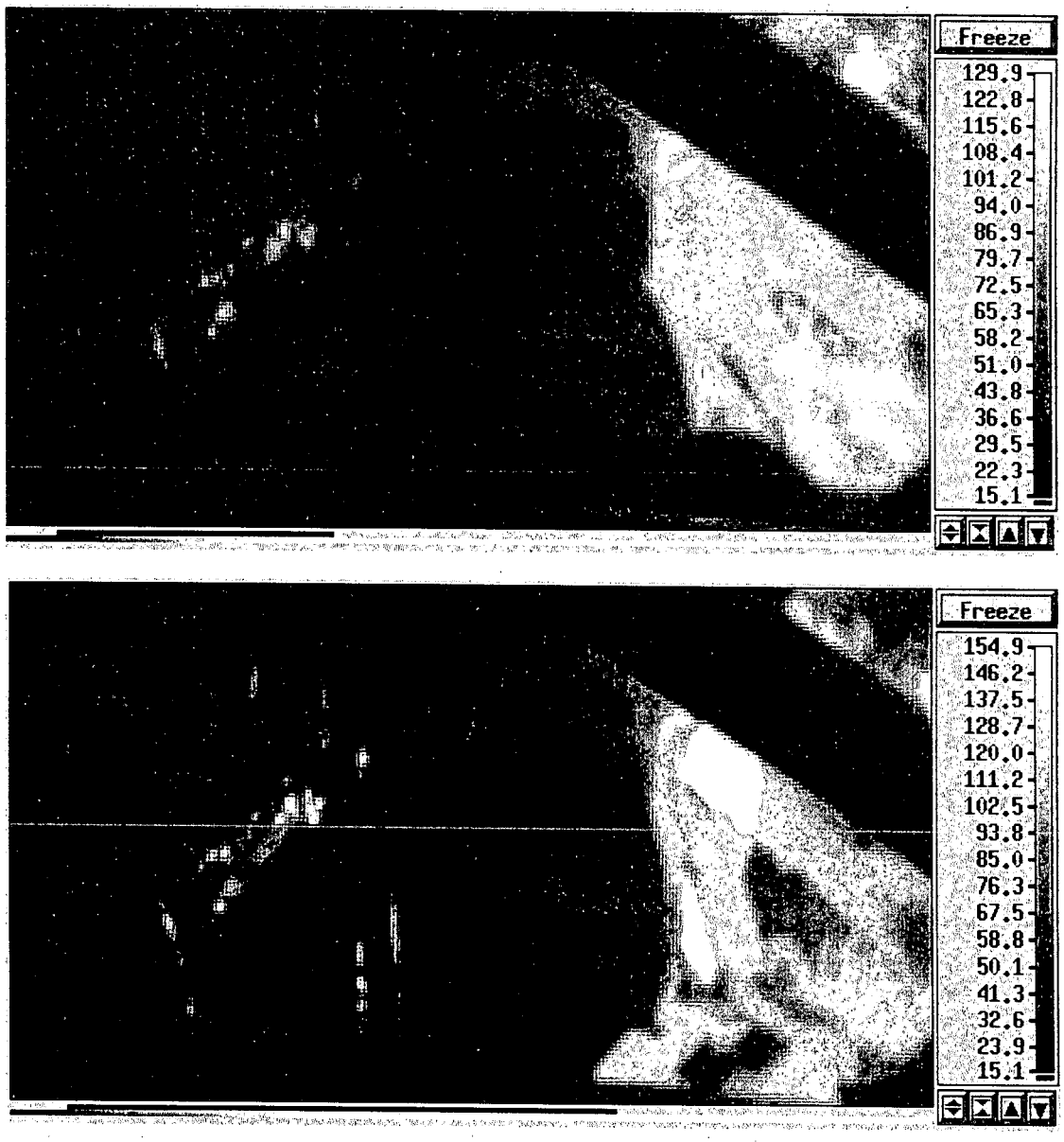

Figure 37. Fire Test F971003. Infrared thermograms from IR04 at 11:00 minutes:seconds post-ignition (upper thermogram) and 11:05 minutes:seconds post-ignition (lower thermogram).

dash sound barrier and instrument panel upper trim panel on the right side of the windshield support panel. The inner layer in these windshield fragments appeared to have liquefied and flowed out around the perimeter of the broken glass, where it ignited and burned (Fig. 39). It was not possible to determine the times of ignition of the instrument panel upper trim panel or the windshield inner layer in the fallen pieces of windshield.

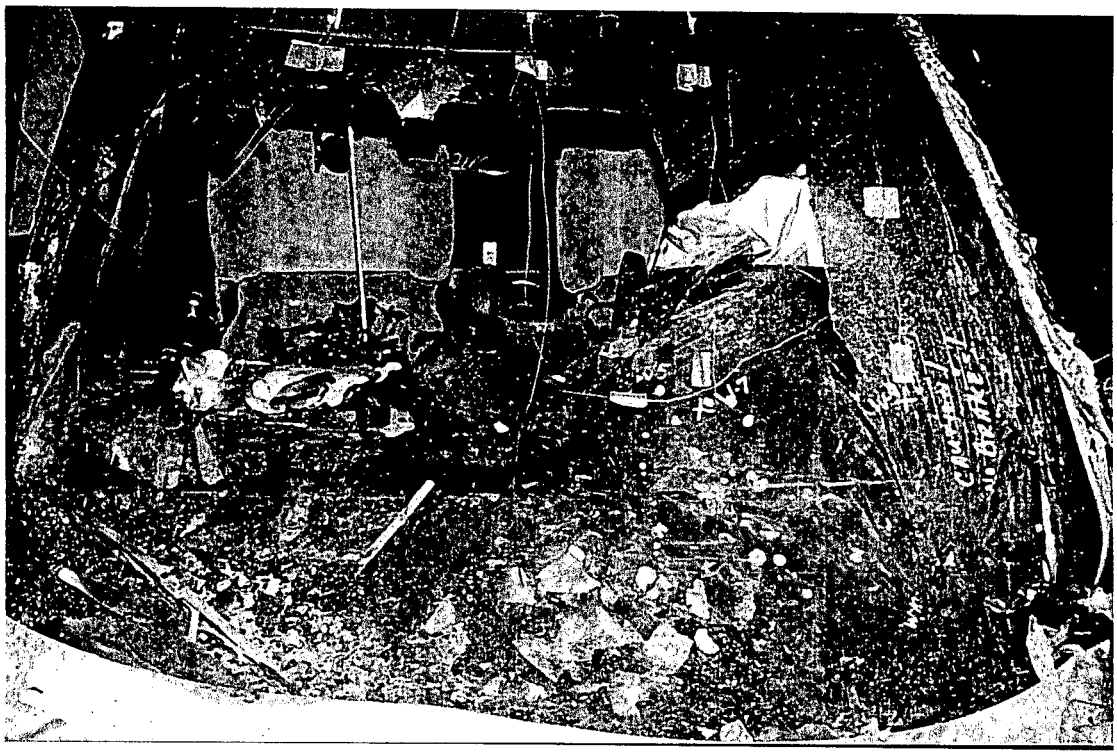

Figure 38. Fire Test F971003. Photograph of the windshield of the test vehicle after this test.

The recorded temperature data indicates that two areas at the exterior surface of the windshield were exposed to flames from 4 through 12 minutes post-ignition. These are the areas where t > 600°C in Figures 24 through 33, which were located along the lower (forward) edge of the windshield below the air inlet screen, and initially were exposed to flames venting from the engine compartment at the rear of the hood (see **SECTION 4**). Flames emerging from under the upper dash extension panel were channeled between the air inlet screen and the windshield (see Fig. 18). Flames attached to the lower surface of the air inlet screen also were channeled between the air inlet screen and the windshield, igniting the forward edge of the instrument panel upper trim panel and the inner layer where the windshield had separated from the windshield support panel. Neither the video record nor the recorded temperature give a clear indication of when the instrument panel upper trim panel and the windshield inner layer ignited in these areas.

Estimated temperature profiles on the instrument panel upper trim panel[12] indicate that flames spread rearward on the top of the right side of the instrument panel between 12 and 13 minutes

[12] The isothermal contour plots in Figures 24 through 32 were estimated from recorded temperature data using a three-dimensional interpolation algorithm available in SigmaPlot for Windows Version 4.00 [3]. This algorithm uses an inverse distance method to generated temperature values for points on a uniformly

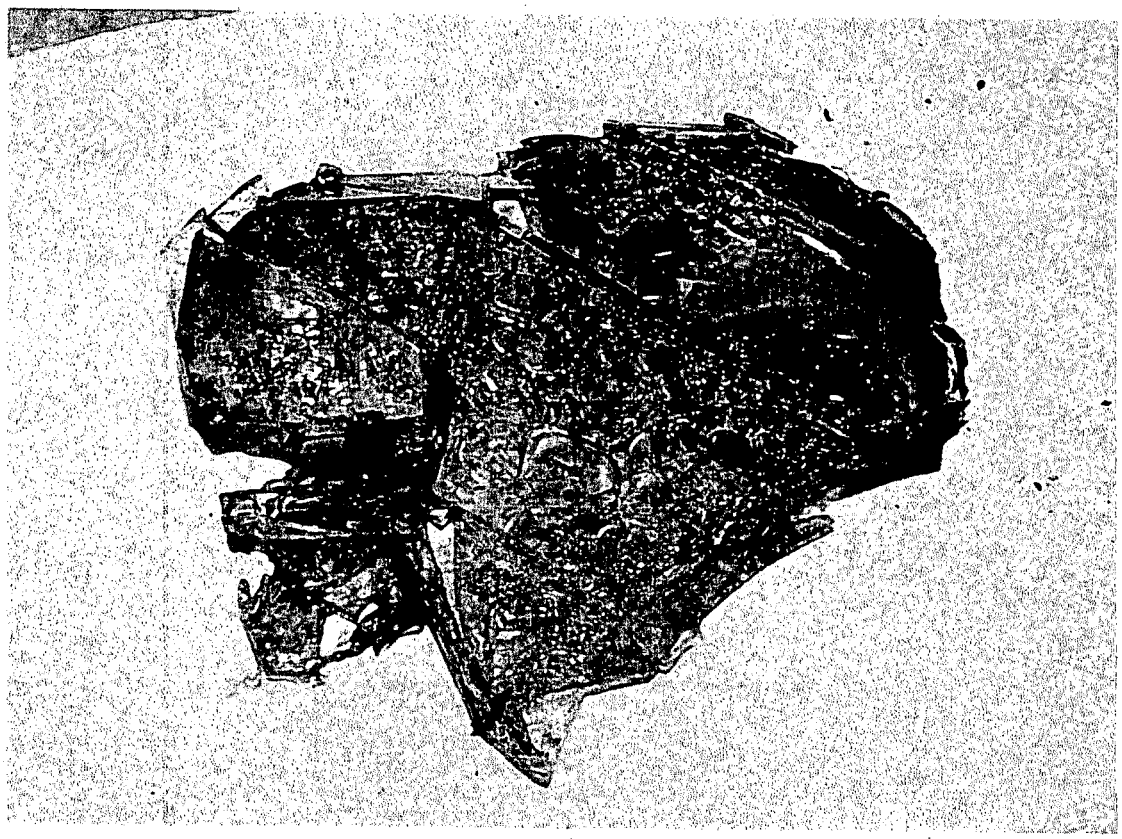

Figure 39. Fire Test F971003. Photograph of the windshield embedded in residue of the dash sound barrier and instrument panel of the test vehicle after this test.

post-ignition (Fig. 40). The isothermal contour plots in Figure 40 show estimated temperature profiles on the instrument panel upper trim panel. Fire damage to the top of the instrument panel extended from the right A-pillar to approximately the right side of the instrument cluster (Fig. 38), suggesting that this area was burning at the end of the test.

The area of the instrument panel where estimated temperatures were greater that 600°C (Fig. 41) was smaller than the area where flames appeared to have been located on the instrument panel at the end of the test (Fig. 41). One possible explanation for this apparent discrepancy is that fragments of the windshield covered some of the thermocouples on the instrument panel upper trim panel. Temperature data recorded from thermocouples insulated from the flames in this manner would reflect the temperature of the materials they were in contact with, rather than flame temperature. If this is the case, then the estimated temperature profiles in Figure 40 are not an

---

spaced Cartesian grid from input [x,y,t] triple data. Data recorded from thermocouples located in front of the upper surface of the instrument panel upper trim panel (Thermocouples I11 through I20).

accurate representation of the distribution of flames on top of the instrument panel. Another possible explanation for this apparent discrepancy is that the distribution of flames on the instrument panel is not clearly discernable in the video from Camera 6. The angle of the instrument panel relative to the camera and the lack of a reference to determine depth in this view make it difficult to distinguish flames above the engine compartment from flames on the instrument panel.

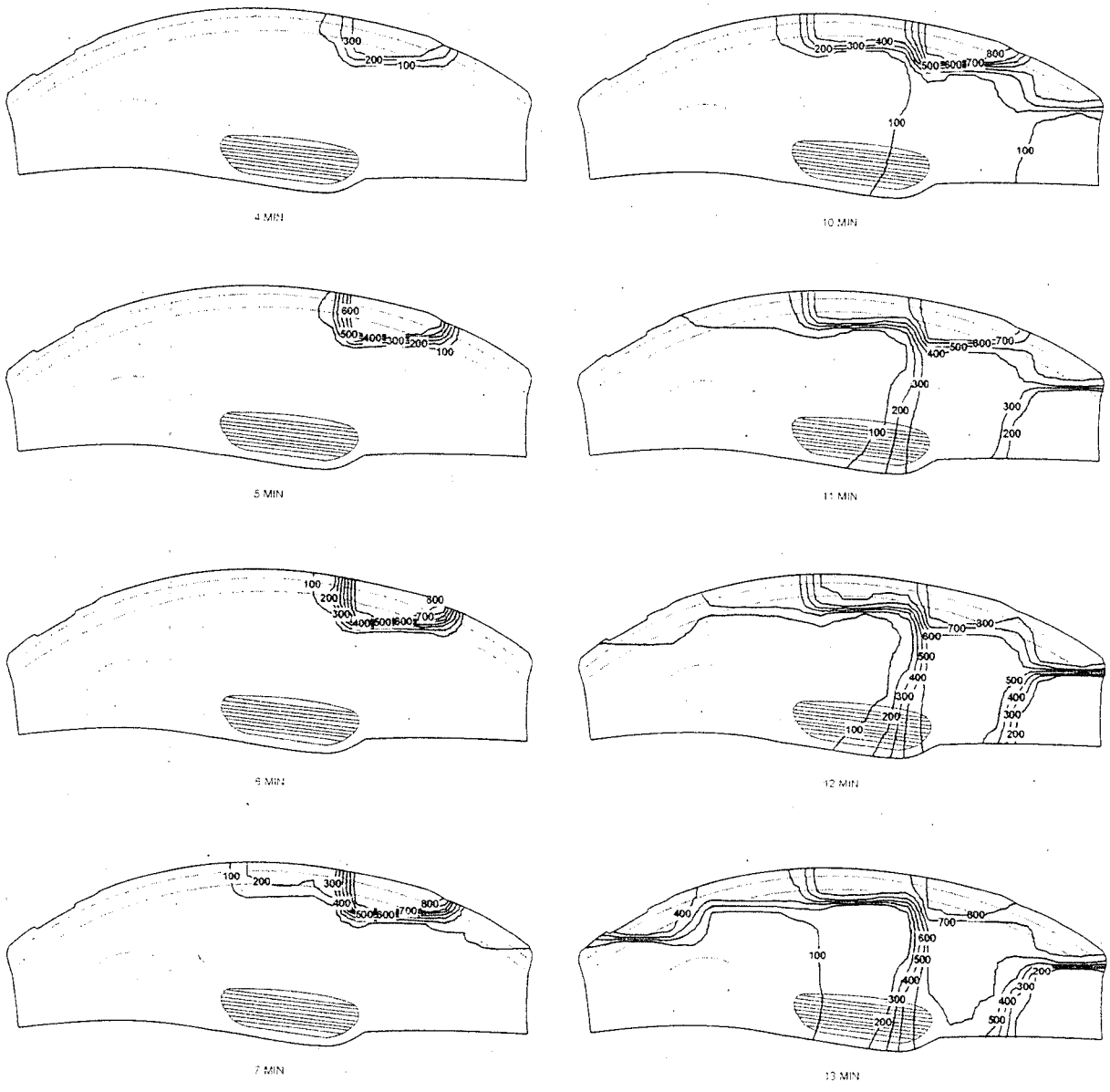

Figure 40. Fire Test F971003. Estimated isothermal contour plots of temperatures on the instrument panel upper trim panel at 4, 5, 6, 7, 8, 9, 10, 11, 12, 13, 14, and 15 minutes post-ignition.

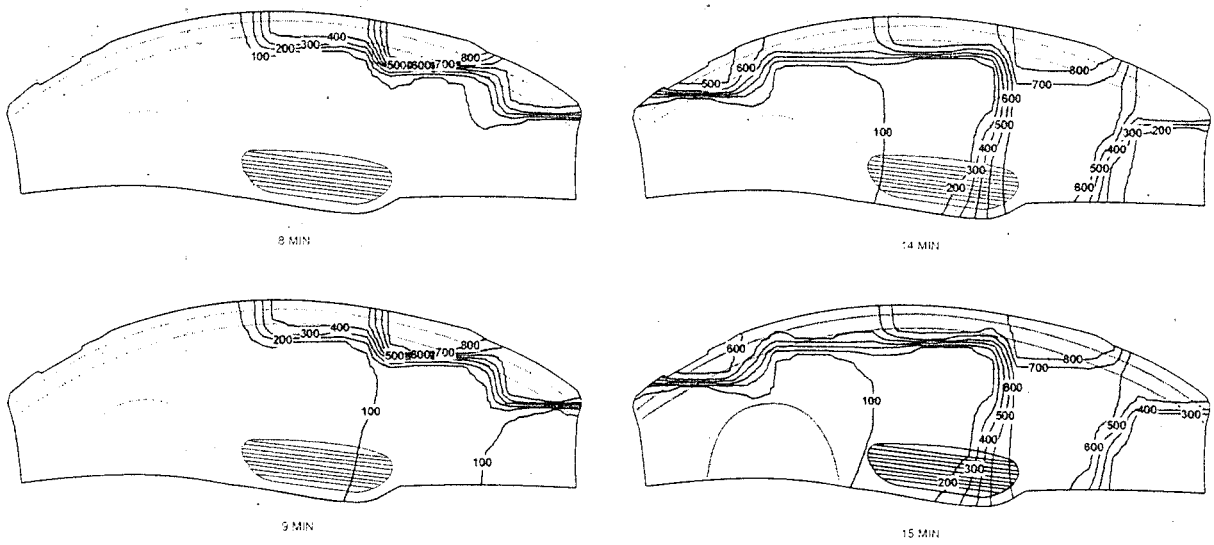

Figure 40, continued. Fire Test F971003. Estimated isothermal contour plots of temperatures on the instrument panel upper trim panel at 4, 5, 6, 7, 8, 9, 10, 11, 12, 13, 14, and 15 minutes post-ignition.

Figure 41. Fire Test F971003. Video still from Camera 6 at 15 minutes post-ignition.

5.2 Flame-Spread through the Dash Panel

One source of evidence of flame spread in the test vehicle was the pattern of fire damage in the instrument panel. This evidence included deposits of soot and tar, melted and charred plastic, and paint discoloration on the dash panel, and was obtained when the vehicle was systematically disassembled after the fire test. This type of evidence was preserved in this test because the fire was extinguished before combustible material in the instrument panel was consumed completely by fire. The water mist used to extinguish the fire cooled the molten plastic rapidly, preserving the geometric shape of the plastic at that instant while avoiding the damage that can be caused by a high-pressure water stream.

The instrument panel top cover was melted and charred, with pieces of the windshield embedded in the residue on top of the windshield support panel (Fig. 42). Flames appeared to have burned-through the right side of the instrument panel where it attached to the dash panel (Fig. 42). The instrument panel compartment door and right side instrument panel compartment insulator were burned and charred, and had fallen onto the carpet under the right side of the instrument panel (Fig. 43). The instrument panel was burned around the instrument panel compartment opening (Fig. 43). The A-pillar trim finishing panel had melted and dripped onto the right side of the instrument panel above the right air outlet (Fig. 43).

Figure 42. Fire Test F971003. Photograph of the right side of the top of the instrument panel in the test vehicle after this test.

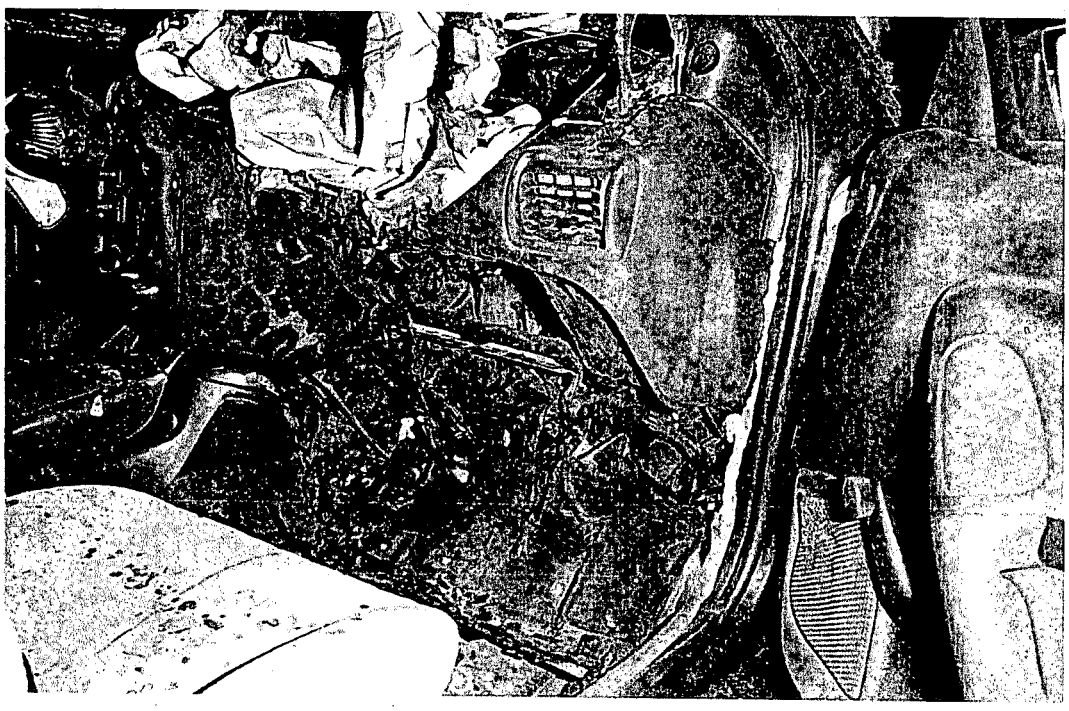

Figure 43. Fire Test F971003. Photograph of the right side of the instrument panel in the test vehicle after this test.

The defroster nozzle, the right side of the air distributor, and the instrument panel compartment box were missing, (Fig. 44). The left side of the air distributor remained mounted in the instrument panel (Fig. 44). The passenger's air bag module and interior of the right side of the instrument panel contained soot deposits (Fig. 44). The residue from the defroster nozzle in the center of the instrument panel was melted and charred (Fig 44).

The auxiliary A/C evaporator and blower upper case, air inlet housing, heater front case, and heater rear case were missing (Fig. 45). The right side of the air distributor case, which contained the model valve doors, was missing (Fig. 45). The left side of the air distributor case was not melted or charred (Fig. 45). The auxiliary A/C evaporator and blower lower case was not melted or charred (Fig. 45). Material from the auxiliary A/C evaporator and blower upper case and air inlet housing softened and flowed downward onto the HVAC blower. Material from the heater front case, the heater rear case, and the air distributor case softened and flowed downward onto the inside of the instrument panel and carpet below the instrument panel (Fig. 43). The residue from these components was melted and charred. The carpet on the toe pan below the HVAC module was melted and charred (Fig. 45).

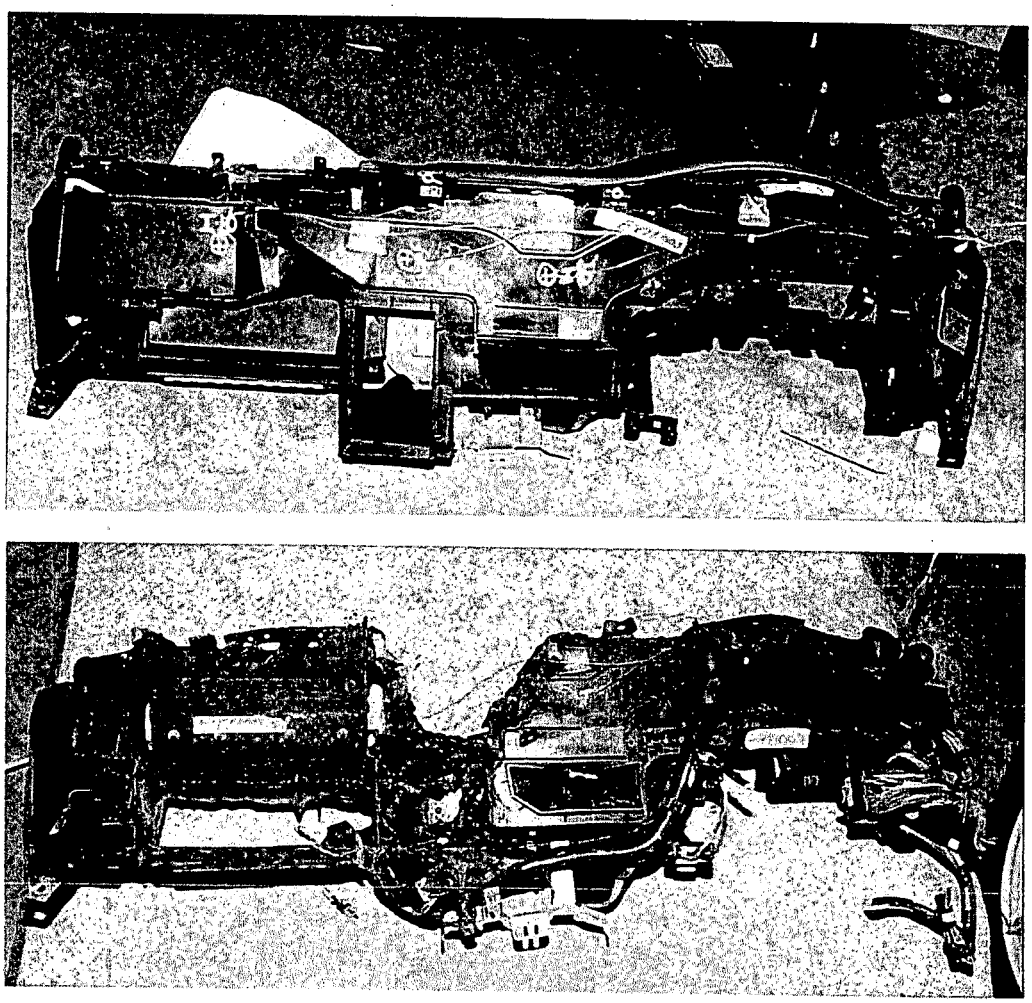

Figure 44. Fire Test F971003. Photographs of the defroster nozzle and air distributor assembly in the instrument from the test vehicle before (upper photograph) and after (lower photograph) this test.

Paint on the right side of the interior of the dash panel and upper dash extension panel was burned in a V-shaped pattern (Fig. 46). Metal was exposed on the section of the upper dash extension panel above the HVAC pass-through (Fig. 46). Melted and charred residue from the dash panel insulator was visible on the right side of the dash panel, and the center and right side of the upper dash extension panel (Fig. 46). Sections of the auxiliary A/C evaporator and blower upper case and heater front case appeared to have softened and sagged into the HVAC pass-through (Fig.'s 45 and 46). There was no evidence of heat or fire damage around the brake linkage pass-through, the steering column pass-through, the two tears in the dash panel, or the seam opening at the lower right corner of the dash panel (Fig. 46).

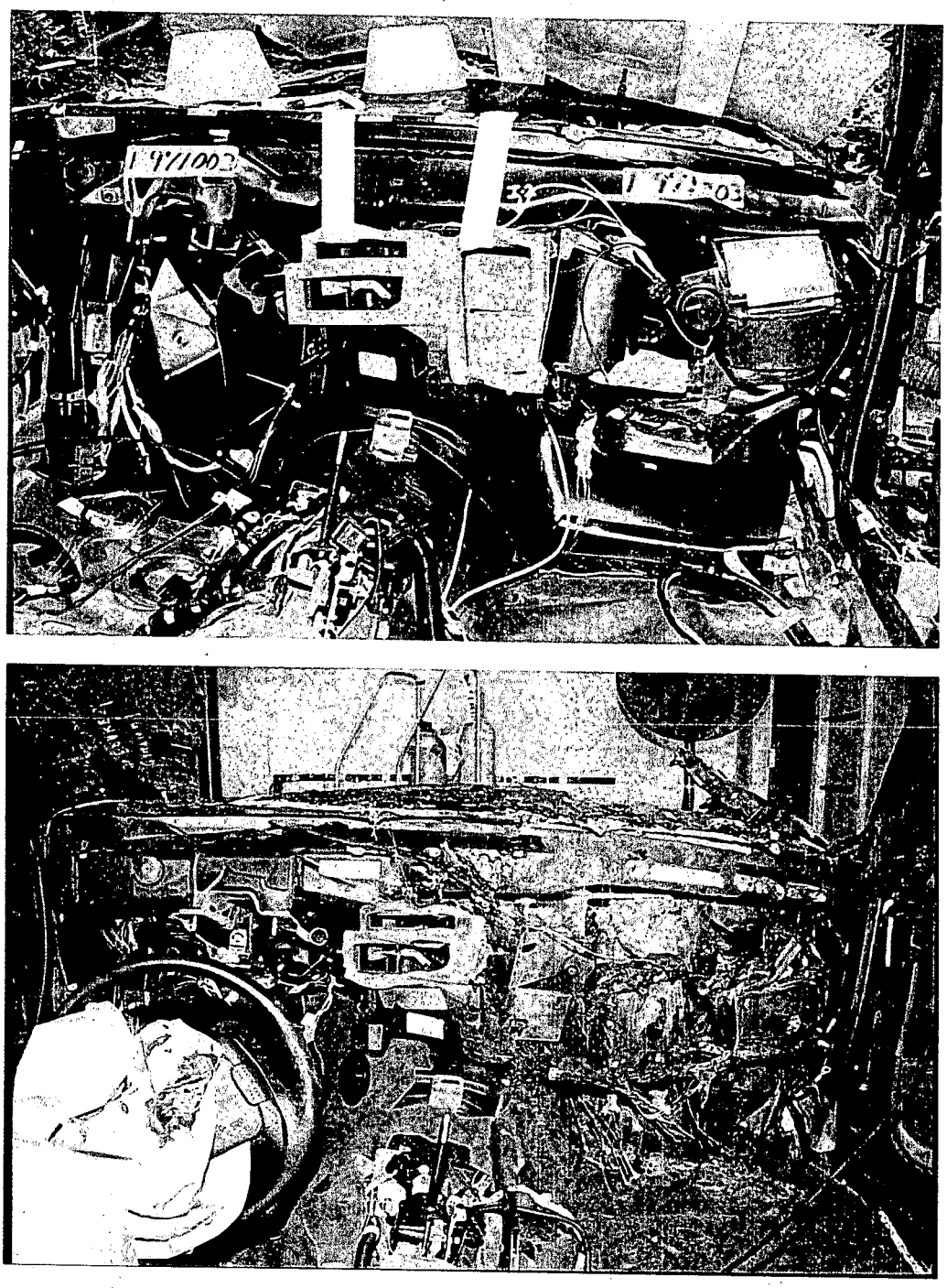

Figure 45. Fire Test F971003. Photograph of the HVAC module in the test vehicle before (upper photograph) and after (lower photograph) this test.

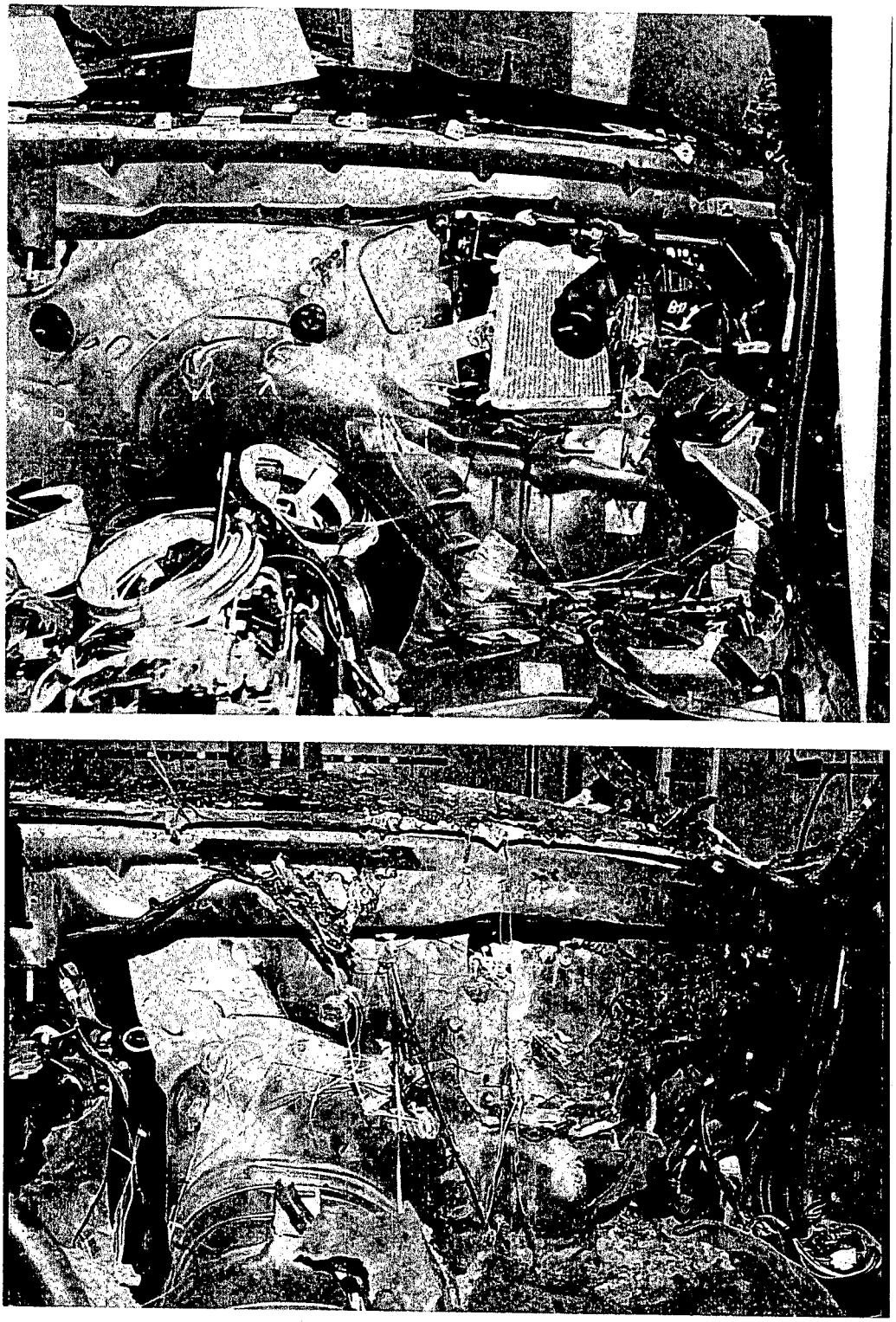

Figure 46. Fire Test F971003. Photograph of the dash panel in the test vehicle before (upper photograph) and after (lower photograph) this test.

Estimated temperature profiles in the HVAC module and the defroster nozzle and air distributor assembly indicate that flames spread rearward into the instrument panel through the HVAC module. The isothermal contour plots[13] in Figures 47 and 48 show estimated temperature profiles in the HVAC module (Fig. 47) and in the defroster and air distributor assembly (Fig. 48). These estimated temperature profiles indicate that flames spread into the auxiliary A/C evaporator and blower upper case and heater front case between 10 and 11 minutes post-ignition (Fig. 47). Flames started to spread laterally to the right into the air inlet housing between 12 and 13 minutes post-ignition and to the left into the air distributor case between 14 and 15 minutes post-ignition (Fig. 47). Flames spread rearward into the right side of the defroster nozzle and air distributor assembly case between 14 and 15 minutes post-ignition (Fig. 48).

The extent of flame-spread in the HVAC module and defroster nozzle and air distributor assembly deduced from the Figures 47 and 48 roughly matched the timing of flame-spread observed in the video record and the pattern of fire damage in the instrument panel of the test vehicle observed after this test. For example, the estimated temperature profiles indicate that flames spread laterally in the HVAC module and defroster nozzle and air distributor assembly toward the center console in the instrument panel between 14 and 15 minutes post-ignition[14] (in Fig.'s 47 and 48). The video record from Camera 6 shows flames emerging from the top of the instrument panel in this area between 14 minutes 50 seconds and 14 minutes 57 seconds post-ignition (Fig. 49). During the inspection of the test vehicle after this test, a hole was observed in the instrument panel where flames apparently burned-through from its interior (Fig. 44).

The video record from Camera 10 shows flames below the right side of the instrument panel at 13 seconds post-ignition (Fig. 50). Melted and charred plastic was observed below the right side of the instrument panel after this test (Fig. 43). The carpet in this area started to burn before the test was ended (Fig.'s 45 and 46). These observations suggests that downward flame-spread in this area involved burning material falling from the HVAC module, the defroster nozzle and air distributor assembly, and the instrument panel compartment box onto the carpet below the right side of the instrument panel.

---

[13] The isothermal contour plots in Figures 46 through 48 were estimated from recorded temperature data using a three-dimensional interpolation algorithm available in SigmaPlot for Windows Version 4.00 [3]. This algorithm uses an inverse distance method to generated temperature values for points on a uniformly spaced Cartesian grid from input [x,y,t] triple data. Data recorded from Thermocouples B1, B3, B4, B5, B6, B10, B11, B15, I2, and I3 were used to calculate the isothermal contour plots in Figure 47. Data recorded from Thermocouples I4, I5, I6, I7, I8, I9, and I10 were used to calculate the isothermal contour plots in Figure 48.

[14] Some of the thermocouples in the instrument panel were attached to components in the HVAC module and the defroster nozzle and air distributor assembly. The locations of these thermocouples changed as these components softened and sagged during the latter stages of this test. The estimated temperature profiles in Figures 47 and 48 do not account for these changes, and therefore may not reproduce the actual temperature profiles in these components during the latter stages of this test.

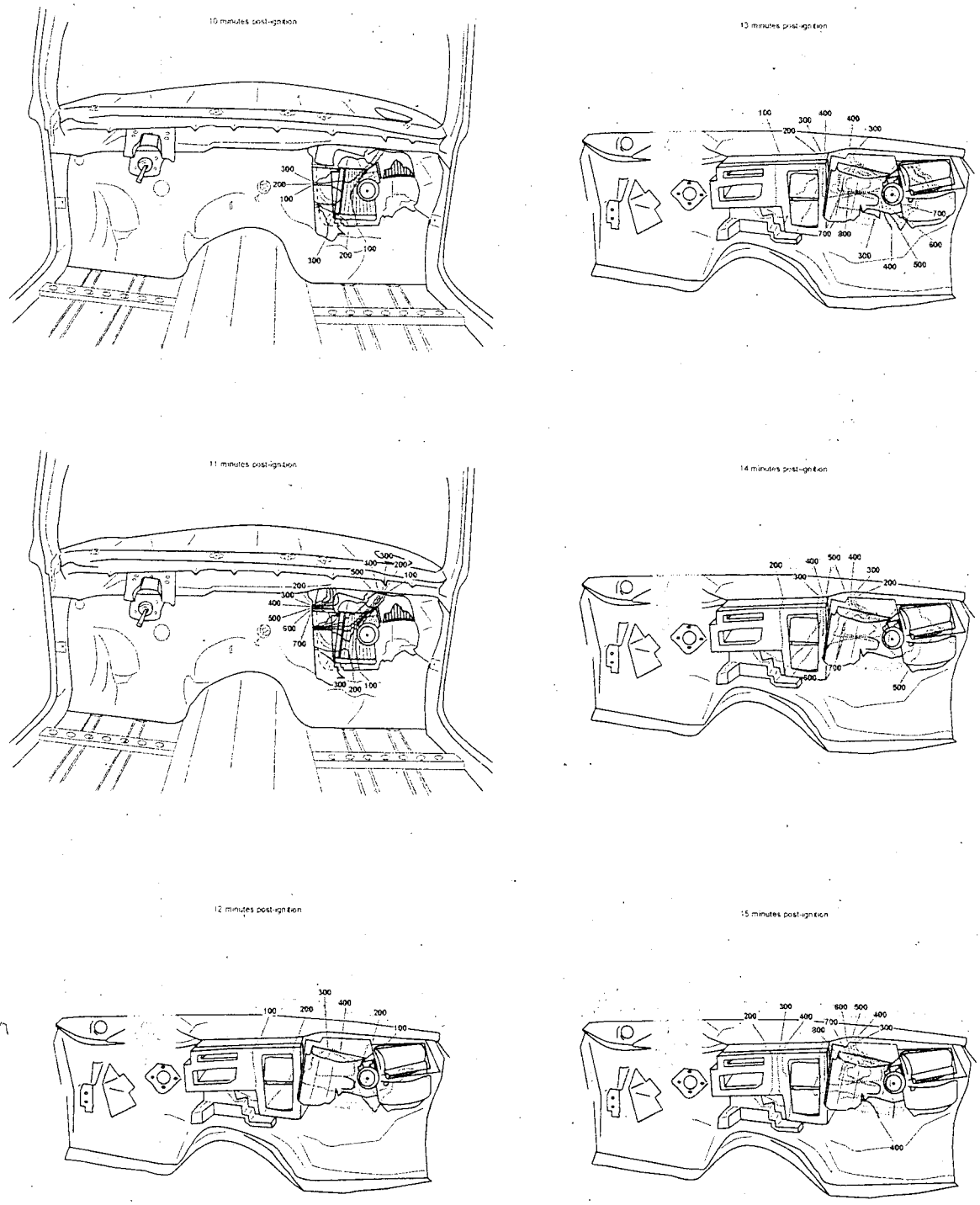

Figure 47. Fire Test 971003. Estimated isothermal contour plots of temperatures in the HVAC module at 10, 11, 12, 13, 14 and 15 minutes post-ignition. The diagrams at 10 and 11 minutes post-ignition show estimated temperature profiles at the dash panel around the HVAC pass-through. The diagrams at 12, 13, 14, and 15 minutes post-ignition show estimated temperature profiles in the HVAC module.

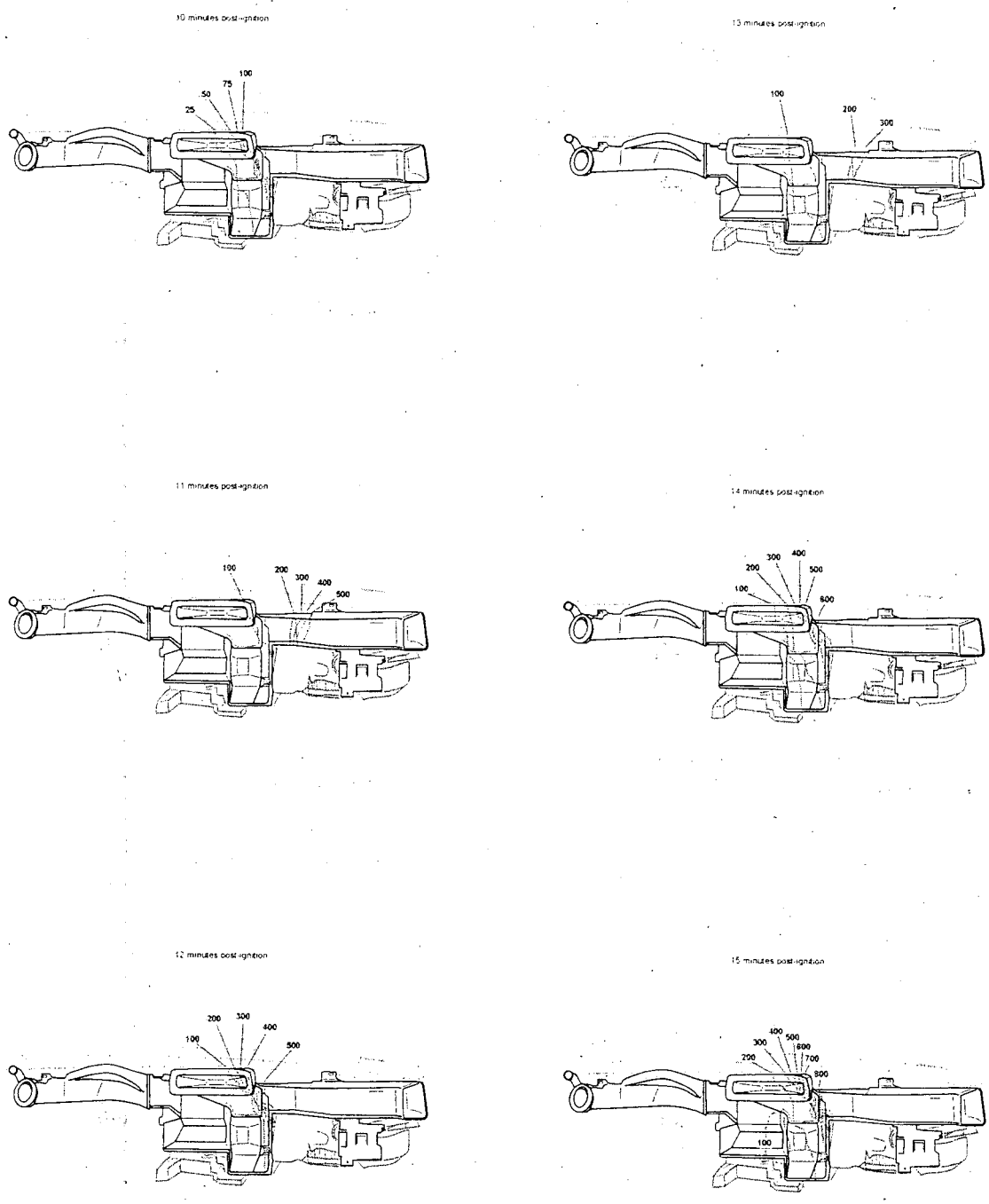

Figure 48. Fire Test 971003. Estimated isothermal contour plots of temperatures in the defroster nozzle and air distributor assembly at 10, 11, 12, 13, 14 and 15 minutes post-ignition.

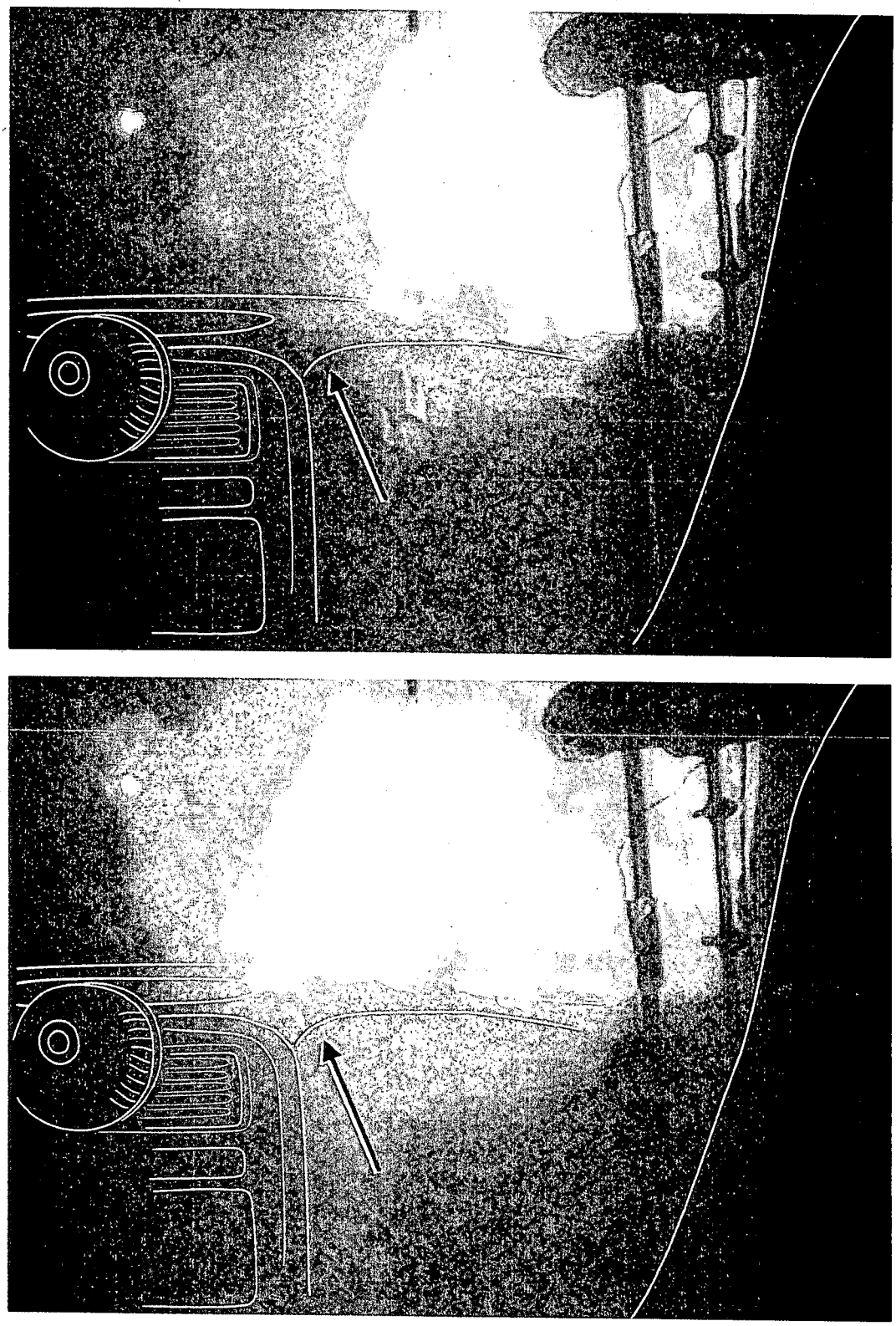

Figure 49. Fire Test F971003. Video stills from Camera 6 at 14 minutes 50 seconds (upper video still) and at 14 minutes 57 seconds (lower video still) post-ignition.

Figure 50. Fire Test F971003. Video still from Camera 10 at 13 minutes post-ignition.

Development of a pressure gradient across the dash panel does not appear to have played a role in flame-spread from the engine compartment into the passenger compartment. Data recorded from pressure taps in the test vehicle indicate that the pressure on both sides of the dash panel started to decrease relative to atmospheric pressure between 8 and 9 minutes post-ignition (Fig. 51). The measured pressures at the exterior and interior surfaces of the dash panel were approximately equal until about 11½ minutes post-ignition, so that there was no net recorded pressure difference between the two surfaces of the dash panel before this time. The estimated temperature profiles in the HVAC module indicate that flames spread into the instrument panel between 10 and 11 minutes post-ignition (Fig. 47). The recorded pressure at the interior surface of the dash panel was greater that the recorded pressure at the exterior surface of the dash panel between about 11½ and 12½ minutes post-ignition (Fig. 51). The net recorded pressure difference across the dash panel was between -0.25 and -0.50 Pascals during this time (Fig. 51), which would have resulted in a net airflow from the passenger compartment into the engine compartment through the HVAC pass-through.

The pressure recorded at the interior surface of the dash panel started to decrease sharply relative to atmospheric pressure at about 13 minutes post-ignition, causing the net recorded

pressure difference across the dash panel to become positive at about 13½ minutes post-ignition (Fig. 51).

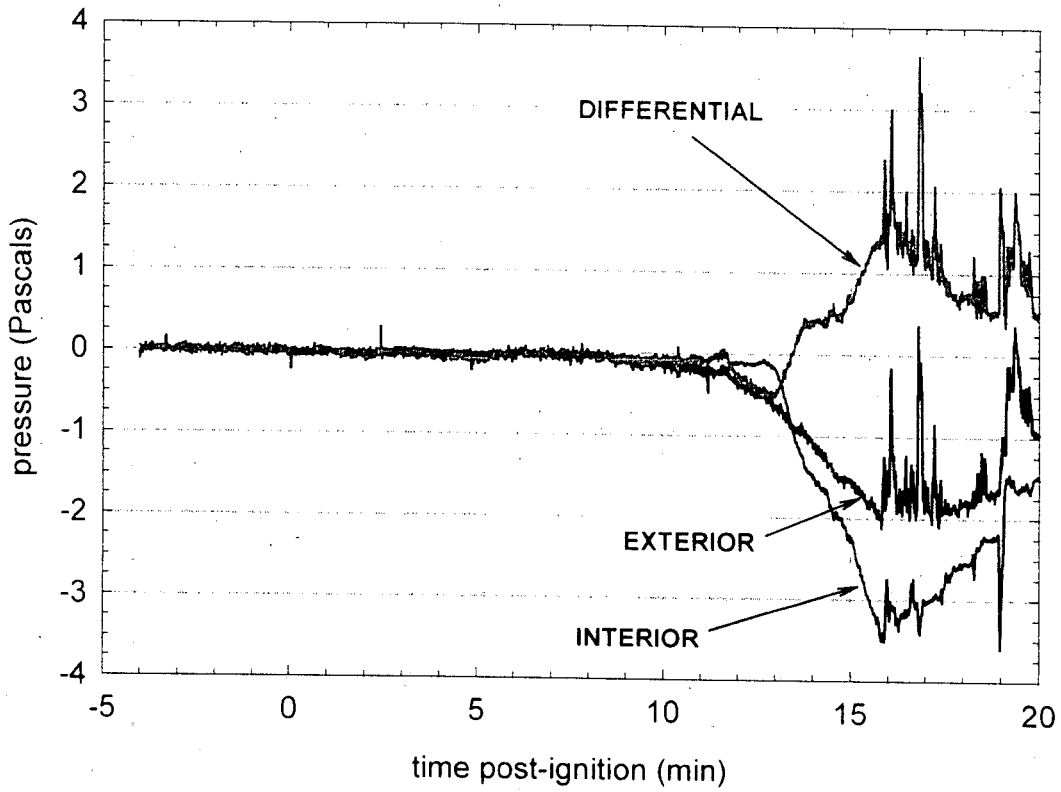

Figure 51. Fire Test F971003. Plots of pressure pressures measured at the exterior surface of the dash panel relative to atmospheric pressure, the interior surface of the dash panel relative to atmospheric pressure, and the differential pressure across the dash panel in the test vehicle. A positive value of pressure indicates that the pressure was greater at the exterior surface of the dash panel.

Pressure data recorded from pressure taps at the dash panel may have been affected by the presence of flames inside the instrument panel. The pressure taps at the dash panel are visible in the lower photograph of Figure 46. Vertical sections of both probes were routed inside the instrument panel and show evidence of being exposed to heat and flames, which can result in a buoyancy-driven upward airflow in the pressure tap and an erroneous low pressure reading. Consequently, it is difficult to determine if the pressure readings plotted in Figure 51 were valid throughout the entire test, or if they were affected by exposure of the pressure tap to heat and flames after flames spread into the instrument panel.

5.3 Heat and Fire Damage to the Headlining Panel and Front Seats

The pattern of heat and fire damage to the headlining panel, estimated temperature profiles along the lower surface of the headlining panel, and data recorded from the aspirated thermocouples located below the headlining panel and extending downward toward the front seat cushions indicated that a burning upper layer did not develop in the passenger compartment during this test. The fabric covers on the sun visors and on the forward part of the headlining panel were exposed to heat and flames during this test (Fig. 52). Estimated temperature profiles along the lower surface of the headlining panel[15] indicate that exposure to heat and flames occurred between 15 and 16 minutes post-ignition (Fig. 53). Temperatures along the headlining panel were less than about 50°C until the first section of windshield fell inward between 10 and 11 minutes post-ignition (Fig. 53).

Figure 52. Fire Test F971003. Photograph of the forward section of the headlining panel in the test vehicle after this test.

[15] The isothermal contour plots in Figure 52 were estimated from recorded temperature data using a three-dimensional interpolation algorithm available in SigmaPlot for Windows Version 4.00 [3]. This algorithm uses an inverse distance method to generated temperature values for points on a uniformly spaced Cartesian grid from input [x,y,t] triple data. Data recorded from Thermocouples R1 through R15 were used to calculate the isothermal contour plots in Figure 53.

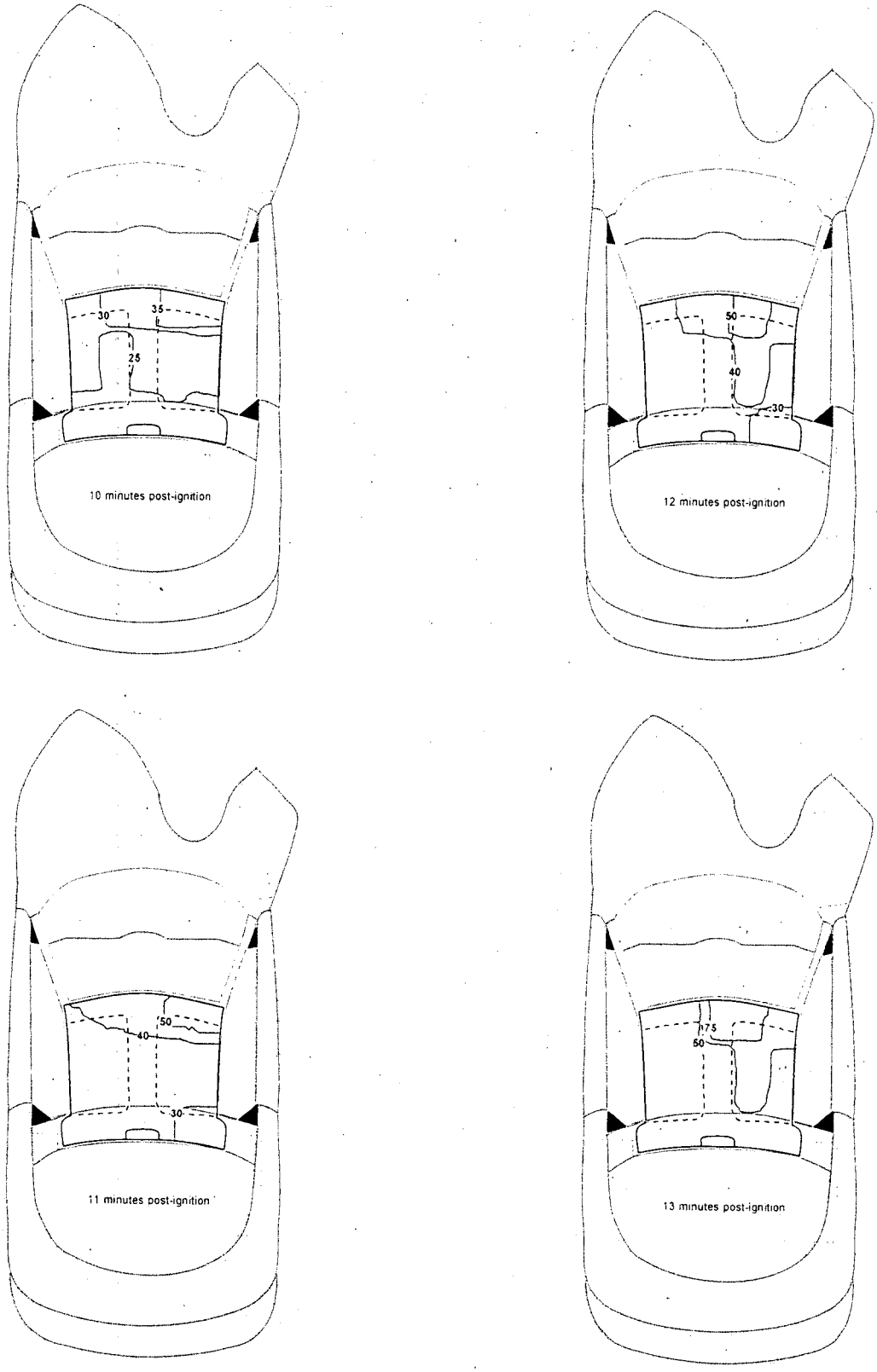

Figure 53. Fire Test 971003. Estimated temperature profiles along the lower surface of the headlining panel in the test vehicle 10, 11, 12, 13, 14, and 15 minutes post-ignition and 15 minutes 50 seconds post-ignition.

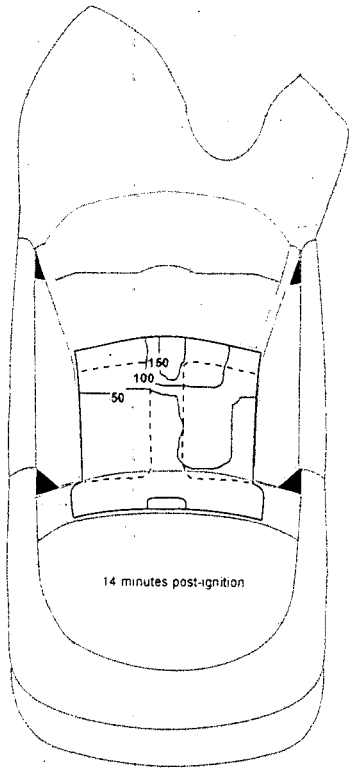

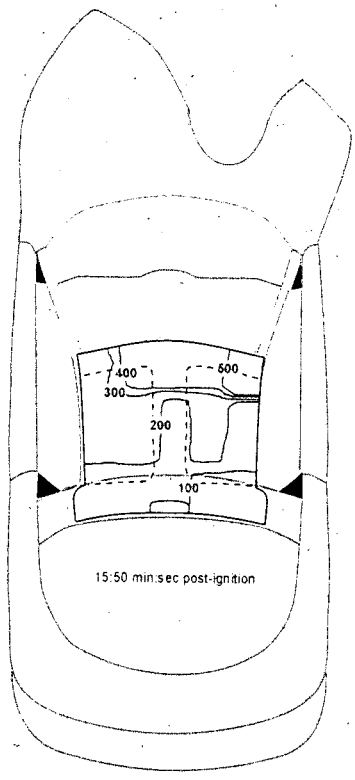

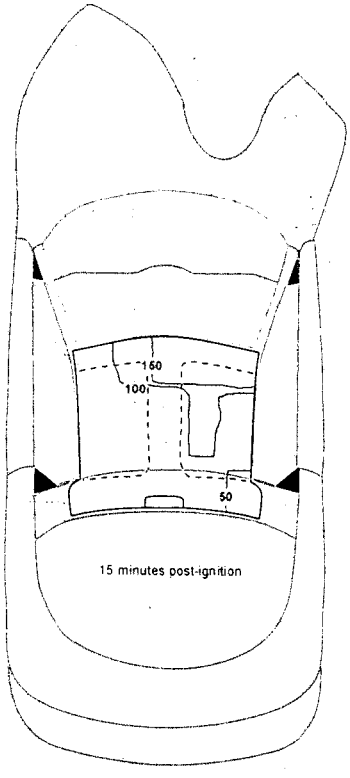

Figure 53, continued. Fire Test 971003. Estimated temperature profiles along the lower surface of the headlining panel in the test vehicle 10, 11, 12, 13, 14, and 15 minutes post-ignition and 15 minutes 50 seconds post-ignition.

The horizontal surface at the top of the dash panel formed by the upper dash extension panel and windshield support panel was forward of the roofline. As flames spread rearward on the right side of the top of the instrument panel, the fire plume from the top of the instrument panel rose upward through the opening in the windshield (Fig. 54). Temperatures along the forward edge of the headlining panel increased to between 150 and 200°C by 15 minutes post-ignition. Development of higher temperatures along the headlining panel between 15 and 16 minutes post-ignition (Fig. 53) correlated with the timing of flame-spread through the top of the instrument panel above the center console. The area where the fabric covering on the headlining panel was charred corresponded roughly to the area where the estimated temperatures were greater than 300°C at 15 minutes 50 seconds post-ignition (Fig. 53).

Temperatures recorded from aspirated thermocouples located just below the headlining panel (Fig.'s 55 and 56) were consistent with the estimated temperature profiles along the headlining above the front seats (Fig. 53). For example, the temperatures recorded from aspirated

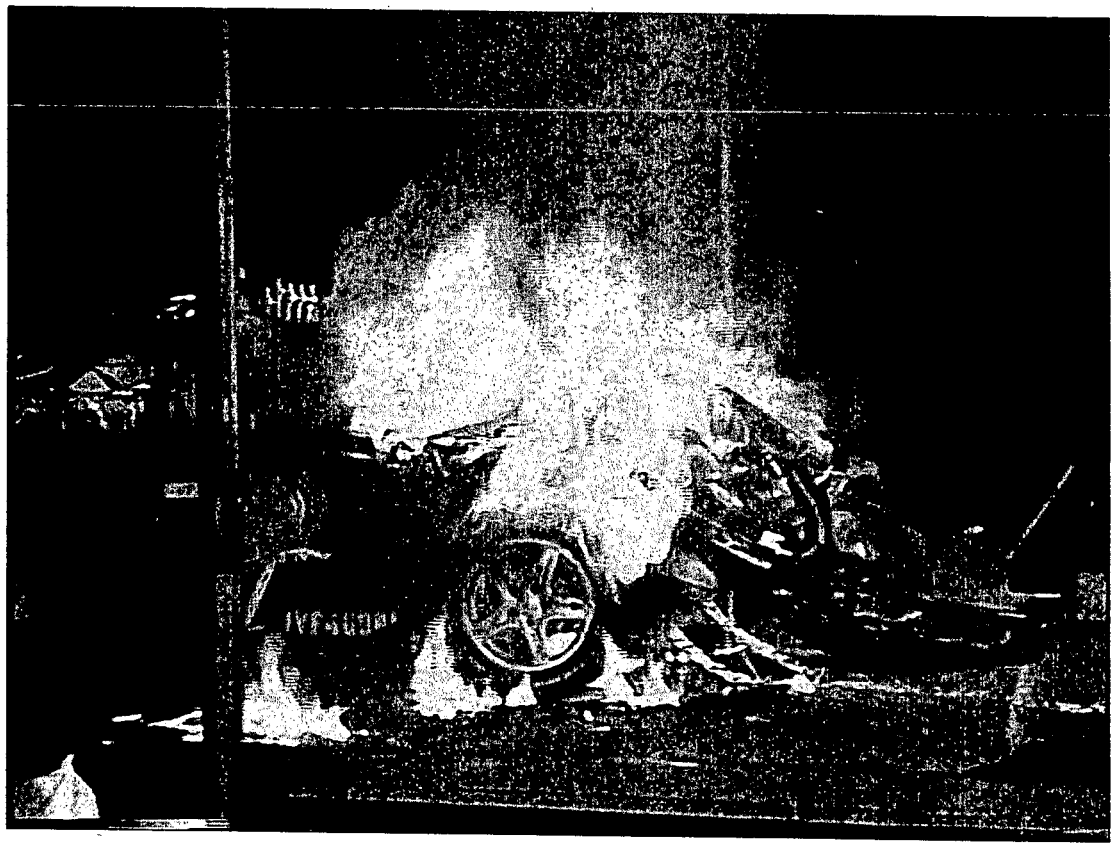

Figure 54. Fire Test F971003. Video still from Camera 2 at 15 minutes post-ignition.

thermocouples located at the lower surface of the headlining panel above the driver's and front passenger's seats were 328 and 256°C, respectively, at 15 minutes 50 seconds (Fig.'s 55 and 56). The estimated temperature profiles along the headlining panel above the front seats were between about 250 and 350°C at this time (Fig. 53).

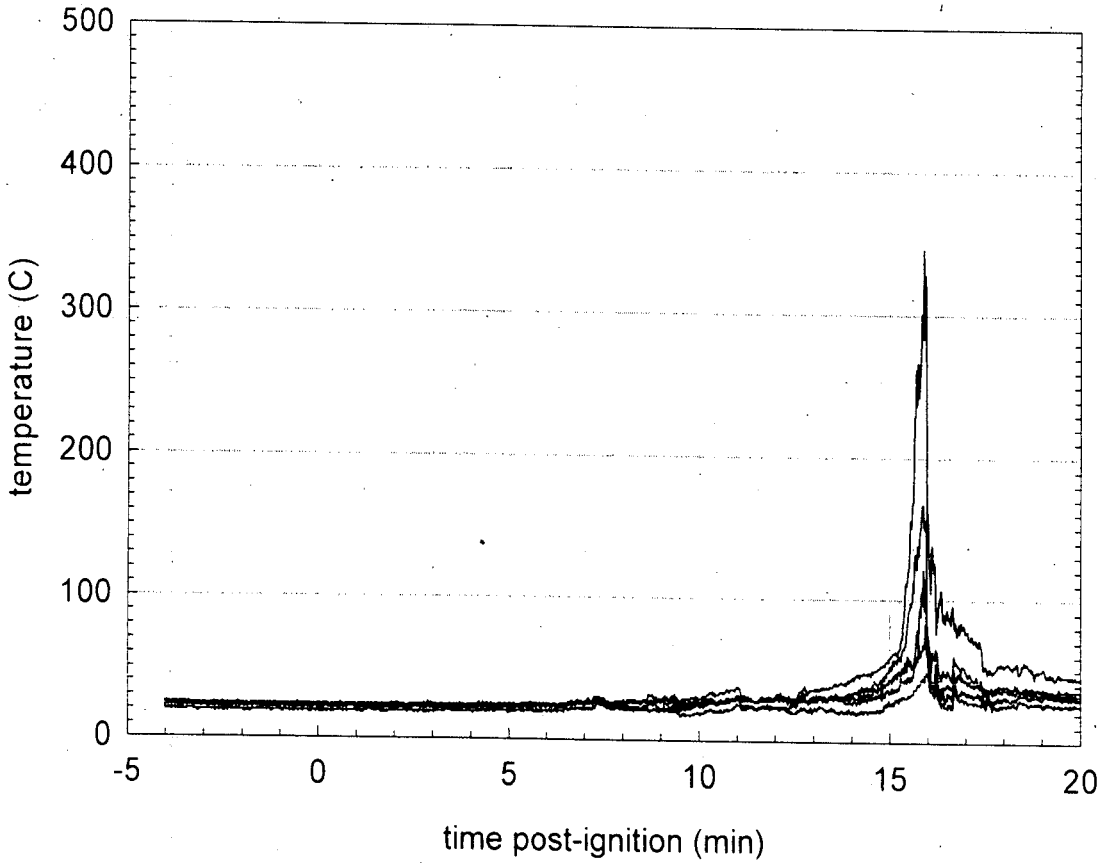

Figure 55. Fire Test F971003. Plots of air temperatures recorded from aspirated thermocouples 0, 3, 6, 9, 12, and 15 in. below the lower surface of the headlining panel above the front driver's seat.

A vertical air temperature gradient developed as flames spread into the passenger compartment in the instrument panel. Air temperatures recorded from the aspirated thermocouples located 6 inches below the lower surface of the headlining panel were 93 and 67°C, respectively, at 15 minutes 50 seconds (Fig.'s 55 and 56). And air temperatures recorded from the aspirated thermocouples located 15 inches below the lower surface of the headlining panel were 43 and 50°C, respectively, at 15 minutes 50 seconds (Fig.'s 55 and 56). Thus, the vertical temperature gradient in the passenger compartment was approximately 20°C/in. above the driver's seat and approximately 14°C/in. above the front passenger's seat.

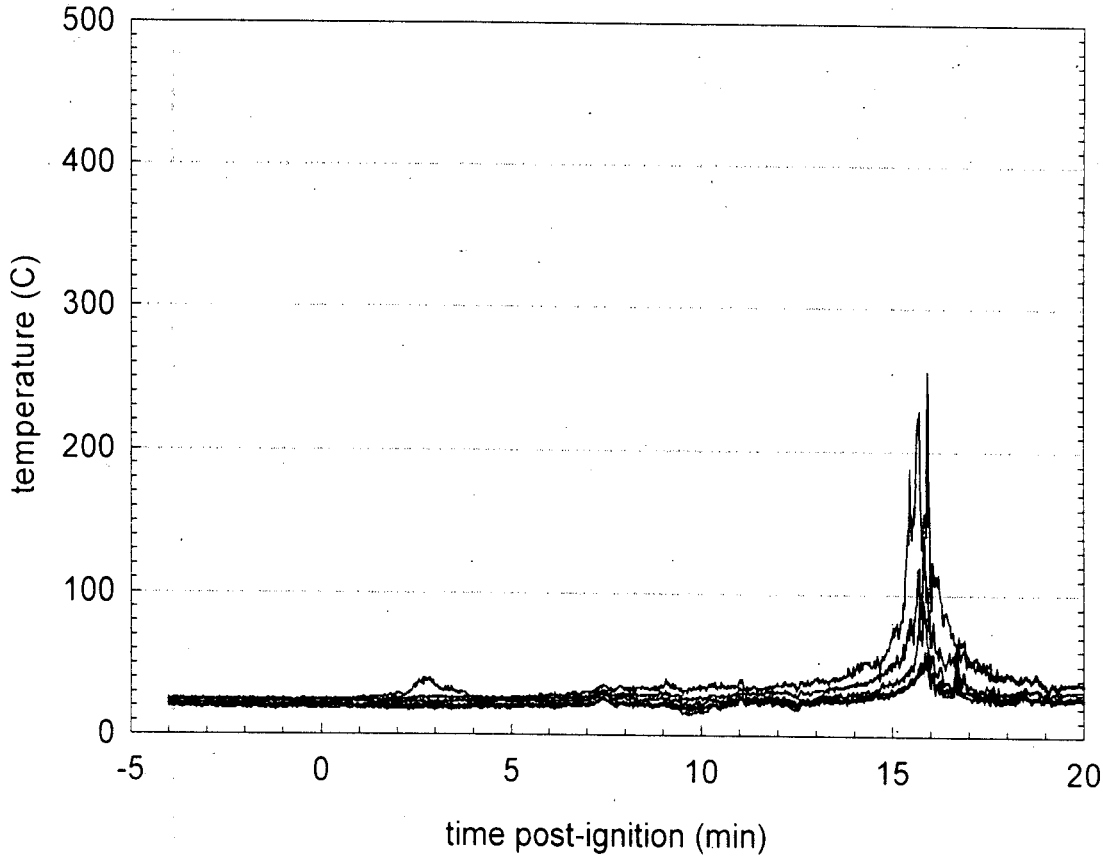

Figure 56. Fire Test F971003. Plots of air temperatures recorded from aspirated thermocouples 0, 3, 6, 9, 12, and 15 in. below the lower surface of the headlining panel above the front passenger's seat.

The lack of heat and fire damage to the tops of the front seat backs also indicated that a burning upper layer did not develop during this test. The fabric covers were melted and charred where pieces of the windshield had fallen onto the front seat cushions (Fig. 57). The seat cushion covers do not appear to have ignited (Fig.57). The seat backs showed no evidence of heat or fire damage. That is, there was no discoloration, melting, or charring of the fabric covers on the front seat backs (Fig. 57).

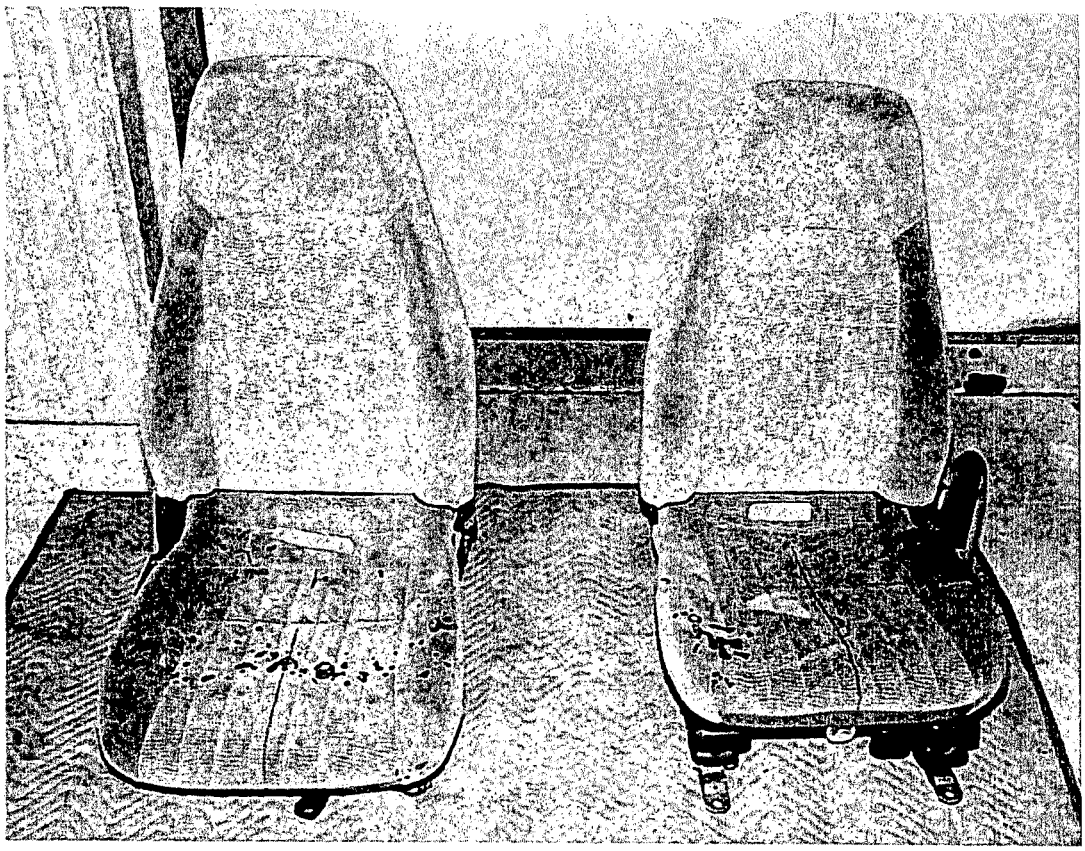

Figure 57. Fire Test F971003. Photograph of the front seats from the test vehicle after this test.

6 Combustion Conditions

The output of combustion products from a fire depends on the material burning and on the supply of air to the flame. A well-ventilated fire is one in which the air supplied to the flames is sufficient for complete combustion. In partially enclosed spaces, such as an engine compartment or passenger compartment, airflow to the flames may be inadequate for complete combustion. In this case, called a ventilation-controlled or under-ventilated fire, the supply of air limits both the heat released by the fire and oxidation (combustion) of the gaseous fuel in the fire zone. As ventilation decreases, the output of carbon monoxide, hydrocarbons, smoke, and other products of incomplete combustion increase. The chemical composition of these gases depends on the chemical compositions of the materials burning and on the burning conditions, primarily ventilation. For fires in an enclosed space, heated buoyant gases can accumulate below the ceiling or roof of the enclosed space, forming what is called the upper layer. The upper layer can be ignited by flames from burning objects (piloted ignition) or can ignite spontaneously (autoignition) when the temperature of the gases exceeds a minimum threshold temperature (autoignition temperature), which depends on the chemical composition and the fuel/oxygen ratio of the gaseous upper layer. Once ignited, radiation from the burning upper layer transfers heat downward, and may ignite combustible materials below the burning upper layer. Ventilation of the flames affects the chemical composition of the gases produced in a fire.

The equivalence ratio is a quantitative measure of the amount of oxygen consumed during combustion, and is defined as follows:

$$\Phi = \frac{\left[fuel/O_2\right]_{fire}}{\left[fuel/O_2\right]_{stoichiometric}}$$

where Φ is the equivalence ratio, $[fuel/O_2]_{fire}$ is the fuel-to-oxygen ratio in the fire, and $[fuel/O_2]_{stoichiometric}$ is the fuel-to-oxygen ratio required for complete (stoichiometric) combustion. Combustion product concentration data, oxygen concentration data, gas temperature data, and airflow data are typically used to calculate a value of the equivalence ratio in laboratory tests [4]. In most instances, the equivalence ratio is not determined for large-scale tess where objects made of different materials may burn in different physical environments. Ventilation and thus the equivalency ratio may be different in each environment. Since it was not possible to isolate and measure the fire products produced by each of the materials burning or to measure airflow into each of the unique environments that existed during this test, the equivalence ratio was not determined here.

Air temperature and gas concentration data collected during this test were used to estimate derived parameters that are related to ventilation. Air temperature and gas concentration data from the Fire Products Collector at the test facility were used to estimate the ratios $[G_{CO}]/[G_{CO2}]$ and $[G_{HC}]/[G_{CO2}]$. Air temperature data from the aspirated thermocouples in the passenger compartment and gas concentration data from the FTIR gas analysis of air in the passenger compartment were used to estimate the ratios $[C_{CO} \times d_{CO}]/[C_{CO2} \times d_{CO2}]$, $[C_{HC} \times d_{HC}]/[C_{CO2} \times d_{CO2}]$, $[C_{CO2} \times d_{CO2}]/[t_{air} \times Cp]$, $[C_{CO} \times d_{CO}]/[t_{air} \times Cp]$, and $[C_{CO2} \times d_{CO2}]/[t_{air} \times Cp]$. Ventilation was assessed by comparing the values of these derived parameters estimated from the test data to reference values obtained during the testing of individual materials in small-scale flammability tests,[15] where the equivalence ratio was measured precisely [4]. The reference parameters used in this comparison include $Y(CO)/Y(CO_2)$, $Y(HC)/Y(CO_2)$, $Y(CO_2)/\Delta H_{CON}$, $Y(CO)/\Delta H_{CON}$, $Y(HC)/\Delta H_{CON}$ (Table 1).

Table 1

Fire Products for Well-ventilated Fires[1,2]

material	$Y(CO)/Y(CO_2)$ (g/g)	$Y(HC)/Y(CO_2)$ (g/g)	$Y(CO_2)/\Delta H_{CON}$ (g/kJ)	$Y(CO)/\Delta H_{CON}$ (g/kJ)	$Y(HC)/\Delta H_{CON}$ (g/kJ)
poly(ethylene)	0.0087	0.0025	0.13	0.0011	0.00032
poly(propylene)	0.0086	0.0022	0.12	0.0011	0.00027
poly(styrene)	0.026	0.0060	0.21	0.0054	0.00127
polyester	0.05	0.019	0.15	0.0065	0.00185
Nylon	0.018	0.0078	0.13	0.0035	0.00098
Flexible urethane foams	0.006 - 0.027	0.0013 - 0.0033	0.15 - 0.21	0.0012 - 0.0055	0.00023 - 0.00069
Rigid urethane foams	0.015 - 0.046	0.006 - 0.036	0.17 - 0.23	0.0028 - 0.0081	0.00011 - 0.00070

[1]Values reported in Table 1 were calculated from data reported in Table 3-4.11 in reference 4.

[2]Y(CO) is the mass-yield of carbon monoxide (g). $Y(CO_2)$ is the mass-yield of carbon dioxide (g). Y(HC) is the mass-yield of gaseous hydrocarbons (g). $Y(CO_2)/\Delta H_{con} = (C_{CO_2}/c_p\Delta T)(\rho_{CO_2}/\rho_{air})$, $Y(CO)/\Delta H_{con} = (C_{CO}/c_p\Delta T)(\rho_{CO}/\rho_{air})$, and $Y(HC)/\Delta H_{con} = (C_{HC}/c_p\Delta T)(\rho_{HC}/\rho_{air})$. ΔH_{CON} is the convective heat of combustion per unit fuel vaporized (kJ/g). The C_i are the gas-phase concentrations (volume fraction) of carbon dioxide, carbon monoxide, and total hydrocarbons. The ρ_i are the gas-phase densities (g/m^3) of carbon dioxide, carbon monoxide, total hydrocarbons, and air. c_p is the heat capacity of air (kJ/g-K). ΔT is the difference between the gas temperature and the temperature of the ambient air (K).

The values of these parameters in Table 1 were determined for the well-ventilated combustion of a poly(ethylene), a poly(propylene), a poly(styrene), a polyester, a Nylon, a group of flexible urethane foams, and a group of rigid urethane foams in controlled small-scale laboratory tests.[16]

---

[15] Small-scale flammability tests to determine combustion properties of materials were conducted in the Factory Mutual Research Corporation Flammability Apparatus is a small-scale test apparatus (see reference 4).

[16] The compositions and physical properties such as density, thermal conductivity, and heat capacity of these materials were not specified.

Analysis of the data from the Fire Products Collector suggests that initially, the production of carbon monoxide relative to carbon dioxide was greater than expected for well-ventilated combustion of materials similar to those used in the test vehicle. Figure 58 shows a plot of $[G_{CO}]/[G_{CO2}]$ versus time post-ignition, where G_{CO} and G_{CO2} are the carbon monoxide- and carbon dioxide-release rates measured using the Fire Products Collector (**APPENDIX H**). The ratio $[G_{CO}]/[G_{CO2}]$ is equivalent to $[Y(CO)]/[Y(CO_2)]$ in Table 1.

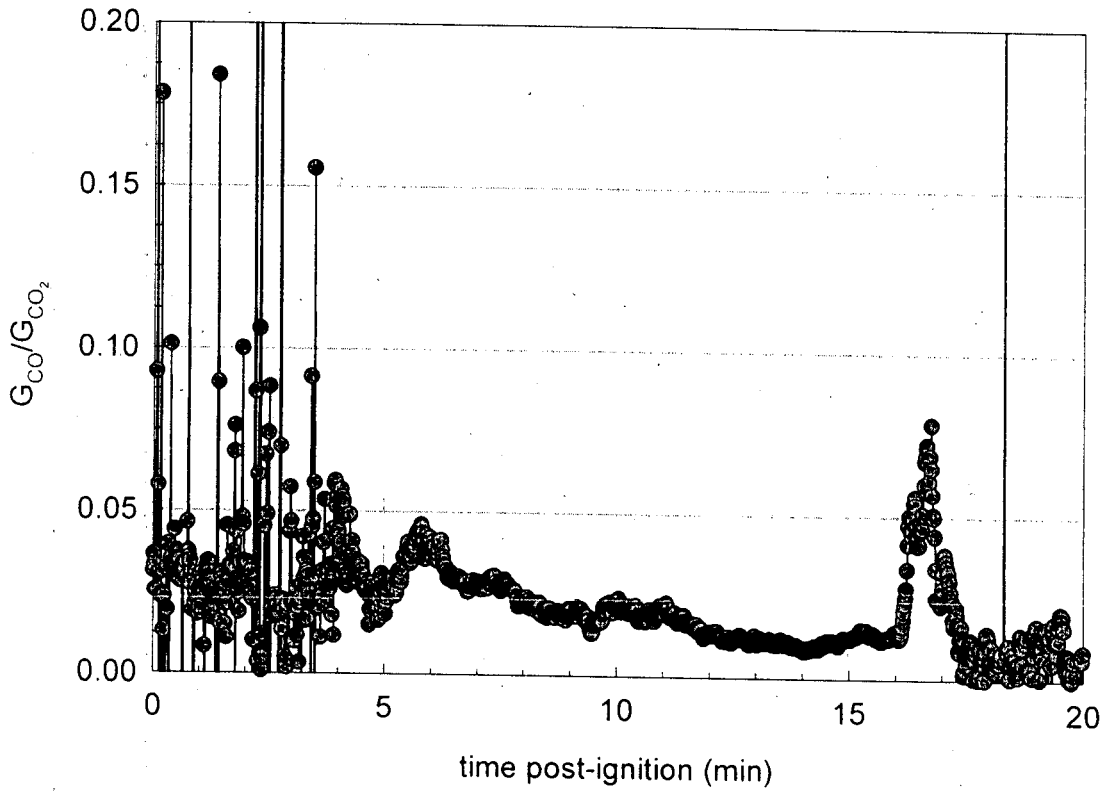

Figure 58. Fire Test F971003. Plots of $[G_{CO}]/[G_{CO2}]$ (—●—) versus time post-ignition determined from the carbon monoxide and carbon dioxide release rates measured by the Fire Products Collector.

Before ignition, $[G_{CO}]/[G_{CO2}]$ was undefined because $G_{CO} = G_{CO2} = 0$. The carbon dioxide- and carbon monoxide-release rates (Plots H2 and H3, respectively) were low during the first 4 minutes of this test, and small absolute variations in the measured values of G_{CO} and G_{CO2} resulted in the relatively large variations in the calculated value of $[G_{CO}]/[G_{CO2}]$ (Fig. 58).

Beginning at about 4 minutes post-ignition, the temperature, concentration of carbon dioxide, and concentration of carbon monoxide in the air entrained into the Fire Products Collector increased significantly above background levels. The timing of this behavior correlated roughly with the observation of flame-spread to the air inlet screen above the propane torch, and resulted in

significant increases in the heat-release rate (Plot H1), the carbon dioxide-release rate (Plot H2), and the carbon monoxide-release rate (Plot H3). The plot of $[G_{CO}]/[G_{CO2}]$ also became uniform, with values decreasing from about 0.05 at 4 minutes post-ignition to about 0.02 at 5 minutes post-ignition (Fig. 58). For well-ventilated combustion of poly(propylene), $[Y(CO)]/[Y(CO_2)] = 0.0086$ (Table 1). Values of $[G_{CO}]/[G_{CO2}] > \sim 0.009$ indicate under-ventilated combustion conditions. One possible explanation for values of $[G_{CO}]/[G_{CO2}] > 0.009$ observed in this test is the progression from pyrolysis to ignition of the air inlet screen exposed to heat and flames emerging from under the upper dash extension panel.

The value of $[G_{CO}]/[G_{CO2}]$ increased from 0.02 at 5 minutes post-ignition to 0.05 at 6 minutes post-ignition, then decreased uniformly to between 0.01 and 0.02 at 16 minutes post-ignition (Fig. 58). It was not possible to make direct comparisons between $[G_{CO}]/[G_{CO2}]$ and the reference values in Table 1 as different materials became involved in the fire and different combustion environments developed. From about 6 minutes post-ignition until the end of this test, the value of $[G_{CO}]/[G_{CO2}]$ decreased. At the end of this test, the value of $[G_{CO}]/[G_{CO2}]$ (Fig. 58) was within the range of reference values ($0.006 < [Y(CO)]/[Y(CO_2)] < 0.05$) for well-ventilated combustion of materials similar to those used in the test vehicle (Table 1). This trend indicates that well-ventilated combustion conditions developed as the heat-release rate increased.

A similar analysis of air temperature and gas concentration data from the passenger compartment is shown in Figures 59 through 63. Air temperature and gas concentration data from the passenger compartment were used to determine $[C_{CO} \times d_{CO}]/[C_{CO2} \times d_{CO2}]$, $[C_{HC} \times d_{HC}]/[C_{CO2} \times d_{CO2}]$, $[C_{CO2} \times d_{CO2}]/[t_{air} \times Cp]$, $[C_{CO} \times d_{CO}]/[t_{air} \times Cp]$, and $[C_{HC} \times d_{HC}]/[t_{air} \times Cp]$. In these formulas, C_j is the gas-phase concentration of species j, d_j is the density of species j, t_{air} is the air temperature, and C_p is the heat capacity of air. The product $[C_j \times d_j]$ equals the mass-concentration of species j in passenger compartment. The concentrations of the gaseous combustion products (C_j) were determined by Fourier Transform Infrared Spectrometry (**APPENDIX I**). Air temperature data from the aspirated thermocouple assemblies in the passenger compartment (**APPENDIX D**) was used to determine t_{air}. The ratios $[C_{CO} \times d_{CO}]/[C_{CO2} \times d_{CO2}]$, $[C_{HC} \times d_{HC}]/[C_{CO2} \times d_{CO2}]$, $[C_{CO2} \times d_{CO2}]/[t_{air} \times Cp]$, $[C_{CO} \times d_{CO}]/[t_{air} \times Cp]$, and $[C_{HC} \times d_{HC}]/[t_{air} \times Cp]$ are equivalent to $[Y(CO)]/[Y(CO_2)]$, $[Y(HC)]/[Y(CO_2)]$, $Y(CO_2)/\Delta H_{CON}$, $Y(CO)/\Delta H_{CON}$, and $Y(HC)/\Delta H_{CON}$, respectively, in Table 1. Interpretation of the plots shown in Figures 58 through 62 was complicated by the intrusion of heat and gaseous combustion products into the passenger compartment prior to flame-spread into the passenger compartment.

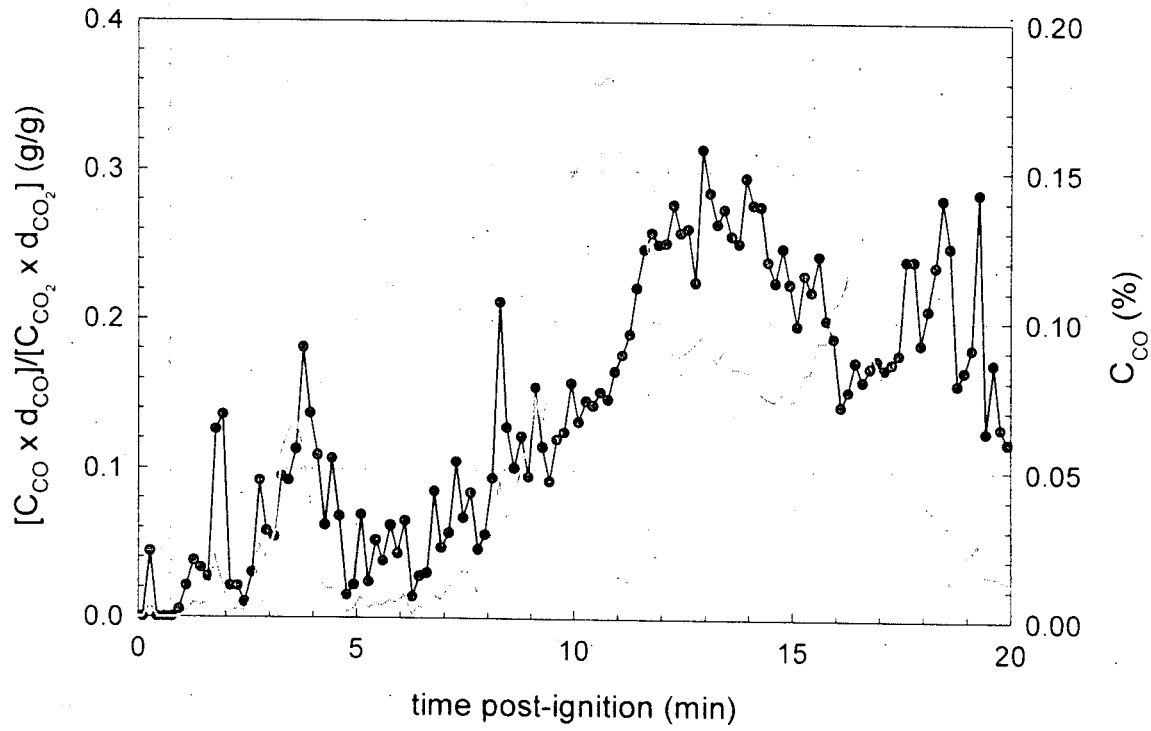

Figure 59. Fire Test F971003. Plots of $[C_{CO} \times d_{CO}]/[C_{CO2} \times d_{CO2}]$ (—●—, left axis) and the concentration of carbon monoxide (—, right axis) in the passenger compartment.

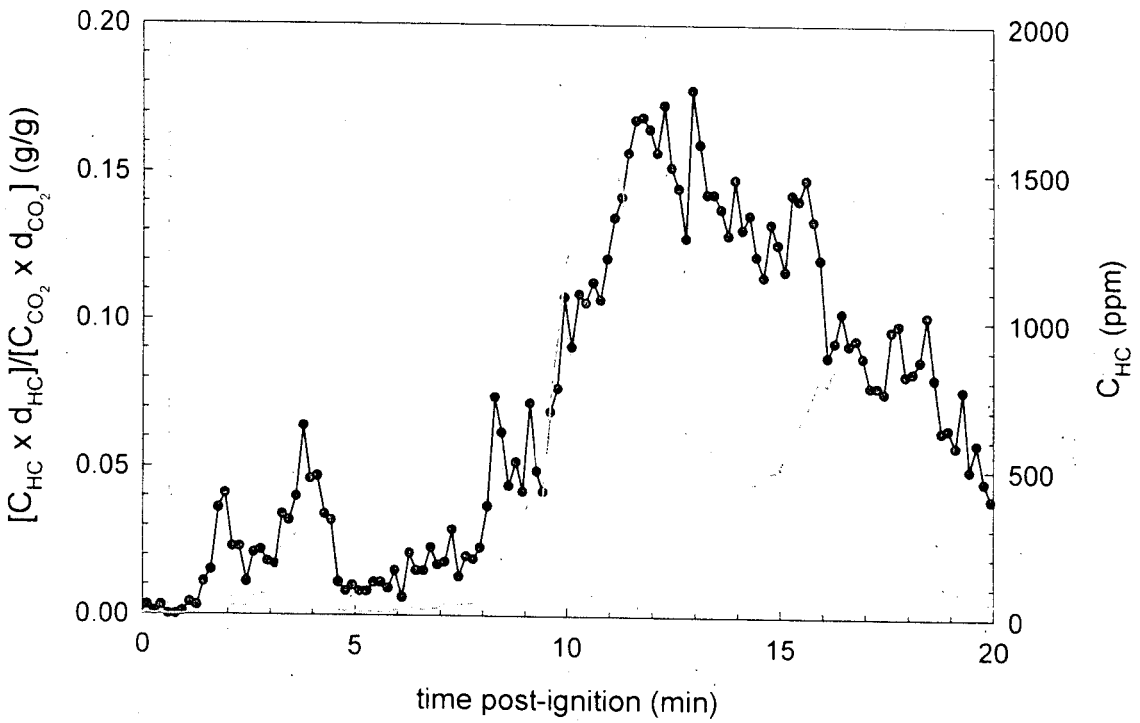

Figure 60. Fire Test F971003. Plots of $[C_{HC} \times d_{HC}]/[C_{CO2} \times d_{CO2}]$ (—●—, left axis) and the concentration of total hydrocarbons (—, right axis) in the passenger compartment.

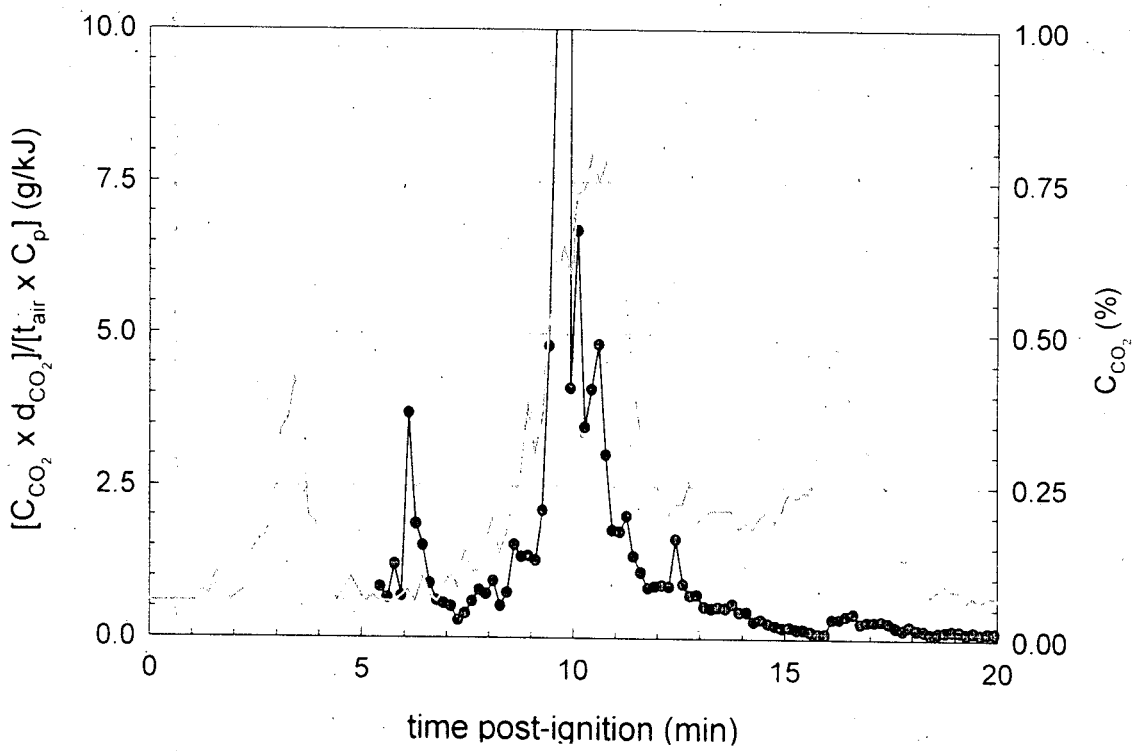

Figure 61. Fire Test F971003. Plots of $[C_{CO2} \times d_{CO2}]/[t_{air} \times Cp]$ (—●—, left axis) and the concentration of carbon dioxide (—, right axis) in the passenger compartment.

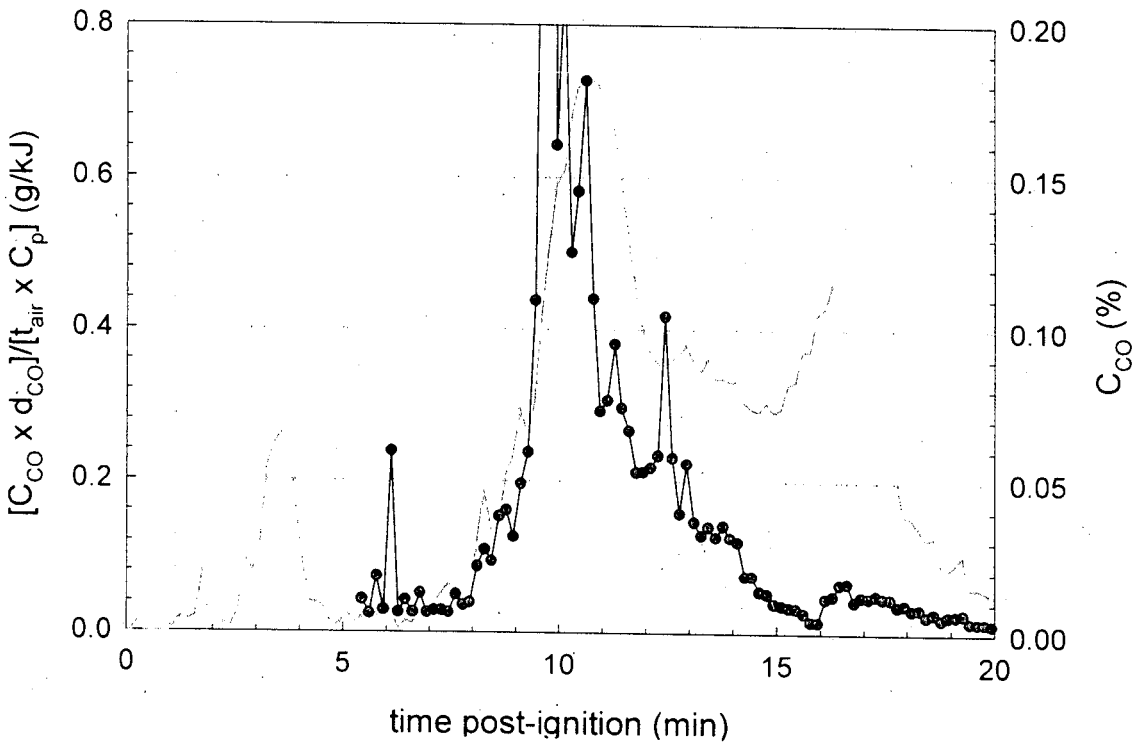

Figure 62. Fire Test F971003. Plots of $[C_{CO} \times d_{CO}]/[t_{air} \times Cp]$ (—●—, left axis) and the concentration of carbon monoxide (—, right axis) in the passenger compartment.

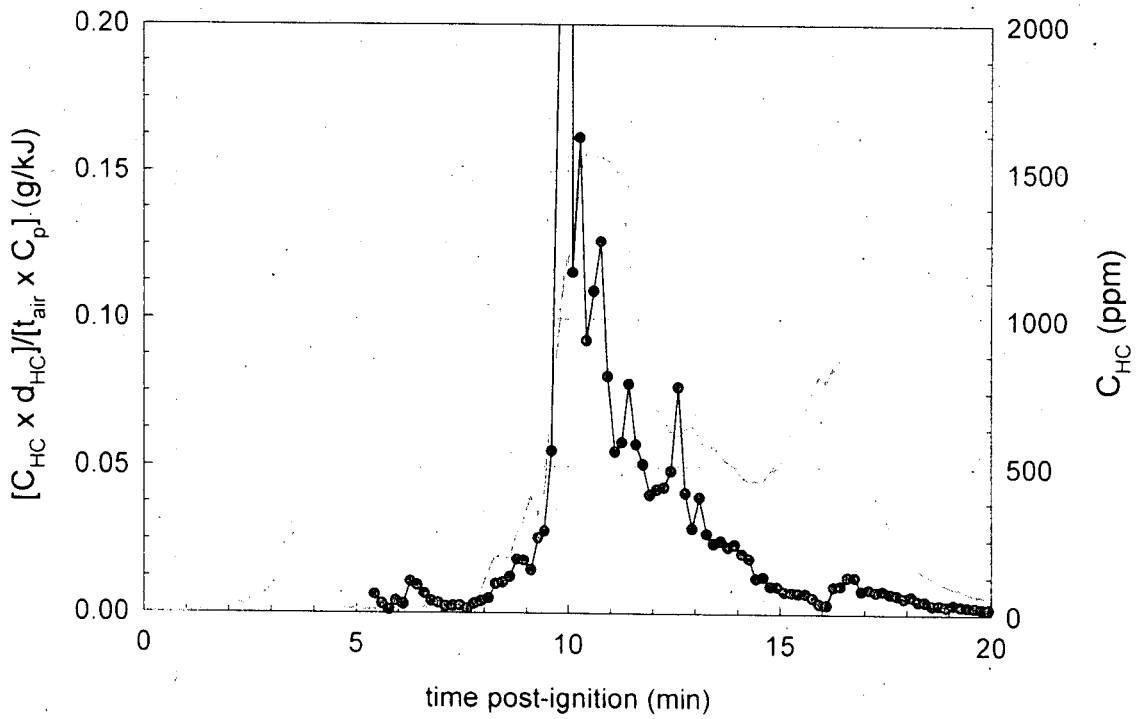

Figure 63. Fire Test F971003. Plots of $[C_{HC} \times d_{HC}]/[t_{air} \times Cp]$ (—●—, left axis) and the concentration of hydrocarbons (—, right axis) in the passenger compartment.

Gaseous combustion products were detected in the passenger compartment before the propane torch was extinguished at 2 minutes post-ignition (APPENDIX I). The air temperature recorded from the aspirated thermocouples located at the lower surface of the headlining panel started to increase at about 5 minutes post-ignition (APPENDIX D). However, the first evidence of flame-spread into the instrument panel was when temperatures recorded from thermocouples in the HVAC module exceeded 600°C between 10 and 11 minutes post-ignition (SECTION 4.1). Data recorded from these thermocouples show that temperatures started to increase between 4 and 5 minutes post-ignition (APPENDIX C), indicating that heat was flowing into the instrument panel through the HVAC module at this time. The forward edges of the windshield and the instrument panel upper trim panel were exposed to flames beginning between 3 and 4 minutes post-ignition (SECTION 4.1). The right edge of the instrument panel upper trim panel was burning by 5 minutes post-ignition (SECTION 4.1).

The plot of $[C_{CO} \times d_{CO}]/[C_{CO2} \times d_{CO2}]$ and $[C_{HC} \times d_{HC}]/[C_{CO2} \times d_{CO2}]$ shows peaks at 2 and 4 minutes post-ignition, a trend toward increasing values (0.04 → 0.25) from 5 to 12 minutes post-ignition, and a trend toward decreasing values (0.25 → 0.15) from 12 to 16 minutes post-ignition (Fig. 59). Similarly, the plot of $[C_{HC} \times d_{HC}]/[C_{CO2} \times d_{CO2}]$ shows peaks from 5 to 12 minutes post-ignition, and a trend toward decreasing values (0.017 → 0.010) from 12 to 16 minutes post-ignition (Fig. 60).

Combustion gases measured in the passenger compartment measured before flames had spread into the instrument panel (10 to 11 minutes post-ignition) were produced in the engine compartment. The values of $[C_{CO} \times d_{CO}]/[C_{CO2} \times d_{CO2}]$ and $[C_{HC} \times d_{HC}]/[C_{CO2} \times d_{CO2}]$ were greater than the respective reference values (Table 1) during this time, indicating that the infiltrating gases were produced in an area where pyrolysis or under-ventilated combustion was occurring. The instrument panel was forward of the roofline. After flames spread into the instrument panel, heat and fire products flowed upward through the opening in the windshield. Components that were rearward of the roofline, such as the front seats, did not ignite during this test. Heat and fire products in the passenger compartment likely resulted from eddy flows from the main fire plume. The complex nature of airflow and gas mixing in the test vehicle cannot be reconstructed from the recorded test data. Therefore, the trends in these plots cannot be related to specific objects burning or specific events that occurred during this test.

The plots of $[C_{CO2} \times d_{CO2}]/[t_{air} \times Cp]$, $[C_{CO} \times d_{CO}]/[t_{air} \times Cp]$, and $[C_{HC} \times d_{HC}]/[t_{air} \times Cp]$ start at about 5 ½ minutes post-ignition, when temperatures recorded from the aspirated thermocouples at the height of the FTIR gas sampling inlet (t_{air}) started to increase (Fig.'s 61 through 63). The values calculated for $[C_{CO2} \times d_{CO2}]/[t_{air} \times Cp]$, $[C_{CO} \times d_{CO}]/[t_{air} \times Cp]$, and $[C_{HC} \times d_{HC}]/[t_{air} \times Cp]$ were greater than the respective reference values (Table 1) from about 5½ minutes post-ignition until the end of the test. The plots of $[C_{CO2} \times d_{CO2}]/[t_{air} \times Cp]$, $[C_{CO} \times d_{CO}]/[t_{air} \times Cp]$, and $[C_{HC} \times d_{HC}]/[t_{air} \times Cp]$ contain peaks between 9 and 10 minutes post-ignition (Fig.'s 61 through 63). The values of each of these parameters increased sharply at about 9½ minutes post-ignition, indicating disproportionate increases in C_{CO}, C_{CO2}, and C_{HC} relative to t_{air}. These peaks occurred approximately 1 minute before flame-spread into the instrument panel, and may have been related to flame spread in the HVAC module.

These peaks may be related to the process of flame-spread into the HVAC module. Pyrolysis of materials in the HVAC module occurring in advance of the flame front is an endothermic chemical reaction yielding volatile unoxidized or partially oxidized products. Thermal decomposition of materials in the HVAC module, caused by the movement of heated gases into the HVAC module prior to flame-spread into this area, would have produced more carbon monoxide (CO) and unburned hydrocarbons (HC), and less carbon dioxide (CO_2) than predicted for well-ventilated combustion. Admixture of these products with air sampled for FTIR analysis would have resulted in momentary increases in the values of $[C_{CO2} \times d_{CO2}]/[t_{air} \times Cp]$, $[C_{CO} \times d_{CO}]/[t_{air} \times Cp]$, and $[C_{HC} \times d_{HC}]/[t_{air} \times Cp]$.

7 Estimation of Skin Temperature Profiles from Measured Heat Flux Data, Fractional Equivalent Dose Parameters from Measured Gas Concentration Data, and Thermal Damage to the Respiratory Tract from Measured Air Temperature Data

The mathematical model "BURNSIM: A Burn Hazard Assessment Model" [5] was used to estimate the time and depth of burns to exposed skin. The inputs to this model were heat fluxes derived from the directional flame thermometer measurements and air temperatures measured using the aspirated thermocouple probe.

Two models were used to estimate the potential for toxicity from exposure to the combustion gases measured in the passenger compartment. The Federal Aviation Administration (FAA) Combined Hazard Survival Model [6] was used to estimate the time to incapacitation and the time to lethality. A model described by Purser [7] also was used to estimate the time to incapacitation. Both models estimate the risk from exposure to hot air, reduced oxygen, carbon monoxide, carbon dioxide, hydrogen cyanide, hydrogen chloride, hydrogen fluoride, hydrogen bromide, acrolein, and nitrogen dioxide. Both models also account for the physiological effect of carbon dioxide-induced hyperventilation, which directly increases the respiratory uptake which, in turn, can result in increased respiratory intake of combustion gases.

7.1 The BURNSIM Model

The computer model BURNSIM was the analytical tool chosen to estimate skin temperature depth profiles from the heat flux data in **APPENDIX E**. The BURNSIM model divides the skin into a series of ten layers, with a uniform thickness of 0.2 mm per layer. The top layer was divided into 8 layers each with a uniform thickness of 0.025 mm to better account for the non-instantaneous heat transfer from the epidermal surface into the first layer.

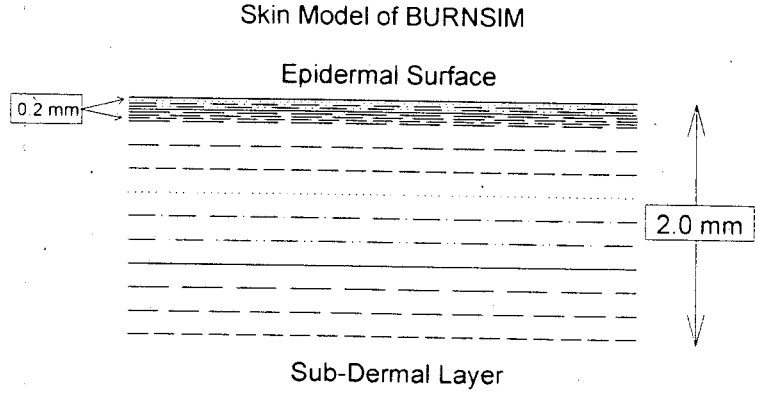

The BURNSIM analysis used here incorporated the following assumptions to estimate skin temperature profiles. The absorbtivity of exposed skin was assumed to be 0.60 (i.e., the skin

absorbs 60% of the radiation incident upon the epidermal surface). The absorbtivity of surface hair was assumed to be 0.05 (i.e., surface hair absorbs 5% of the incident radiation before it reached the skin). Exposed skin was assumed to absorb 100% of the measured convective heat flux to its surface. The temperature of each layer was estimated as a function of the time of exposure to an external heat flux. A portion of the absorbed heat is removed from the skin by the circulatory system. Thermal damage to a layer of skin exceeds the capacity of the physiological repair processes when the temperature of that layer exceeds 45°C.

In estimating skin temperature, the analysis presented in this paper using BURNSIM did not account for the presence of facial or head hair, or clothing covering the skin, all of which may block direct heat transfer to the skin. This analysis also did not account for variations in skin thickness among individuals, or variations in skin thickness at different parts of the body on the same individual. For example, skin thickness can vary from 1 to 5 mm with body location. This analysis also did not account for effect of skin pigmentation on absorbtivity. In using the radiative and convective heat flux estimates shown in **APPENDIX E** to estimate skin temperature profiles, this analysis assumed that the location and orientation of the skin was identical to that of the transducers used to measure heat flux. Small changes in position or angle of the surface of the skin relative to the Heat Flux Transducers in this test can lead to large differences between in the actual incident heat flux to exposed surfaces and that measured by the Heat Flux Transducer (see below). Based on the currently available information and data, the accuracy of the estimated skin temperature depth profiles in humans obtained using BURNSIM with inputs of heat flux levels such as measured in this test has not been determined.

7.1.1 Estimation of Skin Temperature Profiles using BURNSIM

Figures 64 through 69 show skin temperature depth profiles estimated from the heat flux data recorded from the heat flux transducer/radiometer assemblies (HFT/RAD) above the front seats in the test vehicle (**APPENDIX E**). HFT/RAD5, HFT/RAD6, and HFT/RAD7 were located approximately 80 cm above the driver's seat, with HFT/RAD5 facing upward, HFT/RAD6 facing forward, and HFT/RAD7 facing forward at an angle of approximately 45° relative the longitudinal centerline of the test vehicle. HFT/RAD8, HFT/RAD9, and HFT/RAD10 were located approximately 80 cm above the front passenger's seat, with HFT/RAD8 facing upward, HFT/RAD9 facing forward, and HFT/RAD10 oriented at angle of approximately 15° relative to the longitudinal centerline of the test vehicle. The maximum heat fluxes recorded from these transducers occurred between 15 minutes 50 seconds and 16 minutes post-ignition (Plots E7, E8, E13, and E14).

The convective and radiative heat fluxes recorded from HFT/RAD5 between 15 minutes 50 seconds and 16 minutes post-ignition were approximately 0.5 and 2.5 kW/m^2, respectively (Plots E7 and E8). Skin temperature profiles estimated from data recorded from HFT/RAD5 yielded an estimated temperature at the epidermal surface of approximately 42°C during this time (Fig. 64).

The convective and radiative heat fluxes recorded from HFT/RAD6 between 15 minutes 50 seconds and 16 minutes post-ignition were approximately 0.0 and 20.5 kW/m^2, respectively (Plots E9 and E10). Skin temperature profiles estimated from data recorded from HFT/RAD6 yielded an estimated temperature at the epidermal surface of approximately 76°C (Fig. 65).

The convective and radiative heat fluxes recorded from HFT/RAD7 between 15 minutes 50 seconds and 16 minutes post-ignition were approximately –2.5 and 24.5 kW/m^2, respectively (Plots E11 and E12). The negative value of the convective heat flux indicates that there was a net convective heat transfer away from the transducer (cooling) during this time. Skin temperature profiles estimated from data recorded from HFT/RAD7 yielded an estimated temperature at the epidermal surface of approximately 84°C during this time (Fig. 66).

The convective and radiative heat fluxes recorded from HFT/RAD8 between 15 minutes 50 seconds and 16 minutes post-ignition were 1.5 and 21.8 kW/m^2, respectively (Plots E13 and E14). Skin temperature profiles estimated from data recorded from HFT/RAD8 yielded an estimated temperature at the epidermal surface of approximately 43°C during this time (Fig. 67).

The convective and radiative heat fluxes recorded from HFT/RAD9 between 15 minutes 50 seconds and 16 minutes post-ignition were 1.2 and 9.4 kW/m^2, respectively (Plots E15 and E16). Skin temperature profiles estimated from data recorded from HFT/RAD9 yielded an estimated temperature at the epidermal surface of approximately 55°C during this time (Fig. 68).

The convective and radiative heat fluxes recorded from HFT/RAD10 between 15 minutes 50 seconds and 16 minutes post-ignition were 1.3 and 7.2 kW/m^2, respectively (Plots E17 and E18). Skin temperature profiles estimated from data recorded from HFT/RAD10 yielded an estimated temperature at the epidermal surface of approximately 52°C during this time (Fig. 69).

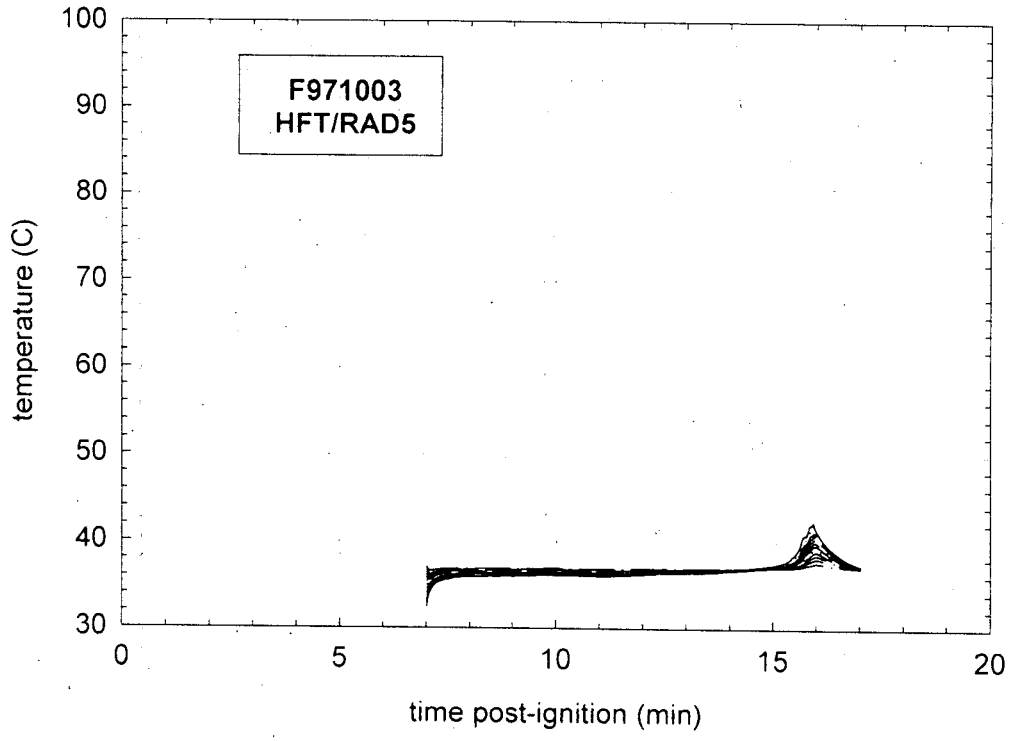

Figure 64. Fire Test F971003. Skin temperature profiles estimated from heat flux data recorded from HFT/RAD5 (**APPENDIX G**, Plots E7 and E8).

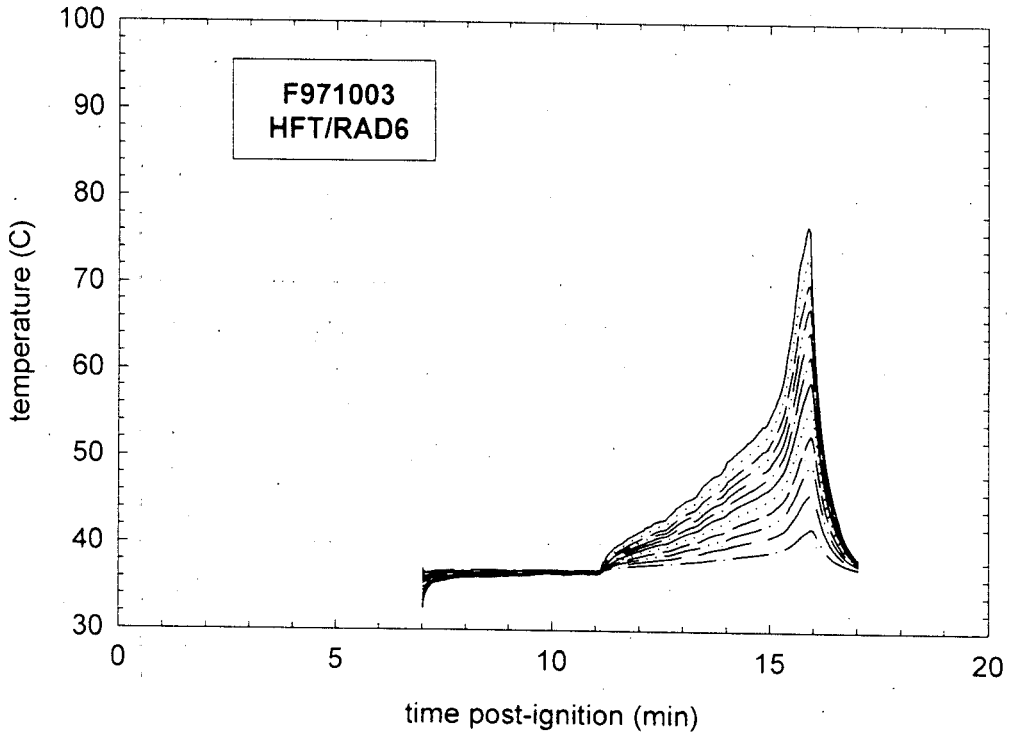

Figure 65. Fire Test F971003. Skin temperature profiles estimated from heat flux data recorded from HFT/RAD 6 (**APPENDIX G**, Plots E9 and E10).

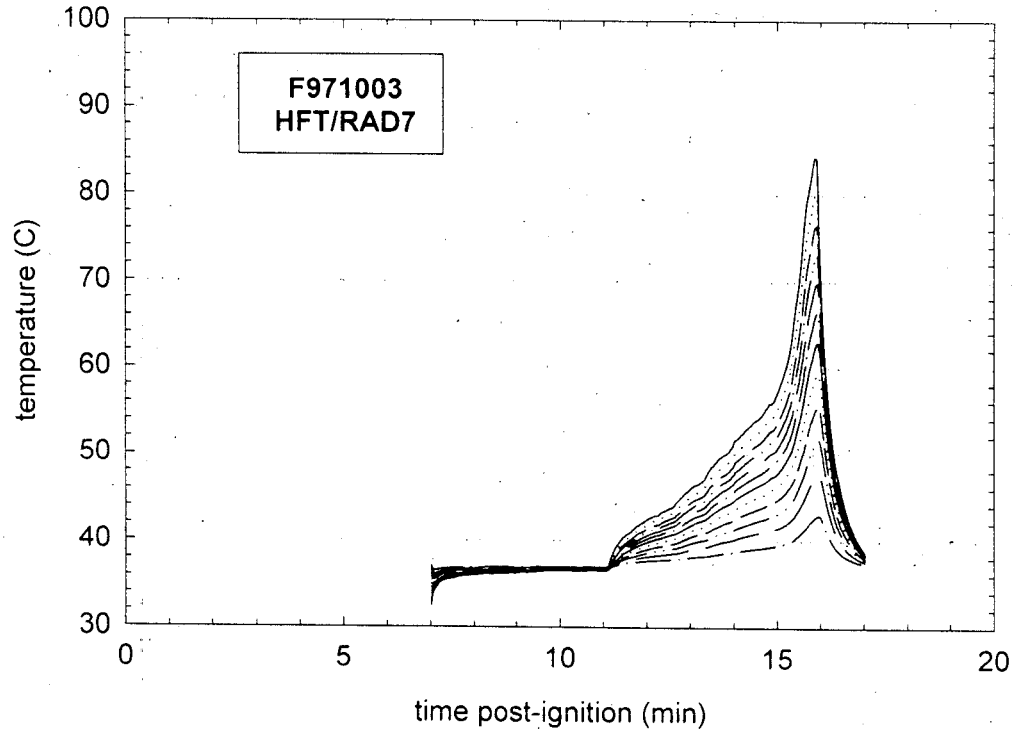

Figure 66. Fire Test F971003. Skin temperature profiles estimated from heat flux data recorded from HFT/RAD7 (**APPENDIX G**, Plots E11 and E12).

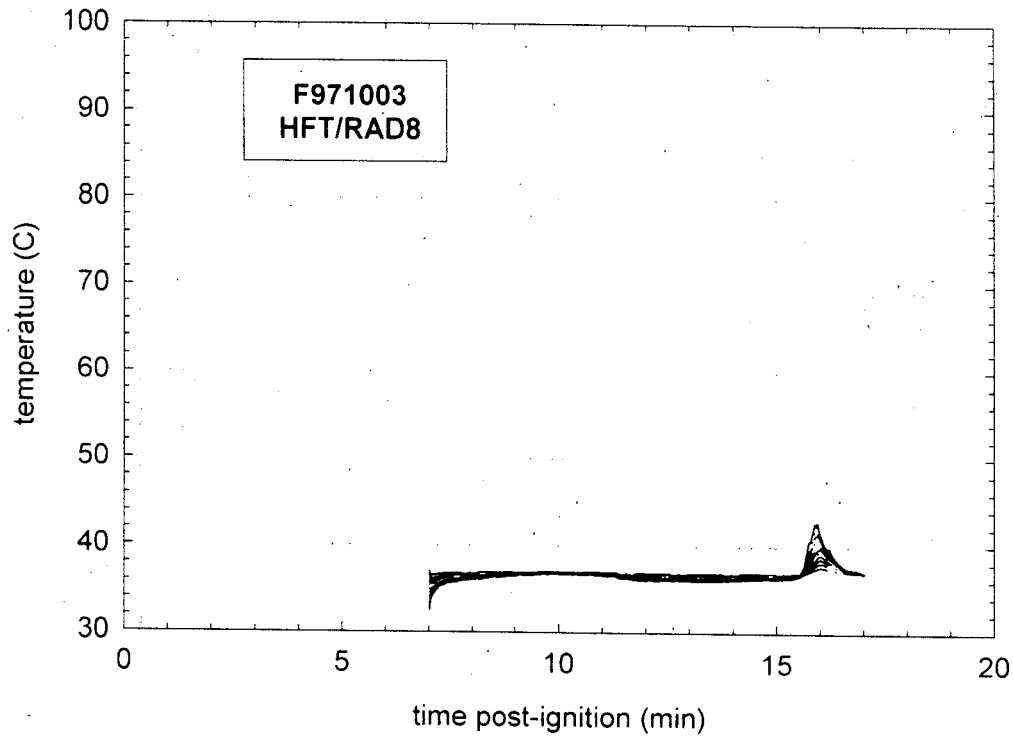

Figure 67. Fire Test F971003. Skin temperature profiles estimated from heat flux data recorded from HFT/RAD8 (**APPENDIX G**, Plots E13 and E14).

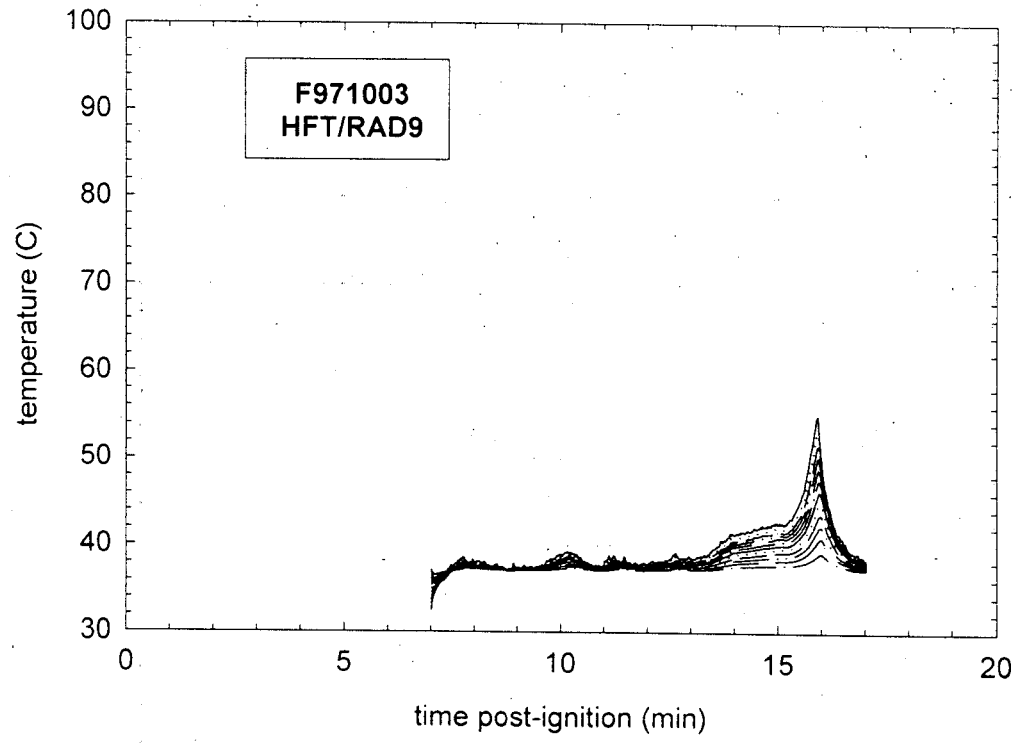

Figure 68. Fire Test F971003. Skin temperature profiles estimated from heat flux data recorded from HFT/RAD9 (**APPENDIX G**, Plots E15 and E16).

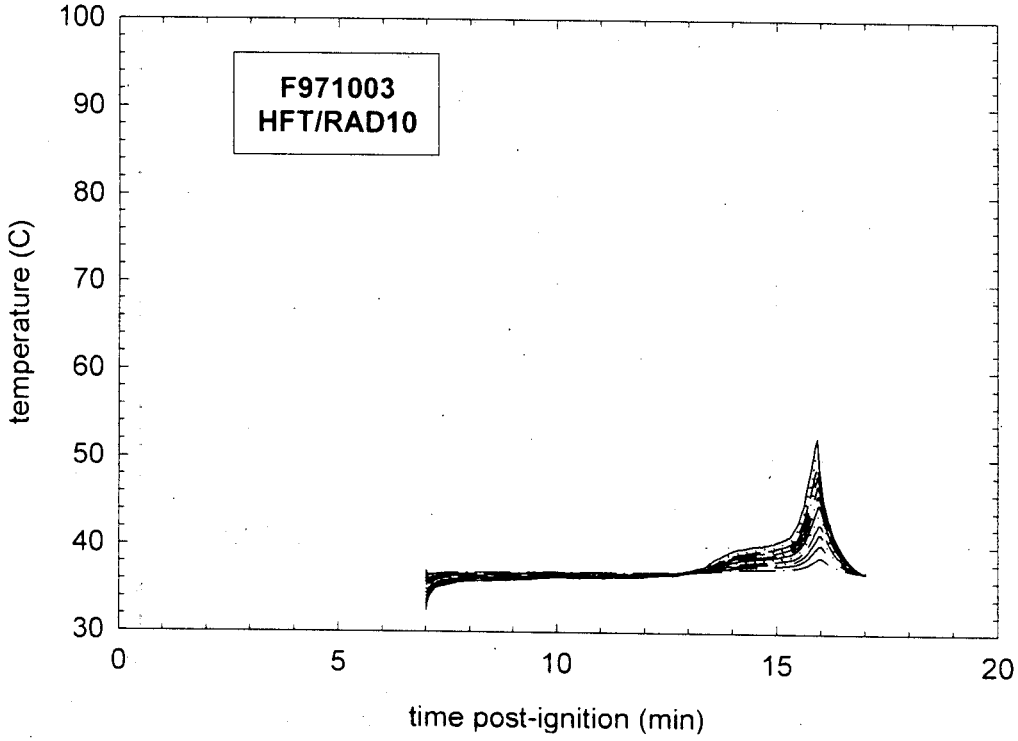

Figure 69. Fire Test F971003. Skin temperature profiles estimated from heat flux data recorded from HFT/RAD10 (**APPENDIX G**, Plots E17 and E18).

7.2 The FAA Combined Hazard Survival Model and Purser's Model of Combustion Gas Toxicity

The FAA Combined Hazard Survival Model and Purser's model utilize the concept of a Fractional Effective Dose [FED] to estimate the cumulative effects of exposure to a mixture of gases produced by burning materials. For exposure to a single gas with an unchanging concentration in air, the Fractional Effective Dose for Incapacitation [FED(I)] is defined as the product of the gas-phase concentration and the time of exposure ($C \times t$) normalized to the concentration-time product that results in incapacitation of 50% of an exposed population [6, 7]. Similarly, the Fractional Effective Dose for lethality [FED(L)] is defined as the product of the gas-phase concentration and the time of exposure normalized to the concentration-time product that results in the death of 50% of an exposed population [see references in 6 and 7]. The estimates of FED(I) and FED(L) obtained using the FAA Combined Hazard Survival Model or Purser's model of combustion gas toxicity and presented in this report cannot be used to predict precisely whether or when the gas concentrations measured in this test would have resulted in incapacitating narcosis or death for a vehicle occupant. Whether exposure to these gases results in toxicity depends on a number of complex physical and physiological variables.

Some of the physical variables include the exact chemical composition of the gaseous mixture, the concentration of each component of the gaseous mixture, and the time of exposure. Exposure to these gases in a burning vehicle can be highly variable, and depend on factors such as elevation in the passenger compartment and airflow through the passenger compartment. As mentioned in the previous section, combustion gases are hotter that the ambient air and form an upper layer. The air temperature data from the aspirated thermocouples indicated that a steep air-temperature gradient developed in the front of the passenger compartment during this test (see **SECTION 7.3**). Since both heat and mass are conserved in a fire, the existence of a steep vertical air-temperature gradient implies the existence of similarly steep vertical concentration gradients for gaseous combustion products accumulating in the passenger compartment. The location of the head and nose in the passenger compartment will effect the exposure concentration. An occupant whose head was located below the level where gases were measured, such as an occupant bent over in the seat, would have been exposed to lower concentrations of combustion gases than those shown in **APPENDIX I** and in Figures 70 through 73. Airflow through the passenger compartment will dilute or remove these gases.

Uncertainties in the responses of humans exposed to these gases complicates the determination of when and whether toxicity occurs. The mathematical equations for the calculation of FED(I) and FED(L) were derived by analysis of data from controlled experiments in which different

species of laboratory animals were exposed to a range of concentrations of each gas. In using data from these laboratory animal experiments to define FED(I) and FED(L), both models implicitly assume that humans respond the same as laboratory animals to exposure to these gases – an assumption that is largely untested and may not be accurate. For example, except for incapacitation from exposure to carbon dioxide, none of the model predictions using either the FAA Combined Hazard Survival Model or Purser's model have been validated for humans. That is, the accuracy of FED(I) and FED(L) in predicting human responses to exposure to the combustion gases measured in this test has not been determined. Consequently, there is a high degree of uncertainty as to the effect exposure to these levels of combustion gases would actually have on a human vehicle occupant. In addition, neither of these models accounts for variation in individual responses to these gases nor the effect of trauma suffered during the crash on an occupant's response to these gases.

The equations presented in both the FAA Combined Hazard Survival Model and in Purser's model divide the exposure into one-minute intervals when the concentration of the gaseous species changes with time. In this test, Fourier Transform Infrared spectra were obtained at seven-second intervals to characterize the changing gas concentrations observed in the passenger compartment. The equations presented in the FAA Combined Hazard Survival Model and in Purser's model were modified to account for the faster sampling times used in this test. These modified equations are shown below and were used to derive the estimated of FED(I) and FED(L) shown in **SECTION 7.2.1.**

Carbon dioxide-induced hyperventilation can increase the respiratory uptake of airborn combustion products. The FAA Combined Hazard Survival Model uses a multiplication factor to account for the increased respiratory uptake of gaseous combustion products because of exposure to elevated levels of carbon dioxide [V_{CO2}]:

$$V_{CO_2} = \frac{\exp(1.9086 + 0.2496 \times C_{CO_2})}{6.8} \qquad (1)$$

where the units of C_{CO2} are %. This equation was not modified for the analysis presented in **SECTION 7.2.1**.

The Fractional Effective Doses for Incapacitation from exposure to carbon dioxide, carbon monoxide, hydrogen chloride, hydrogen cyanide and decreased oxygen were calculated using the following equations modified to account for sampling intervals of less than 1 minute:

$$FED(I)_{CO_2} = \left(\frac{t}{60}\right) \times \sum \left\{ \frac{1}{2193.8 - \left(311.6 \times C_{CO_2}\right)} \right\} \quad (2)$$

when $5.5 \leq C_{CO2} \leq 7.0\%$,

$$FED(I)_{CO_2} = \left(\frac{t}{60}\right) \times \sum \left\{ \frac{1}{\exp\left(6.1623 - \left(0.5189 \times C_{CO_2}\right)\right)} \right\} \quad (3)$$

when $C_{CO2} > 7.0\%$,

$$FED(I)_{CO} = \left(\frac{t}{60}\right) \times \left(\frac{1}{3.4250}\right) \times \sum \left\{ V_{CO_2} \times C_{CO} \right\} \quad (4)$$

when $V_{CO2} \times C_{CO} > 0.01\%$,

$$FED(I)_{HCl} = \left(\frac{t}{60}\right) \times \sum \left\{ \frac{1}{3 + \frac{336{,}000}{\left(V_{CO_2} \times C_{HCl}\right) - 300}} \right\} \quad (5)$$

when $V_{CO2} \times C_{HCl} > 300$ ppm;

$$FED(I)_{HCN} = \left(\frac{t}{60}\right) \times \left(\frac{1}{564}\right) \times \sum \left\{ \left(V_{CO_2} \times C_{HCN}\right) - 63 \right\} \quad (6)$$

when $V_{CO2} \times C_{HCN} > 63$ ppm; and

$$FED(I)_{O_2} = \left(\frac{t}{60}\right) \times \sum \left\{ \frac{1}{\exp\left(8.55 - \left(0.511 \times \left(20.9 - C_{O_2}\right)\right)\right)} \right\} \quad (7)$$

when $C_{O2} < 11\%$. The value of t in these equations was the time in seconds between acquisition of FTIR spectra. The overall Fractional Effective Dose for Incapacitation was calculated by summing the terms in equations 2 through 7:

$$FED(I)_{TOTAL} = FED(I)_{CO_2} + FED(I)_{CO} + FED(I)_{HCl} + FED(I)_{HCN} + FED(I)_{O_2} \quad (8)$$

The Fractional Effective Doses for Lethality from exposure to carbon monoxide and hydrogen cyanide were calculated using the following equations modified to account for sampling intervals of less than 1 minute:

$$FED(L)_{CO} = \left(\frac{t}{60}\right) \times \sum \left\{ \frac{1}{\exp\left(5.85 - \left(0.00037 \times V_{CO_2} \times C_{CO}\right)\right)} \right\} \qquad (9)$$

when $2000 \leq V_{CO2} \times C_{CO} \leq 9000$ ppm,

$$FED(L)_{CO} = \left(\frac{t}{60}\right) \times \sum \left\{ \frac{1}{0.4 + \left(\frac{58{,}000}{V_{CO_2} \times C_{CO}}\right)} \right\} \qquad (10)$$

when $V_{CO2} \times C_{CO} > 9000$ ppm, and

$$FED(L)_{HCN} = \left(\frac{t}{60}\right) \times \left(\frac{1}{2586}\right) \times \sum \left\{ \left(V_{CO_2} \times C_{HCN}\right) - 43.2 \right\} \qquad (11)$$

when $V_{CO2} \times C_{HCN} > 43.2$ ppm;

The overall Fractional Effective Dose for Lethality was calculated by summing the terms in equations 8 through 10:

$$FED(L)_{TOTAL} = FED(L)_{CO} + FED(L)_{HCN} \qquad (12)$$

The model described by Purser also uses a multiplication factor to account for the enhanced respiratory uptake of toxic gases because of exposure to elevated levels of carbon dioxide:

$$V_{CO_2} = \frac{\exp\left(1.9086 + \left(0.2496 \times C_{CO_2}\right)\right)}{6.8} \qquad (13)$$

The Fractional Effective Doses for Incapacitation from exposure to carbon monoxide and hydrogen cyanide were calculated using the following equations modified to account for sampling intervals of less than 1 minute:

$$FED(I)_{CO_2} = \left(\frac{t}{60}\right) \times \sum \left\{ \frac{1}{\exp\left(6.1623 - \left(0.5189 \times C_{CO_2}\right)\right)} \right\} \quad (14)$$

when $C_{CO2} > 5\%$,

$$FED(I)_{CO} = \left(\frac{t}{60}\right) \times V_{CO_2} \times \sum \left\{ \frac{0.00082925 \times C_{CO}}{30} \right\} \quad (15)$$

where the units of C_{CO} are ppm,

$$FED(I)_{HCN} = \left(\frac{t}{60}\right) \times V_{CO_2} \times \sum \left\{ \frac{4.4}{185 - C_{HCN}} \right\} \quad (16)$$

when $80 \leq C_{HCN} \leq 180$ ppm,

$$FED(I)_{HCN} = \left(\frac{t}{60}\right) \times V_{CO_2} \times \sum \left\{ \frac{1}{\exp\left(5.396 - \left(0.023 \times C_{HCN}\right)\right)} \right\} \quad (17)$$

when $C_{HCN} > 180$ ppm; and

$$FED(I)_{O_2} = \left(\frac{t}{60}\right) \times \sum \left\{ \frac{1}{\exp\left(8.13 - \left(0.54 \times \left(20.9 - C_{O_2}\right)\right)\right)} \right\} \quad (18)$$

when $C_{O2} < 11.3\%$.

As in the FAA model, the value of t in these equations was the time in seconds between acquisition of FTIR spectra. The overall Fractional Effective Dose for Incapacitation was calculated by summing the terms in equations 14 through 18:

$$FED(I)_{TOTAL} = FED(I)_{CO_2} + FED(I)_{CO} + FED(I)_{HCN} + FED(I)_{O_2} \quad (19)$$

Both the FAA Combined Hazard Survival model and Purser's model predict that 50% of an exposed population would experience incapacitating narcosis (*i.e.*, an occupant loses consciousness and would be unable to exit a vehicle without assistance) when $FED(I)_{TOTAL} = 1.0$. Similarly, both of these models predict that 50% of an exposed population would die when $FED(L)_{TOTAL} \geq 1.0$.

7.2.1 Estimation of Fractional Equivalent Dose Parameters

The analysis presented in this section includes estimates of FED(I) and FED(L) for carbon dioxide, carbon monoxide, hydrogen cyanide, hydrogen chloride and oxygen using the FAA Combined Hazard Survival Model and Purser's model for assessment of the toxicity of combustion products. Other gaseous species included in the FAA Combined Hazard Model and Purser's model were not measured during this test; therefore, values of FED(I) or FED(L) were not estimated for these gases. Figures 70 through 74 show plots of $FED(I)_{co2}$, $FED(I)_{co}$, $FED(I)_{HCN}$, $FED(I)_{HCL}$, and $FED(I)_{O2}$ computed using the FAA Combined Hazard Survival Model and Purser's model for assessment of the toxicity of combustion products.

The concentrations of carbon dioxide, hydrogen cyanide, hydrogen chloride, and oxygen were less than the respective threshold concentrations for computing $FED(I)_{CO2}$ (Fig. 70), $FED(I)_{HCN}$ (Fig. 72), $FED(I)_{HCl}$ (Fig. 73), and $FEC(I)_{O2}$ (Fig. 74) at all times during this test. The threshold conditions for computing $FED(I)_{CO2}$ are $C_{CO2} > 5.5$ % in the FAA model and $C_{CO2} > 5$ % in Purser's model. The maximum concentration of carbon dioxide in the passenger compartment was 0.8% occurring at approximately 10½ minutes post-ignition (Plot I2 and Fig. 70).

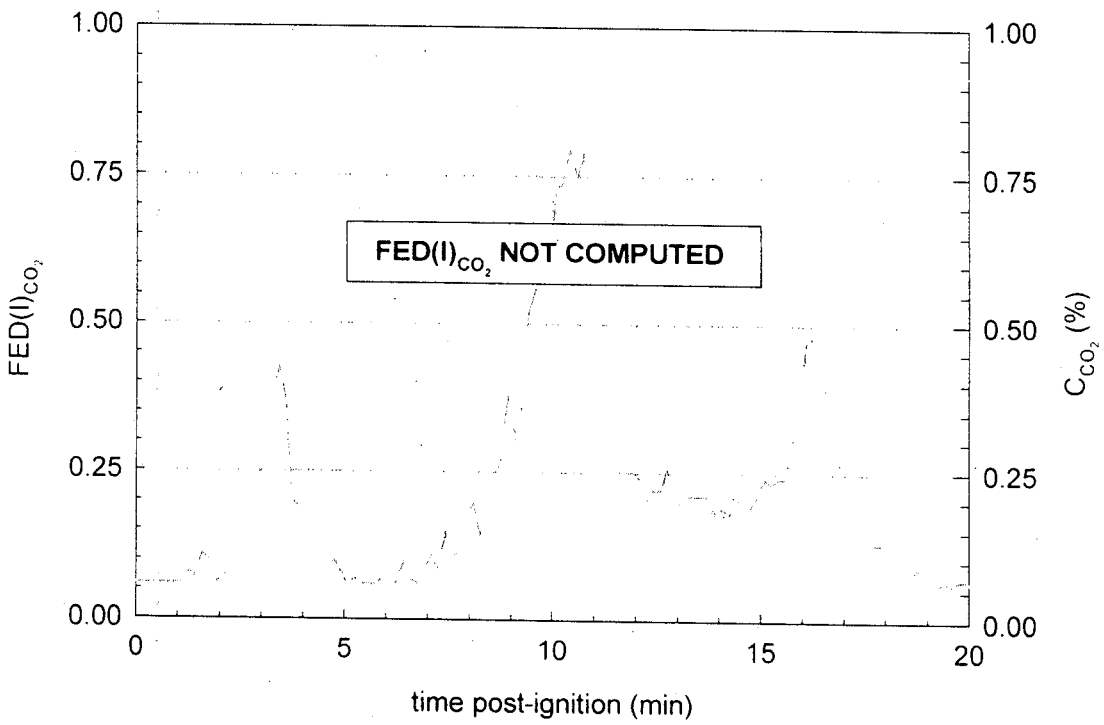

Figure 70. Fire Test F971003. The concentration of CO_2 was less than the threshold concentration for computing $FED(I)_{CO2}$ at all times during this test. A plot of C_{CO2} (——) is shown for reference.

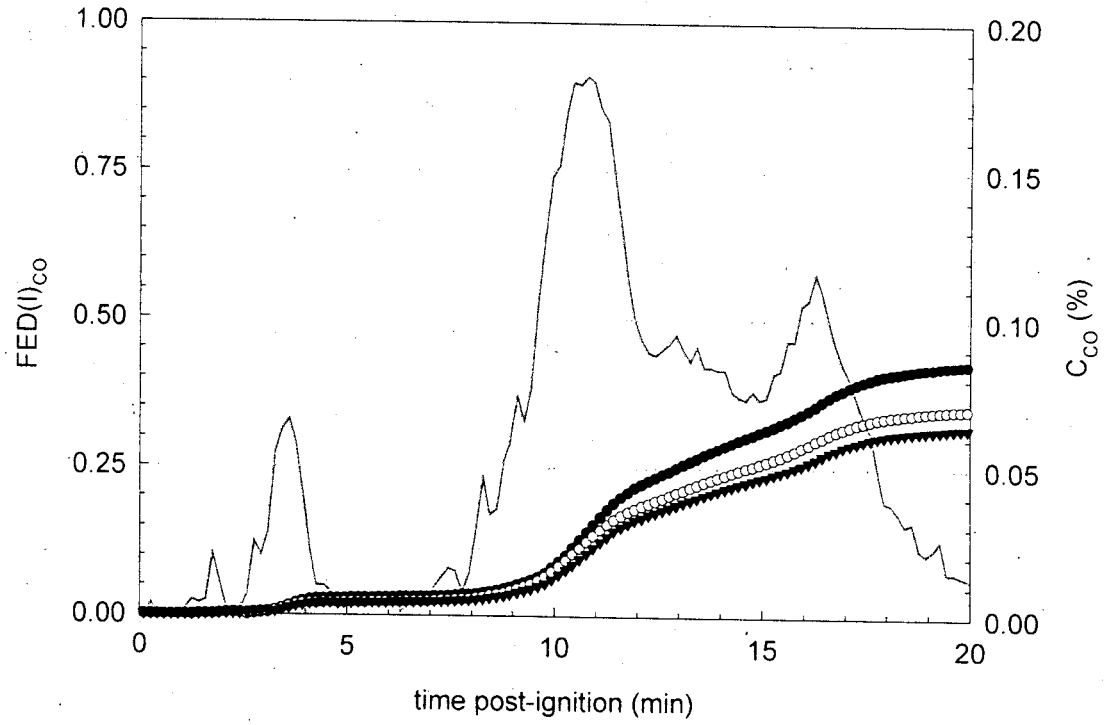

Figure 71. Fire Test F971003. Plots of estimates of $FED(I)_{CO}$ versus time post-ignition computed using the FAA Combined Hazard Survival Model (—○—), the Purser model with a respiratory minute volume of 8.5 L/min (—▼—), and the Purser model with a respiratory minute volume of 25 L/min (—●—). A plot of C_{CO} (——) is included for reference.

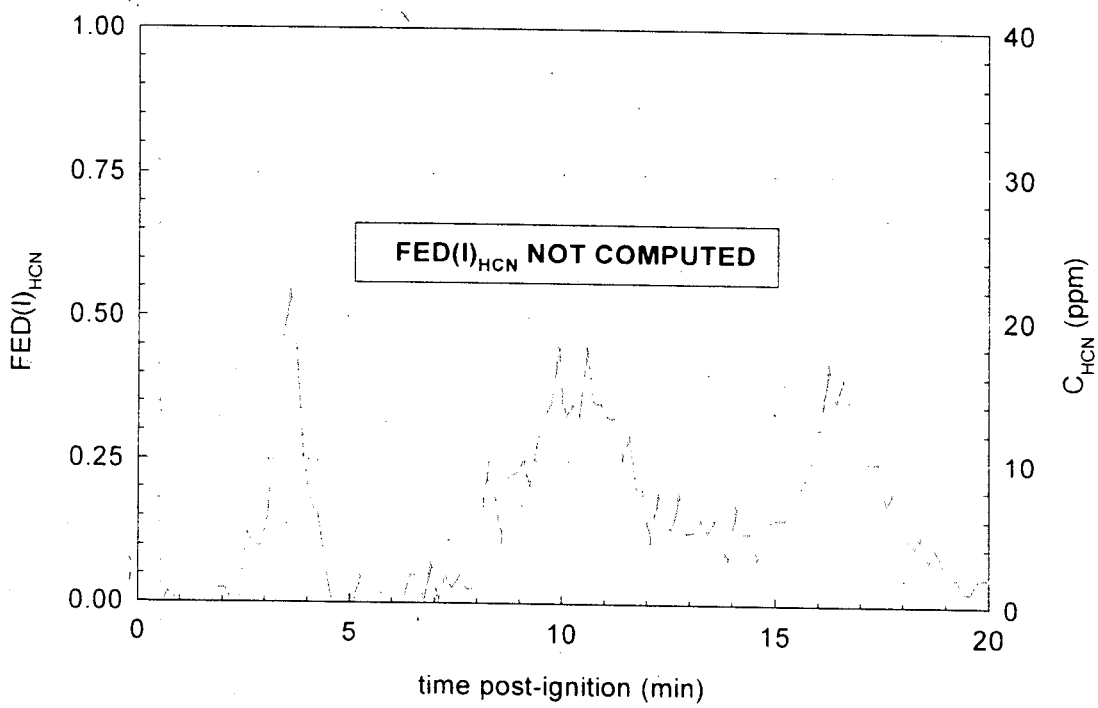

Figure 72. Fire Test F971003. The threshold conditions for computing $FED(I)_{HCN}$ were not satisfied at any time during this test. A plot of C_{HCN} (——) is shown for reference.

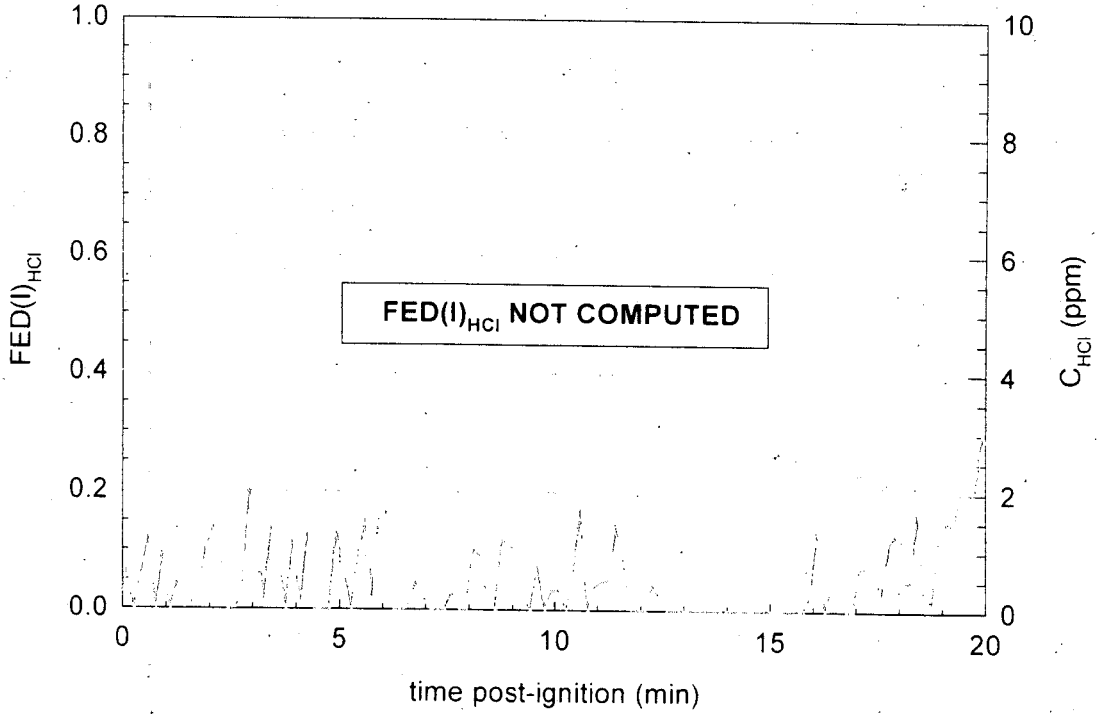

Figure 73. Fire Test F971003. The concentration of HCl was less that the threshold concentration for computing $FED(I)_{HCl}$ at all times during this test. A plot of C_{HCl} (——) is included for reference.

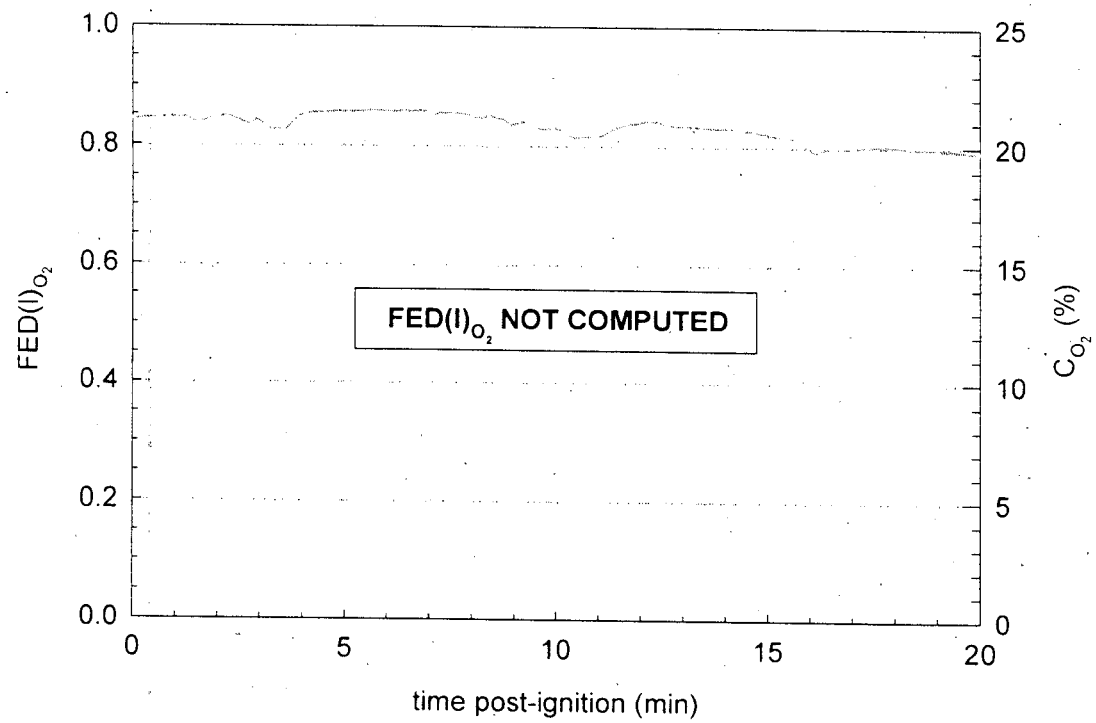

Figure 74. Fire Test F971003. The concentration of O_2 was greater that the threshold concentration for computing $FED(I)_{O2}$ at all times during this test. A plot of C_{O2} (——) is shown for reference.

The threshold conditions for computing $FED(I)_{HCN}$ are $(V_{CO2} \times C_{HCN}) > 63$ ppm in the FAA model and $C_{HCN} > 80$ ppm in Purser's model. The maximum concentration of hydrogen cyanide in the passenger compartment was 22 ppm occurring at approximately 3½ minutes post-ignition (Plot I7), with $(V_{CO2} \times C_{HCN}) \approx 24$ at this time. The threshold for computation for computing $FED(I)_{HCl}$ are $(V_{CO2} \times C_{HCl}) > 300$ ppm in the FAA model. Hydrogen chloride was not detected in the passenger compartment during this test (Plot I6 and Fig. 72). The threshold concentrations for computing $FEC(I)_{O2}$ are $C_{O2} < 11\%$ in the FAA model and 11.3% in Purser's model. The concentration of oxygen decreased from 21% at the start of this test to approximately 19% when the test was ended at about 16 minutes post-ignition (Fig. I9 and Fig 73).

Plots of the $FED(I)_{co}$ parameters estimated using both models are shown in Figure 71. The equations presented in the Purser model for computation of $FED(I)_{co}$ include a term for respiratory minute volume. Minute volumes corresponding to respiration during rest (8.5 L/min) and light activity (25 L/min) were used in these calculations [9]. Purser's model also accounts for the effect of exposure to carbon dioxide on respiratory rate. The FAA Combined Survival Hazard Model computes only one estimate of $FED(I)_{co}$, which accounts for the effect of exposure to carbon dioxide on respiratory rate [8]. The estimate of $FED(I)_{co}$ using the FAA model was approximately 0.29 at 16 minutes post-ignition and reached a maximum value of 0.35 at 20 minutes post-ignition. The estimate of $FED(I)_{co}$ using Purser's model with a respiratory minute volume of 8.5 L/min was approximately 0.34 at 16 minutes post-ignition and reached a maximum value of 0.43 at 20 minutes post-ignition.

Plots of the $FED(I)_{TOTAL}$ parameters estimated using both models are shown in Figure 75. Since $FED(I)_{CO2}$, $FED(I)_{HCN}$, $FED(I)_{HCl}$, and $FEC(I)_{O2}$ were not computed, $FED(I)_{CO}$ was the only contribution to the estimated of $FED(I)_{TOTAL}$ shown in Figure 75.

The concentrations of carbon dioxide, carbon monoxide, and hydrogen cyanide were less than the respective threshold concentrations for computing $FED(L)_{CO}$, $FED(L)_{HCN}$, or $FED(I)_{TOTAL}$ (Fig. 76). The threshold condition for computing $FED(L)_{CO}$ is $(V_{CO2} \times C_{CO}) > 9000$ ppm. The maximum concentration of carbon monoxide in the passenger compartment was approximately 1440 ppm occurring at approximately 10.75 minutes post-ignition (Plot I1), with $(V_{CO2} \times C_{CO}) \approx 0.22$ at this time. The threshold condition for computing $FED(L)_{HCN}$ is $(V_{CO2} \times C_{HCN}) > 43.2$ ppm. The maximum concentration of hydrogen cyanide in the passenger compartment was 22 ppm occurring at approximately 3.5 minutes post-ignition (Fig. I7), with $(V_{CO2} \times C_{HCN}) \approx 24$ at this time

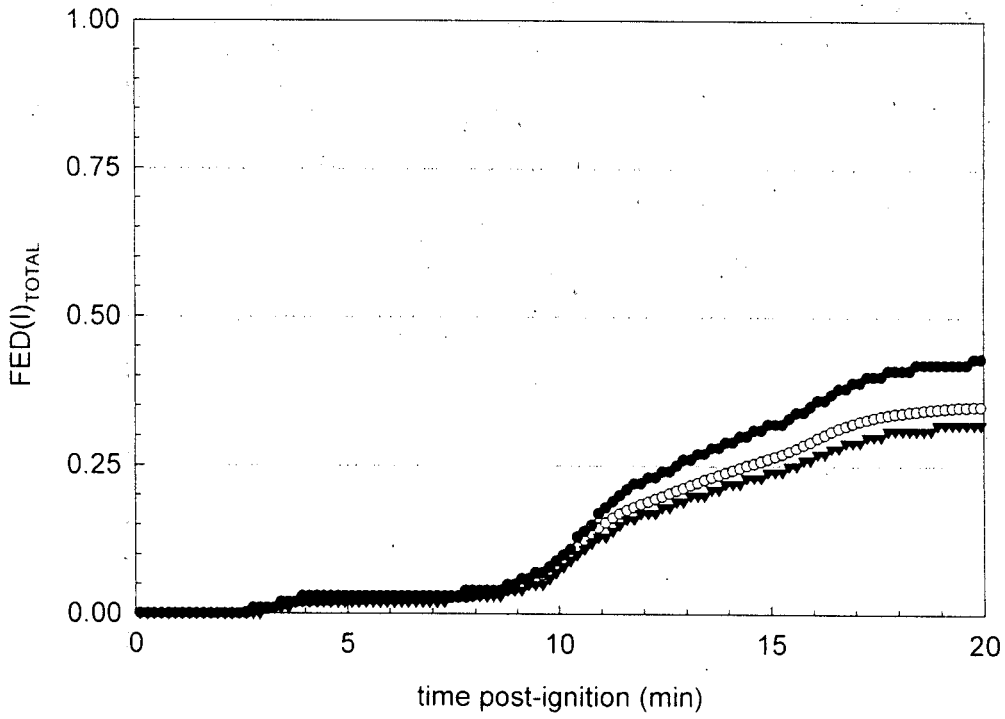

Figure 75. Fire Test F971003. Plots of $FED(I)_{TOTAL}$ versus time post-ignition: FAA Combined Hazard Survival Model (—○—); Purser's model with RMV = 8.5 L/min (—▼—); and Purser's model with RMV = 25 L/min (—●—).

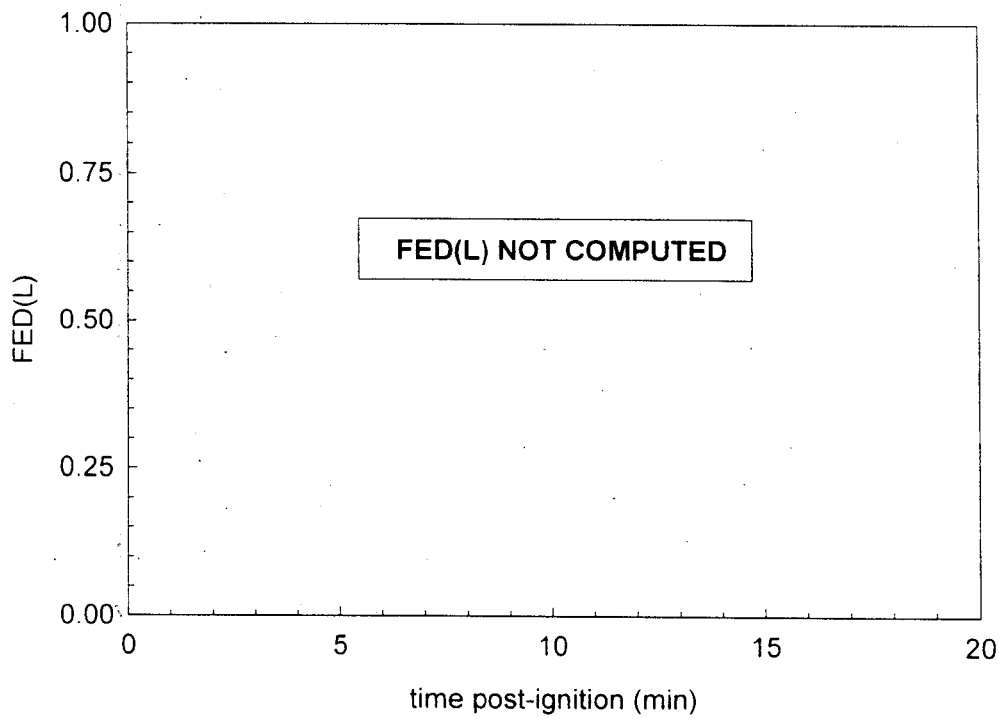

Figure 76. Fire Test F971003. The concentrations of CO and HCN were less that the threshold concentrations for computing $FED(L)_{CO}$, $FED(L)_{HCN}$, or $FED(L)_{TOTAL}$ at all times during this test.

As stated previously, the estimates of FED(I) and FED(L) obtained using the FAA Combined Hazard Survival Model and Purser's model of combustion gas toxicity cannot predict precisely whether or when the gas concentrations measured in this test would have resulted in incapacitating narcosis or death. This is especially true for prediction of lethality, where the mathematical relationships in these models were derived from experiments using laboratory animals or accidental, uncontrolled human exposures [8, 9]. Variation in the susceptibility to these hazards among the human population also will contribute to the uncertainty in these predictions. In addition, the effect of trauma caused by the crash on an occupant's tolerance to these toxic gases is impossible to quantify.

Another variable that may affect an occupant's susceptibility to the combustion products is the location of the head. The data from the aspirated thermocouples indicated that a steep air-temperature gradient developed in the front of the passenger compartment during this test. Since both heat and mass are conserved in a fire, the existence of a steep vertical air-temperature gradient implies the existence of a similarly steep vertical concentration gradient for combustion products accumulating in the passenger compartment. The inlet to the gas sampling tube in the passenger compartment was in the breathing zone of that of a six-foot tall adult male sitting upright in either the driver's or front passenger's seat. An occupant whose head was located below the level where gases were sampled would have been exposed to lower concentrations of combustion gases that those shown in **APPENDIX I**. And the estimated values of FED(I) and FED(L) for this occupant would have been lower than those shown in Figures 61 through 67.

7.3 Estimation of Burn-Injury to the Respiratory Tract

The plots of air temperature shown in Figures 55 and 56 indicate the temperature of the air inhaled by an occupant in the front of the test vehicle would have depended on the height of the occupant's head. Maximum air temperatures occurred at 15:50 minutes:seconds post-ignition. Air temperatures of 328 and 256°C were recorded at the headlining panel above the driver's and front passenger's seats, respectively. The air temperature decreased by approximately 8°C/cm below the headlining panel above the driver's seat and by approximately 5.6°C/cm below the headlining panel above the front passenger's seat.

It is not possible to estimate the potential for burn injury to the respiratory tract caused by inhalation of hot air by relying solely on air temperature data. Water and particulate produced by the fire increase the heat capacity of the air. The concentrations of these species in the inhaled air have been shown to affect both the severity and depth of burn injury in the respiratory system.

Neither the water- nor the particulate-concentrations of air in the passenger compartment were measured in this test. Purser states that a robust quantitative relationship between the temperature, water-content, and particulate-content of inhaled air and subsequent burn injury to respiratory airways has not been established [7]. A few controlled animal studies indicate that inhalation of steam at 100°C caused burns to the larynx and trachea similar to those produced by inhalation of dry air at 350°C or flames at 500°C [see references in 7]. In these controlled animal studies, death was not immediate, but resulted from obstructive edema in the burned airways a few to twenty-four hours after the exposure. As the concentration of water vapor in the air sampled from the passenger compartment was not measured during this test, the potential for burn injury to the respiratory airways from inhalation of hot gas cannot be determined accurately from the air temperature data shown.

8 Experimental Fire Detectors

Two experimental fire detectors were installed in the engine compartment of the test vehicle for this test. One of the experimental fire detectors was a linear device supplied by Santa Barbara Dual Spectrum (Goleta, CA). The other experimental fire detector was a pneumatic device also supplied by Santa Barbara Dual Spectrum (Goleta, CA). Both of these experimental fire detectors were attached to the underside of the deformed hood and spanned the width of the engine compartment (See **APPENDIX G**). Plots of the output signals from these experimental fire detectors are shown in Figure 77.

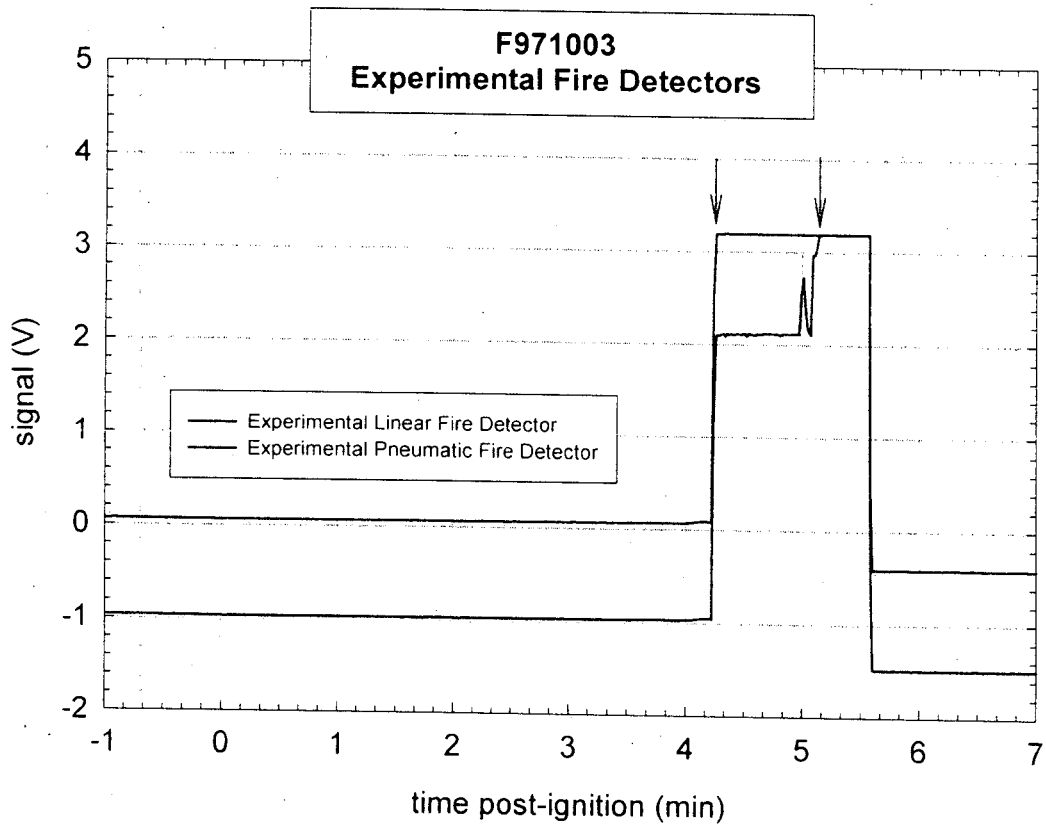

Figure 77. Fire Test F971003. Plots of output signals from the experimental linear fire detector and the experimental pneumatic fire detector installed in the test vehicle for this test. The arrows indicate the times of contact closure in the respective experimental fire detectors.

The experimental linear fire detector was a length of two insulated, twisted wires. The insulation on the wired melted or burned when exposed to heat of flames, causing contact to be made between the two wires. The signal for fire detection with this device was a contact closure.

The experimental pneumatic fire detector consisted of a metal tube packed with a metal hydride. This tube was sealed at one end and connected to a pressure transducer at the other end. The metal hydride inside the sealed tube released hydrogen gas when exposed to heat of flames, causing the pressure inside the tube which results in contact closure in the pressure transducer. The signal for fire detection with this device was a contact closure.

These data plots in Figure 77 indicate that contact closure occurred at 4 minutes 14 seconds post-ignition in the experimental linear fire detector and at 5 minutes 36 seconds post-ignition in the experimental pneumatic fire detector.

ACKNOWLEDGEMENTS

Dr. Thomas Ohlemiller and Thomas Cleary of the Building and Fire Research Laboratory, National Institute of Standards and Technology were responsible for video taping this fire test, and provided an initial analysis of the test data for fire propagation. Dr. Archibald Tewarson of Factory Mutual Research Corporation provided the data from the Fire Products Collector at the test facility that was collected during this test.

REFERENCES

1. Jack L. Jensen and Jeffrey Santrock. Evaluation of Motor Vehicle Fire Initiation and Propagation. Part 1: Vehicle Crash Test and Fire Propagation Test Program. Submitted to the National Highway Transportation Safety Administration pursuant to the Settlement Agreement between General Motors and the Department of Transportation. Submitted July 31, 1997.

2. Jack L. Jensen and Jeffrey Santrock. Evaluation of Motor Vehicle Fire Initiation and Propagation. Part 5: Crash Tests on a Rear Wheel Drive Passenger Car. To be submitted to the National Highway Transportation Safety Administration pursuant to the Settlement Agreement between General Motors and the Department of Transportation.

3. SigmaPlot® 4.0 for Windows®, SPSS Inc., 444 North Michigan Avenue, Chicago, IL 60611. Copyright © 1997 by SPSS Inc..

4. Archibald Tewarson. "Generation of Heat and Chemical Compounds in Fires" Section 3/Chapter 4, SFPE Handbook of Fire Protection Engineering, 2nd Edition, 1995, pp. 3:53-124.

5. F. S. Knox III, Dena Bonetti, and Chris Perry. User's Manual for BRNSIM/BURNSIM: A Burn Hazard Assessment Model. United States Army Aeromedical Research Laboratory Report No. 93-13. Fort Rucker, Alabama 36362-5292. February 1993.

6. L. C. Speitel. Toxicity Assessment of Combined Gases and Development of a Survival Model. DOT/FAA/AR-95-5. July 1995.

7. David A. Purser. "Toxicity Assessment of Combustion Products" Section 2/Chapter 8, SFPE Handbook of Fire Protection Engineering, 2nd Edition, 1995, pp. 2:85-146

APPENDIX A
VIDEO CAMERA SET-UP

Scientific and technical personnel from the Building and Fire Research Laboratory, National Institute of Standards and Technology were primarily responsible for obtaining a video record of this test. Ten video cameras were used in this test. Figure A1 shows the approximate locations of the video cameras relative to the test vehicle during this test.

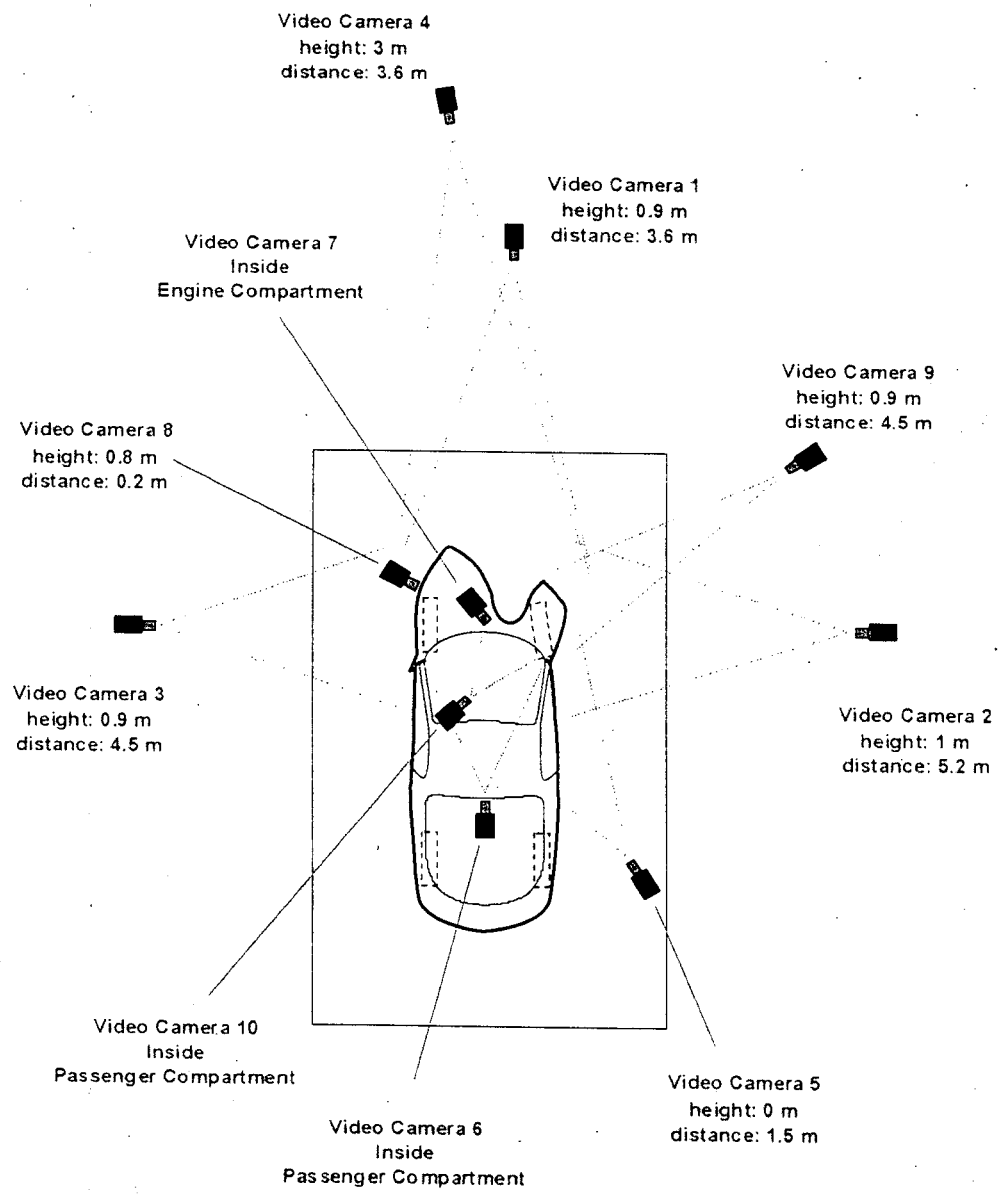

Figure A1. Fire Test F971003 Diagram showing the approximate locations of the video cameras during this test. Distances in this figure are not to scale in this diagram.

Camera 1 was a Hi-8 camcorder mounted on a tripod. It had a field-of-view that included the full height and width of the front of the test vehicle. Camera 2 was a Hi-8 camcorder mounted on a tripod. It had a field-of-view that included the full height of the test vehicle from the front bumper fascia to the middle of the right door. Camera 3 was a Hi-8 camcorder mounted on a tripod. It had a field-of-view that included the full height of the test vehicle from the front bumper fascia to the middle of the left door. Camera 4 was a Hi-8 camcorder mounted on a tower fixture approximately 3m above the test vehicle. Its field-of-view included the front of the test vehicle from the hood to the top of the windshield. Camera 5 was a Hi-8 camcorder mounted on a tripod approximately 27cm above the surface of the fluid containment pan. Its field of view included was a right rear quarter angle view, that shows the right side passenger door and front fender and underneath of the vehicle. Camera 6 was a black and white CCD device. Mounted on the package shelf behind the rear seat back. Its field-of-view included the top of the IP to the floor on passenger side of vehicle. Camera 7 was a black and white CCD device located inside the engine compartment mounted on the engine. Its field of view included the area where the propane torch was located. A small photo light was added to illuminate this area. Camera 8 was a black and white CCD device mounted on the left front fender. Its field of view included the left side of the engine compartment. Camera 9 was a Hi 8 video camera, mounted on a tripod. Its field of view included the right side of the engine compartment. Camera 10 was a black and white CCD device. It was suspended from the roof by a steel threaded rod. Its field of view included from the drivers' seatback, looking toward mid console and passenger airbag area.

All video cameras were started before the test. A microphone on each camera recorded the air horn, which signaled removal of the plug from the hole in filler neck, ignition of the gasoline, and the end of the test.

Quartz-halogen floodlights were used to illuminate the exterior of the vehicle. The level of illumination provided by these lamps was insufficient to balance the intensity of light reflecting from the vehicle surfaces with the brightness of the flames. To compensate for this imbalance, the light sensitivity adjustments on the Hi-8 camcorders were set to the manual position so that the apparent brightness of the vehicle surfaces did not change as the fire developed. As a result, the flames were overexposed, causing them to appear more opaque than they actually were.

APPENDIX B
INFRARED THERMOGRAPHY

Infrared thermal imaging radiometers were used to help determine fire propagation, flame, and surface temperatures during this test. These imaging systems measure thermal radiation within a definite waveband, over a variable field of view. The data obtained from these measurements can be analyzed to produce a two-dimensional map of apparent temperature called a thermogram.

Thermal imaging systems produce a spatially resolved map of surface temperatures from the radiant energy emitted in the field of view. The response time of these systems is nanoseconds, giving them the capability to acquire over 1 million discrete measurements per second. The capability of high-speed data acquisition is advantageous in that it can provide a tremendous amount of thermal data during a vehicle fire test, which can be over in only a few minutes. Thermal imaging radiometers can be used concurrently as a vision system and a measurement system. However, the thermal sensitivity, scan speed, and spatial resolution must be optimized for a particular application.

B.1 Infrared Camera Location

Figure B1 shows the approximate locations of the infrared cameras relative to the test vehicle during this test. IR1 through IR5 were mounted outside the test vehicle. IR1 was an Agema Model 900 thermal imaging system with an optical window of 3 to 14 μm. It's filed-of-view included the front of the test vehicle. IR2 was an Inframetrics Model 760 thermal imaging system with an optical window of 3 to 14 μm. Its field-of-view included the front right quarter of the test vehicle. IR3 was an Inframetrics Model 760 thermal imaging system with an optical window of 3 to 14 μm. Its field-of-view included the front left side of the test vehicle. IR4 was an Agema Model 900 thermal imaging system with an optical window of 3 to 14 μm. It was focused through the right side window opening into the interior of the test vehicle. It's field-of-view included the portions of the instrument panel, the front seats, and the left door interior trim panel. IR5 was an Inframetrics 740 thermal imaging system (Inframetrics Inc, Billerica, MA) with an optical window of 3 to 14 μm. It was focused through the right side window opening into the interior of the test vehicle. It's field-of-view included portions of the windshield and instrument panel.

IR6 was located inside the test vehicle. IR6 was a Flir Model 7300 thermal imaging radiometer (Flir Systems, Inc., Portland, OR) with an optical window of 3 to 5 μm. This system was placed in an insulated metal box located in the rear compartment. Its field-of-view included the central portions of the windshield and upper instrument panel.

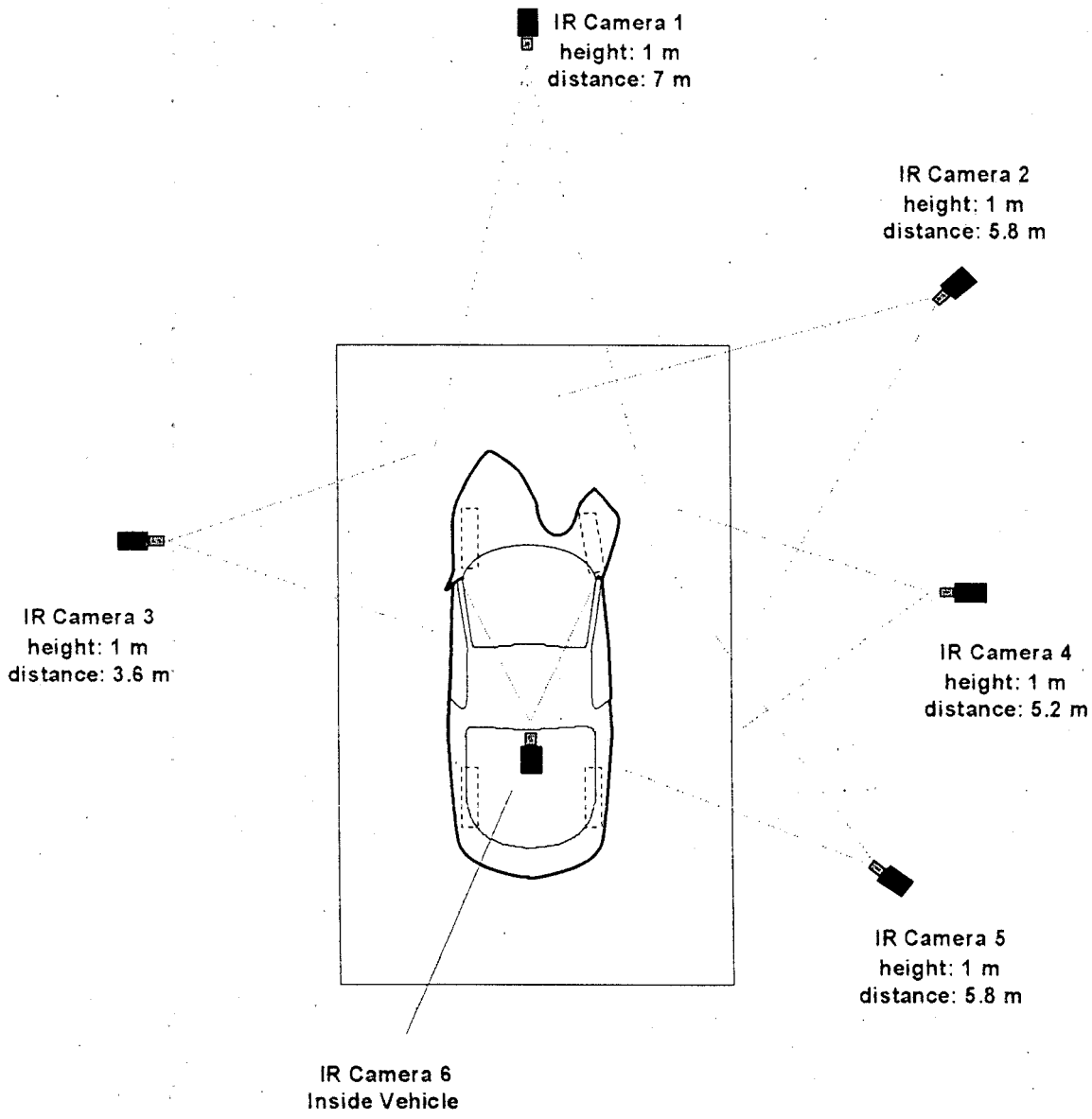

Figure B1. Fire Test F971003. Placement of infrared thermal imaging systems around the test vehicle during this test. Distances and heights are approximate and not to scale in this diagram.

B.2 Data Analysis

Thermal imaging systems measure infrared radiation within a certain spectral band and must be calibrated to convert radiant intensity in that spectral band to temperature. Due to variations in system response, every system has to be calibrated. Calibration curves for the basic thermal imaging radiometers are measured at the factory and stored in read-only memory or in analysis

software programs. Additional calibrations are needed for the optical filters. These calibrations are stored in the analysis software programs. Since thermal imaging radiometers are AC coupled devices, they measure differences in thermal radiation. To get absolute temperatures, there must be a reference to provide DC restoration. In these instruments, the reference is an internal blackbody reference source that is viewed periodically by the detector.

The general radiometric equation was used to convert radiant energy to temperature:

$$\hat{I} = [E_t \times F(T_t)] + [(1 - E_t) \times F(T_b)] - [E_r \times F(T_r)] - [(1 - E_r) \times F(T_b)] \qquad \text{(B1)}$$

Where I is the difference in radiance between the target and a reference surface; E_t is the emittance of the target surface, generally unknown; E_r is the emittance of the reference surface, T_t is the temperature of the target surface; T_b is the temperature of background surfaces (i.e., ambient temperature), or other emitters such as flames reflected from the target; T_r is the temperature of the reference surface; $F(T_t)$ is the radiance from an ideal emitting surface (i.e., black body) at the temperature of the target surface (T_t); $F(T_r)$ is the radiance from an ideal emitting surface at the temperature of the reference (T_r); and $F(T_b)$ is the radiance from the background relative to the radiance value from the reference surface when $E_r = 1$. Factors other than temperature determine the emittance of an object. These factors include the type of material, the texture of the surface, the wavelength of the detector, and the view-angle. In determining temperatures from the radiant energy from an object, the operator can set the emittance of an unknown target surface to a value of between .01 and 1.0.

Radiant intensity measured by the thermal imaging system is converted to a gray-scale value. An 8 bit system provides gray scale values from 0 to 255 for the radiant energy at each pixel in the instantaneous field of view. A 12 bit system provides gray scale values from 0 to 4095. As the radiometer scans the image, each pixel is assigned a gray scale value, and the gray scale image is stored either in a computer memory or onto videotape. When stored in computer memory, a single frame (1 thermogram) can contain up to 68,000 pixels (discrete measurements) with an assigned 8 bit or 12 bit value. Videotape provides a temporal resolution of 30 frames per second. Depending on the thermal range of the thermal imaging radiometer, a temperature value was assigned to each pixel using either the factory calibration curves accompanying each instrument, or calibration curves stored in IR analysis software.

Separation of the apparent temperatures of various surfaces on and inside a burning vehicle from the captured data is not a trivial task. The data represent a complex combination of emitted infrared energy from those surfaces as well as reflected infrared energy from the flames, and

reflected infrared energy from high intensity lights used to illuminate the vehicle for visual data capture. In addition, the flames themselves were emitting infrared radiation due to their sooty content, some part of which was captured by the infrared thermal imaging systems. Also, some of the infrared radiation being emitted by the vehicle surfaces had to pass through flames containing soot from incomplete combustion of synthetic polymers or through clear (clean) flames where more complete combustion was occurring, and/or a combination of both types of flames. In all of these cases, gases in the flame absorbed some of the infrared radiation emitted by objects behind the flame.

The following steps were taken to minimize the impact of unwanted infrared radiation being captured by the thermal imaging systems.

- Anti-reflection tapes, paint, and glazes were applied to highly reflective surfaces on the test vehicle to minimize interference from reflections of the video floor and spot lights on the test vehicle.
- The thermal imaging systems were located in the shadows of the vehicle to block the video lights from shining directly into the radiometer.
- In some cases, flame filters (3.9 μm) were used in an attempt to screen out a portion of the infrared radiation from flames.

Despite these precautions, accurate surface temperatures could not be determined for areas of the vehicle blocked by intense flame. As a result, only surface temperatures determined to be reliable by the IR analysts are reported here. In some cases, specialized data analysis techniques were used to obtain reliable surface temperatures from areas in close proximity to, but not shielded by flame. Where possible, temperature data were reported from areas that lie in the shadow of the flames, which comes from highly emissive surfaces not affected by the flame radiation, and/or is deemed reliable based on the experience of the analysts. Data from nearby thermocouples were compared to IR temperature readings for a more comprehensive analysis.

During the data analysis, the videotapes were reviewed frame-by-frame to observe the burn sequence. The analyst captured images from selected frames on a video board. The image was processed to produce a digitized gray scale value for each element in the pixel matrix utilizing the camera settings automatically documented between video frames on the videotape during data acquisition. Thermograms were produced from the digitized image matrix using a commercial software package (Thermogram Pro V1.3, sold by Inframetrics, Inc., Billerica, MA). This software utilized the NIST traceable calibration tables supplied by the manufacturer with each thermal imaging system.

APPENDIX C
THERMOCOUPLE DATA

The thermocouples used in this test were type-N thermocouples fabricated by Medtherm Corporation (Huntsville, AL). Each thermocouple consisted of an ungrounded thermocouple junction (30 AWG thermocouple wire) enclosed in an Inconel 600 sheath insulated with magnesium oxide (o.d. = 0.040 in. (1 mm), length = 50 ft. (15.2 m)). A transition was made through a stress-relief bushing to a duplex thermocouple extension cable (24 AWG) with fiberglass insulation and a stainless steel over-braid (length = 1 ft. (0.28 m)). Each thermocouple wire terminated in a grounded, compensated Type-N thermocouple plug. The thermocouples were connected to the data acquisition system using Type-N thermocouple extension cables (length = 50 ft. (15.2 m)).

The data acquisition system consisted of a PC (75 MHz Pentium Processor, 16 MB RAM, an 814 MB hard disk, and a 16-bit, Model BG45-AP5CP, ACER Inc., Taiwan R. O. C.) with a 100 kHz I/O board with 16 analog input channels (DaqBoard 200A, IOTech, Inc., Cleveland, OH). Thermocouple multiplex expansion cards (DBK-19, IOTech, Inc., Cleveland, OH) were used for data acquisition from the thermocouples. The expansion cards were mounted in an electronics cabinet and hard-wired to a panel containing compensated Type-N thermocouple jacks.

To reduce electronic noise on the thermocouples, the ground leads from each thermocouple jack was connected to the electronic chassis ground of the thermocouple mutliplex extension cards. The vehicle chassis was connected to the electronic chassis ground by a large-gauge cable. The electronic chassis ground was connected to an isolated earth ground.

The data acquisition software (DASYLab, Daten System Technik GmbH, Mönchengladbach, Germany) was configured to sample each channel at a rate of 10 Hz and store the data in 10-point block averages.

Figures C1 through C7 show the approximate locations of thermocouples in the test vehicle. Plots C1 through C100 show plots of the temperature data recorded from these thermocouples during this test.

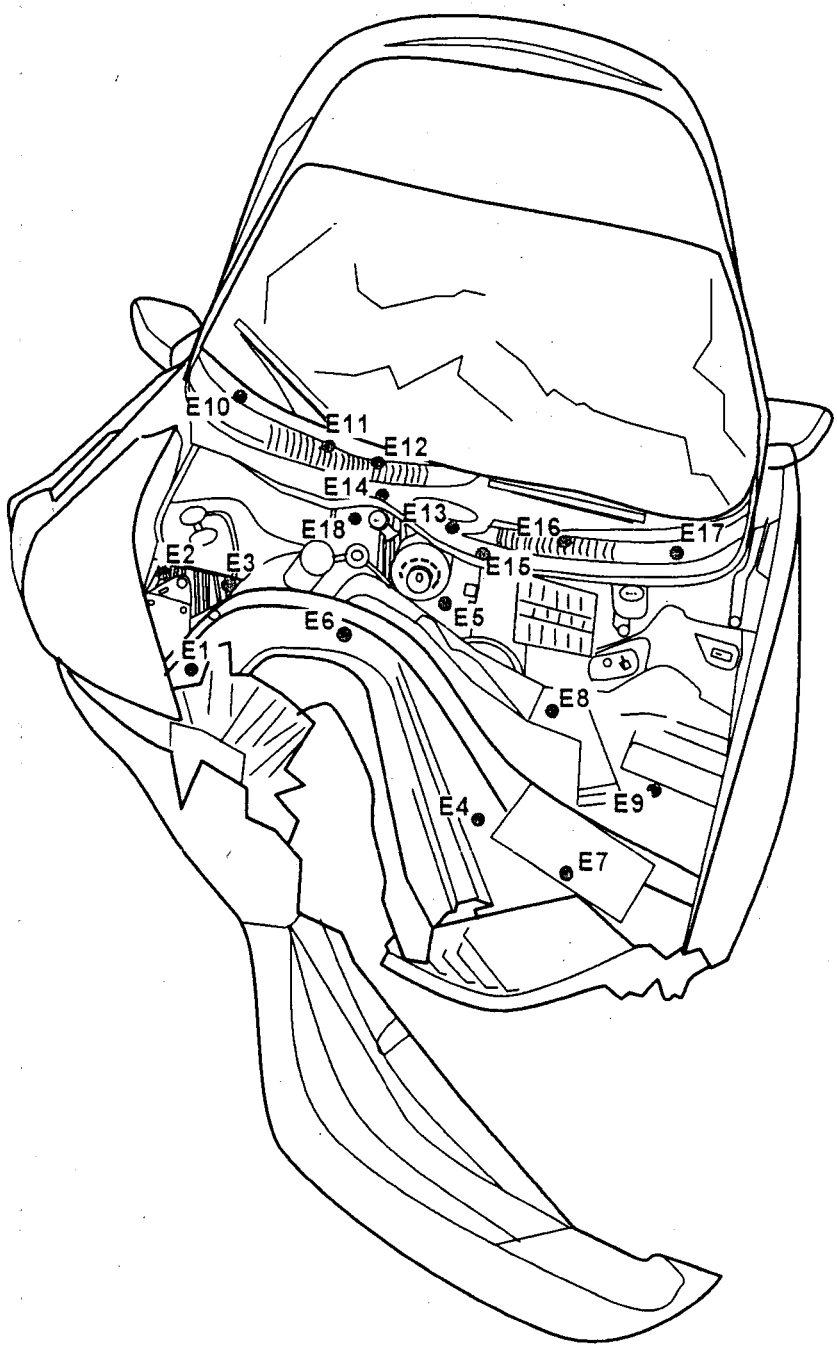

Figure C1. Fire Test F971003. Diagram showing the approximate locations of thermocouples in the engine compartment of the test vehicle. Thermocouple E1 was on the right front inner fender. Thermocouple E2 was on the coolant overflow reservoir cap. Thermocouple E3 was on the battery. Thermocouples E4 and E6 were on the windshield washer fluid reservoir. Thermocouples E5, E8, and E9 were on the air intake. Thermocouple E7 was on the upper radiator support member. Thermocouples E10, E11, E12, E13, E14, E16, and E17 were located under the HVAC Air Intake Screen. Thermocouple E18 was located under the HVAC Air Intake Cowl above the propane torch igniter installed in the engine compartment for this test. Thermocouple E15 was located on HFT/RAD3 (see Figure D2).

Figure C2. Fire Test F971003. Diagram showing the approximate locations of thermocouples on the windshield of the test vehicle. Thermocouples W1 through W10 were located approximately 1 cm in front of the outer surface of the windshield.

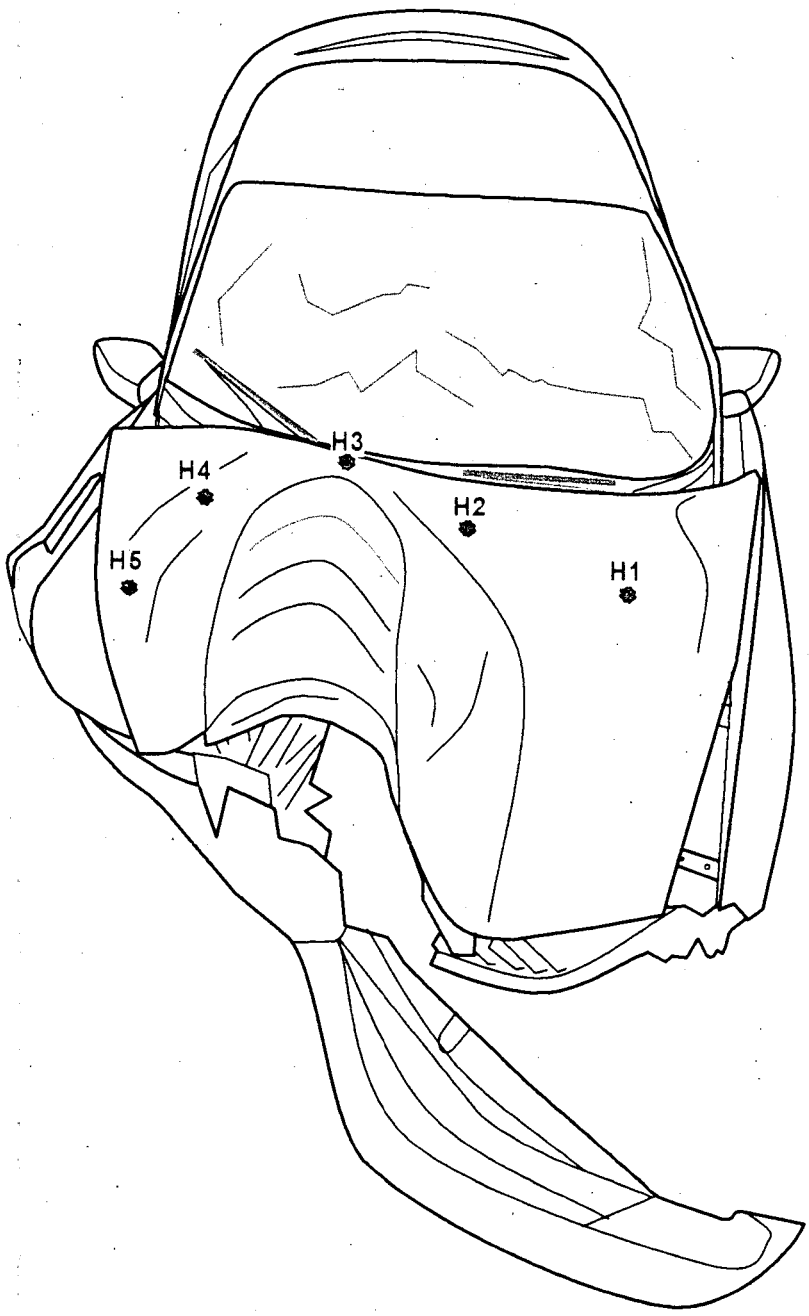

Figure C3. Fire Test F971003. Diagram showing the approximate locations of thermocouples on the hood of the test vehicle. Thermocouples H1 through H5 were located approximately 1 cm below the lower surface of the hood liner on the under-side of the hood.

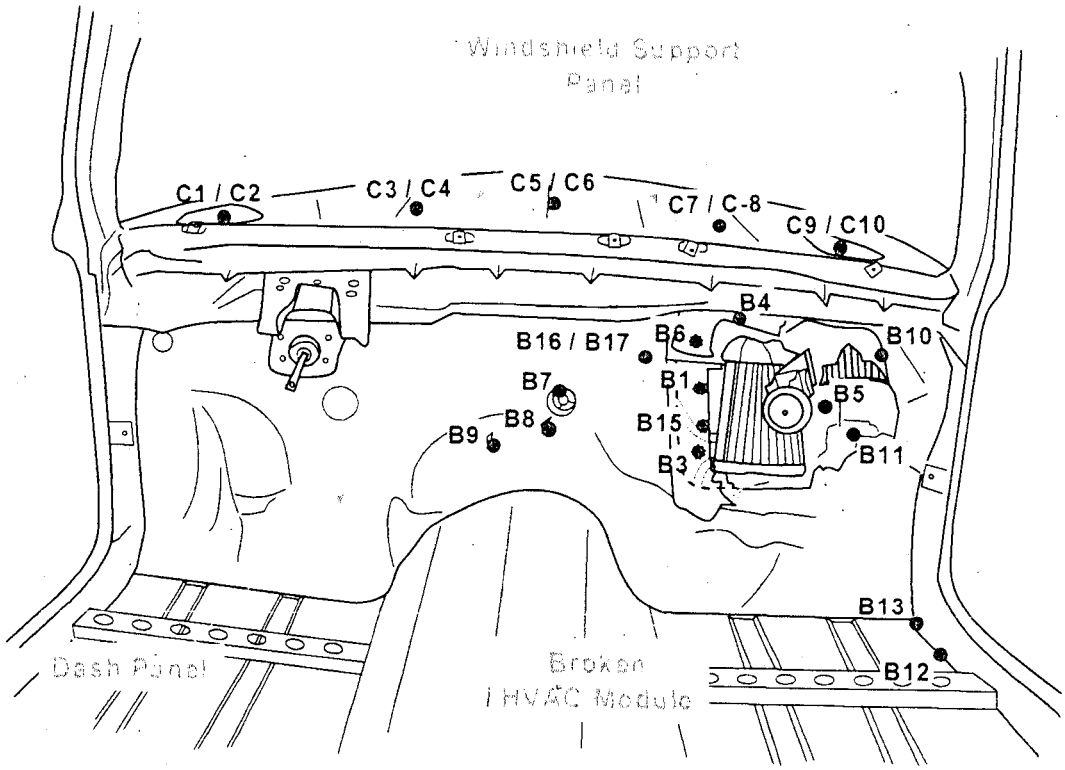

Figure C4. Fire Test F971003. Diagram showing the approximate locations of thermocouples on the windshield support panel, dash panel, and HVAC module in the test vehicle. Thermocouples C1, C3, C5, C7, and C9 were located approximately 1 cm below the lower surface of the windshield support panel. Thermocouples C2, C4, C6, C8, and C10 were located on the upper surface of the windshield support panel. Thermocouples B1, B3, and B15 were located in the HVAC pass-through in the dash panel. Thermocouples B7, B8, and B9 were located in tear-holes in the dash panel from transmission housing mounting bolts. Thermocouples B4, B5, B6, B10, and B11 were located on pieces of the broken HVAC module. Thermocouples B12 and B13 were located in seam openings between the floor pan panel and rocker panel. Thermocouple B16 was located approximately 1 cm in front of the outer surface of the dash panel. Thermocouple B17 was located on the inner surface of the dash panel. Thermocouples B2 and B14 were located on HFT/RAD1 and HFT/RAD2, respectively (see Figure D1).

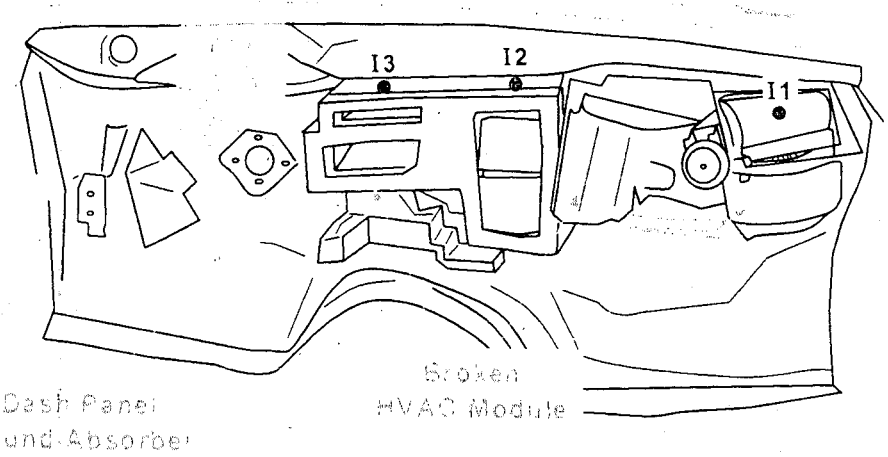

Figure C5. Fire Test F971003. Diagram showing the approximate locations of thermocouples on the HVAC module in the test vehicle. Thermocouple I1 was located on the air selector mode door. Thermocouples I2 and I3 were located in the airspace inside of the distribution case of the HVAC module.

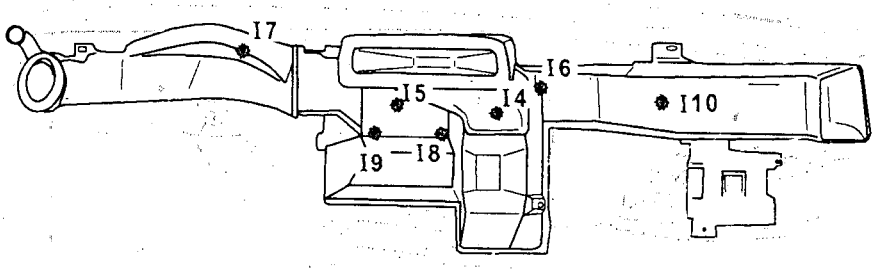

Figure C6. Fire Test F971003. Diagram showing the approximate locations of thermocouples on the HVAC distribution duct assembly of the test vehicle. Thermocouples I4 through I10 were located in the airspace inside of the distribution case of the HVAC distribution ducts.

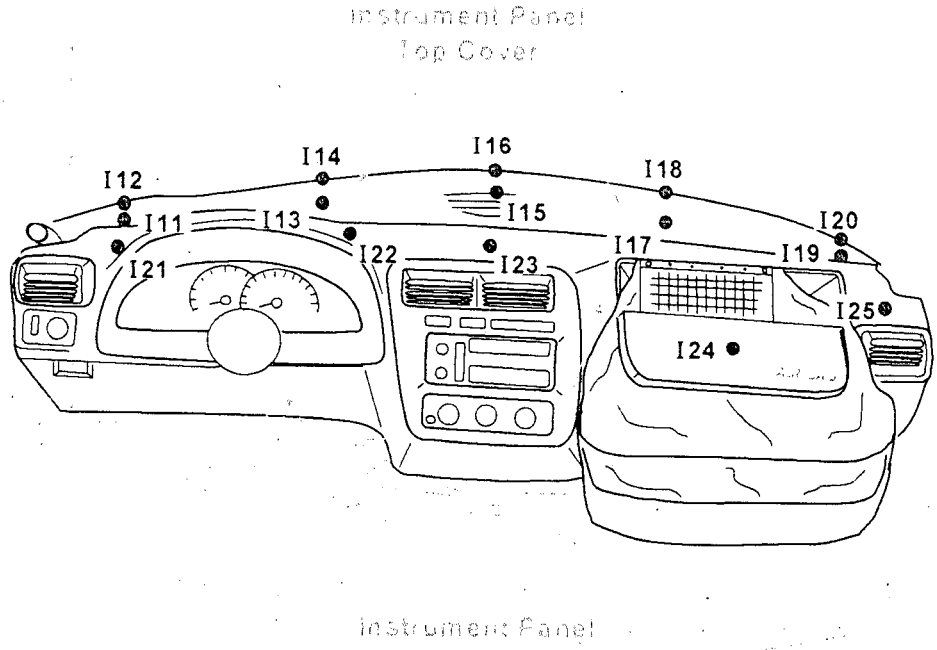

Figure C7. Fire Test F971003. Diagram showing the approximate locations of thermocouples on the instrument panel and instrument panel top cover of the test vehicle. Thermocouples I11 through I20 were located on the upper surface of the instrument panel top cover. Thermocouples I21 through I25 were located on the outer surface of the instrument panel.

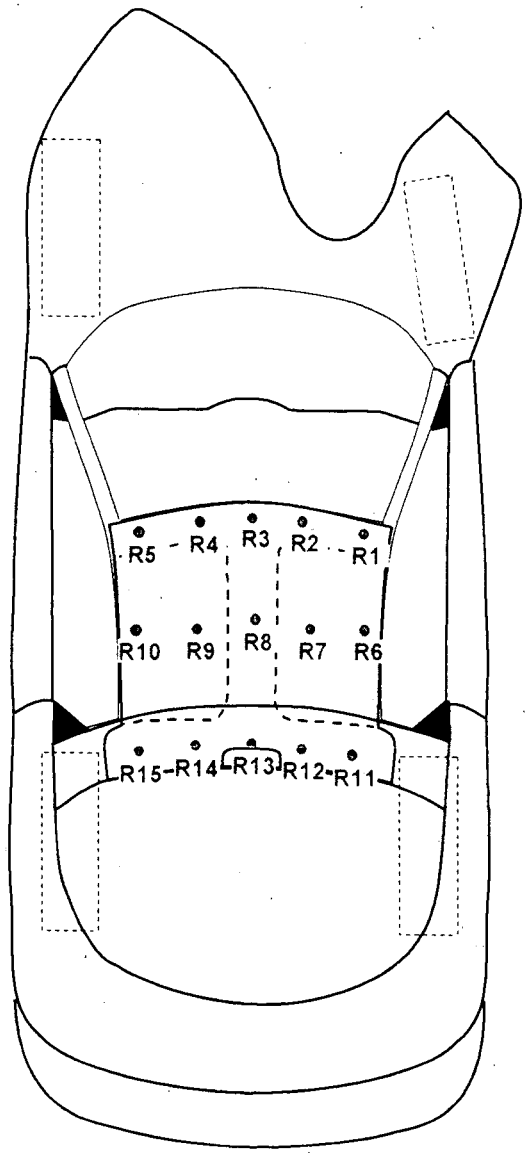

Figure C8. Fire Test F071003. Diagram showing the approximate locations of thermocouples on the headlining panel of the test vehicle. Thermocouples R1 through R15 were located approximately 1 cm below the lower surface of the head lining panel.

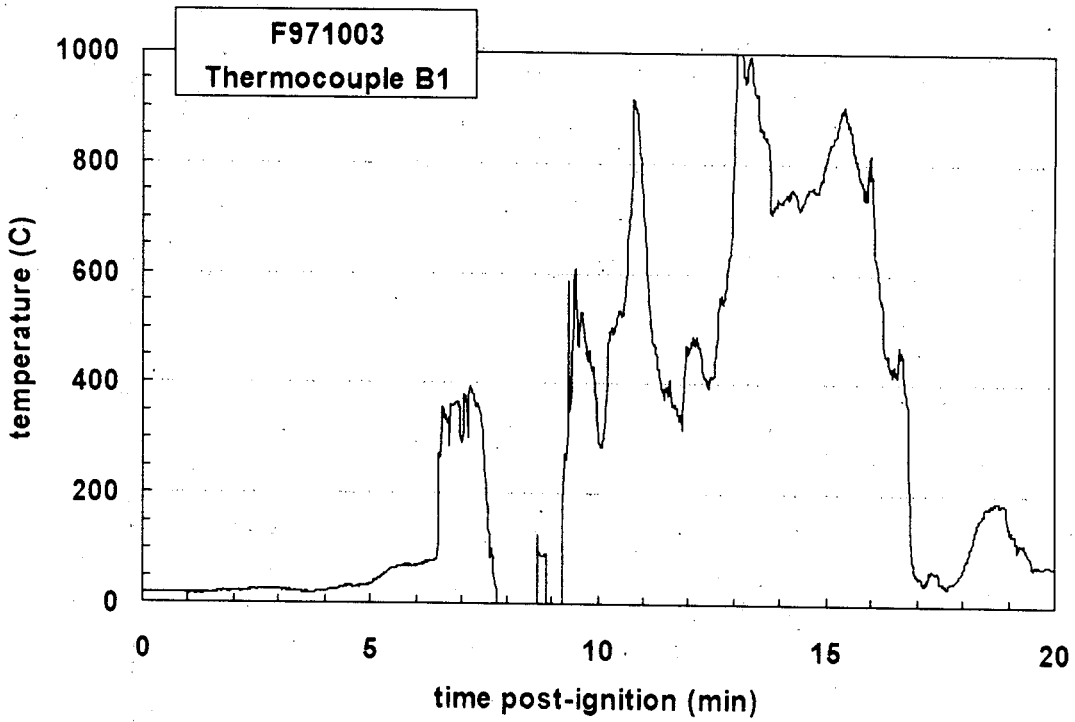

Plot C1. Fire Test F971003. Data plot from Thermocouple B1. Thermocouple B1 began to malfunction at 07:78 (min:sec) post-ignition.

Intentionally Left Blank

Plot C2. Fire Test F971003. See Appendix E for data from Thermocouple B2.

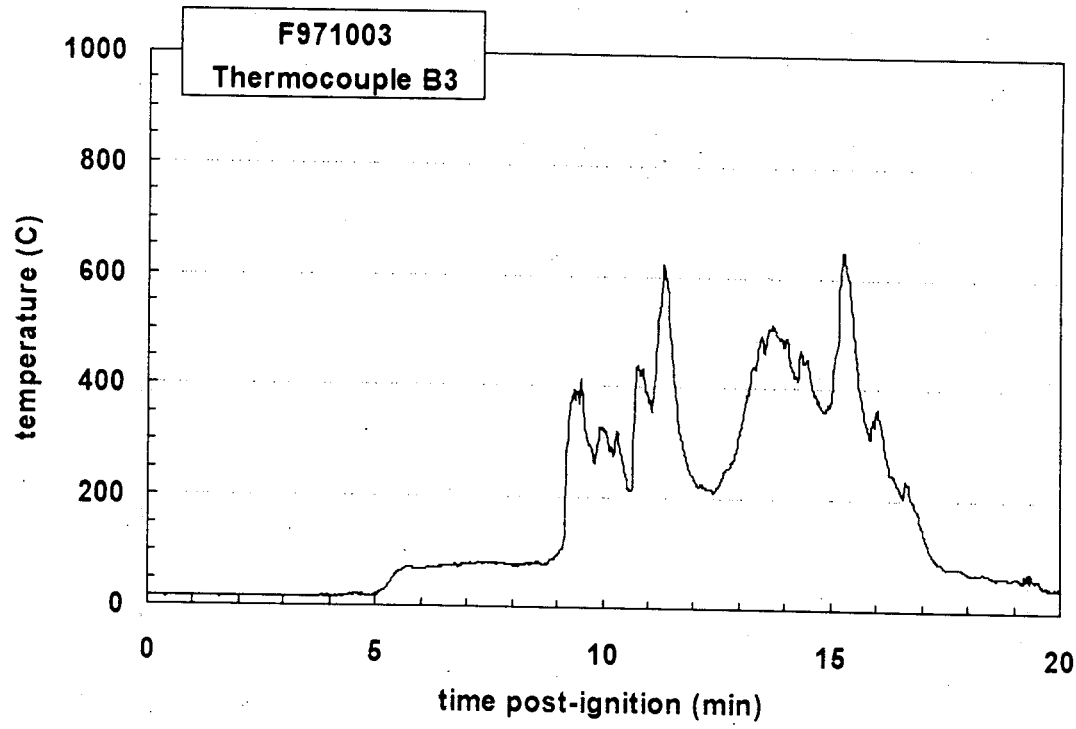

Plot C3. Fire Test F971003. Data plot from Thermocouple B3.

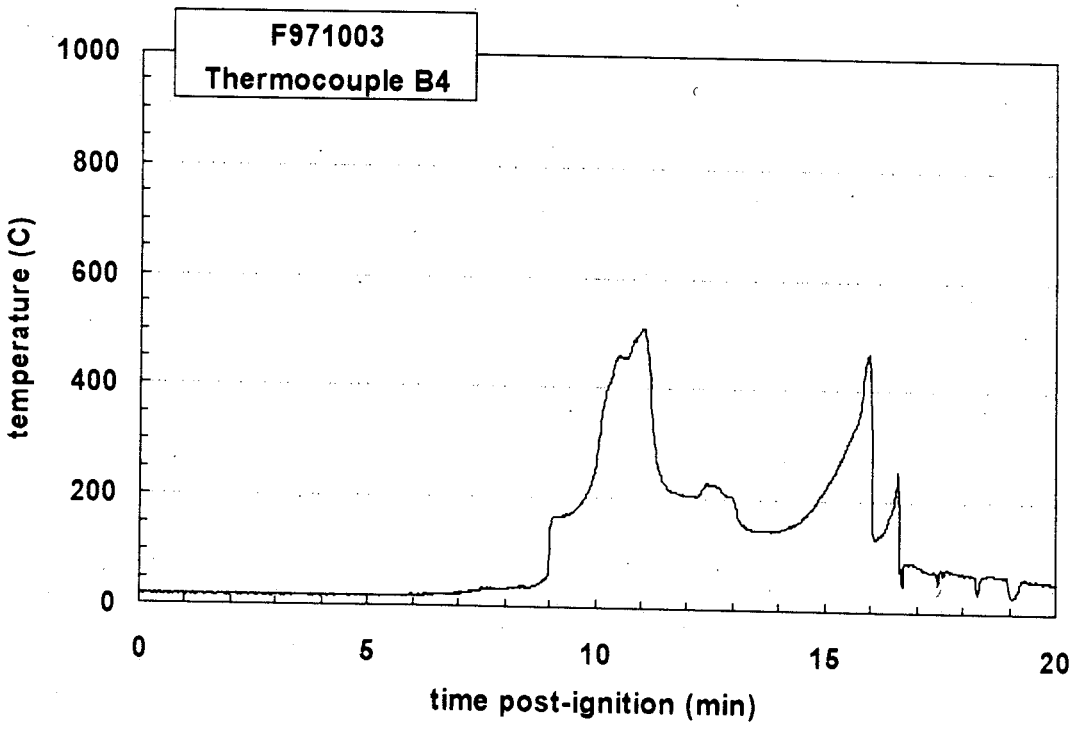

Plot C4. Fire Test F971003. Data plot from Thermocouple B4.

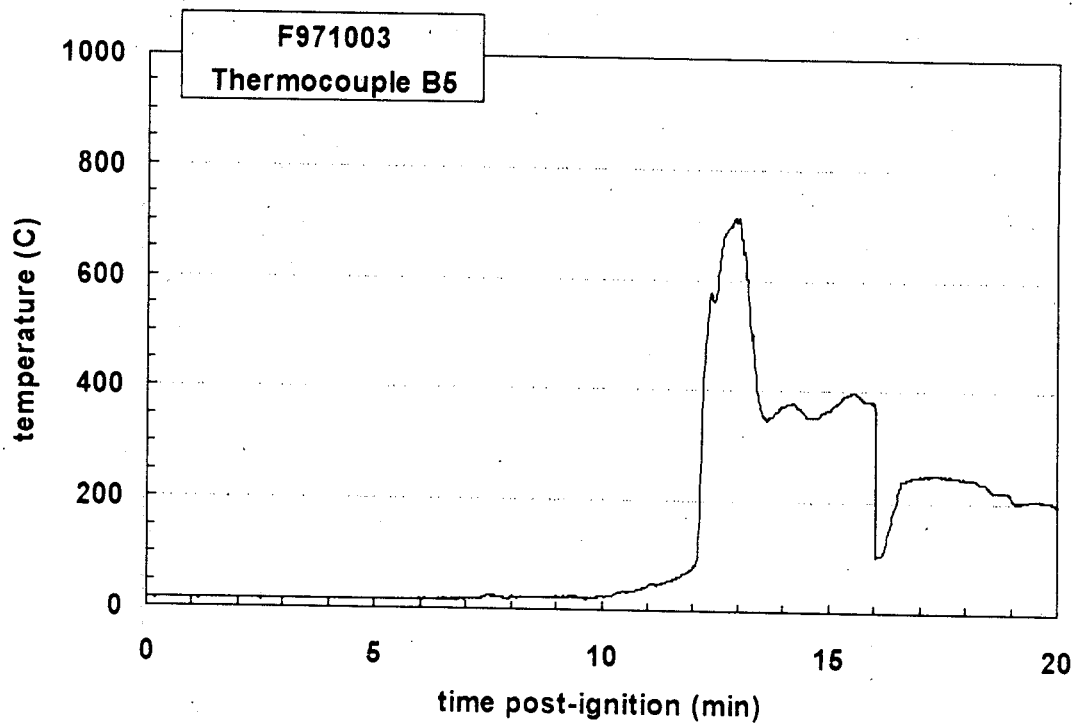

Plot C5. Fire Test F971003. Data plot from Thermocouple B5.

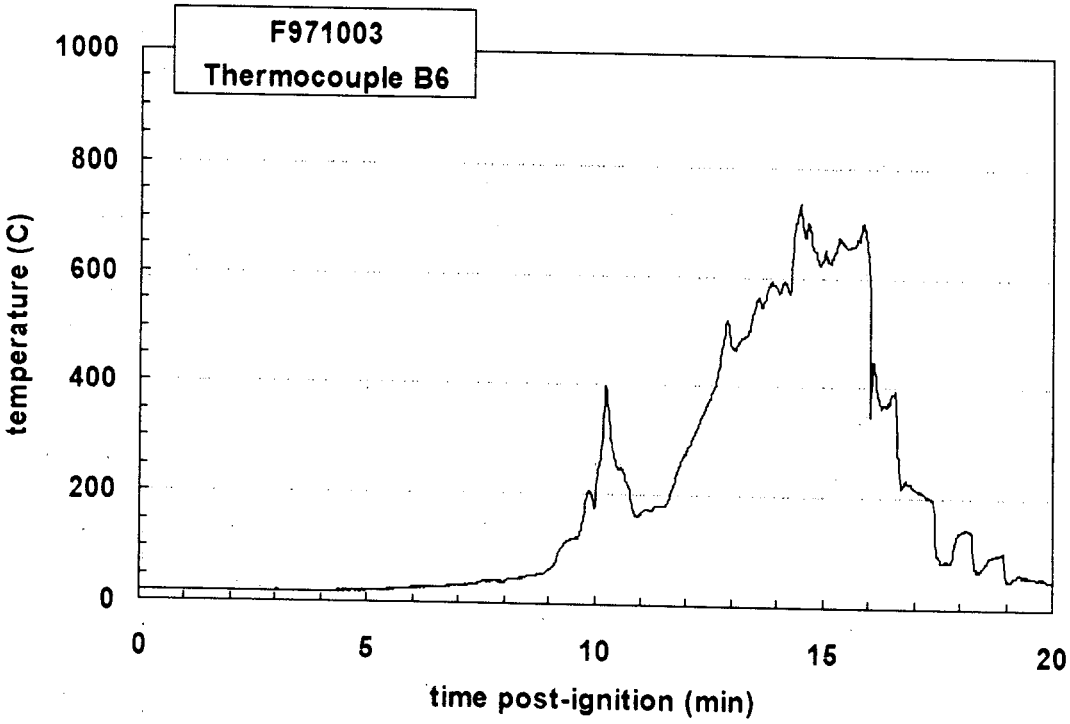

Plot C6. Fire Test F971003. Data plot from Thermocouple B6.

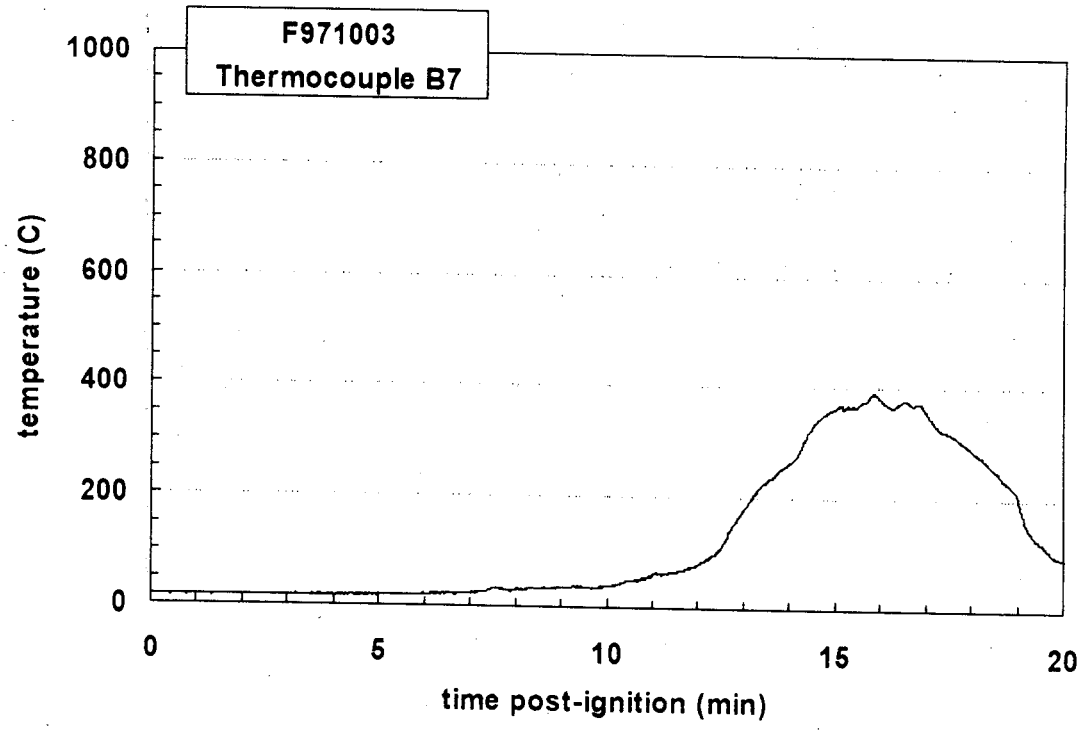

Plot C7. Fire Test F971003. Data plot from Thermocouple B7.

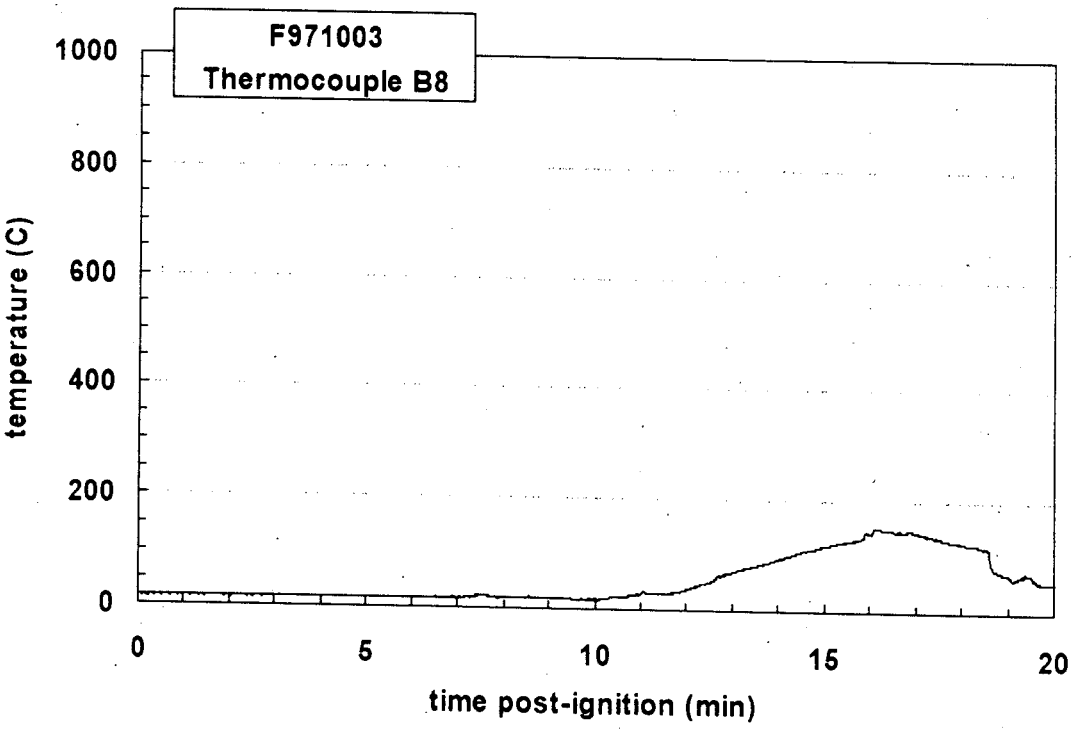

Plot C8. Fire Test F971003. Data plot from Thermocouple B8.

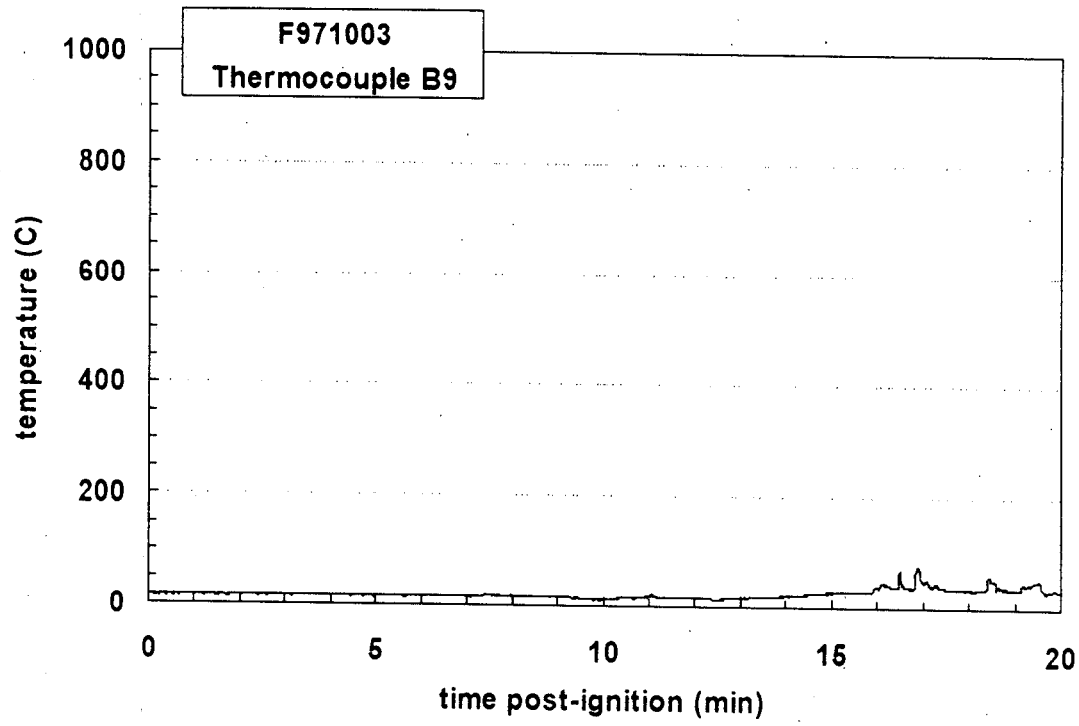

Plot C9. Fire Test F971003. Data plot from Thermocouple B9.

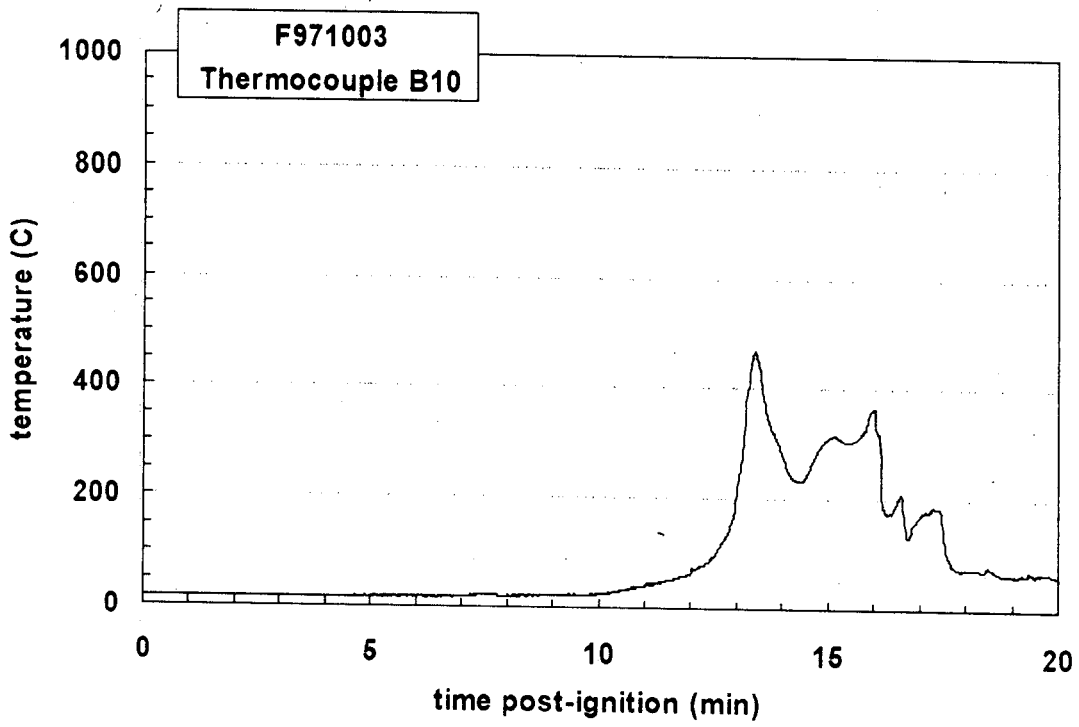

Plot C10. Fire Test F971003. Data plot from Thermocouple B10.

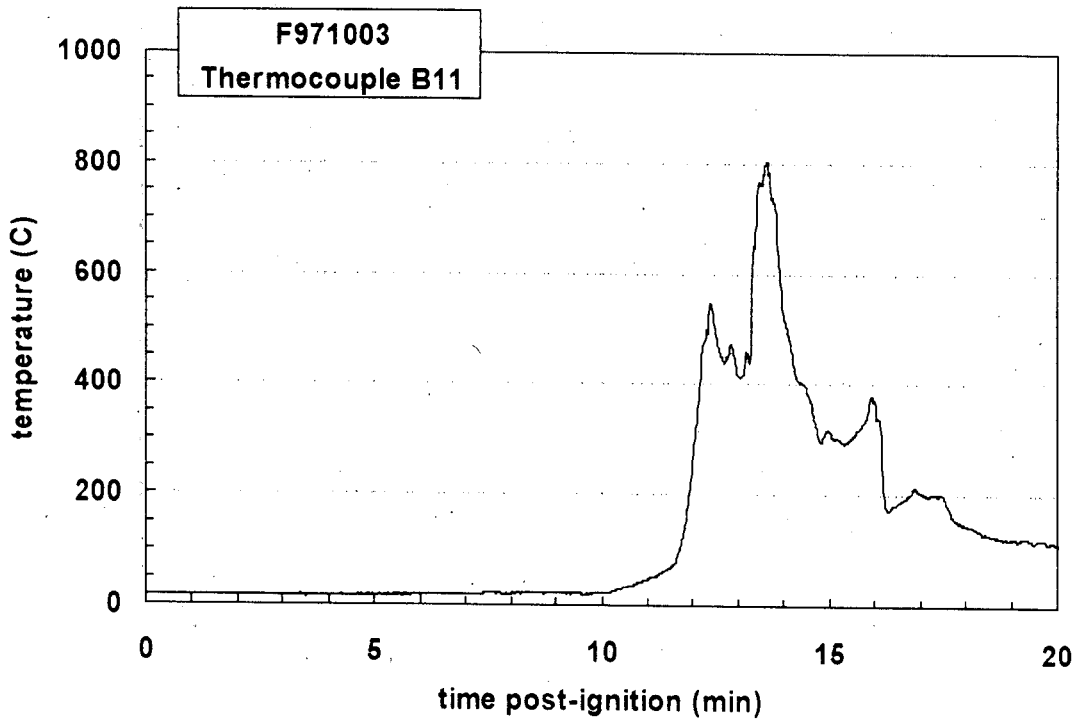

Plot C11. Fire Test F971003. Data plot from Thermocouple B11.

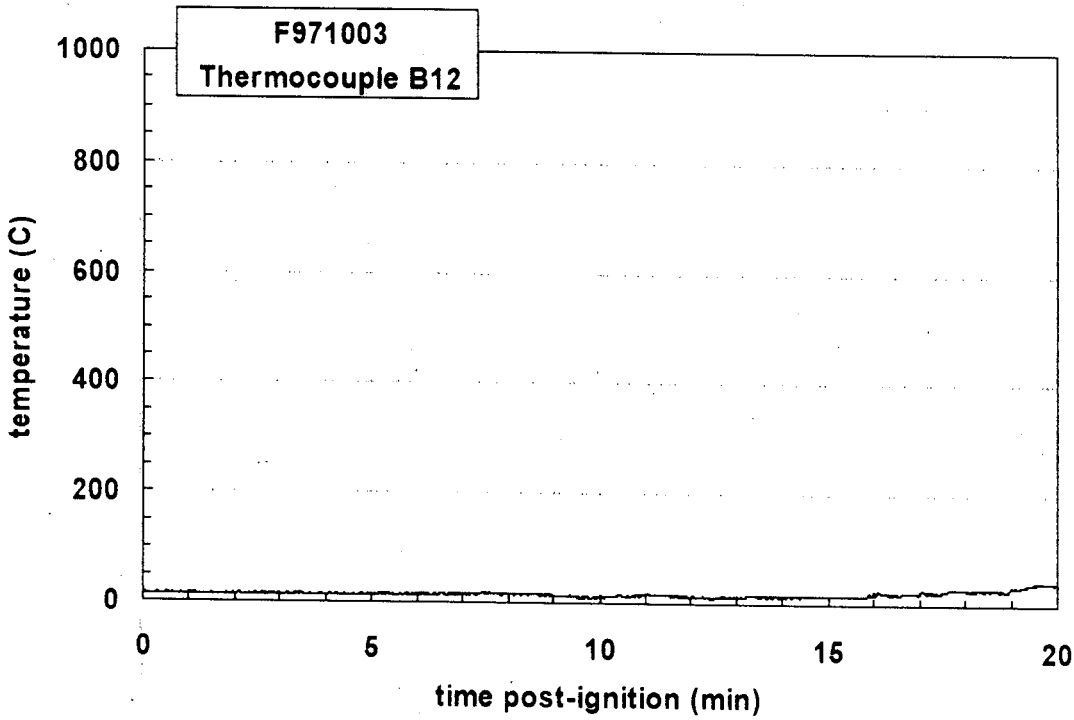

Plot C12. Fire Test F971003. Data plot from Thermocouple B12.

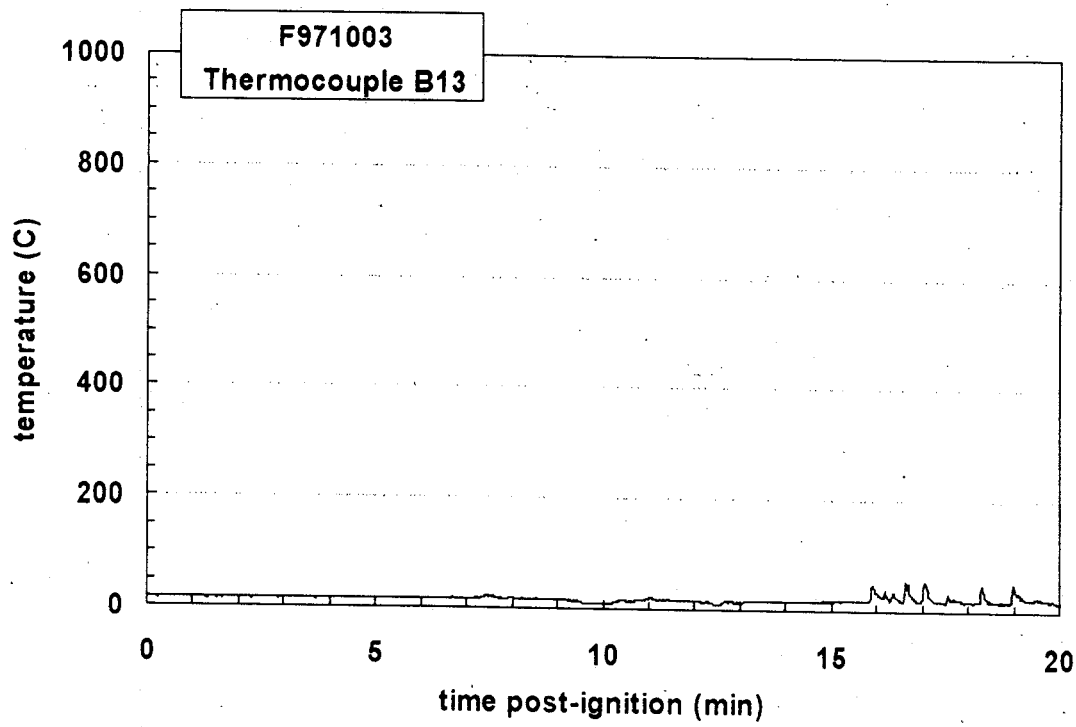

Plot C13. Fire Test F971003. Data plot from Thermocouple B13.

Intentionally Left Blank

Plot C14. Fire Test F971003. See Appendix D for data from Thermocouple B14.

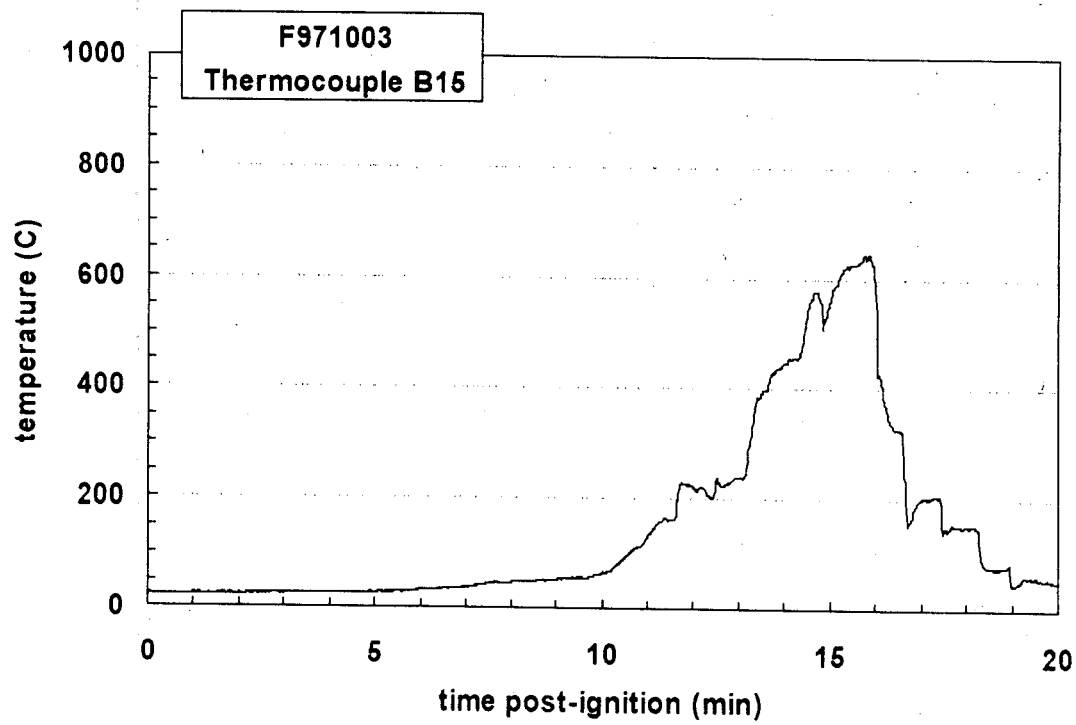

Plot C15. Fire Test F971003. Data plot from Thermocouple B15.

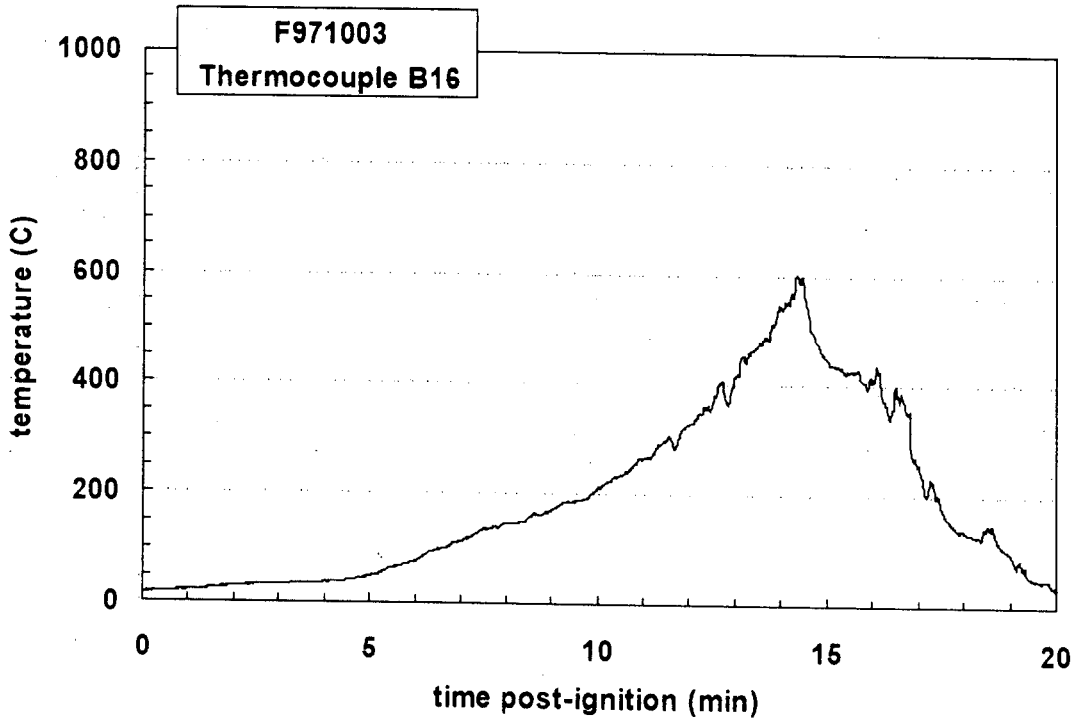

Plot C16. Fire Test F971003. Data plot from Thermocouple B16.

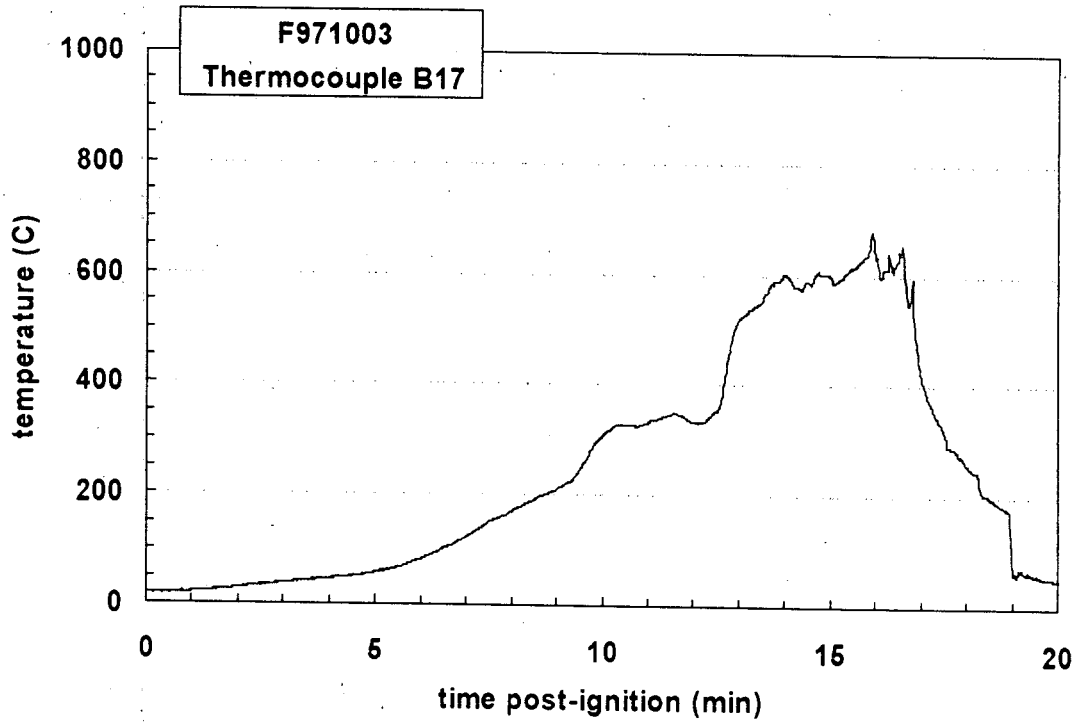

Plot C17. Fire Test F971003. Data plot from Thermocouple B17.

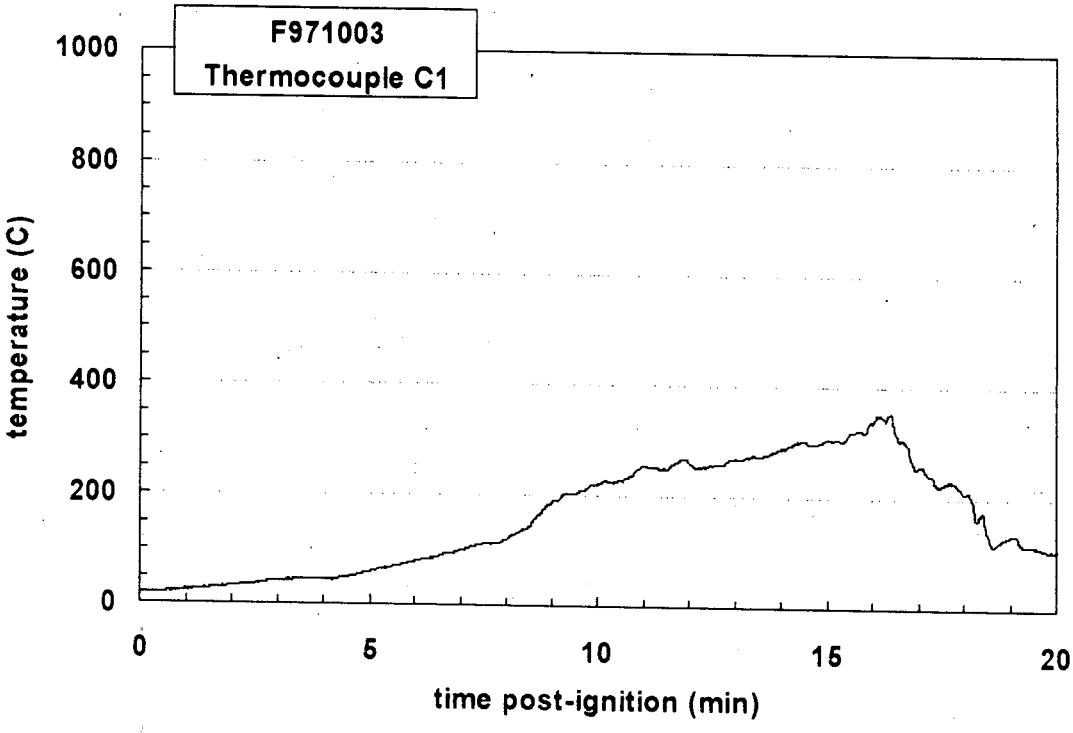

Plot C18. Fire Test F971003. Data plot from Thermocouple C1.

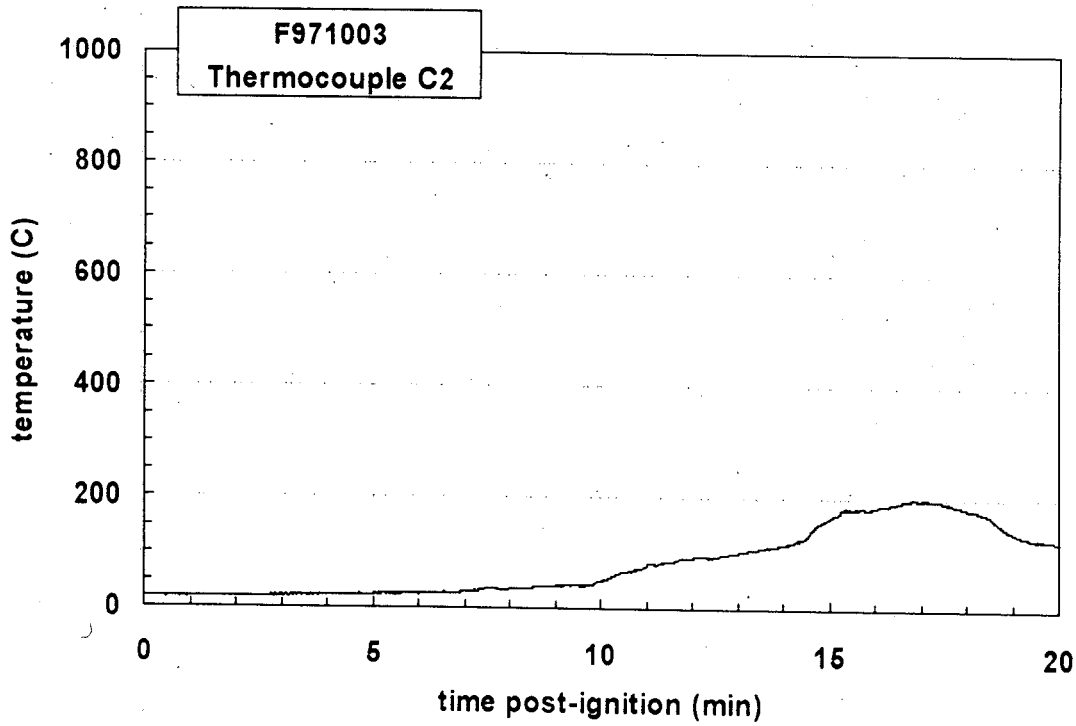

Plot C19. Fire Test F971003. Data plot from Thermocouple C2.

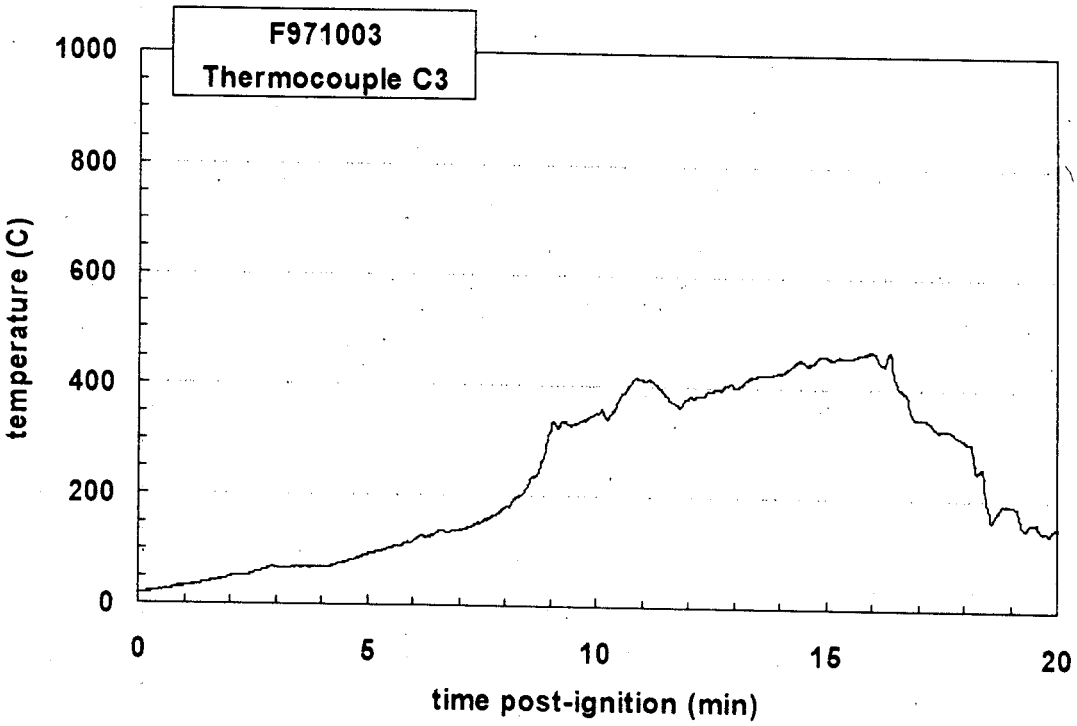

Plot C20. Fire Test F971003. Data plot from Thermocouple C3.

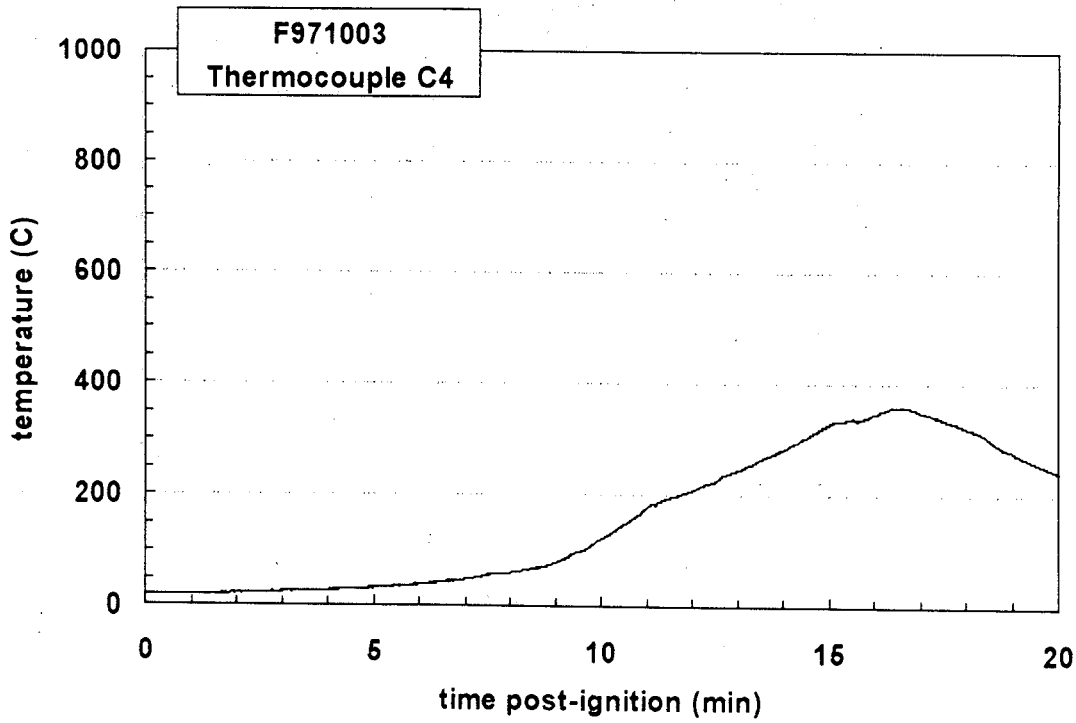

Plot C21. Fire Test F971003. Data plot from Thermocouple C4.

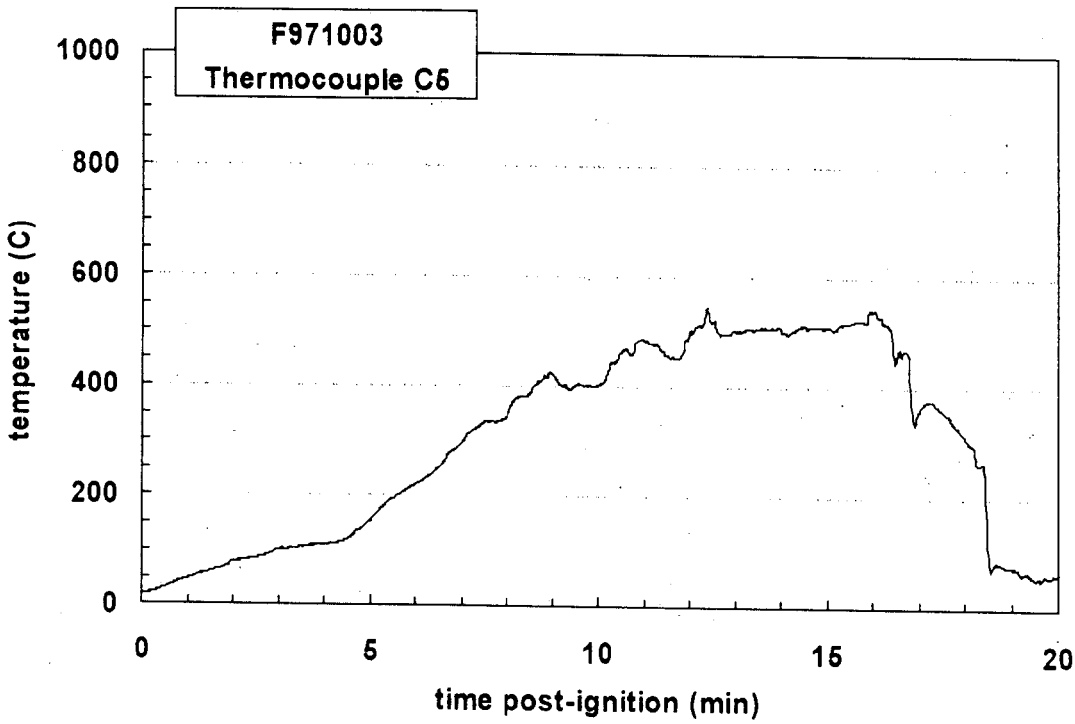

Plot C22. Fire Test F971003. Data plot from Thermocouple C5.

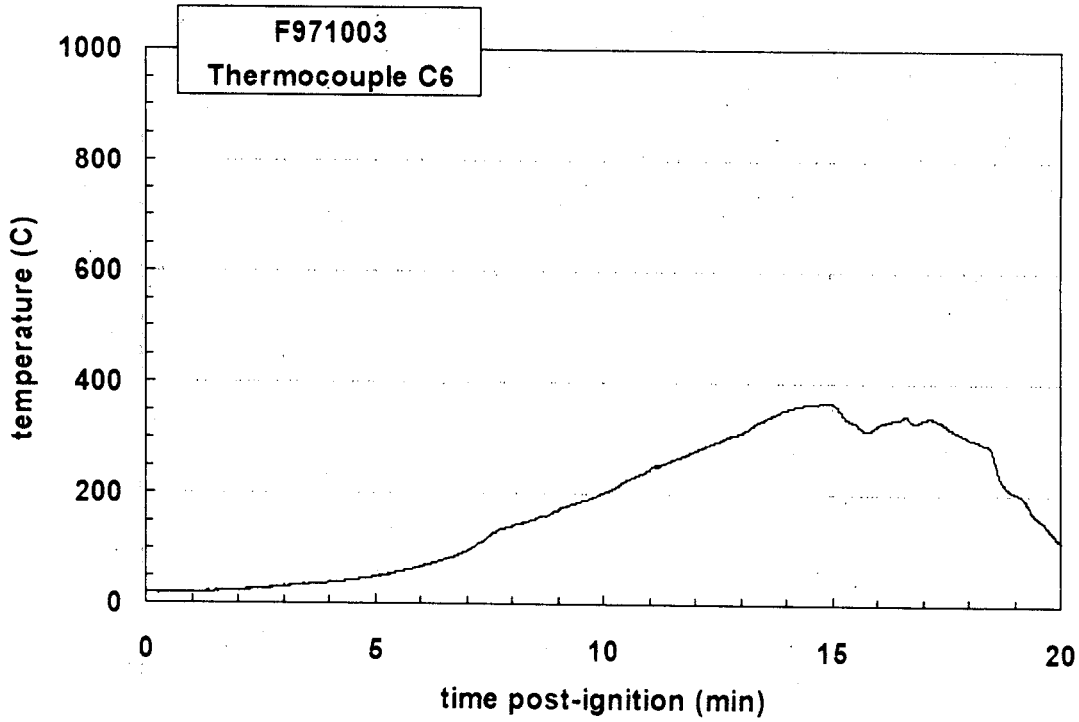

Plot C23. Fire Test F971003. Data plot from Thermocouple C6.

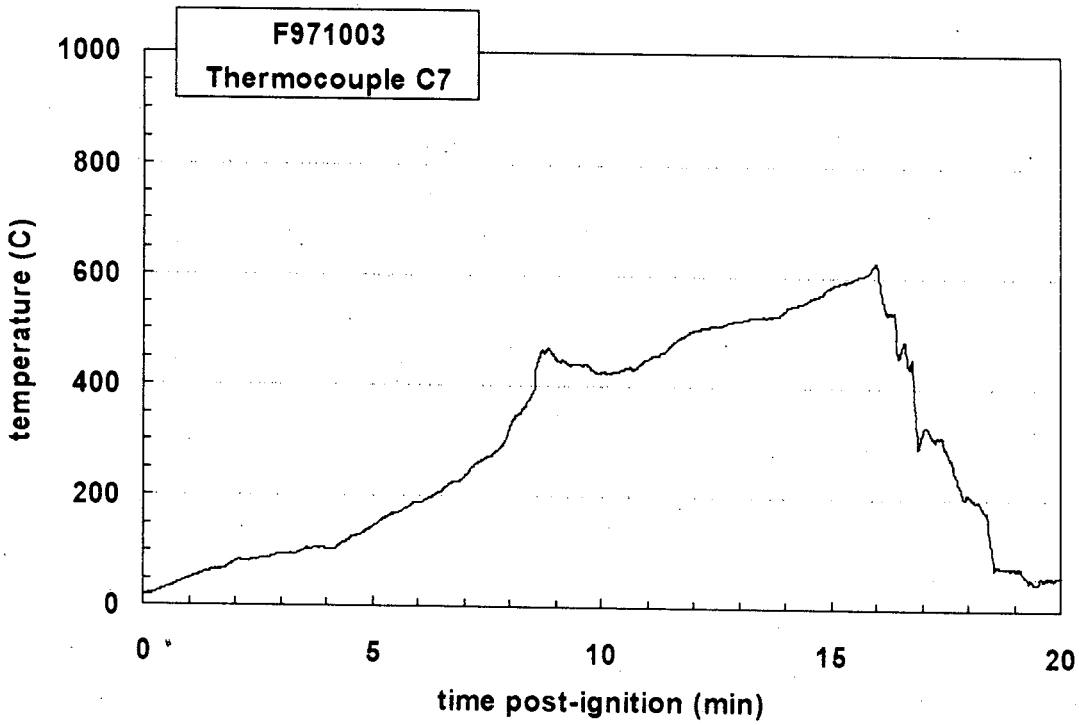

Plot C24. Fire Test F971003. Data plot from Thermocouple C7.

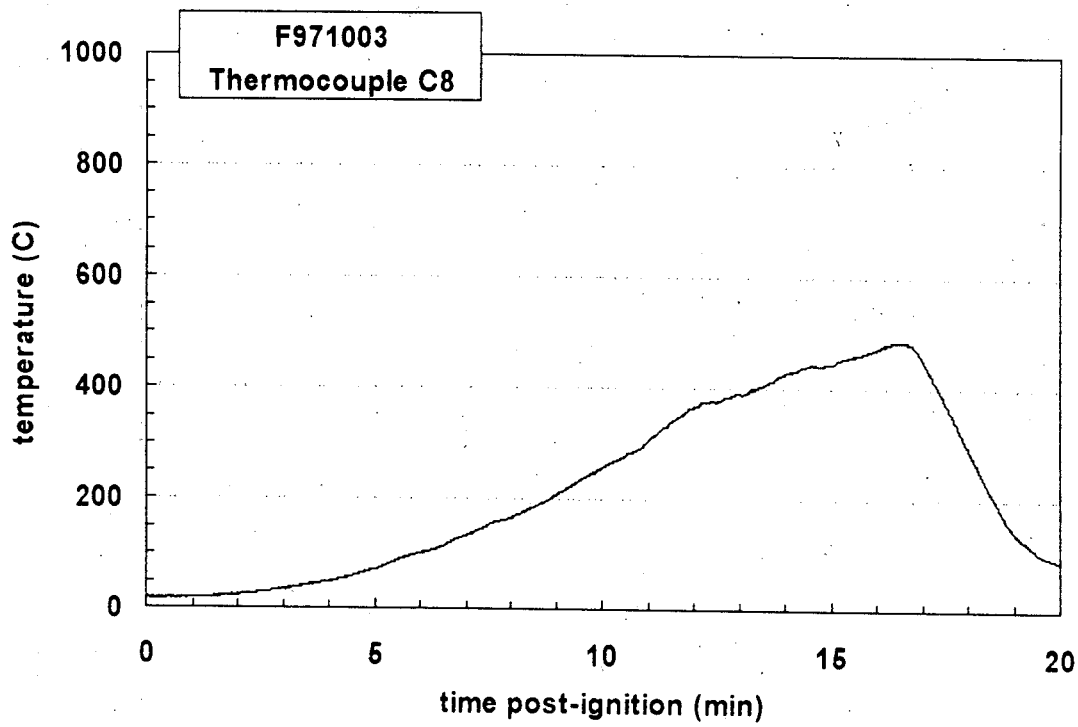

Plot C25. Fire Test F971003. Data plot from Thermocouple C8.

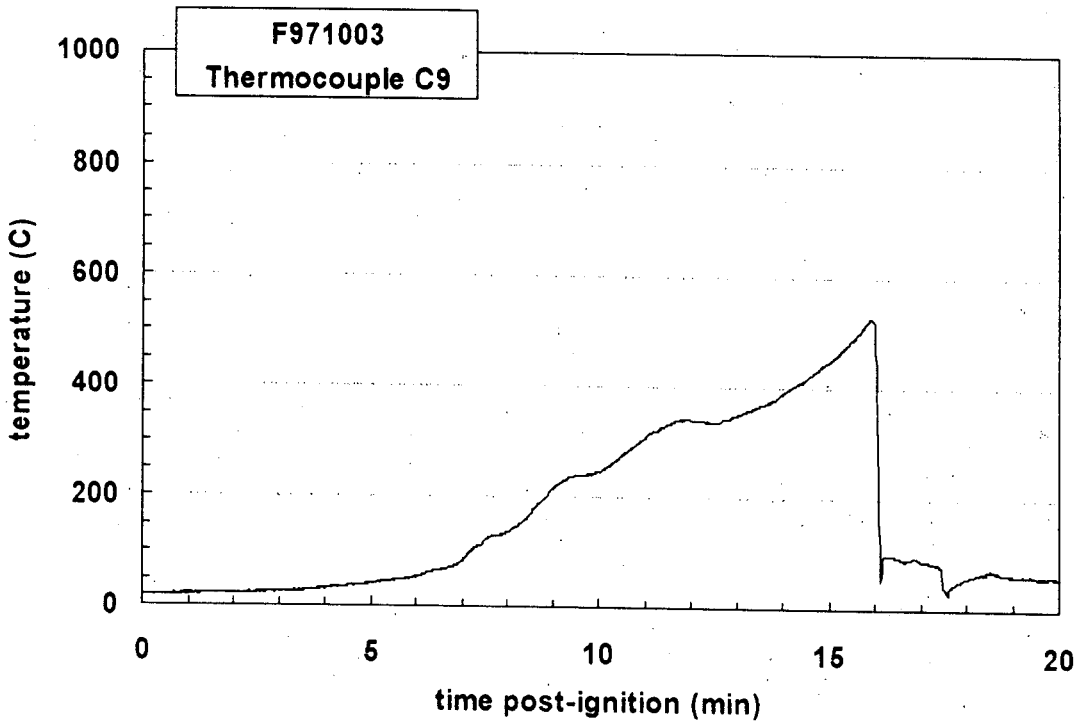

Plot C26. Fire Test F971003. Data plot from Thermocouple C9.

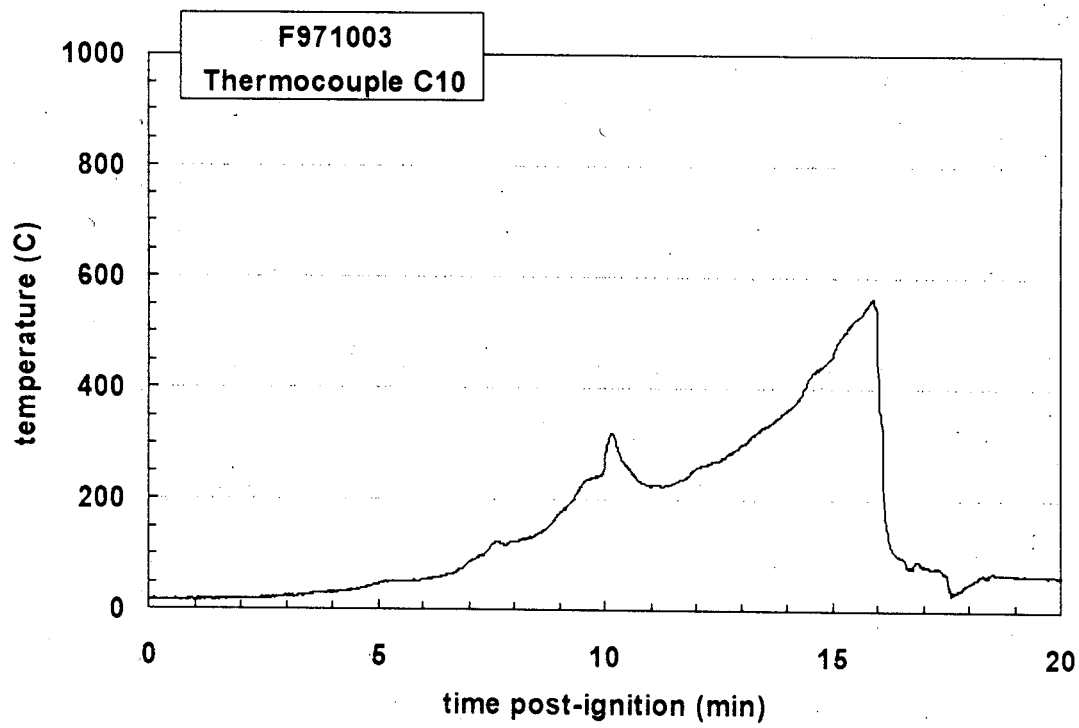

Plot C27. Fire Test F971003. Data plot from Thermocouple C10.

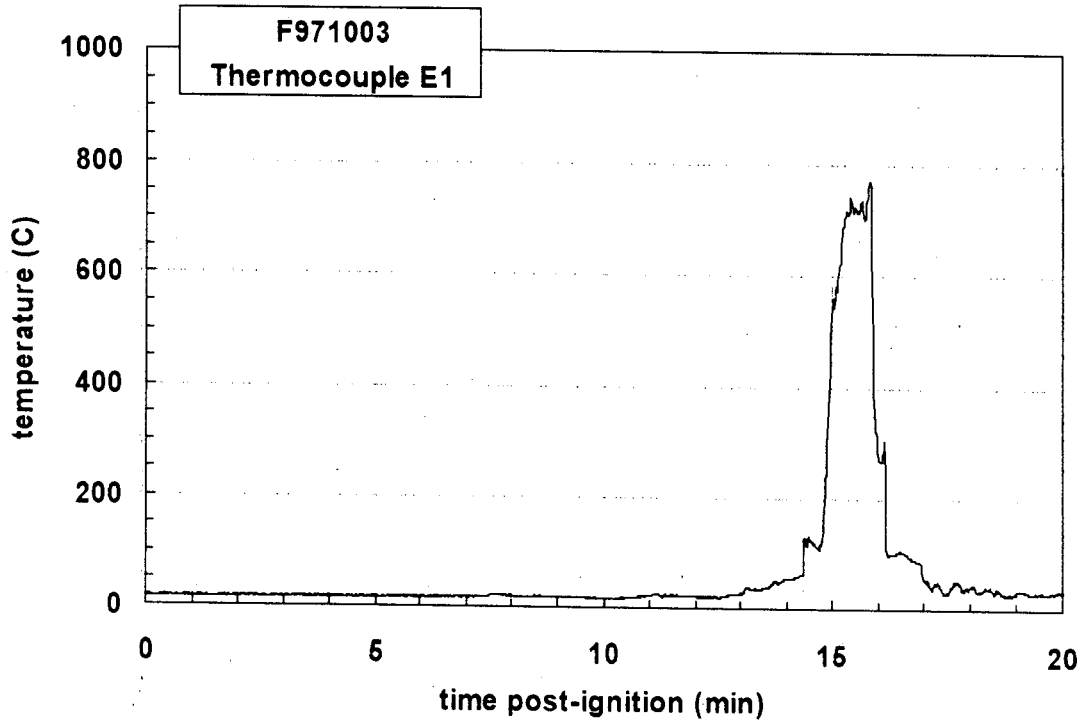

Plot C28. Fire Test F971003. Data plot from Thermocouple E1.

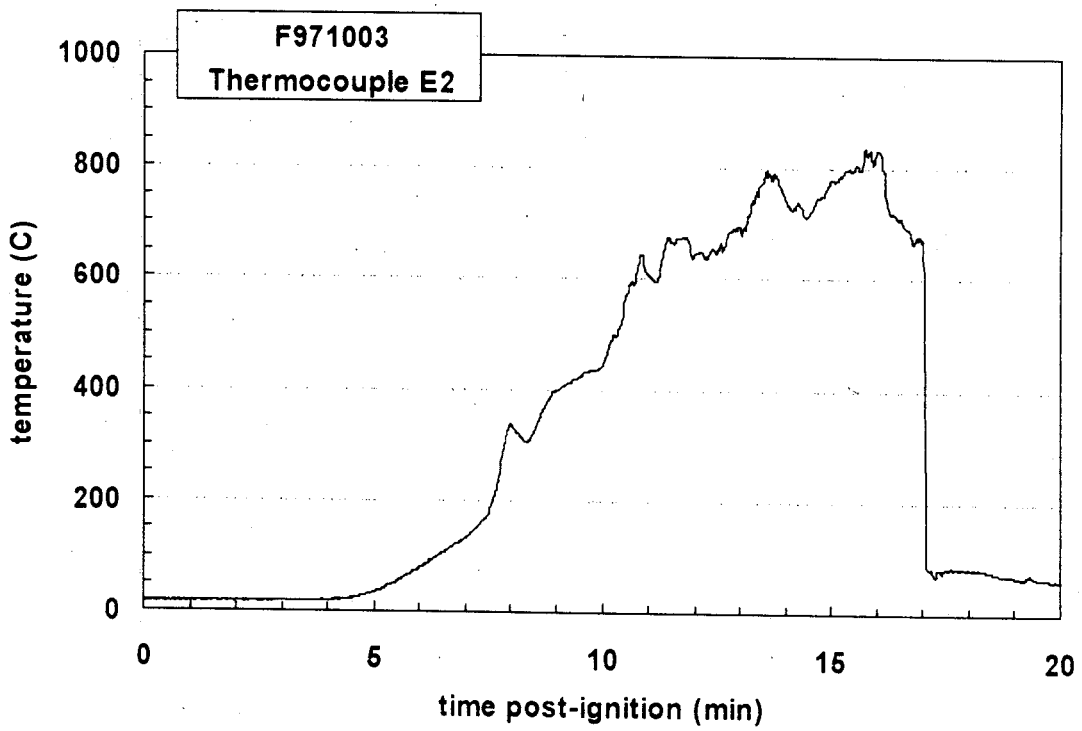

Plot C29. Fire Test F971003. Data plot from Thermocouple E2.

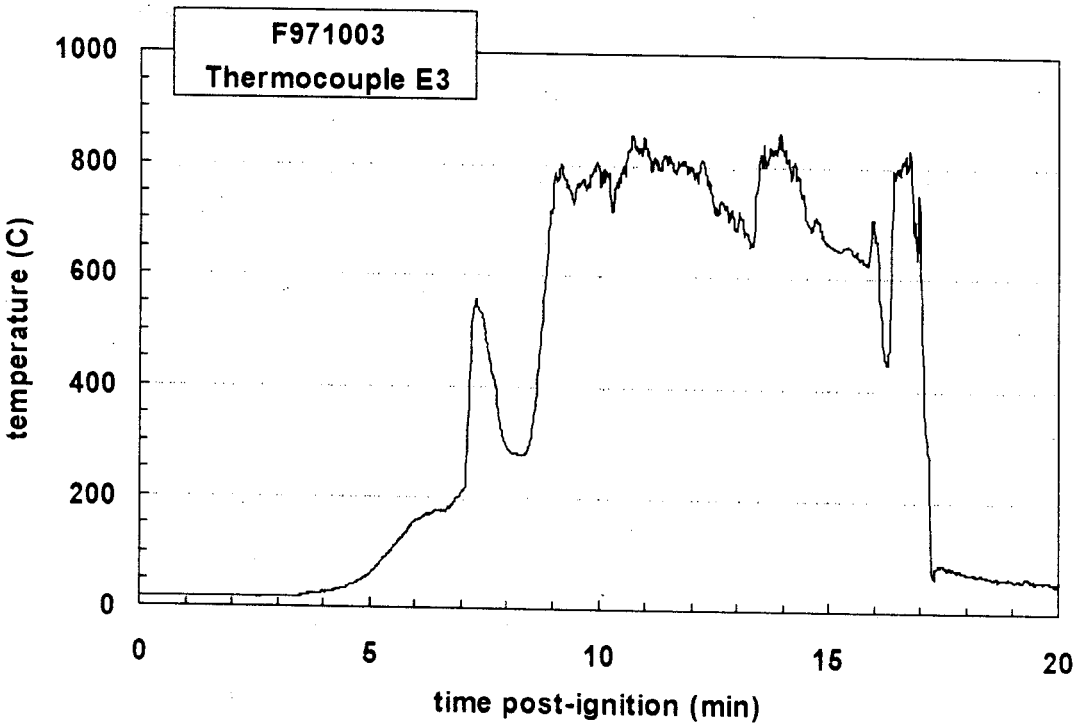

Plot C30. Fire Test F971003. Data plot from Thermocouple E3.

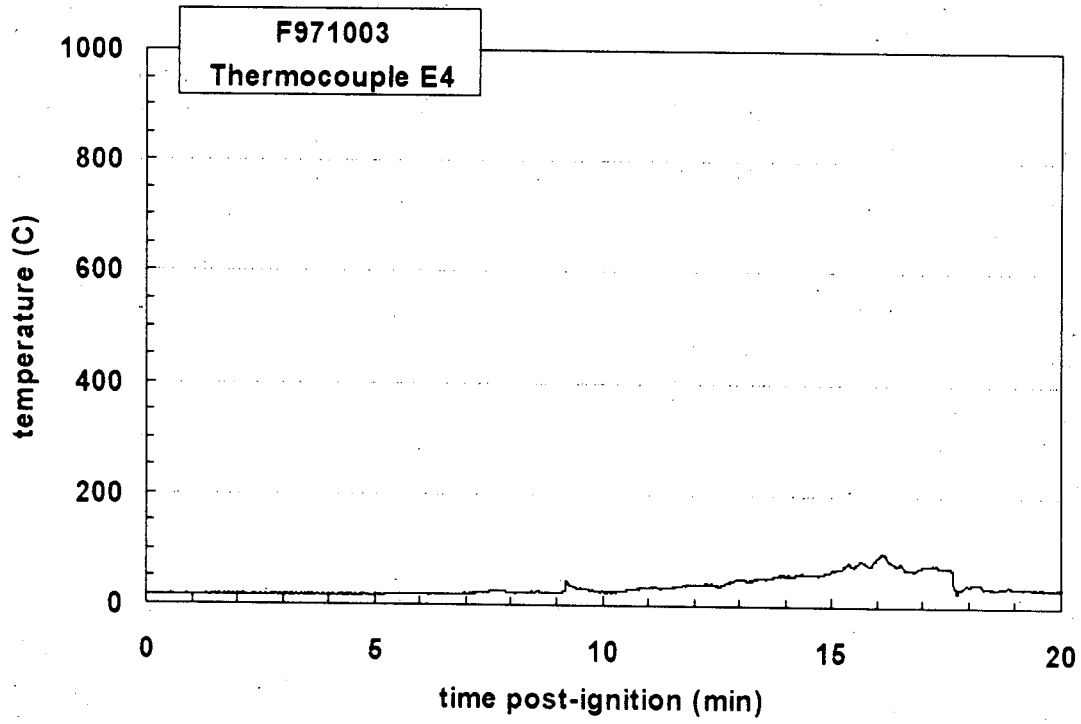

Plot C31. Fire Test F971003. Data plot from Thermocouple E4.

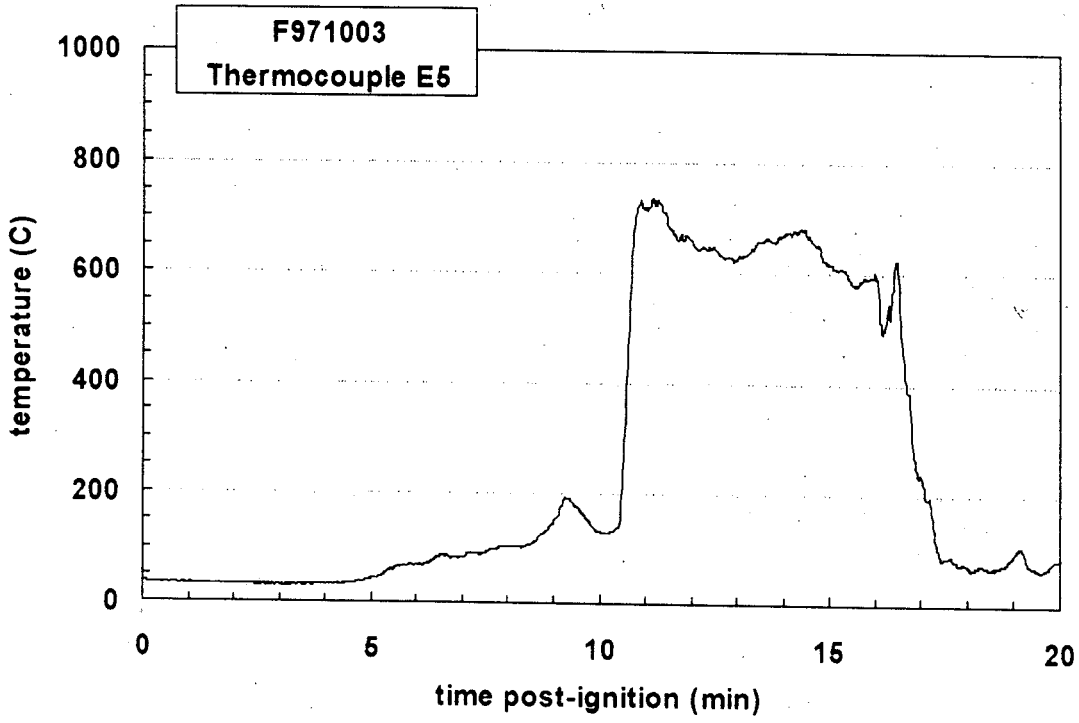

Plot C32. Fire Test F971003. Data plot from Thermocouple E5.

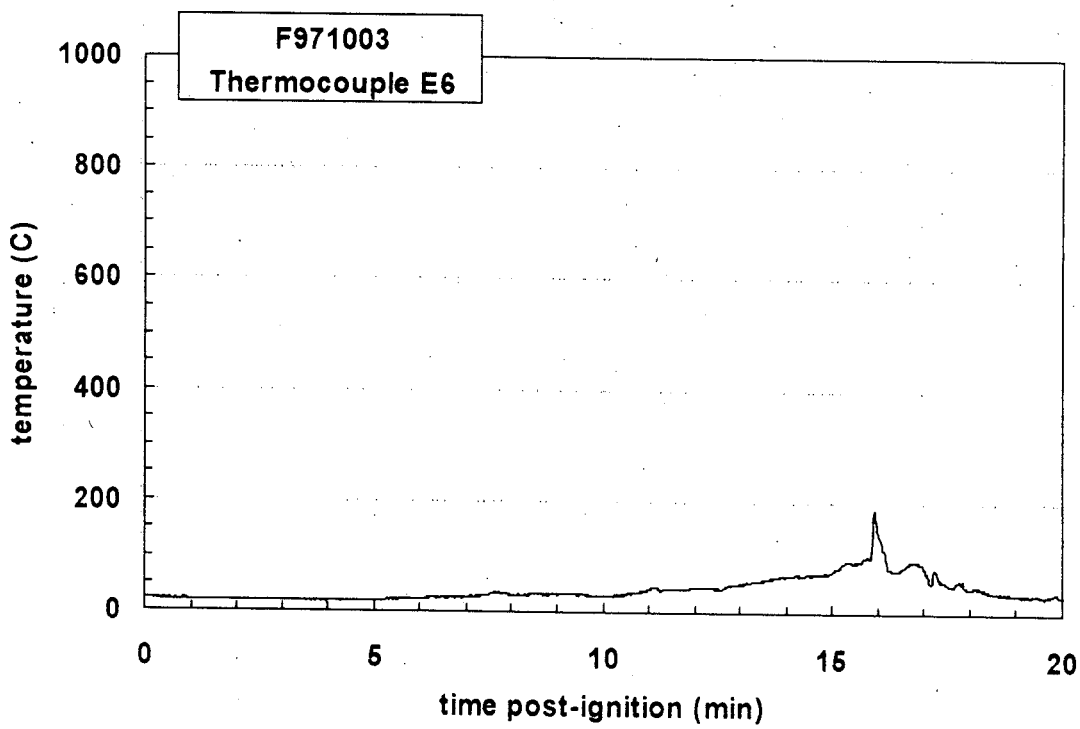

Plot C33. Fire Test F971003. Data plot from Thermocouple E6.

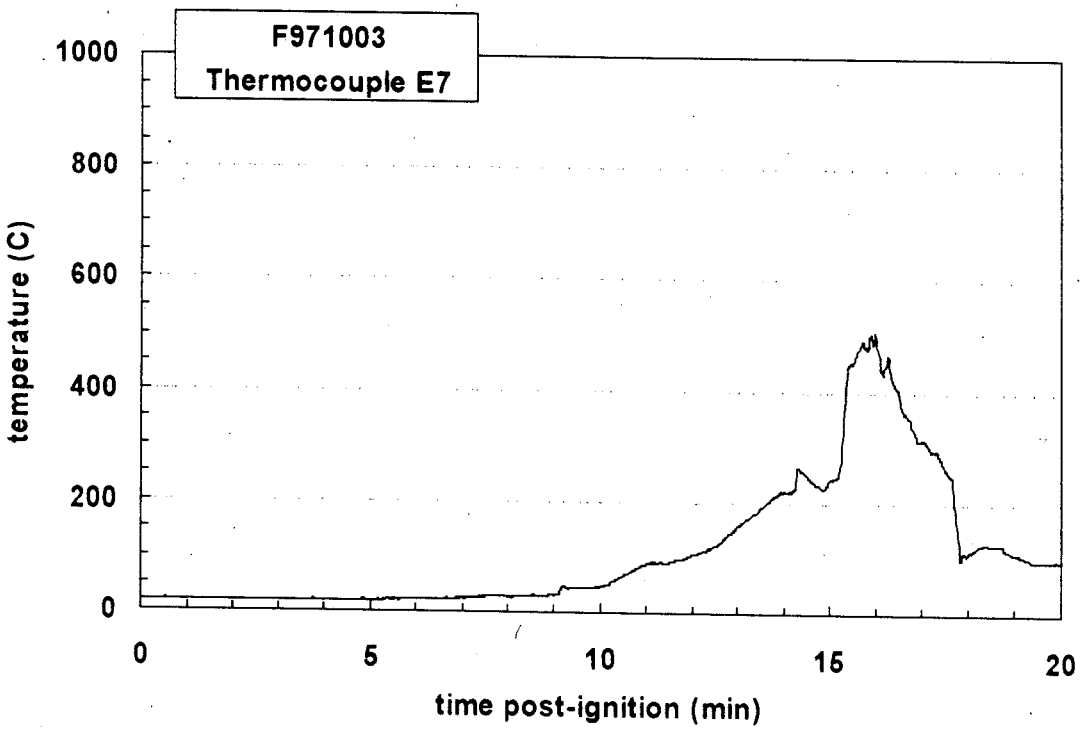

Plot C34. Fire Test F971003. Data plot from Thermocouple E7.

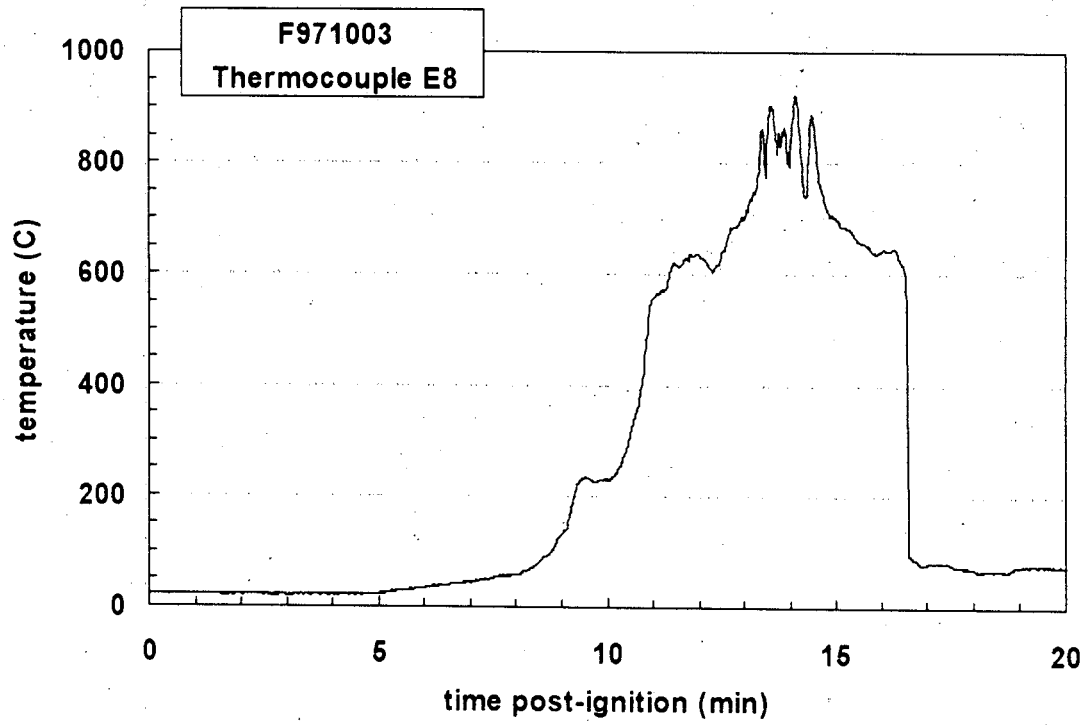

Plot C35. Fire Test F971003. Data plot from Thermocouple E8.

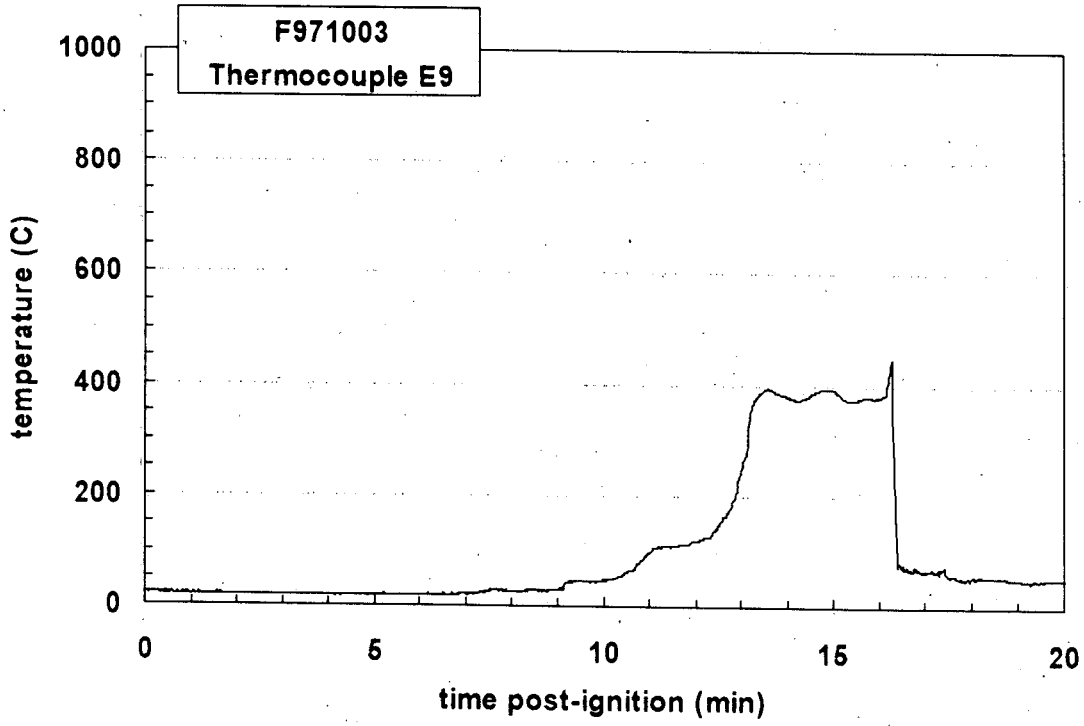

Plot C36. Fire Test F971003. Data plot from Thermocouple E9.

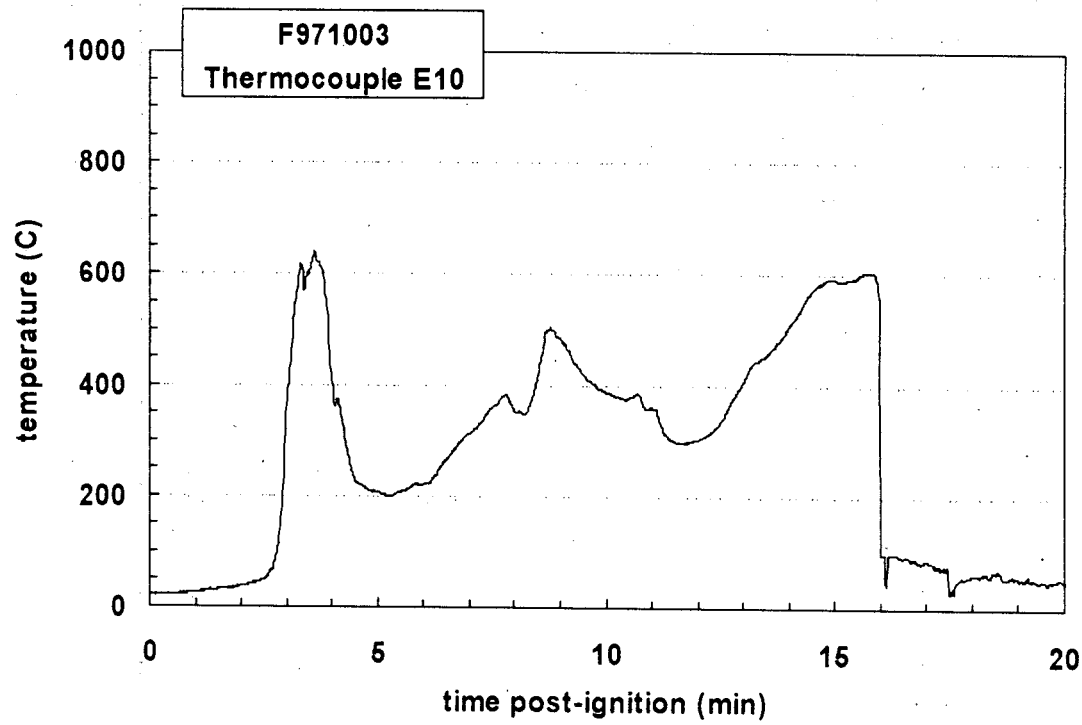

Plot C37. Fire Test F971003. Data plot from Thermocouple E10.

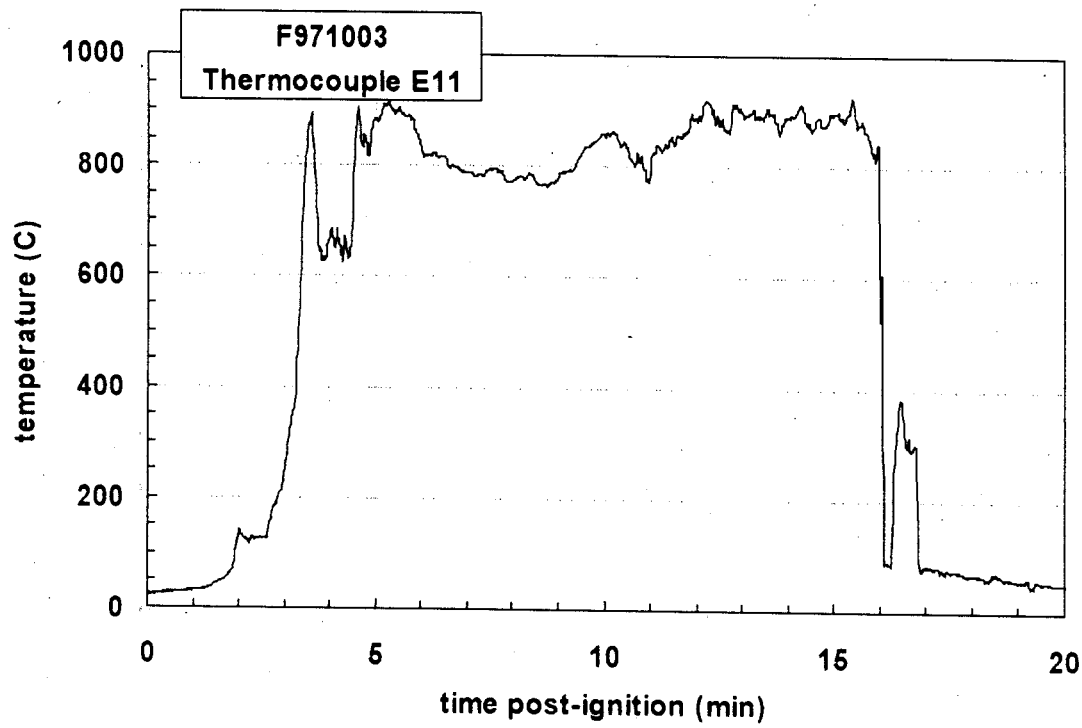

Plot C38. Fire Test F971003. Data plot from Thermocouple E11.

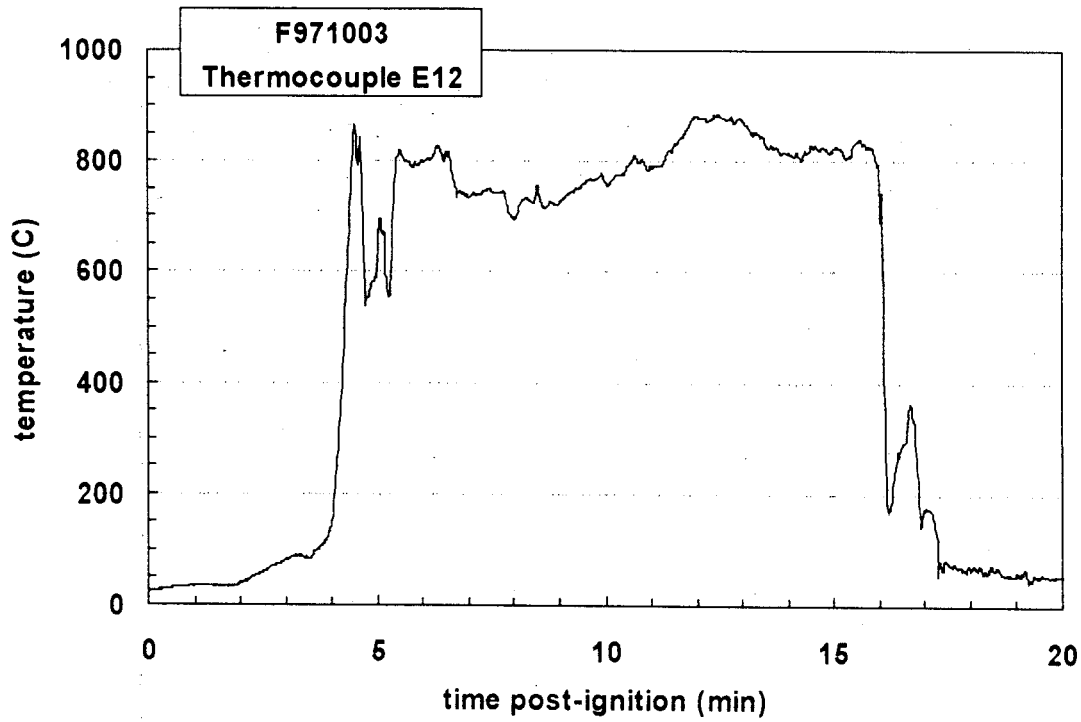

Plot C39. Fire Test F971003. Data plot from Thermocouple E12.

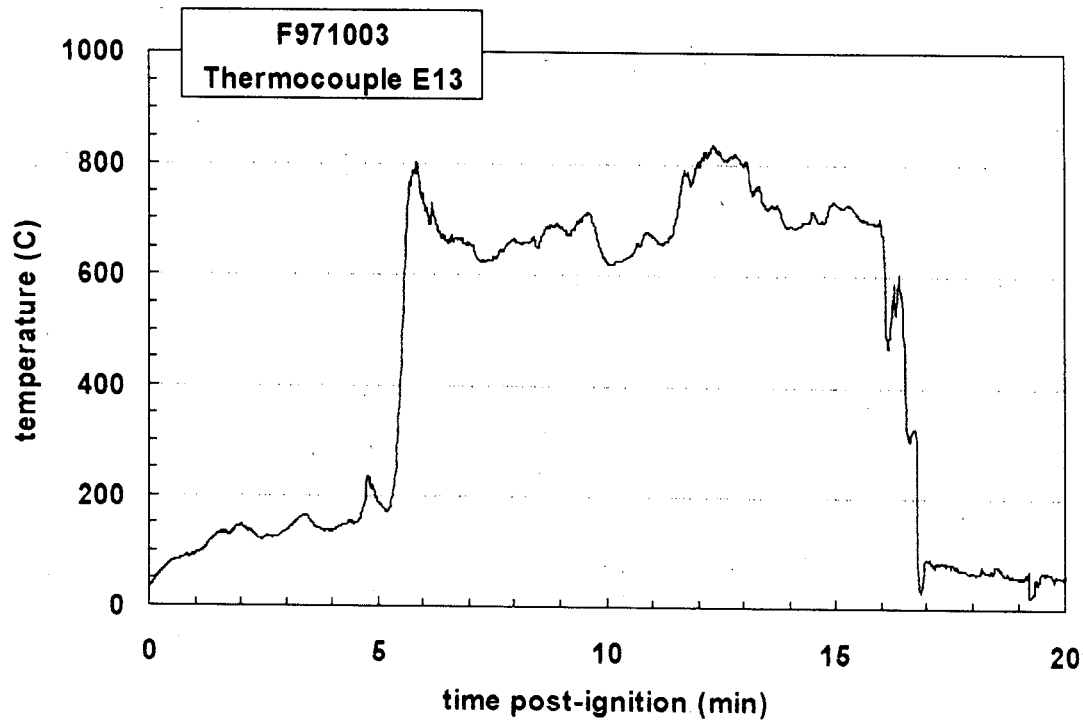

Plot C40. Fire Test F971003. Data plot from Thermocouple E13.

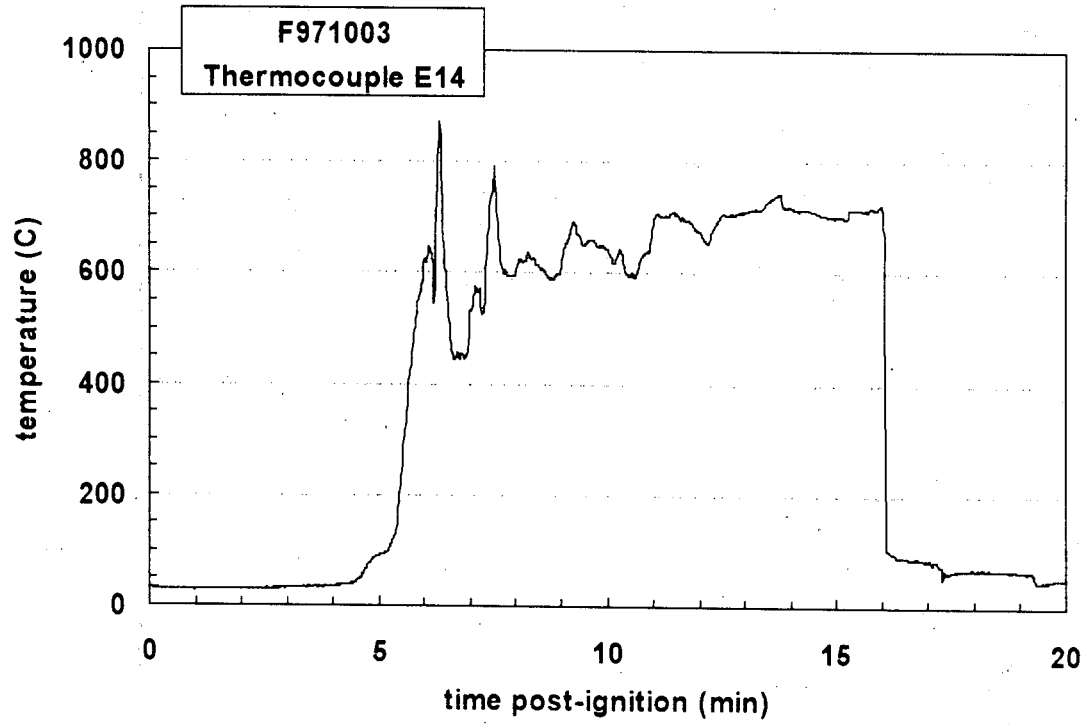

Plot C41. Fire Test F971003. Data plot from Thermocouple E14.

Intentionally Left Blank

Plot C42. Fire Test F971003. See Appendix E for data from Thermocouple E15.

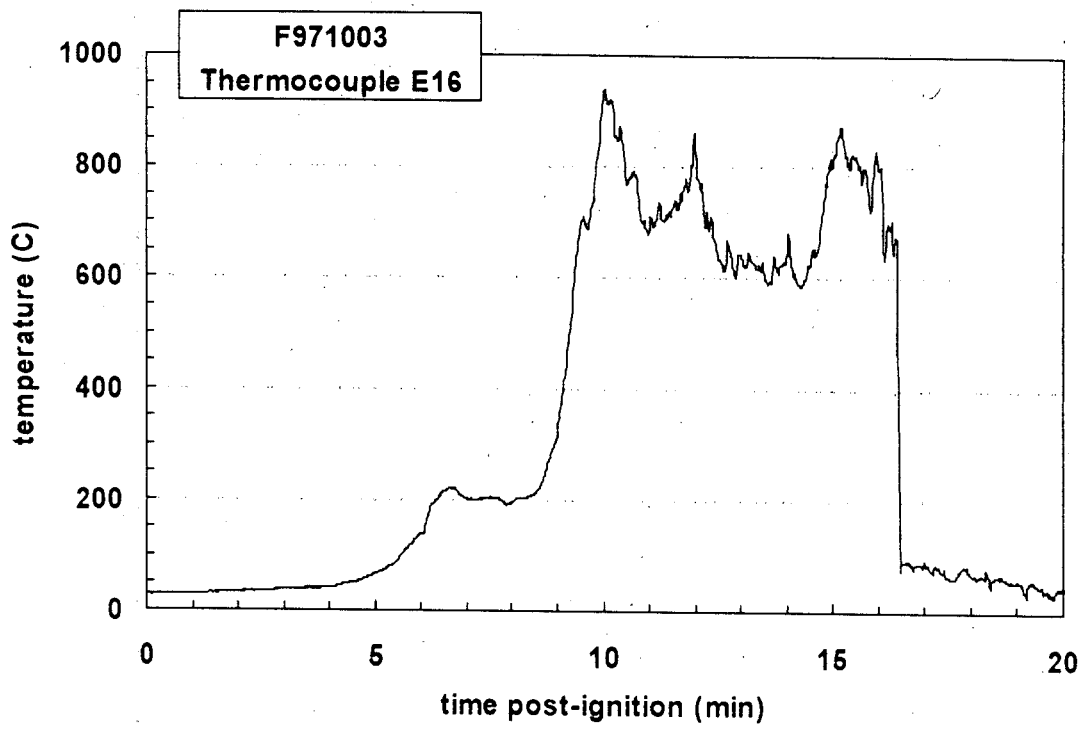

Plot C43. Fire Test F971003. Data plot from Thermocouple E16.

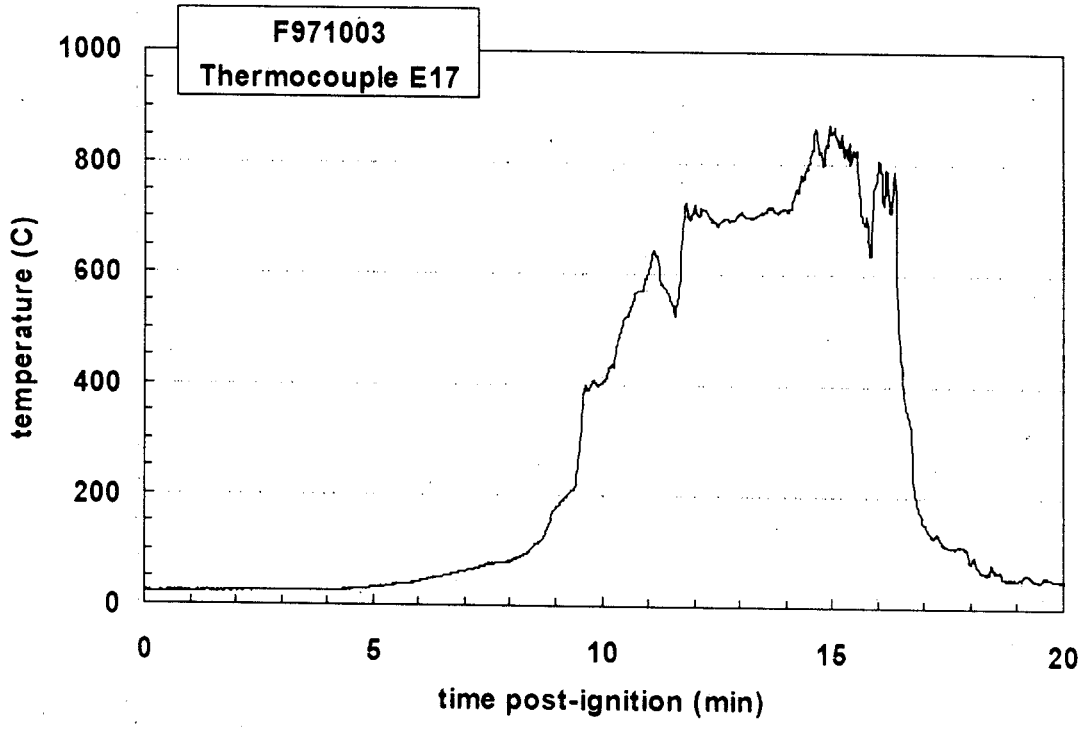

Plot C44. Fire Test F971003. Data plot from Thermocouple E17.

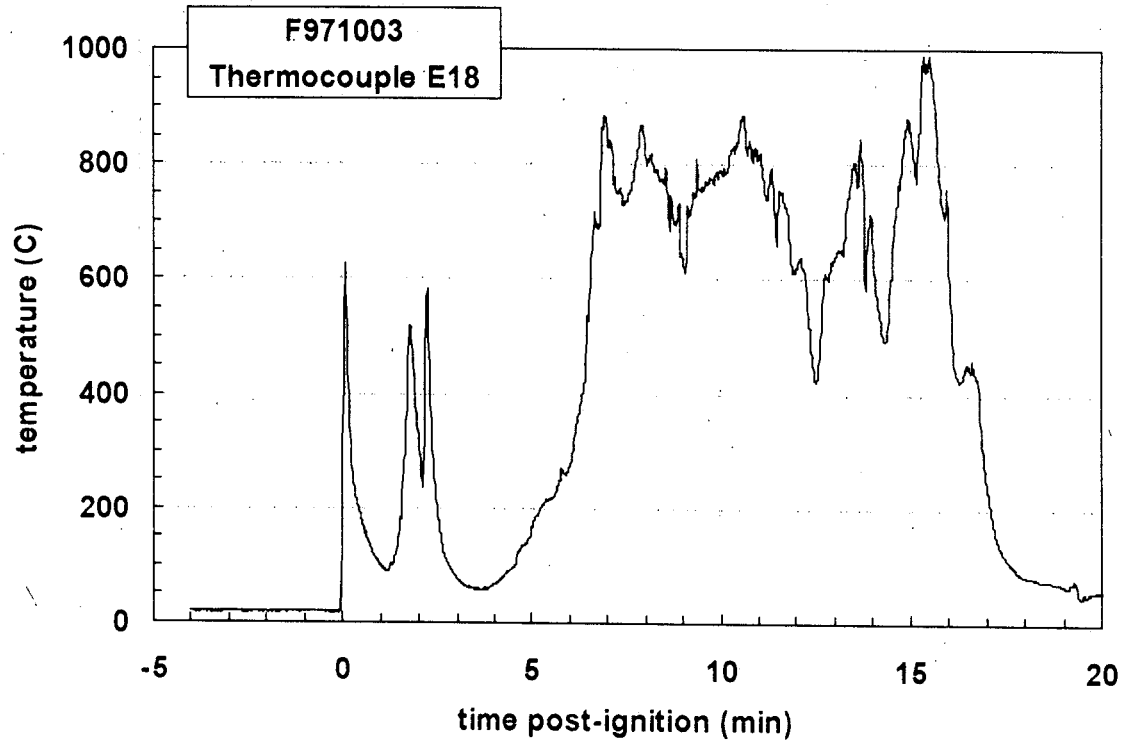

Plot C45. Fire Test F971003. Data plot from Thermocouple E18.

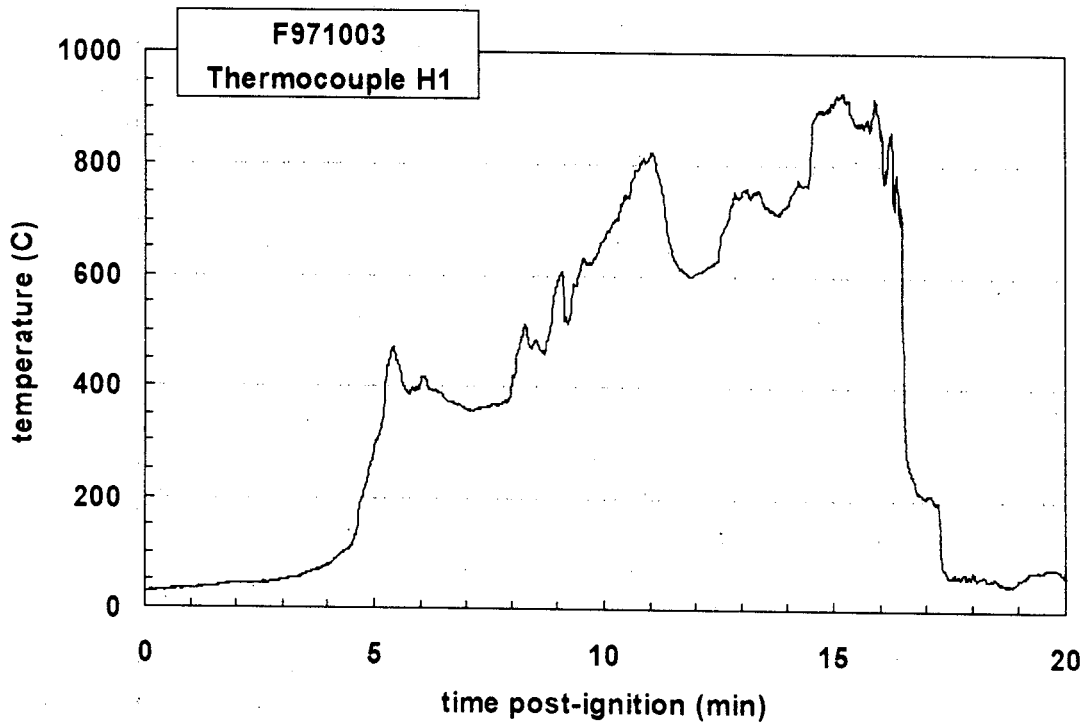

Plot C46. Fire Test F971003. Data plot from Thermocouple H1.

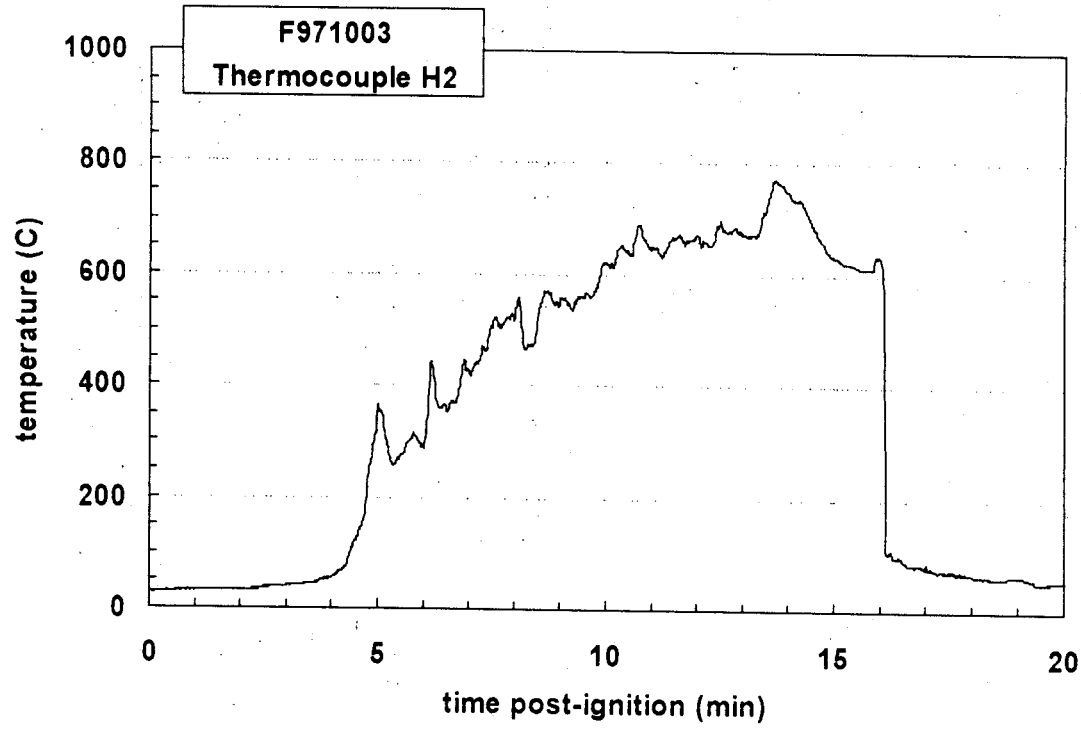

Plot C47. Fire Test F971003. Data plot from Thermocouple H2.

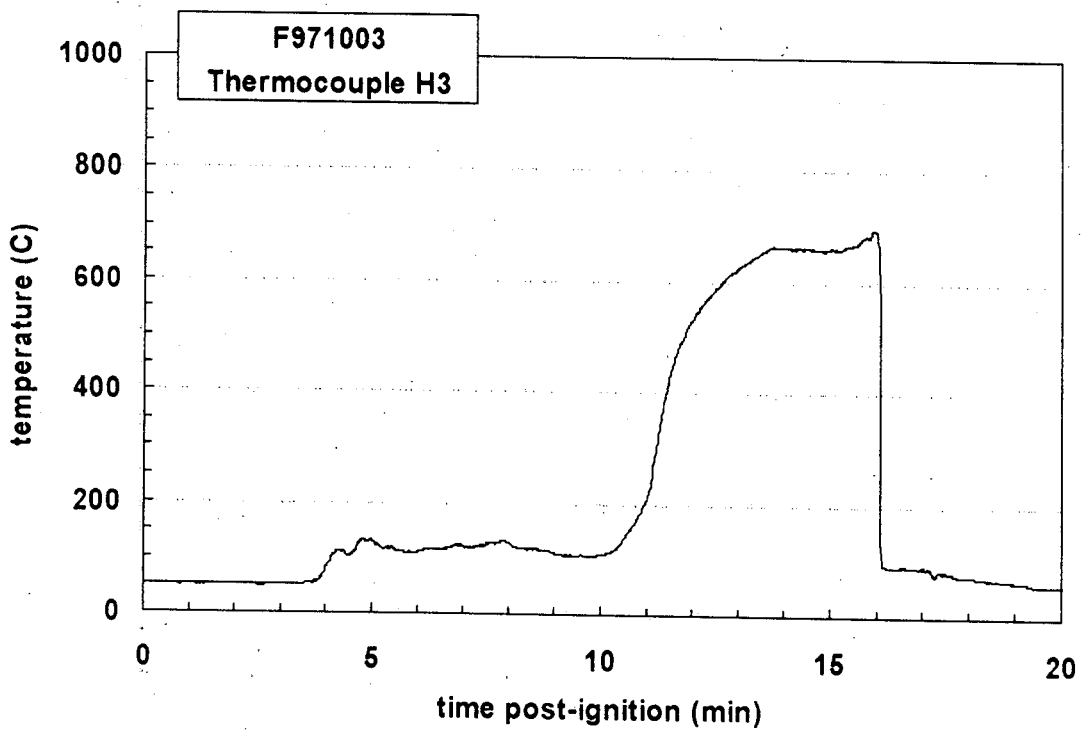

Plot C48. Fire Test F971003. Data plot from Thermocouple H3.

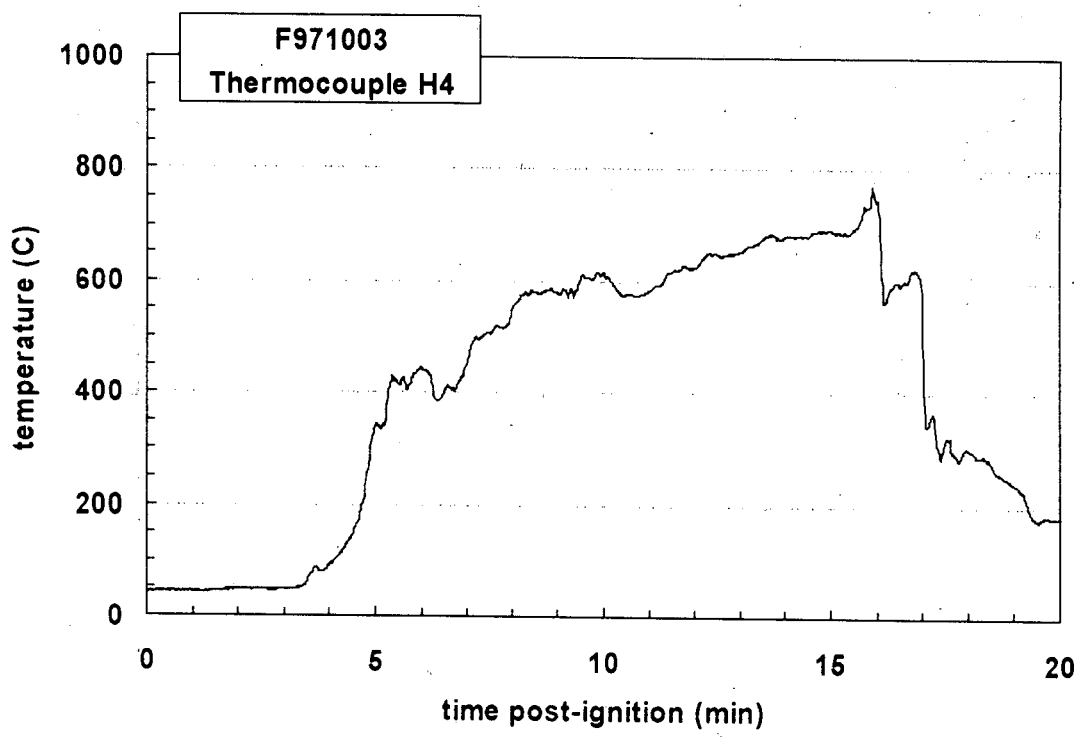

Plot C49. Fire Test F971003. Data plot from Thermocouple H4.

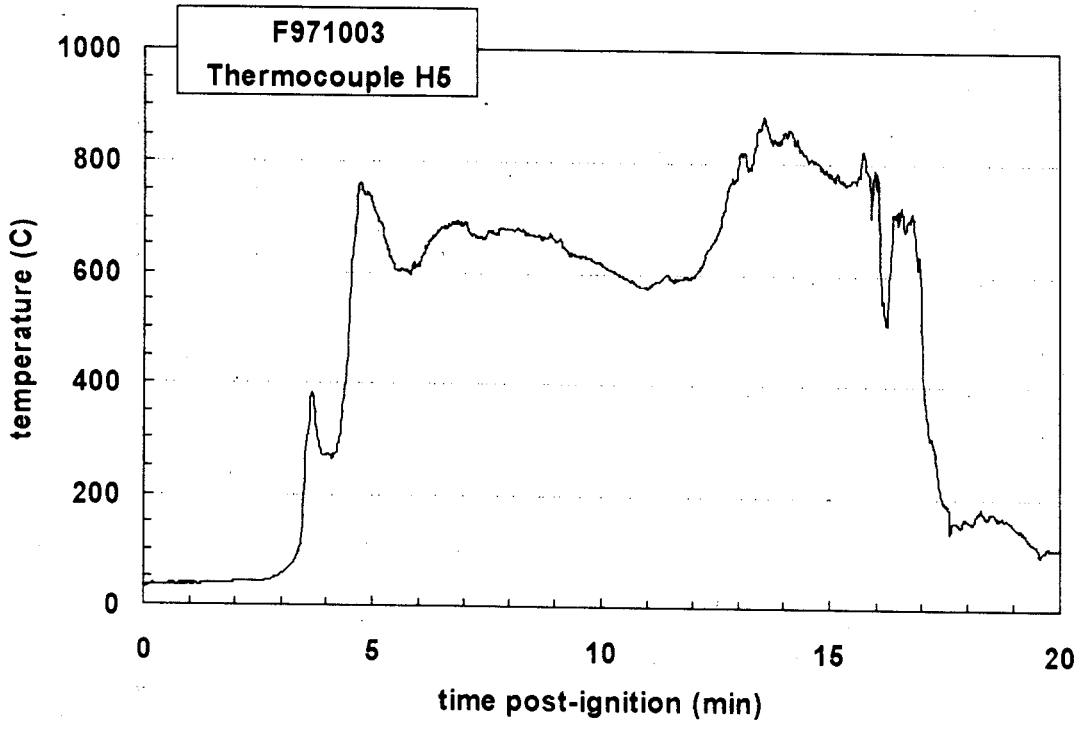

Plot C50. Fire Test F971003. Data plot from Thermocouple H5.

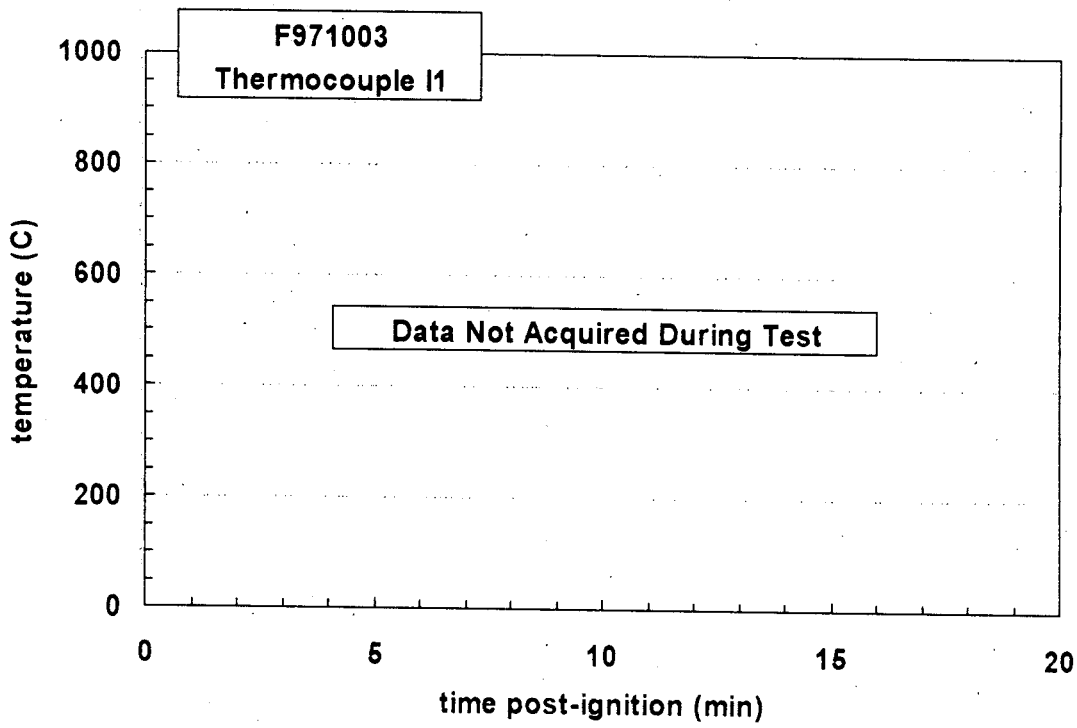

Plot C51. Fire Test F971003. Data plot from Thermocouple I1.

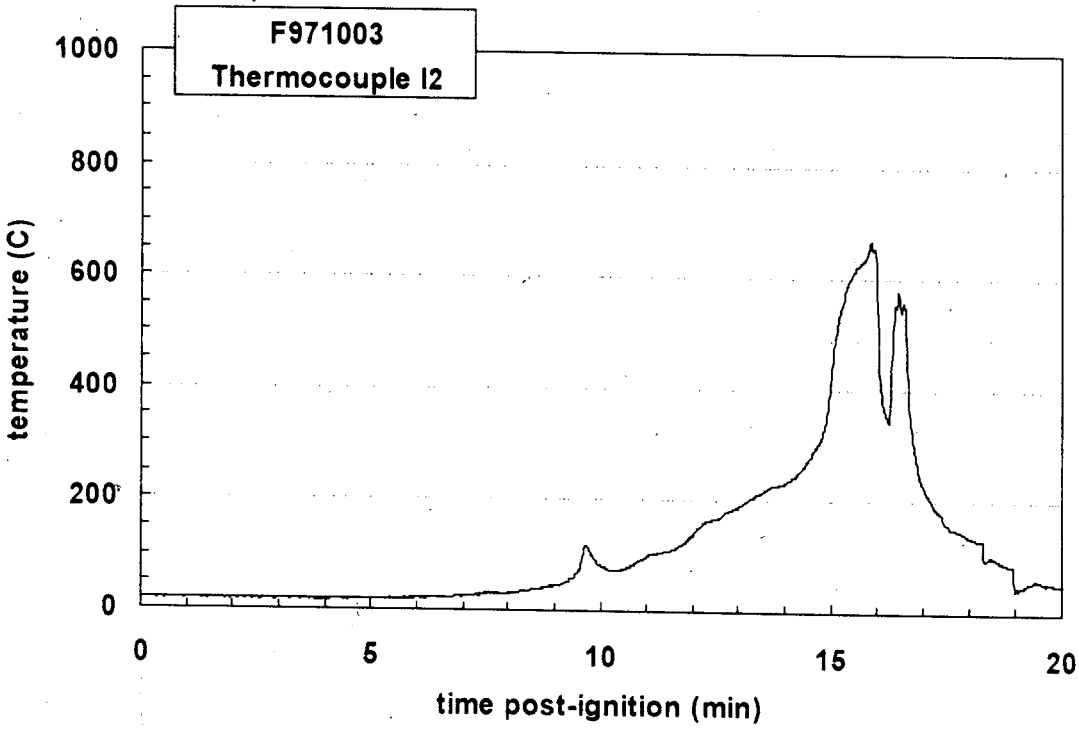

Plot C52. Fire Test F971003. Data plot from Thermocouple I2.

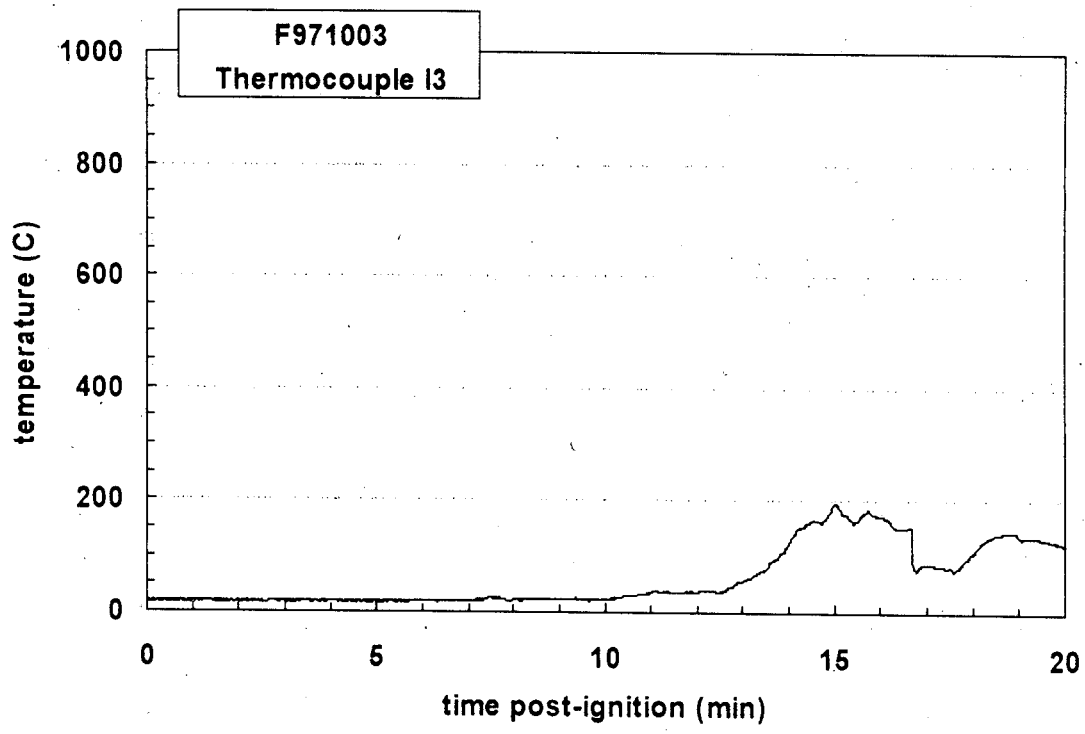

Plot C53. Fire Test F971003. Data plot from Thermocouple I3.

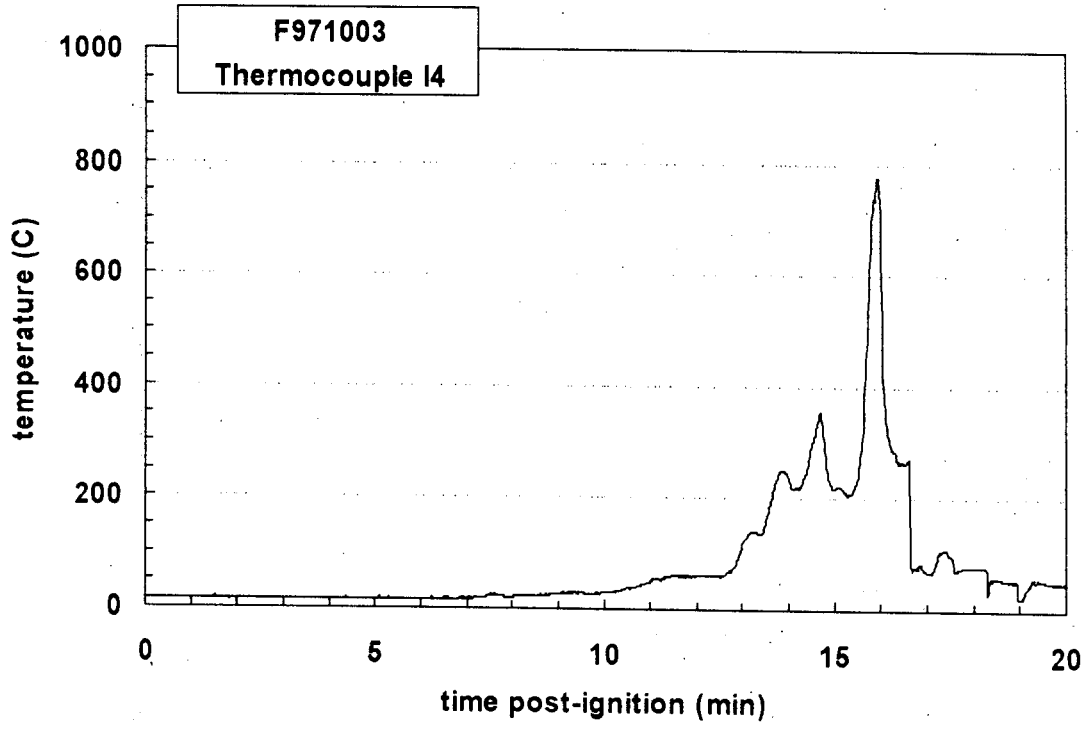

Plot C54. Fire Test F971003. Data plot from Thermocouple I4.

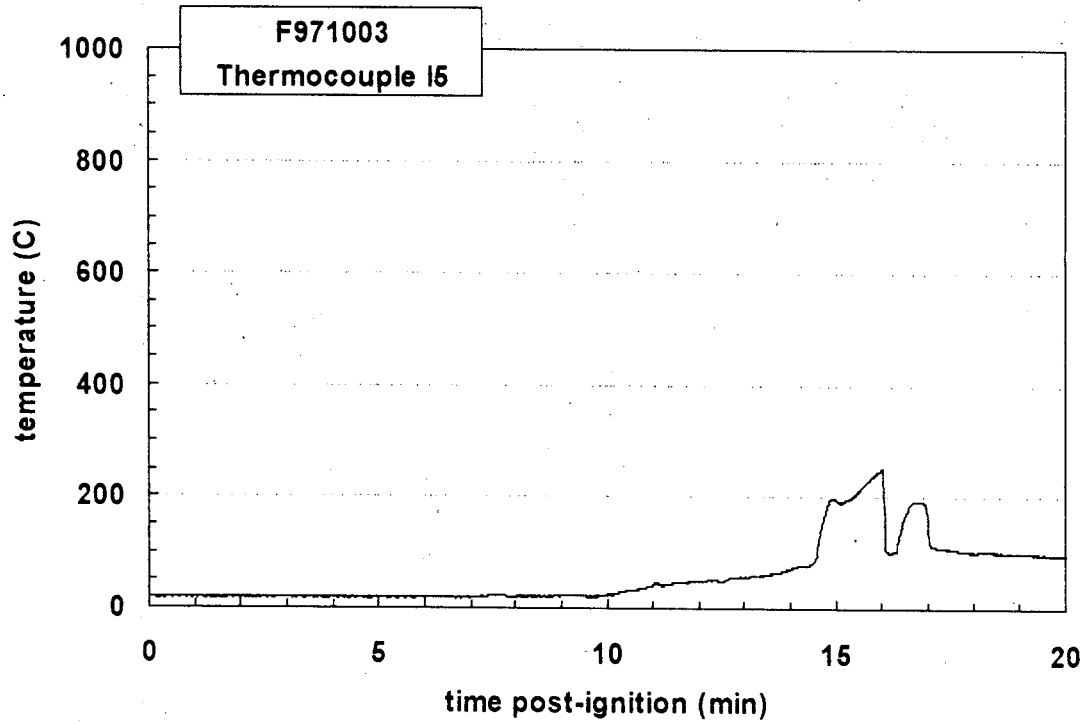

Plot C55. Fire Test F971003. Data plot from Thermocouple I5.

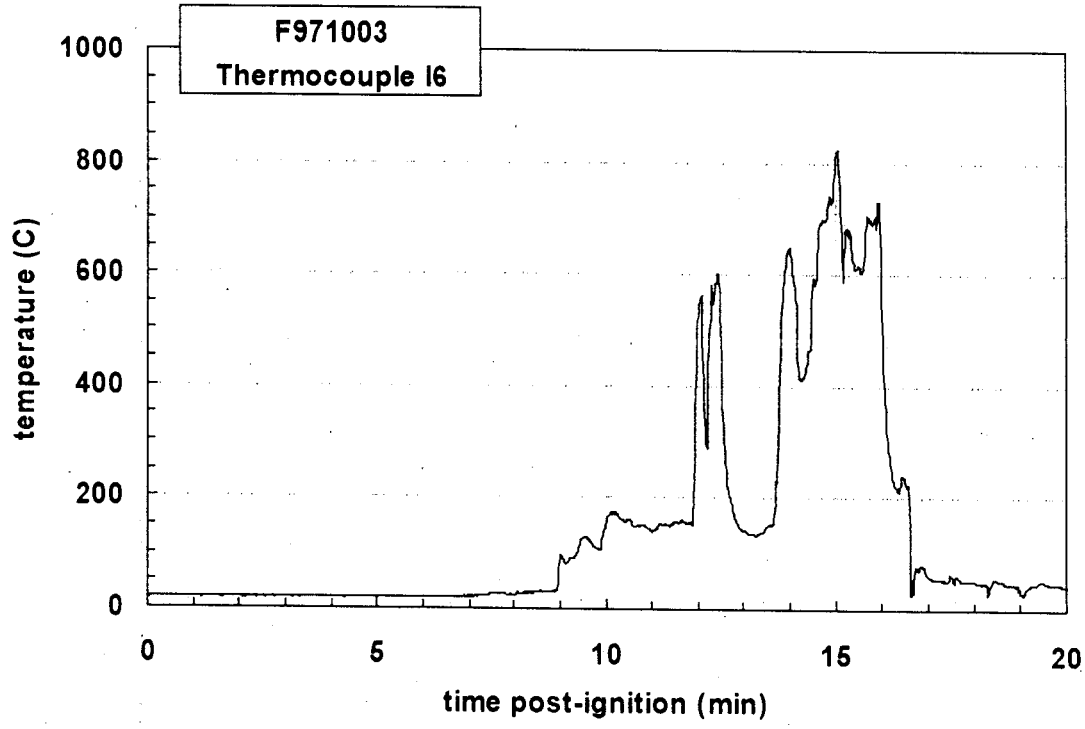

Plot C56. Fire Test F971003. Data plot from Thermocouple I6.

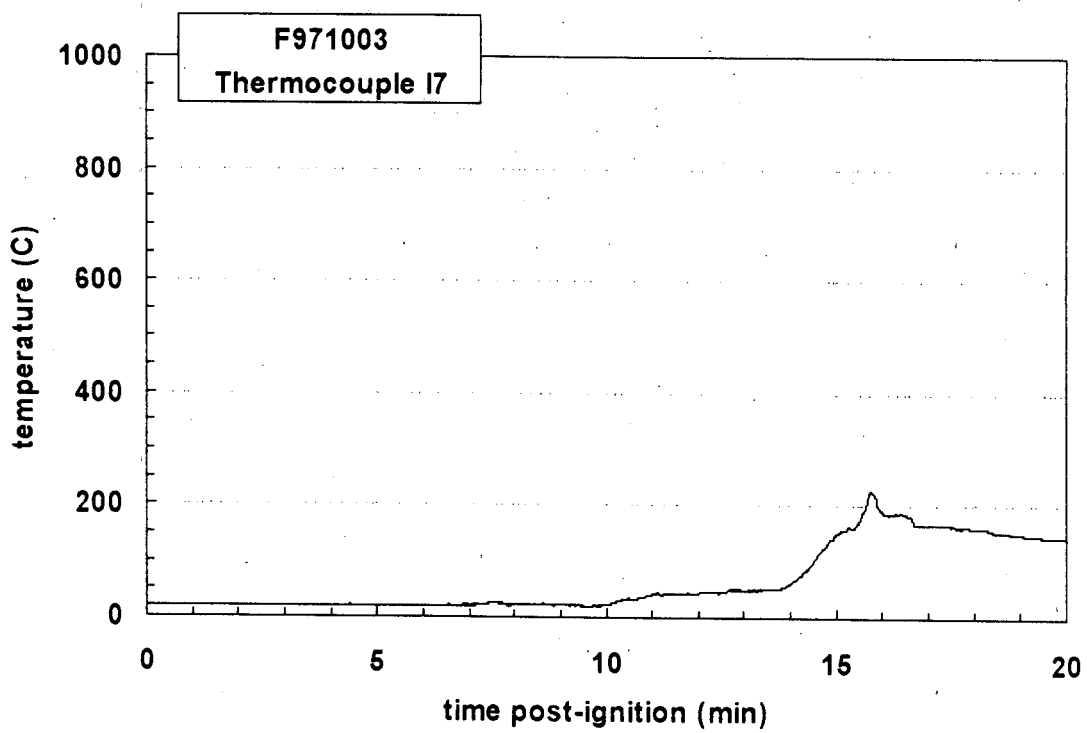

Plot C57. Fire Test F971003. Data plot from Thermocouple I7.

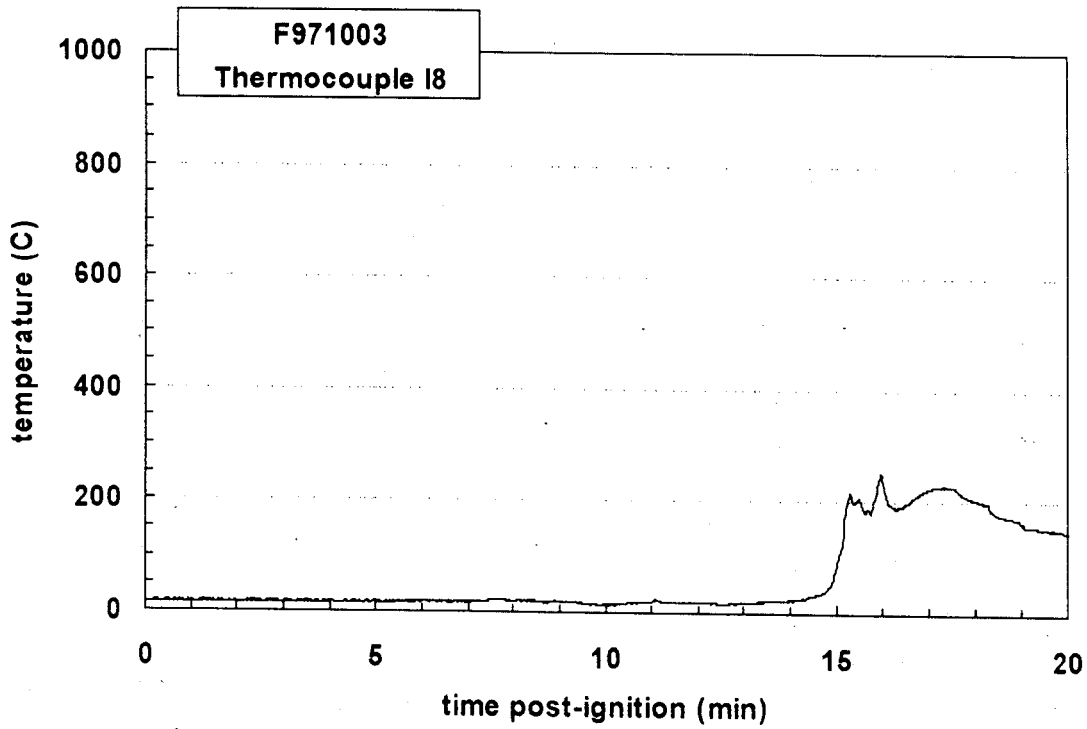

Plot C58. Fire Test F971003. Data plot from Thermocouple I8.

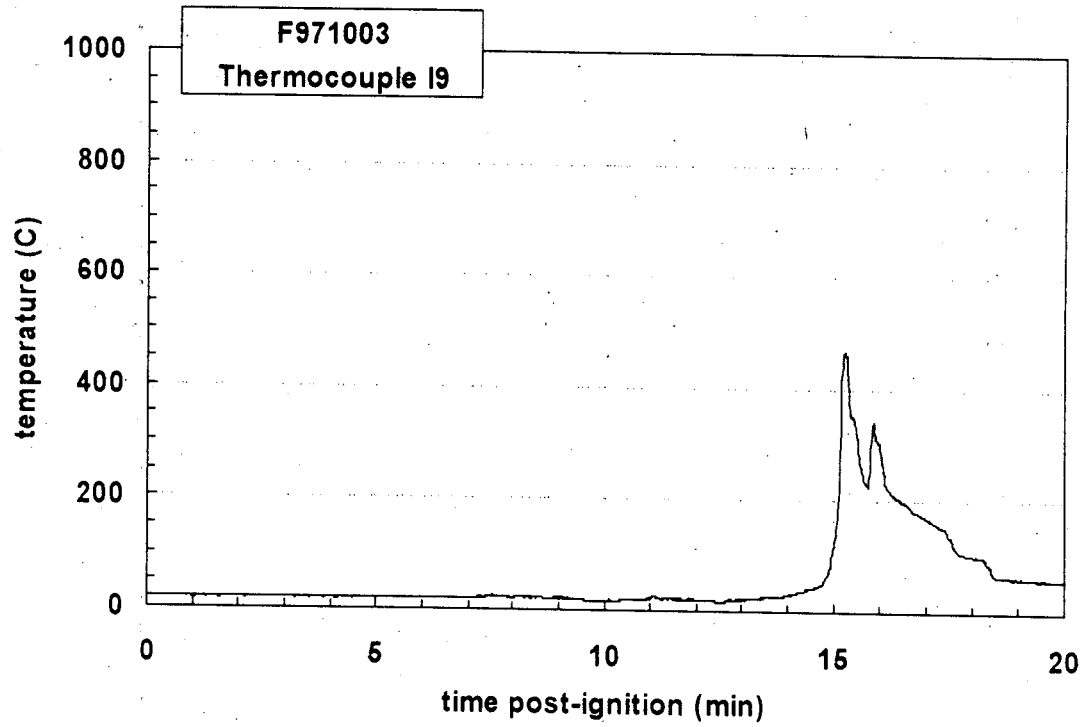

Plot C59. Fire Test F971003. Data plot from Thermocouple I9.

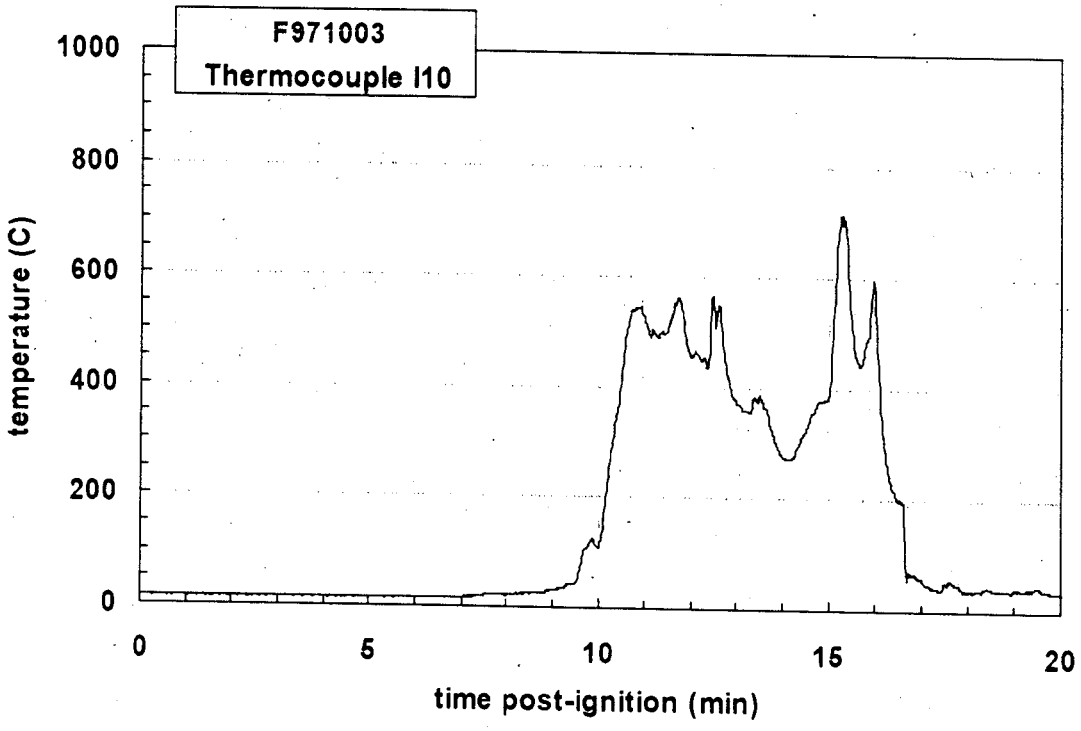

Plot C60. Fire Test F971003. Data plot from Thermocouple I10.

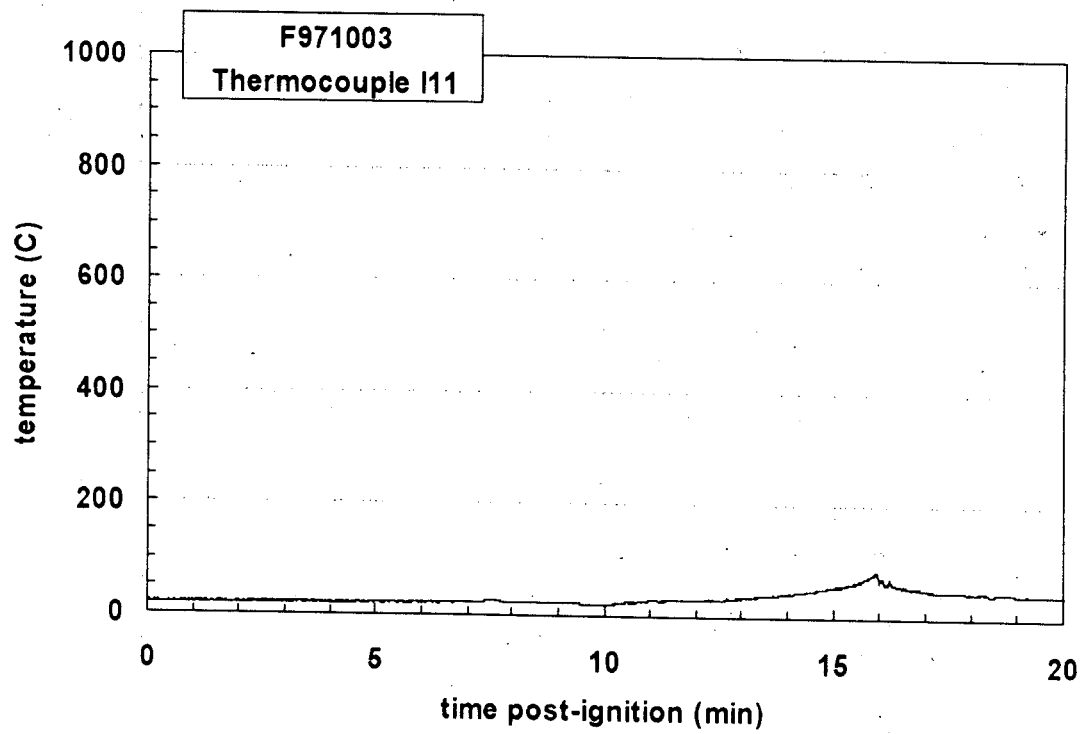

Plot C61. Fire Test F971003. Data plot from Thermocouple I11.

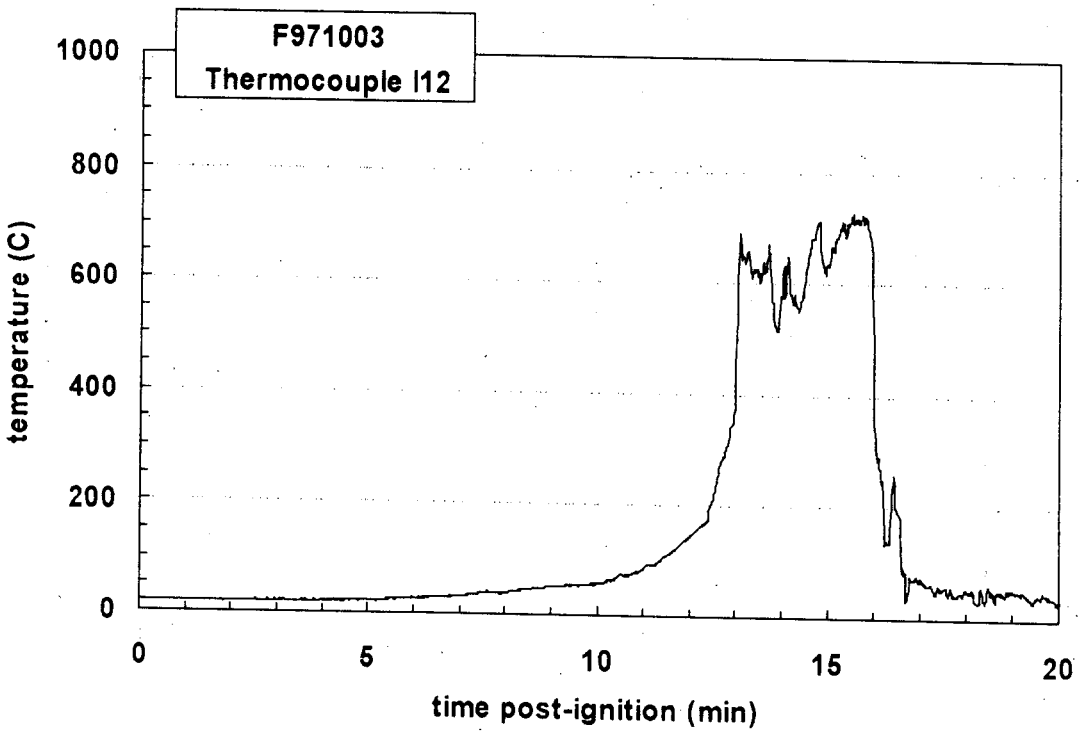

Plot C62. Fire Test F971003. Data plot from Thermocouple I12.

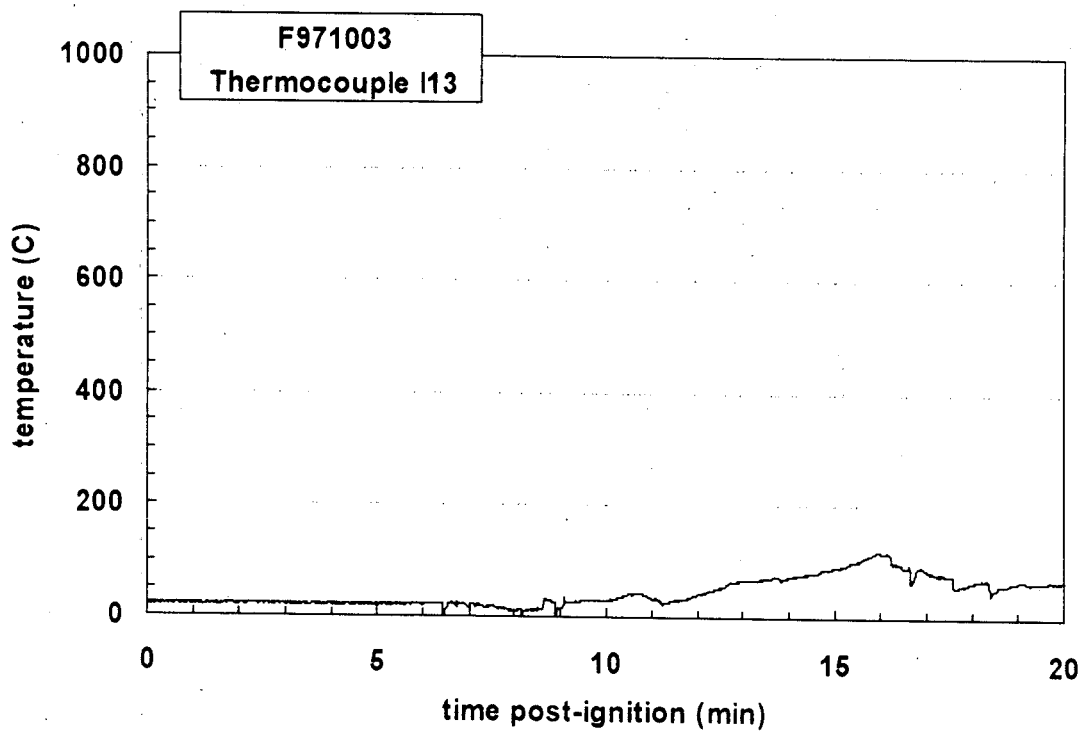

Plot C63. Fire Test F971003. Data plot from Thermocouple I13.

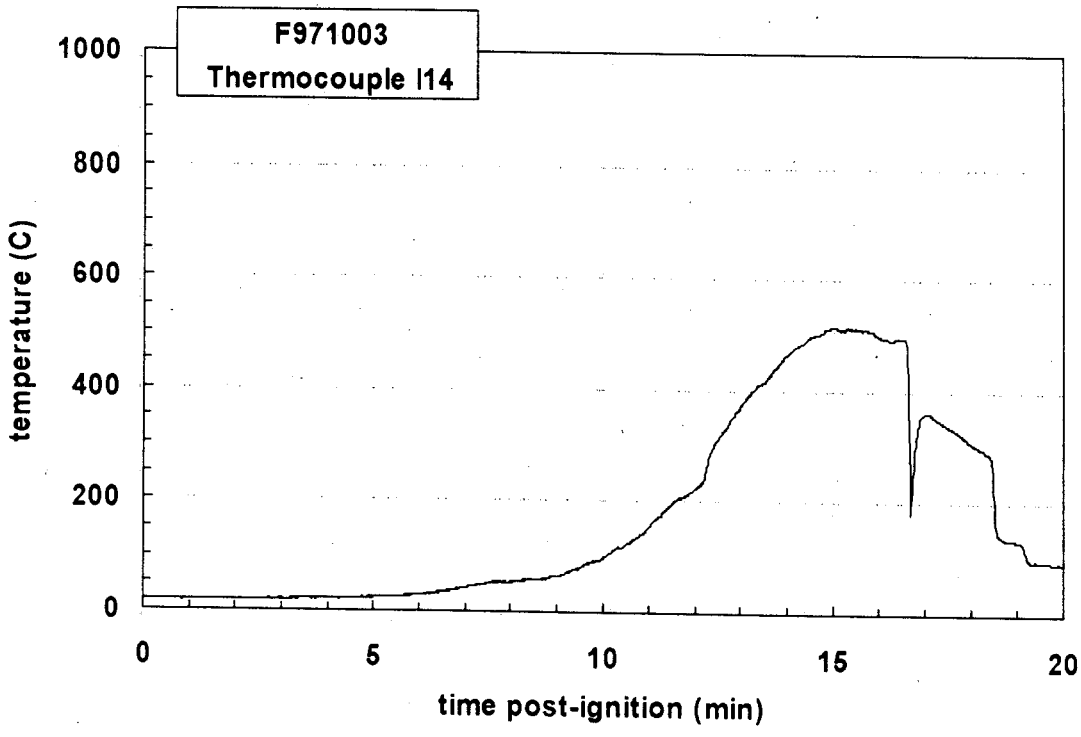

Plot C64. Fire Test F971003. Data plot from Thermocouple I14.

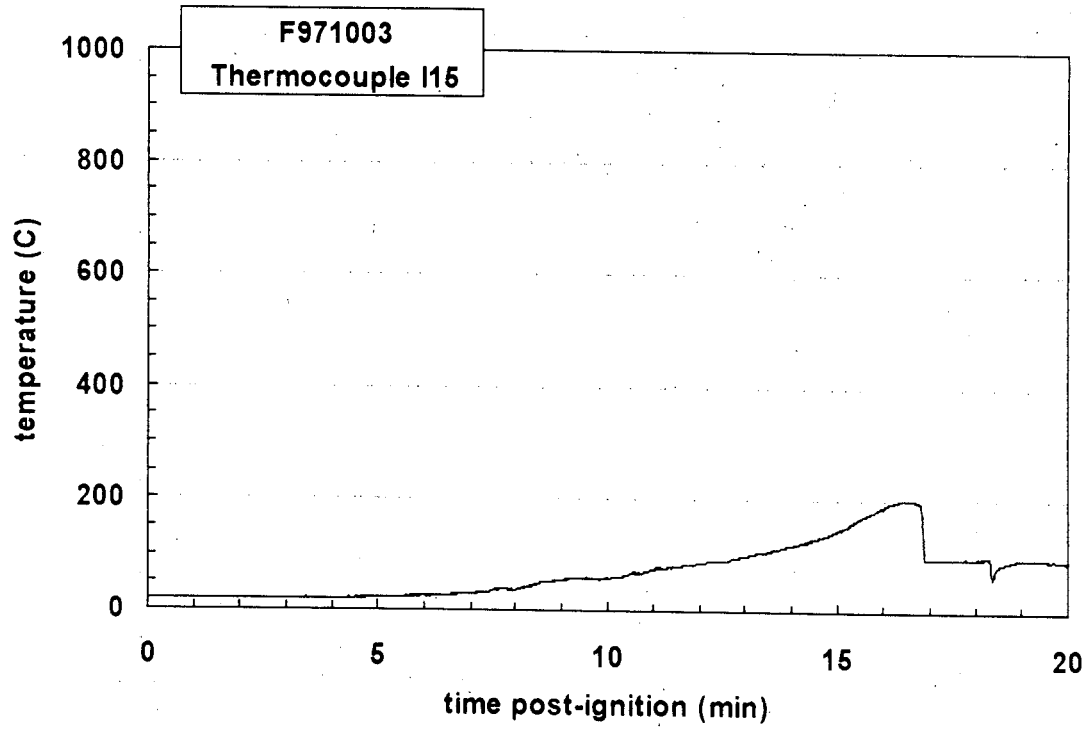

Plot C65. Fire Test F971003. Data plot from Thermocouple I15.

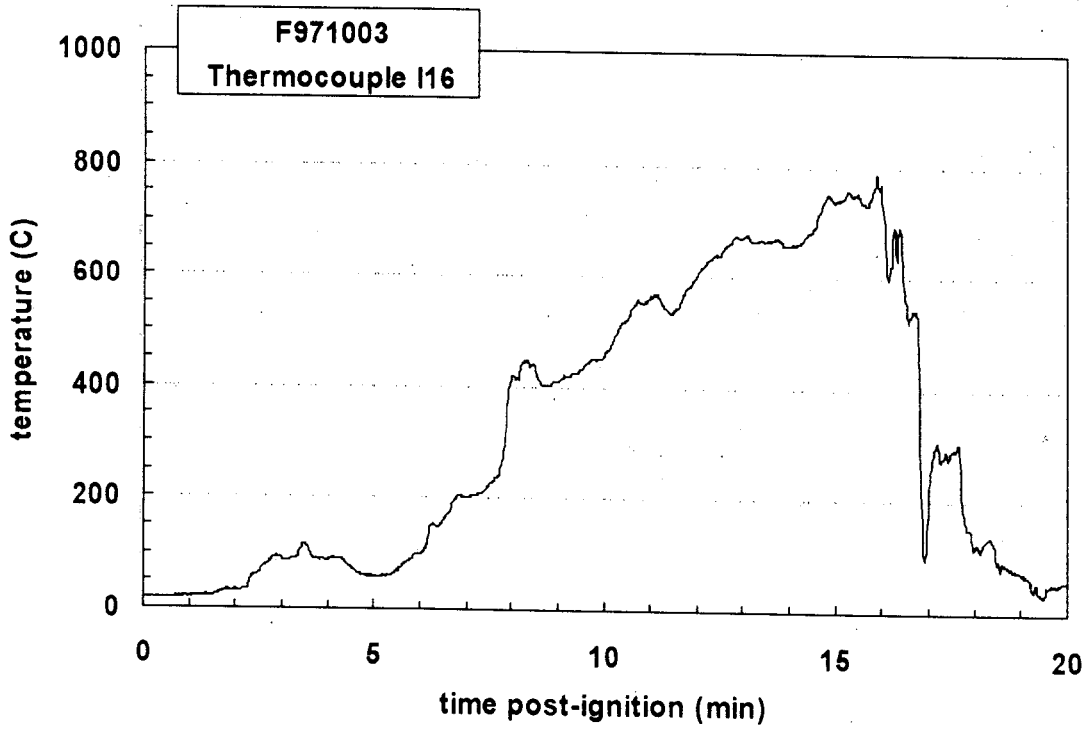

Plot C66. Fire Test F971003. Data plot from Thermocouple I16.

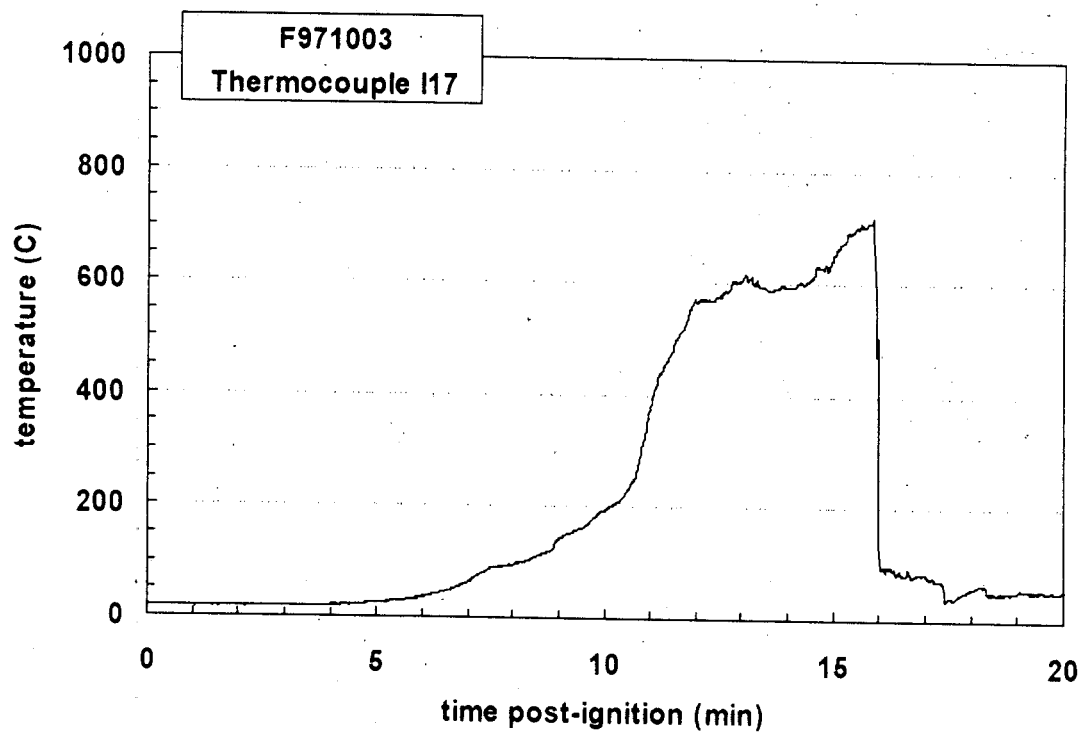

Plot C67. Fire Test F971003. Data plot from Thermocouple I17.

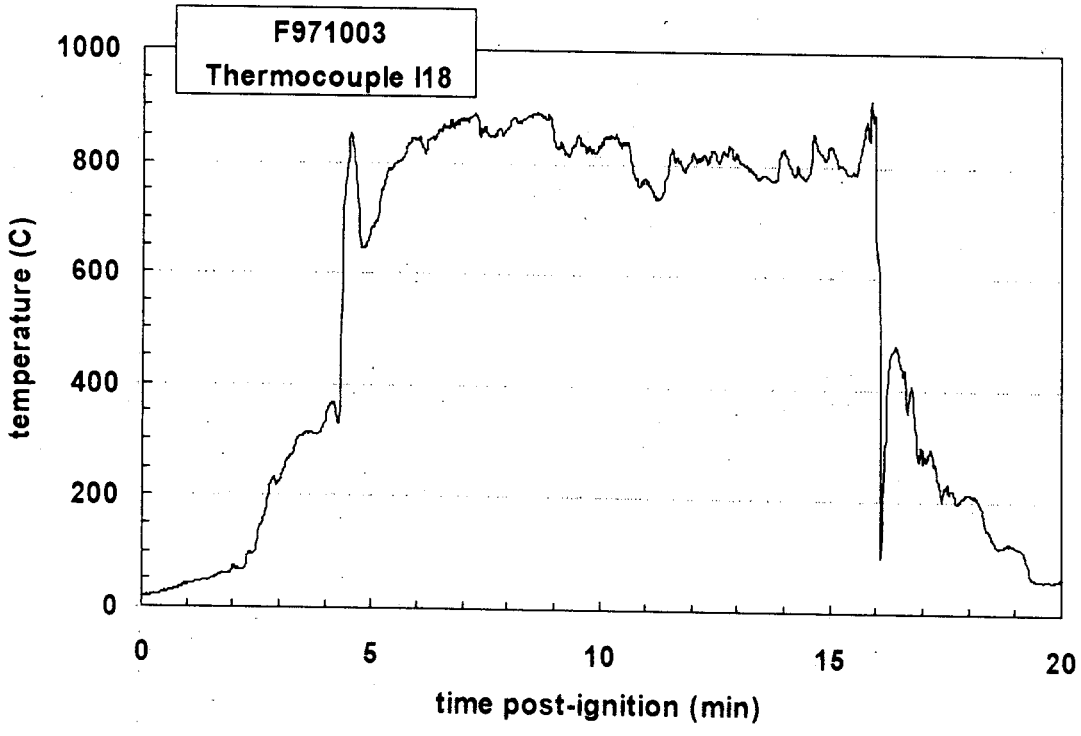

Plot C68. Fire Test F971003. Data plot from Thermocouple I18.

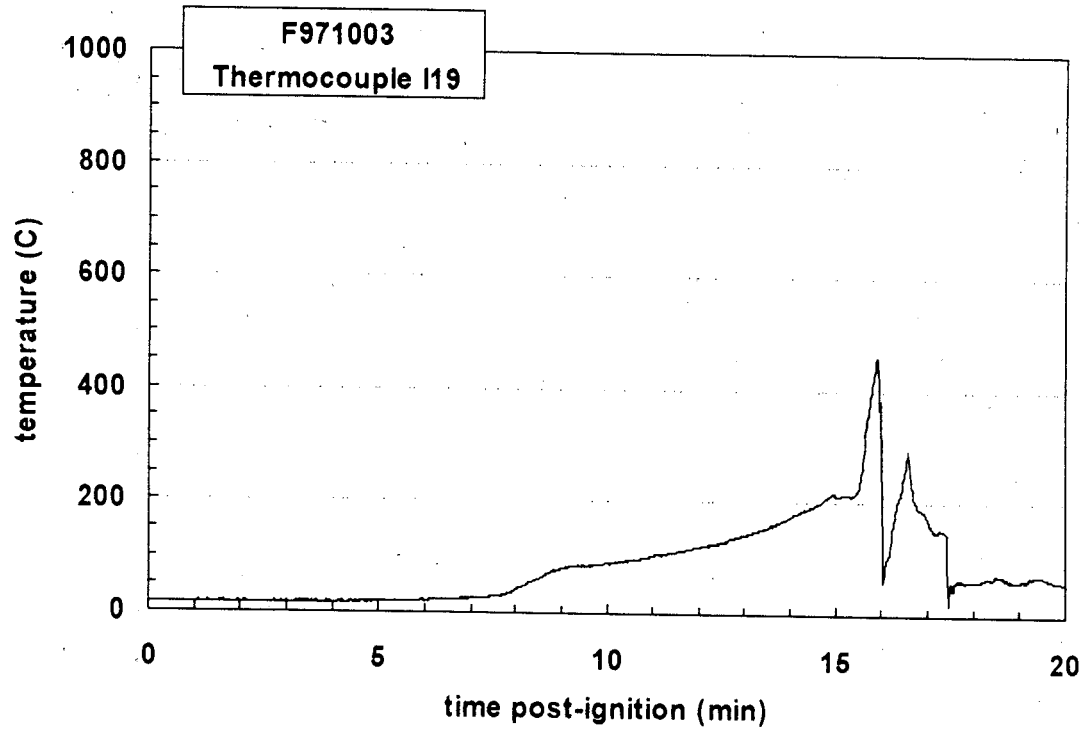

Plot C69. Fire Test F971003. Data plot from Thermocouple I19.

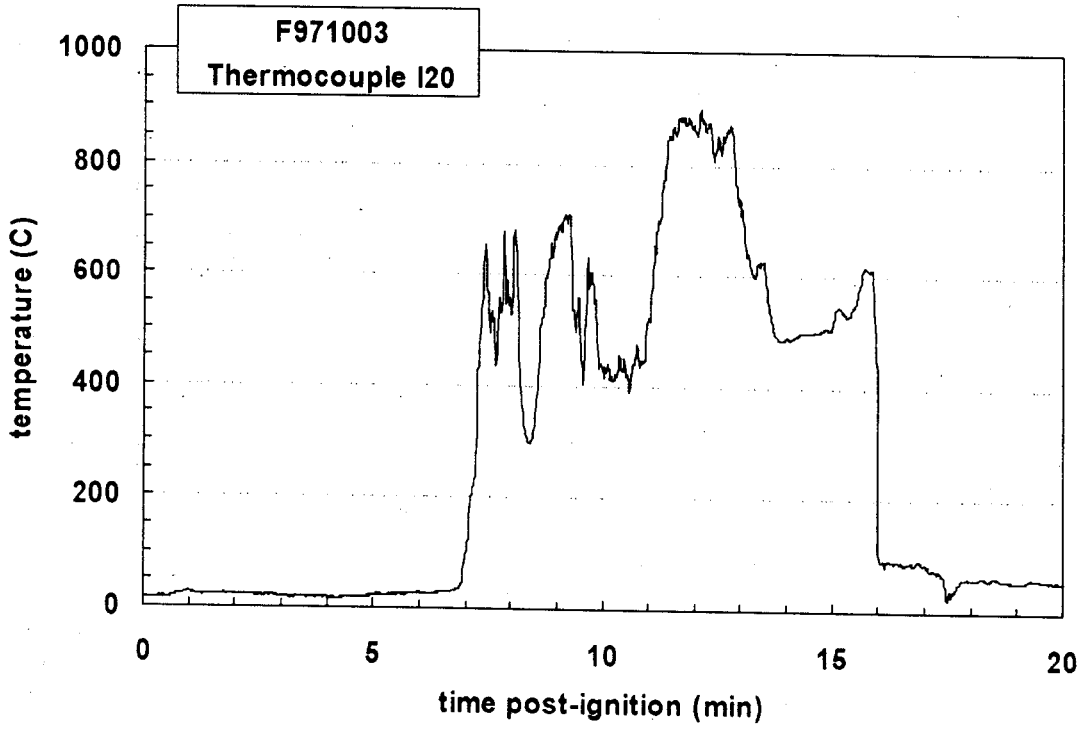

Plot C70. Fire Test F971003. Data plot from Thermocouple I20.

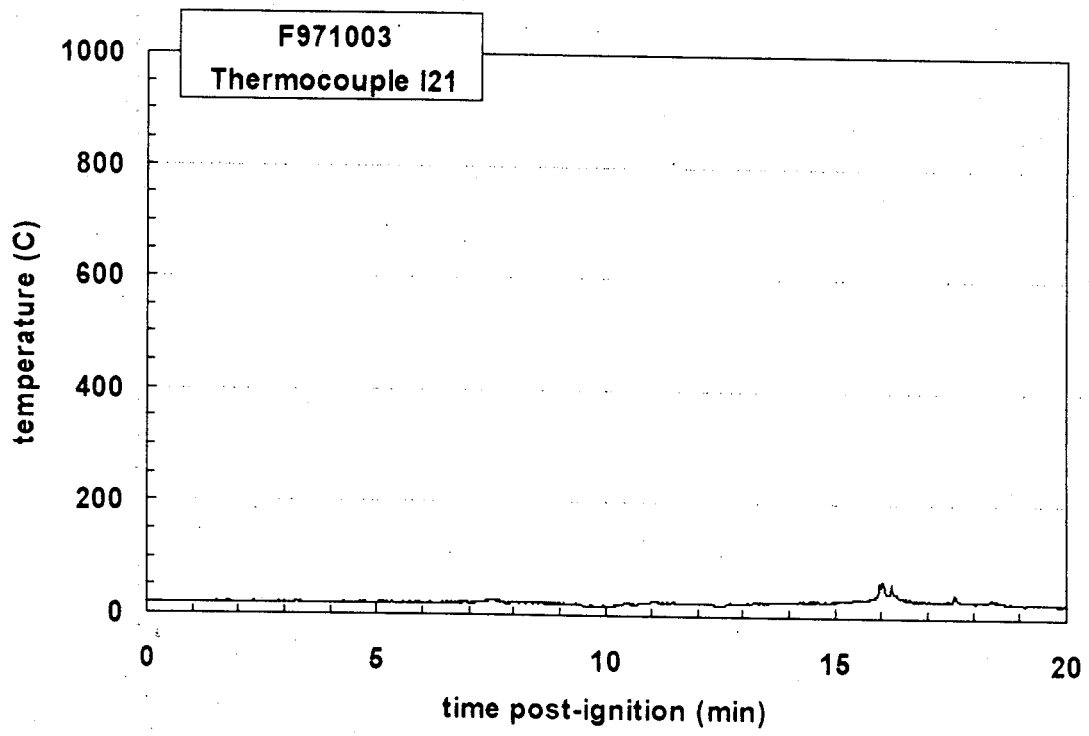

Plot C71. Fire Test F971003. Data plot from Thermocouple I21.

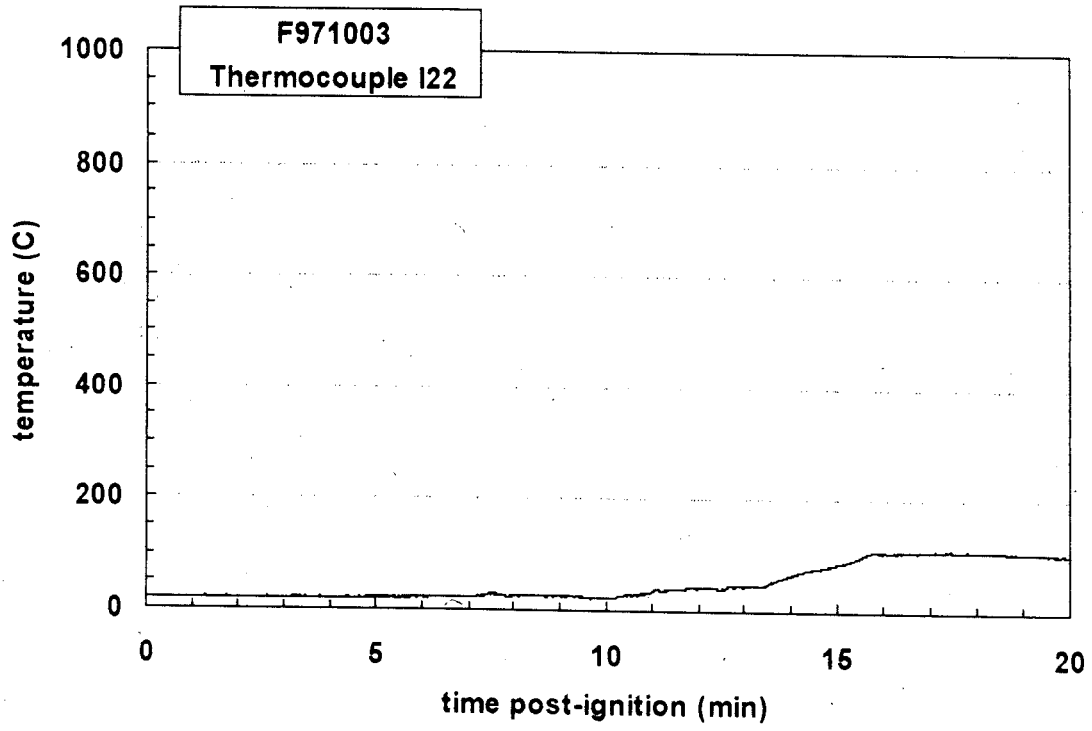

Plot C72. Fire Test F971003. Data plot from Thermocouple I22.

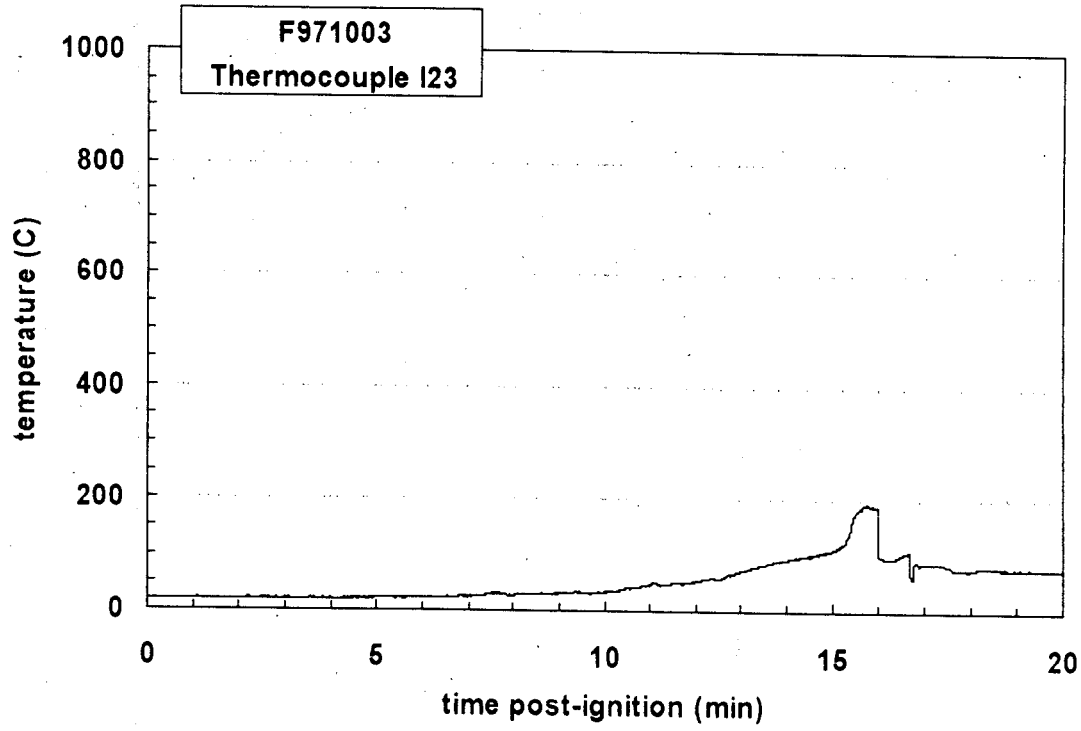

Plot C73. Fire Test F971003. Data plot from Thermocouple I23.

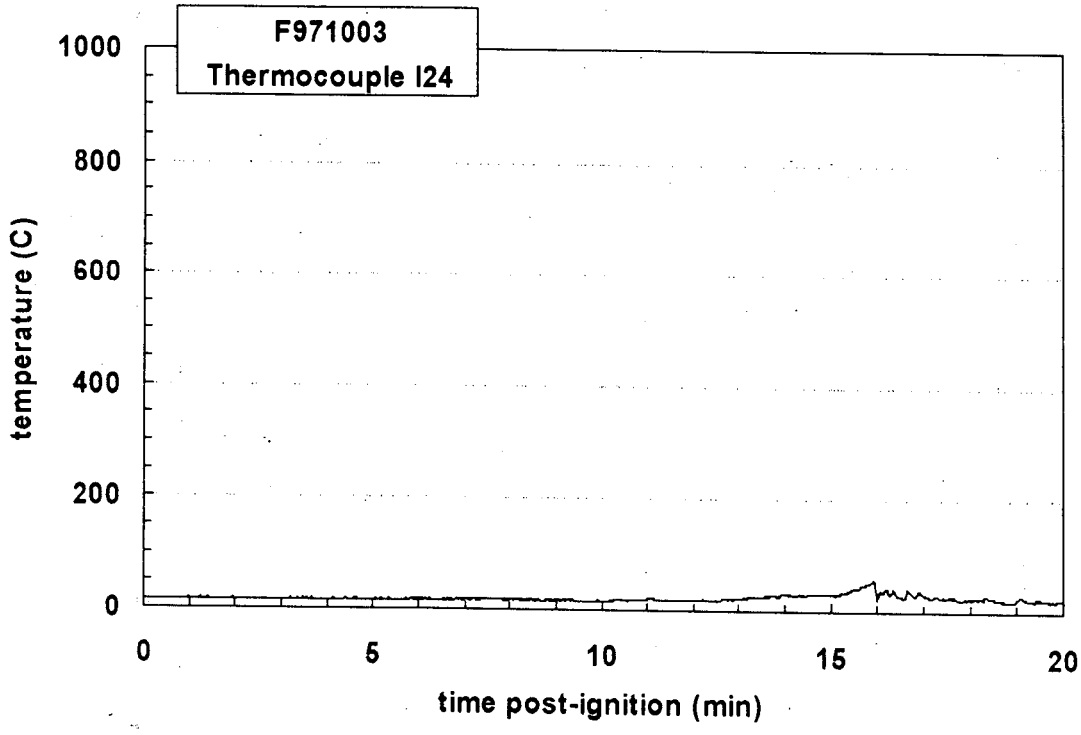

Plot C74. Fire Test F971003. Data plot from Thermocouple I24.

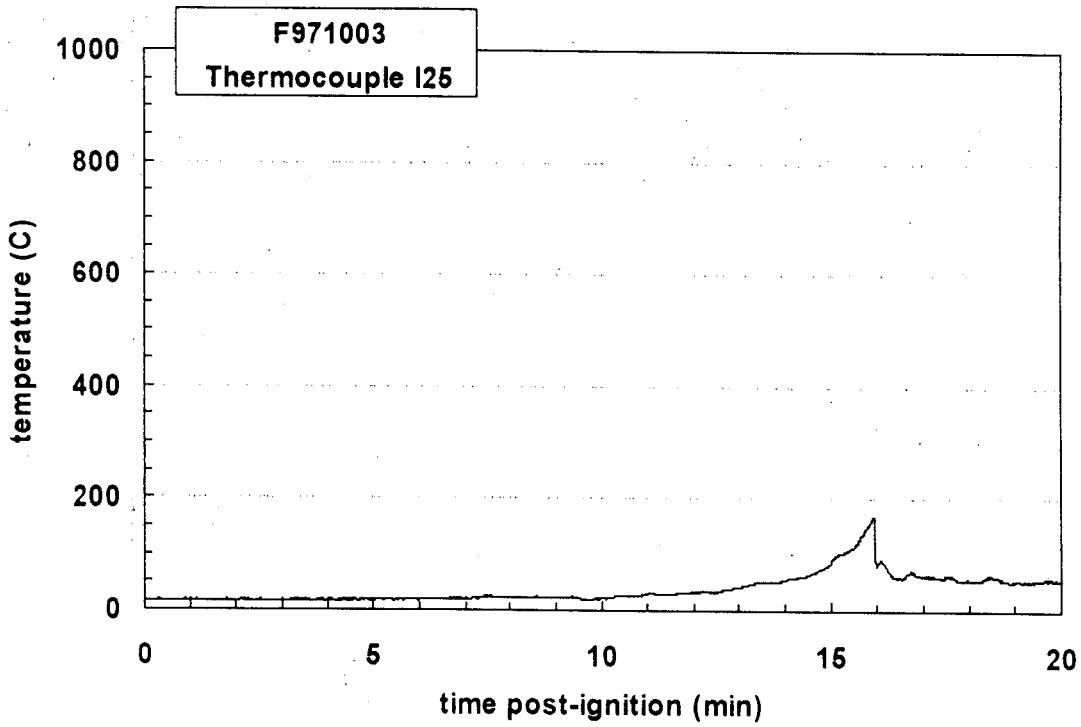

Plot C75. Fire Test F971003. Data plot from Thermocouple I25.

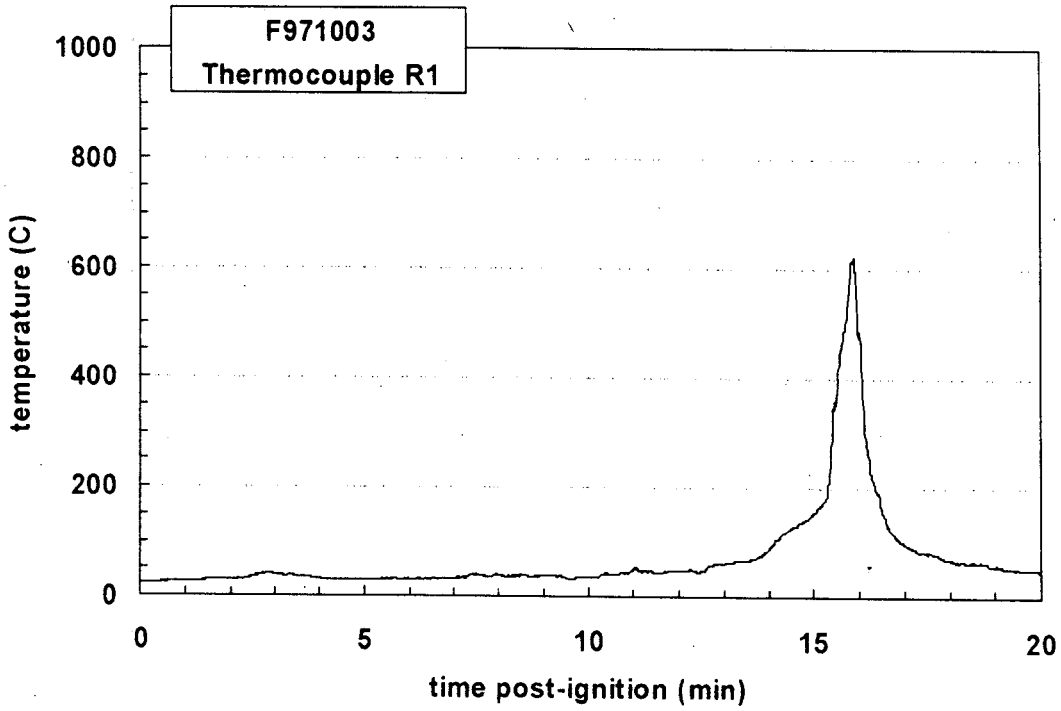

Plot C76. Fire Test F971003. Data plot from Thermocouple IR1.

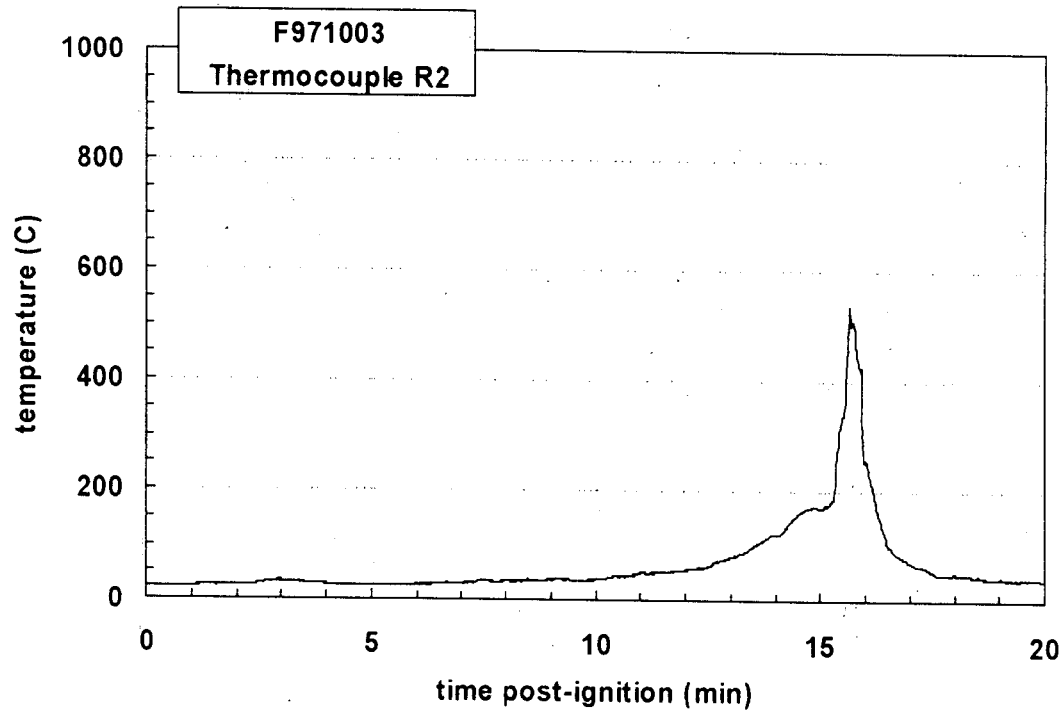

Plot C77. Fire Test F971003. Data plot from Thermocouple R2.

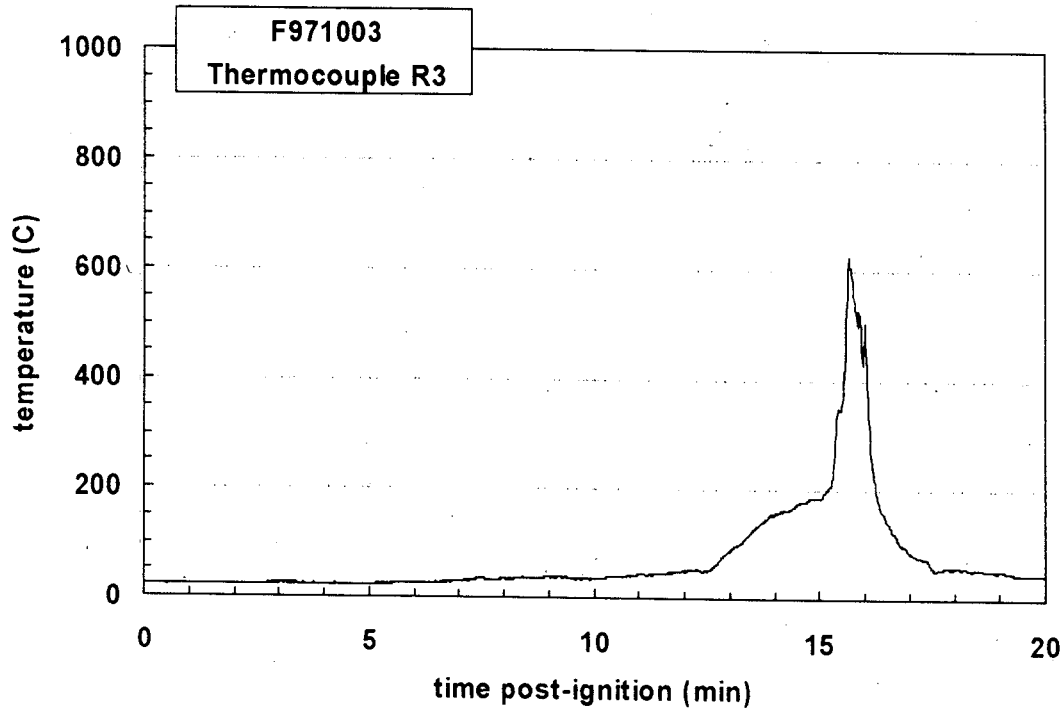

Plot C78. Fire Test F971003. Data plot from Thermocouple R3.

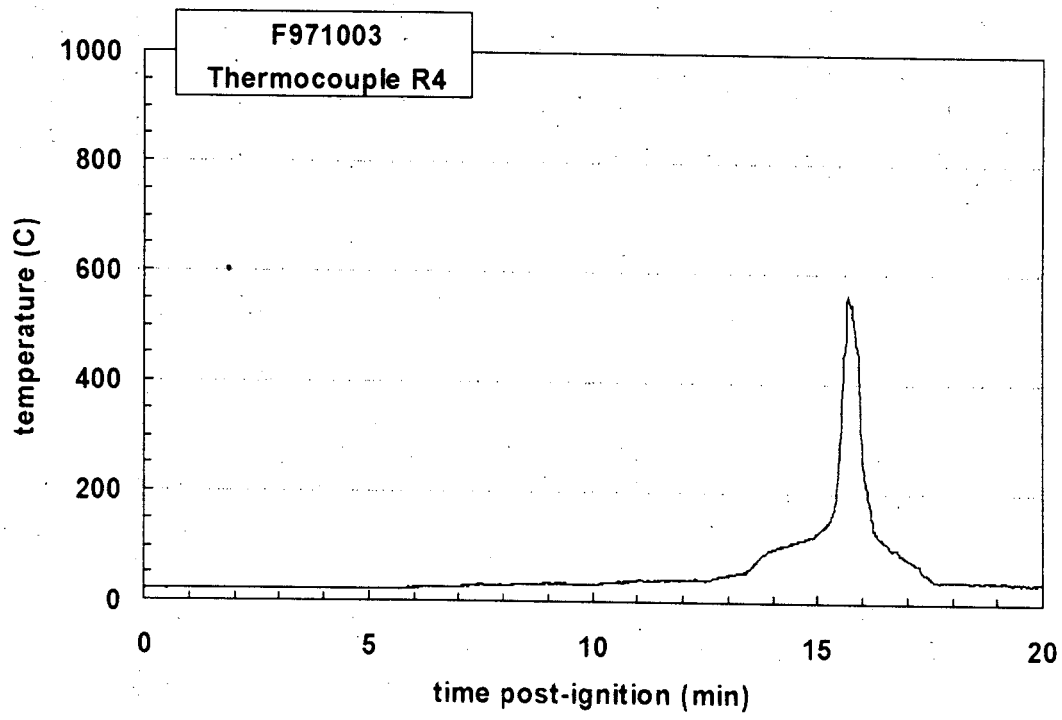

Plot C79. Fire Test F971003. Data plot from Thermocouple R4.

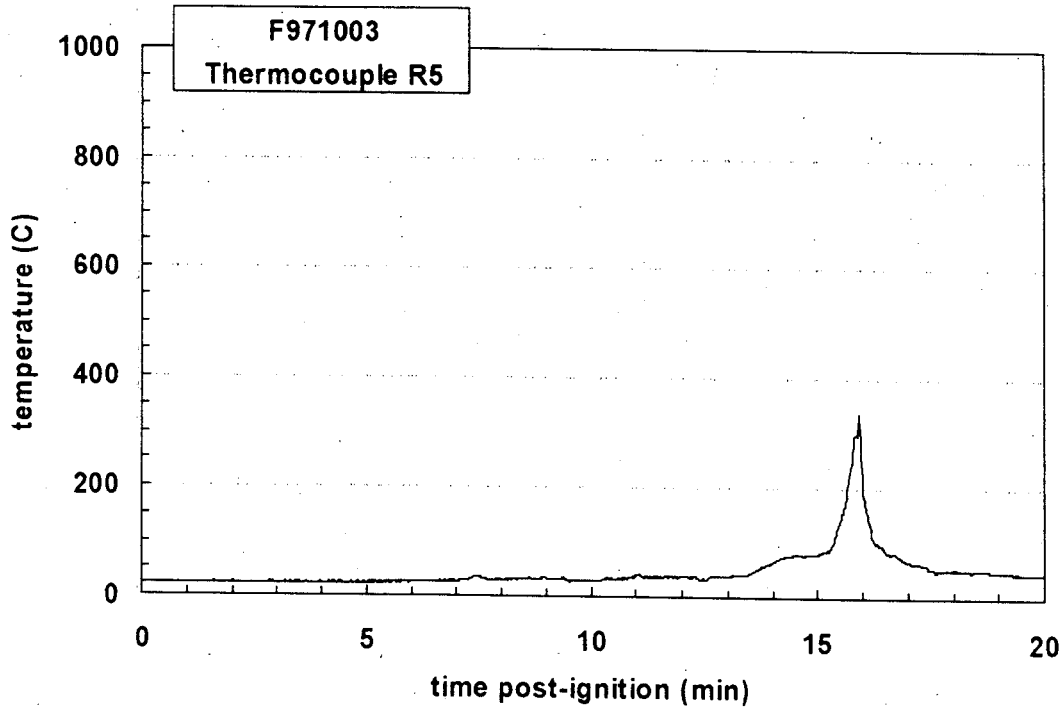

Plot C80. Fire Test F971003. Data plot from Thermocouple R5.

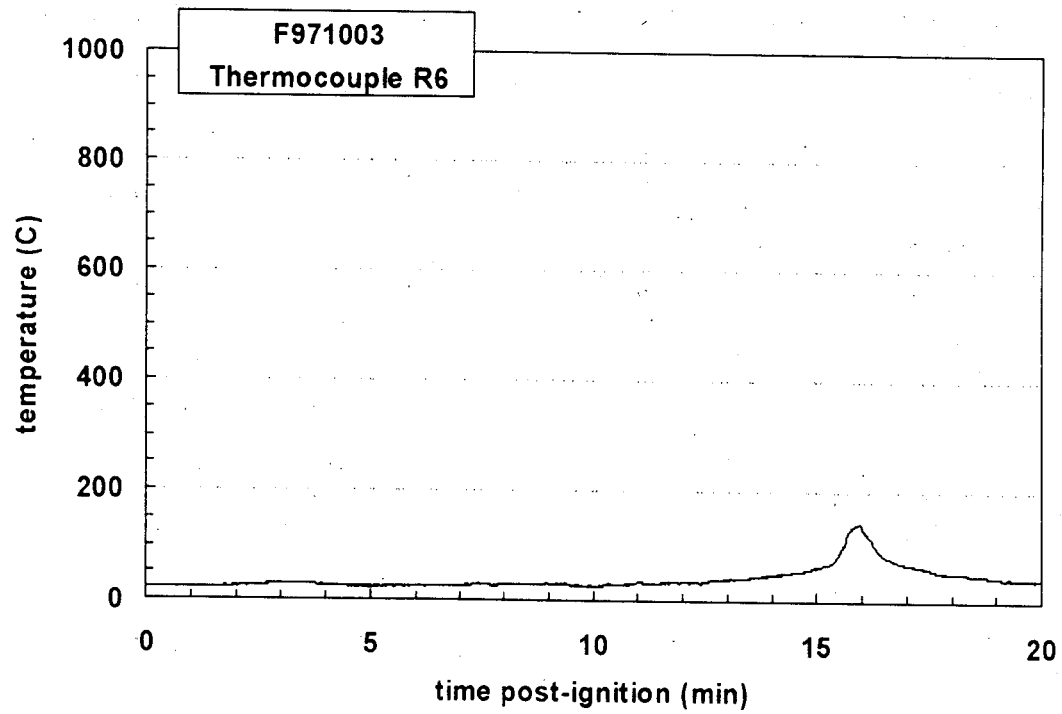

Plot C81. Fire Test F971003. Data plot from Thermocouple R6.

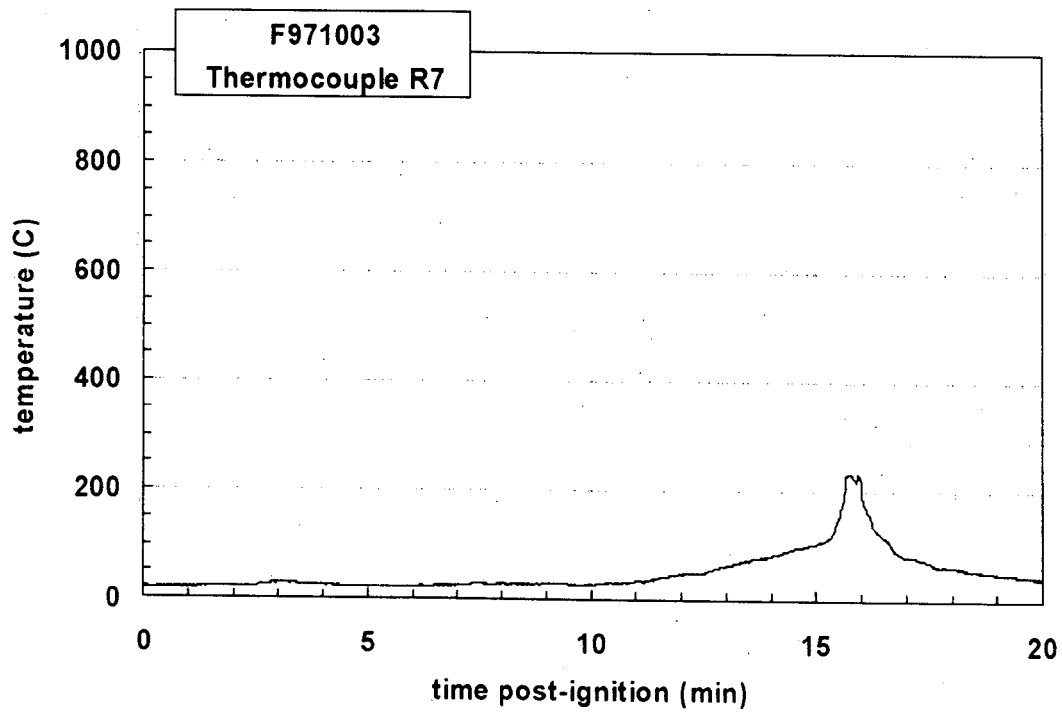

Plot C82. Fire Test F971003. Data plot from Thermocouple R7.

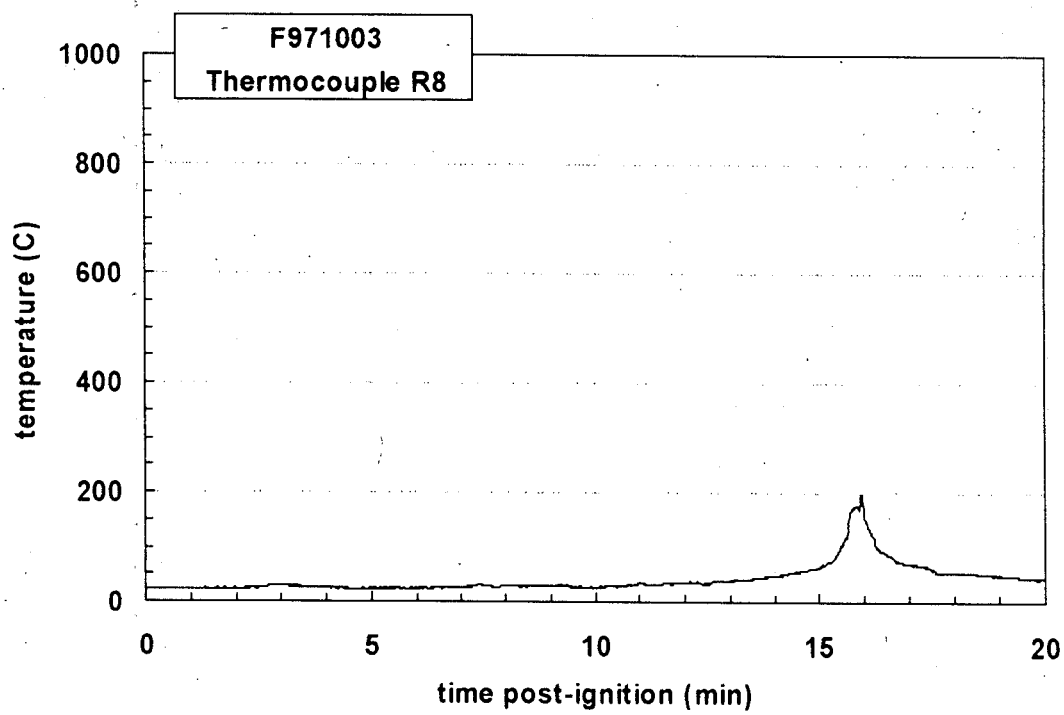

Plot C83. Fire Test F971003. Data plot from Thermocouple R8.

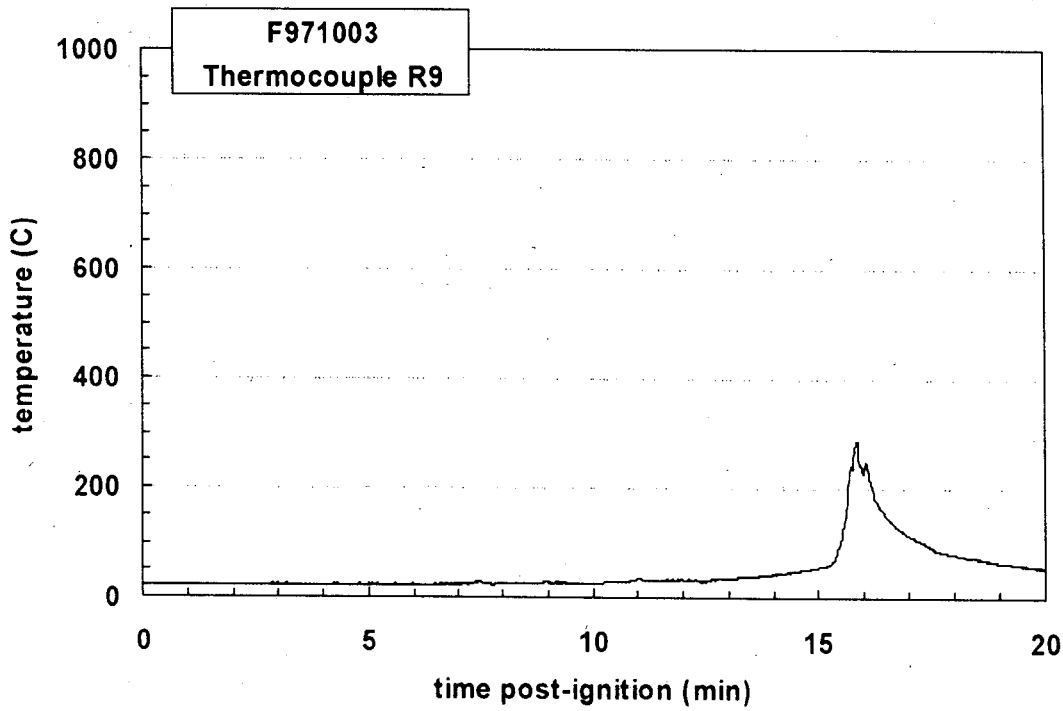

Plot C84. Fire Test F971003. Data plot from Thermocouple R9.

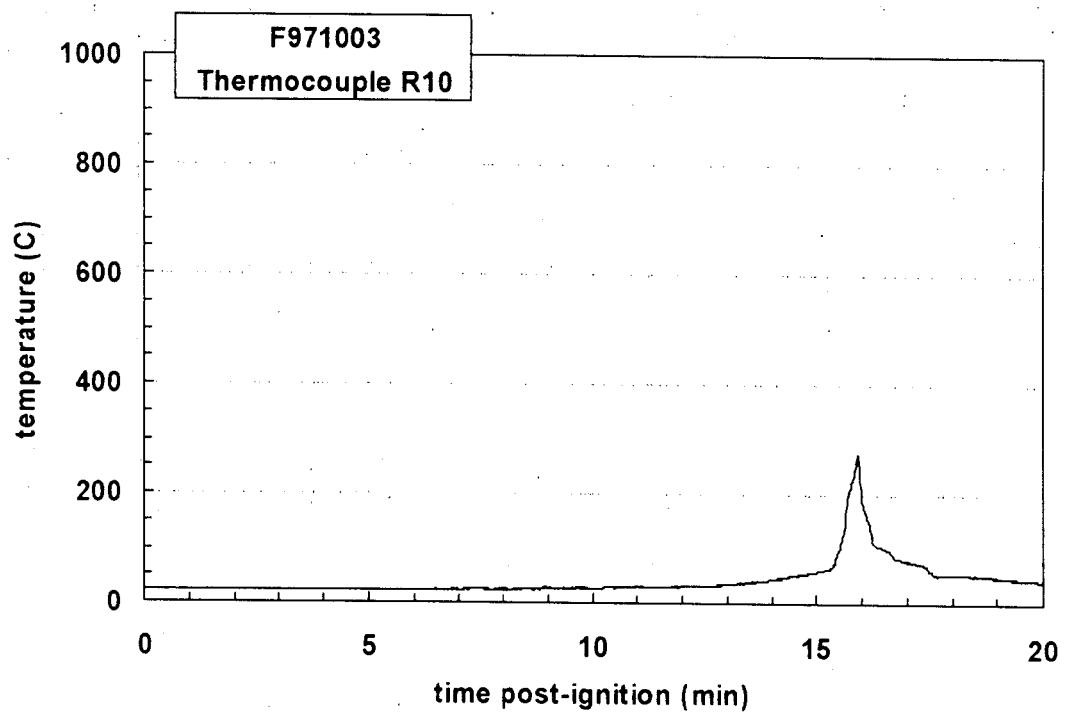

Plot C85. Fire Test F971003. Data plot from Thermocouple R10.

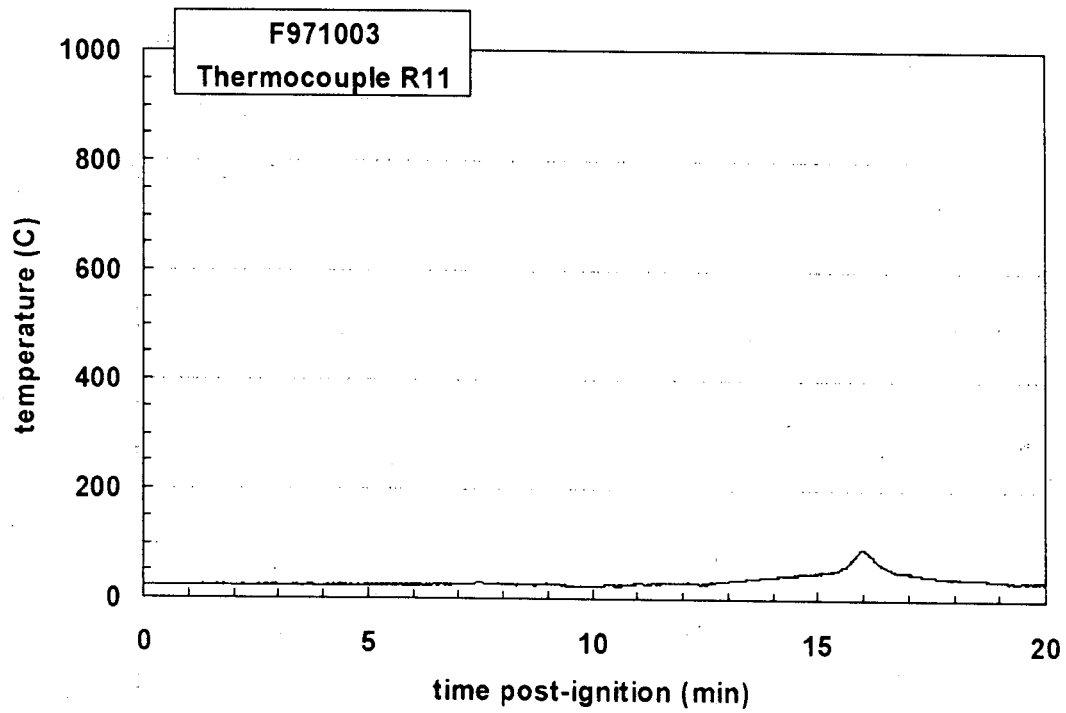

Plot C86. Fire Test F971003. Data plot from Thermocouple R11.

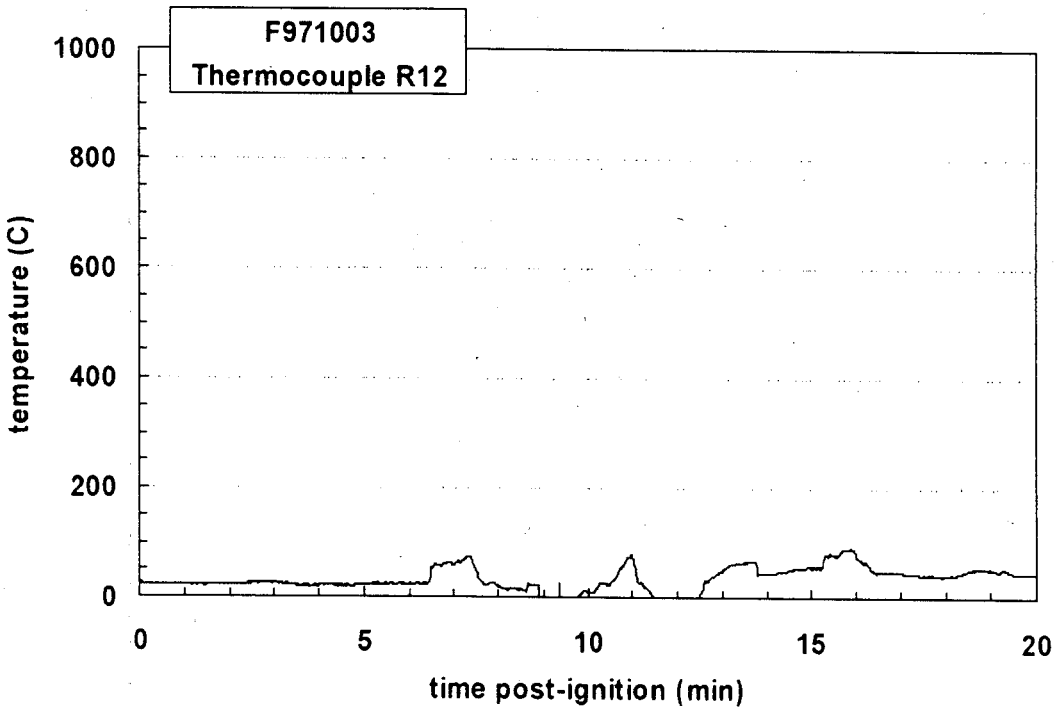

Plot C87. Fire Test F971003. Data plot from Thermocouple R12. The Thermocouple began to malfunction at 08:90 (min:sec) post-ignition.

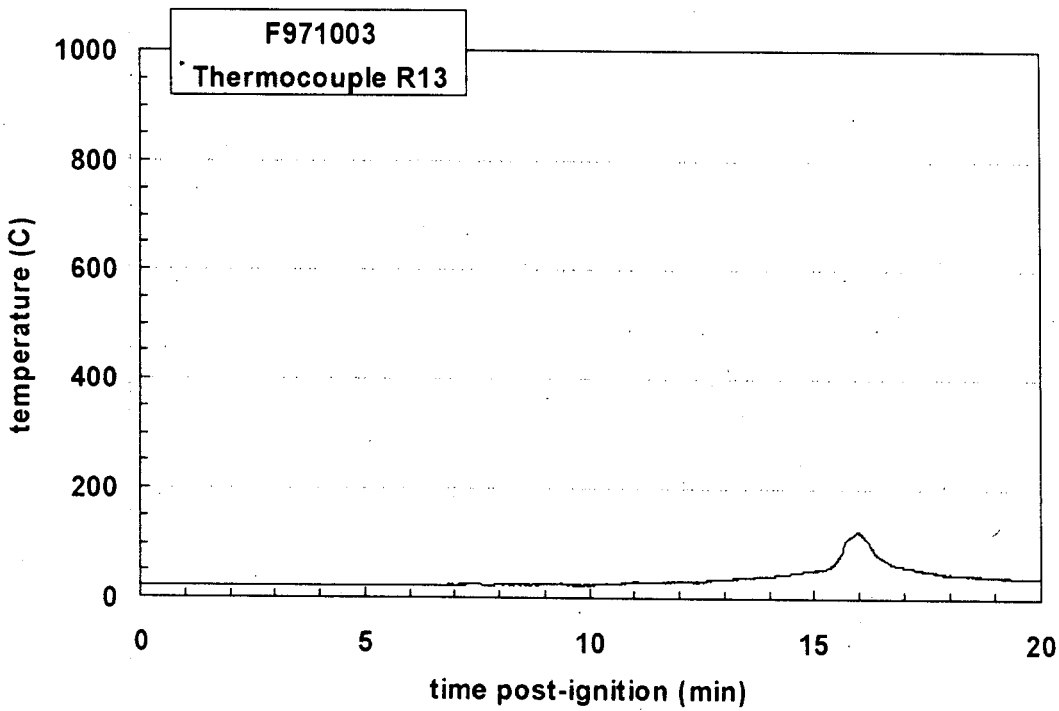

Plot C88. Fire Test F971003. Data plot from Thermocouple R13.

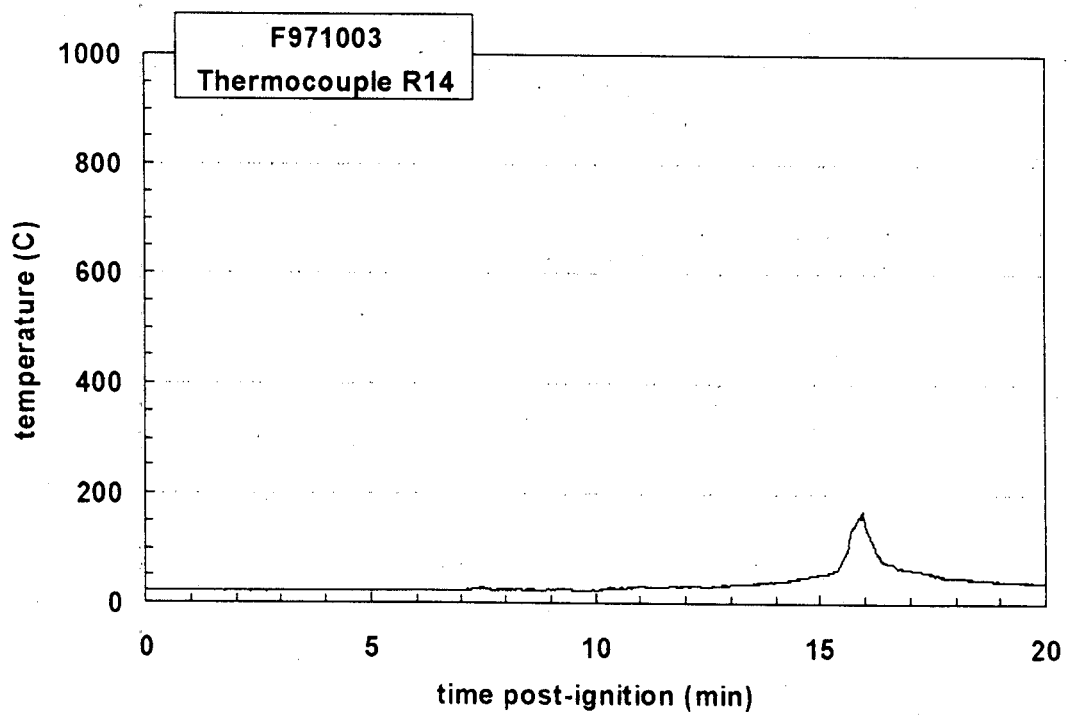

Plot C89. Fire Test F971003. Data plot from Thermocouple R14.

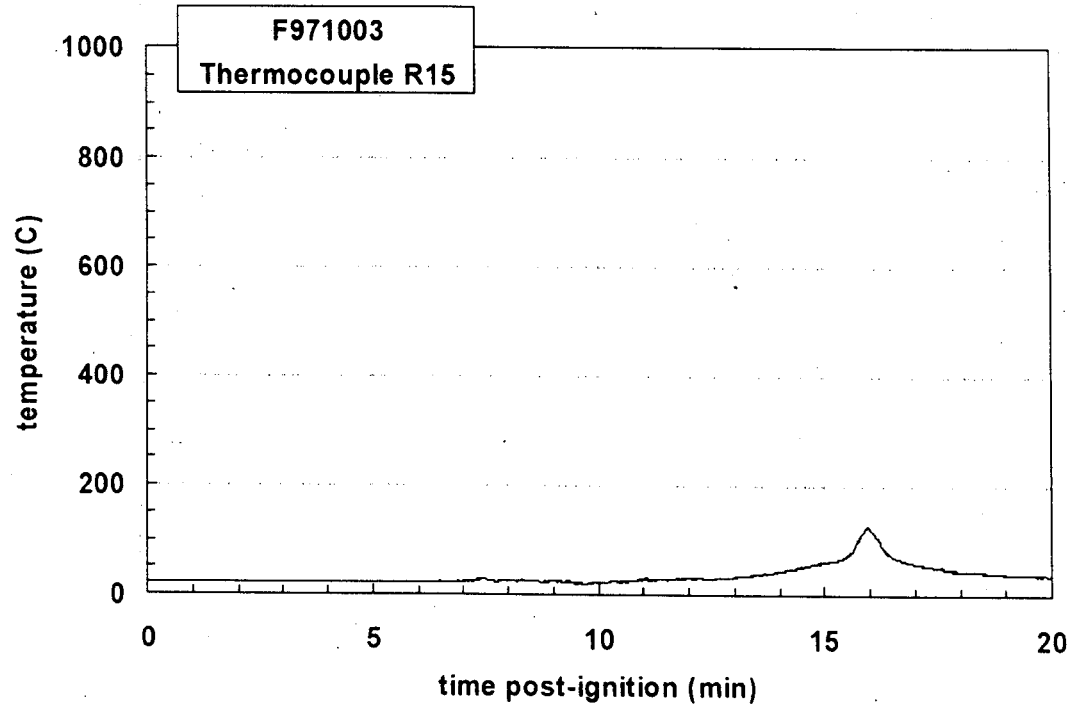

Plot C90. Fire Test F971003. Data plot from Thermocouple R15.

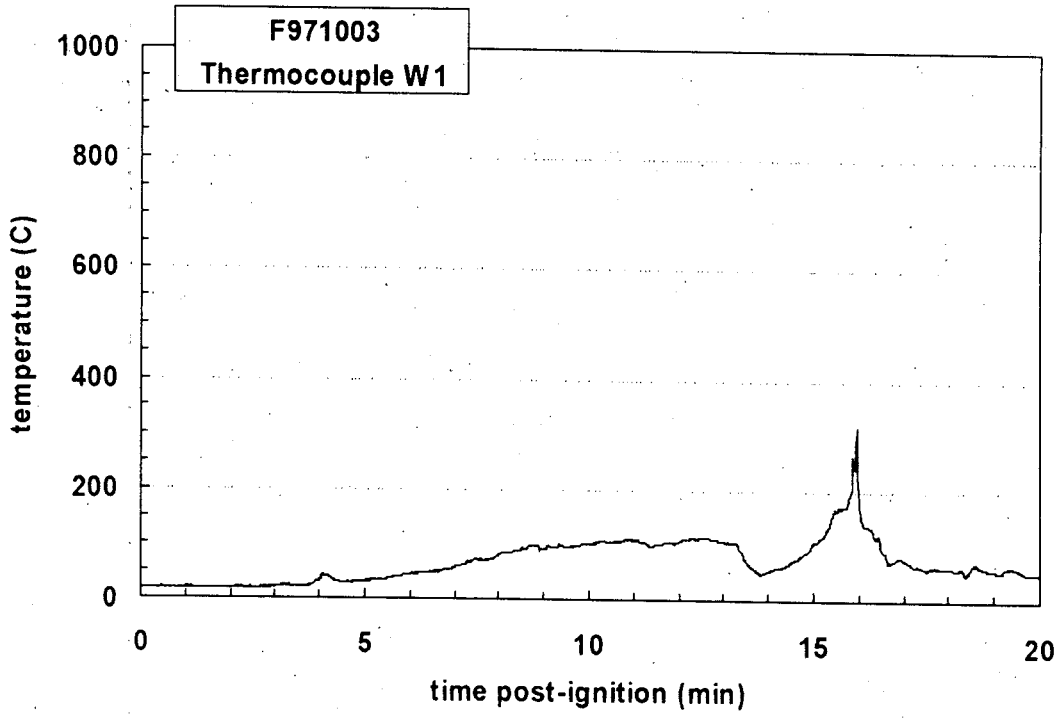

Plot C91. Fire Test F971003. Data plot from Thermocouple W1.

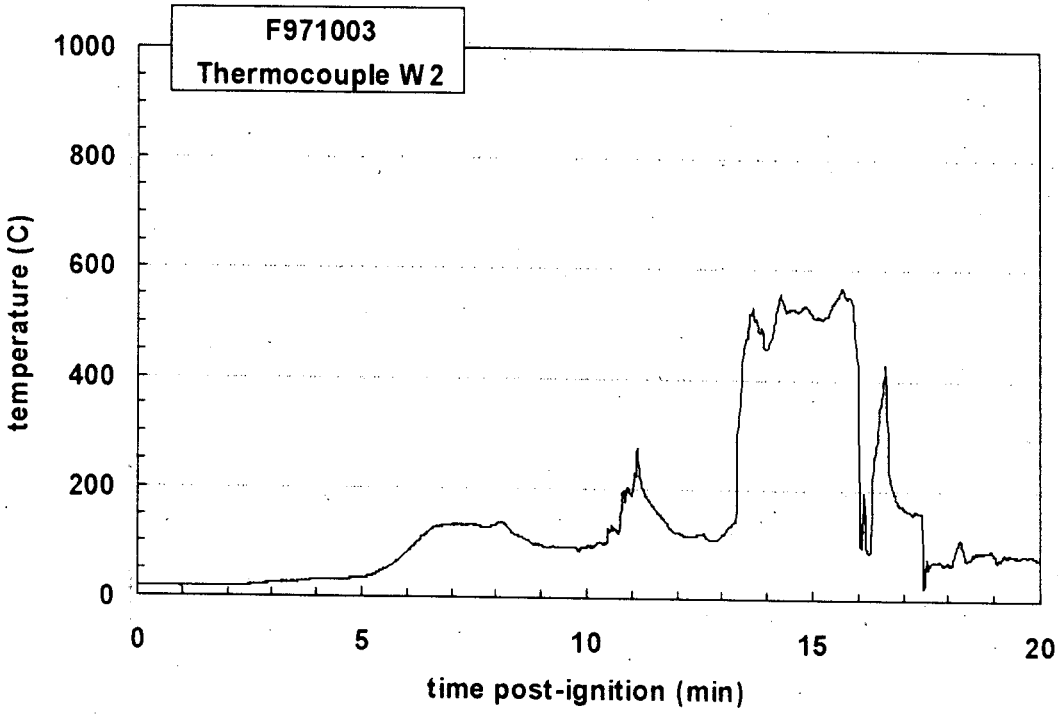

Plot C92. Fire Test F971003. Data plot from Thermocouple W2.

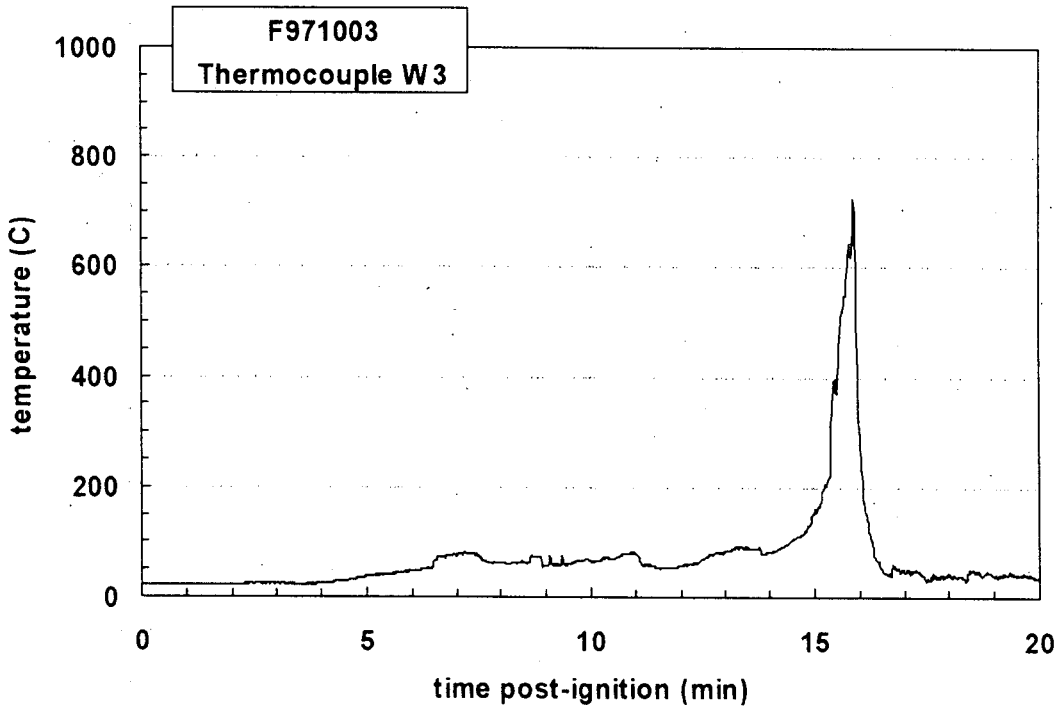

Plot C93. Fire Test F971003. Data plot from Thermocouple W3.

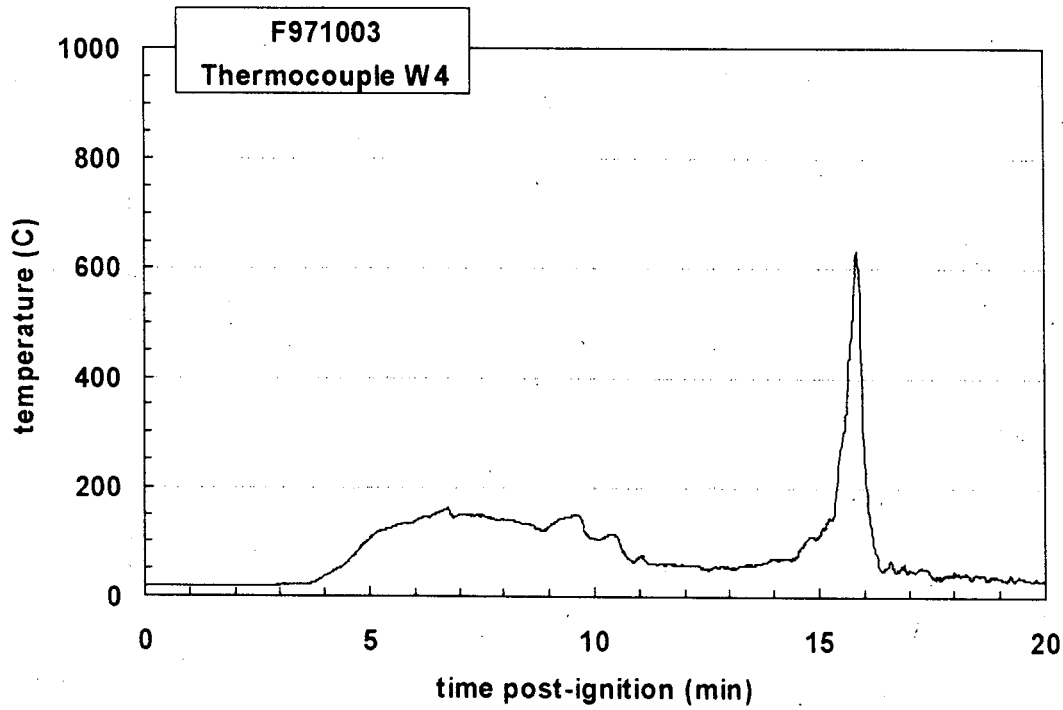

Plot C94. Fire Test F971003. Data plot from Thermocouple W4.

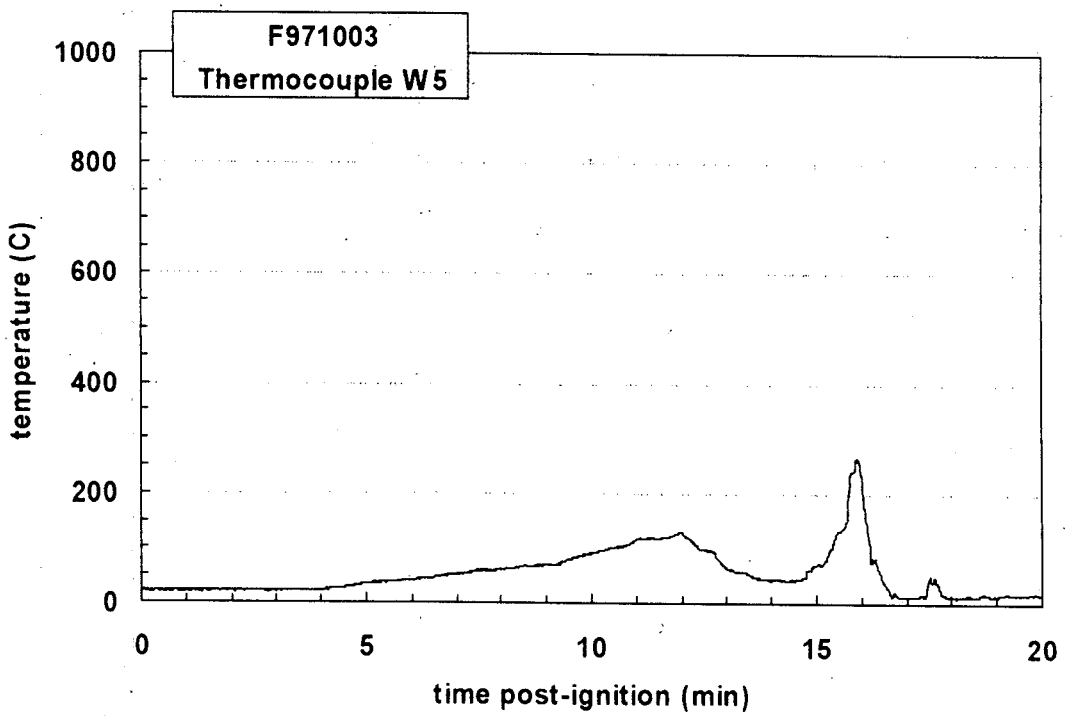

Plot C95. Fire Test F971003. Data plot from Thermocouple W5.

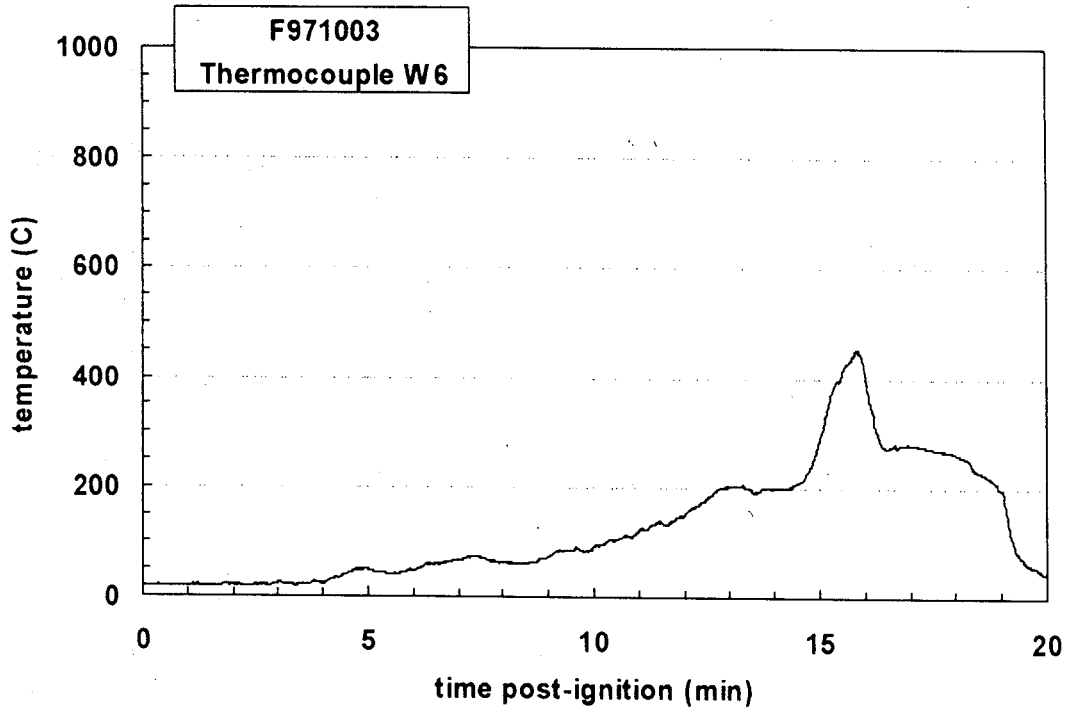

Plot C96. Fire Test F971003. Data plot from Thermocouple W6.

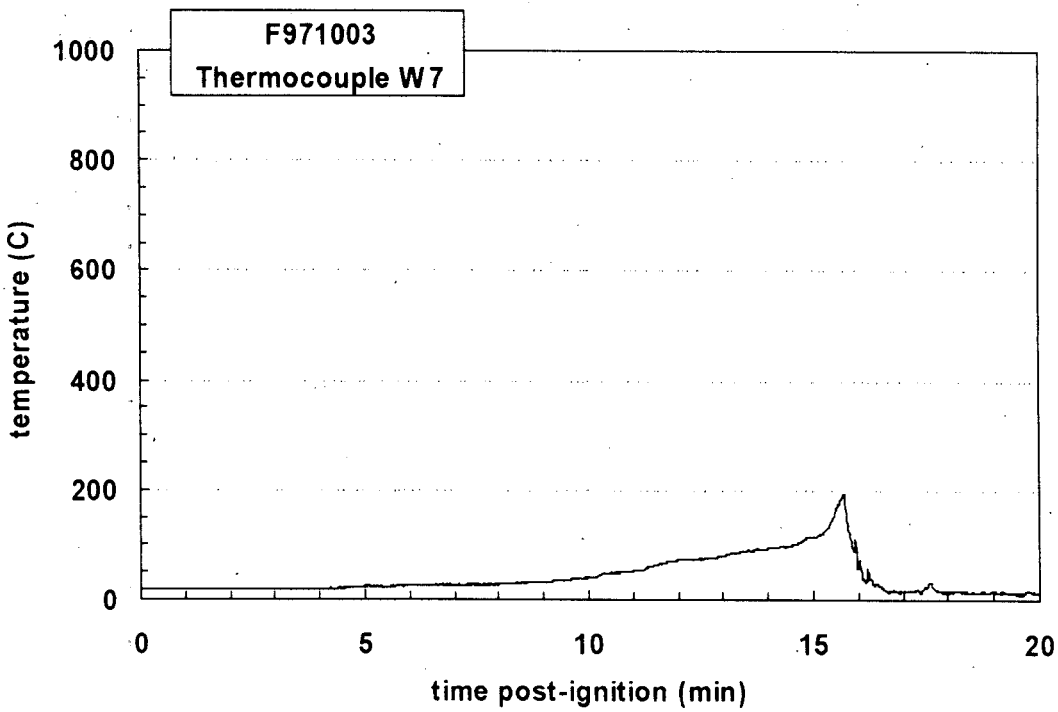

Plot C97. Fire Test F971003. Data plot from Thermocouple W7.

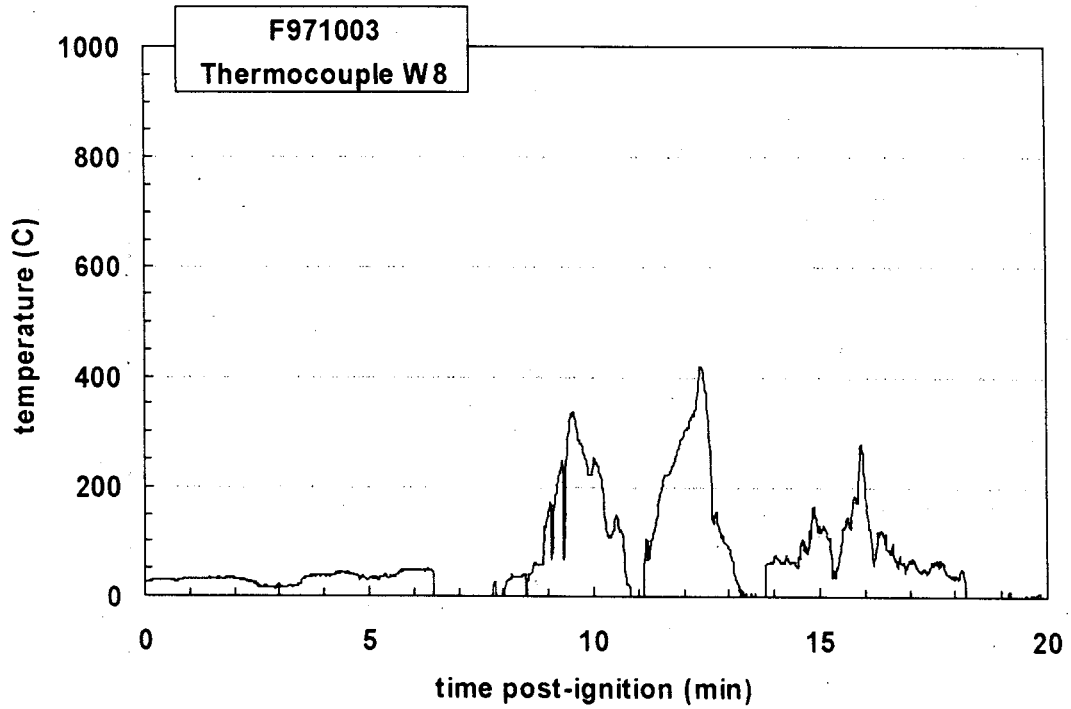

Plot C98. Fire Test F971003. Data plot from Thermocouple W8. The Thermocouple began to malfunction at 06:47 (min:sec) post-ignition.

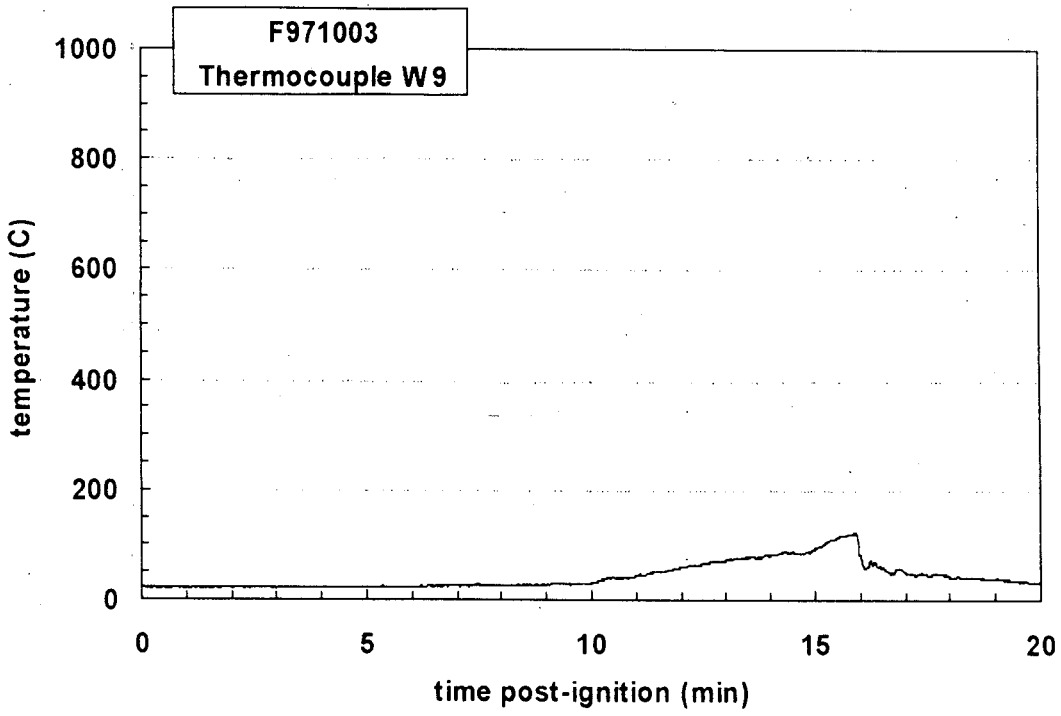

Plot C99. Fire Test F971003. Data plot from Thermocouple W9.

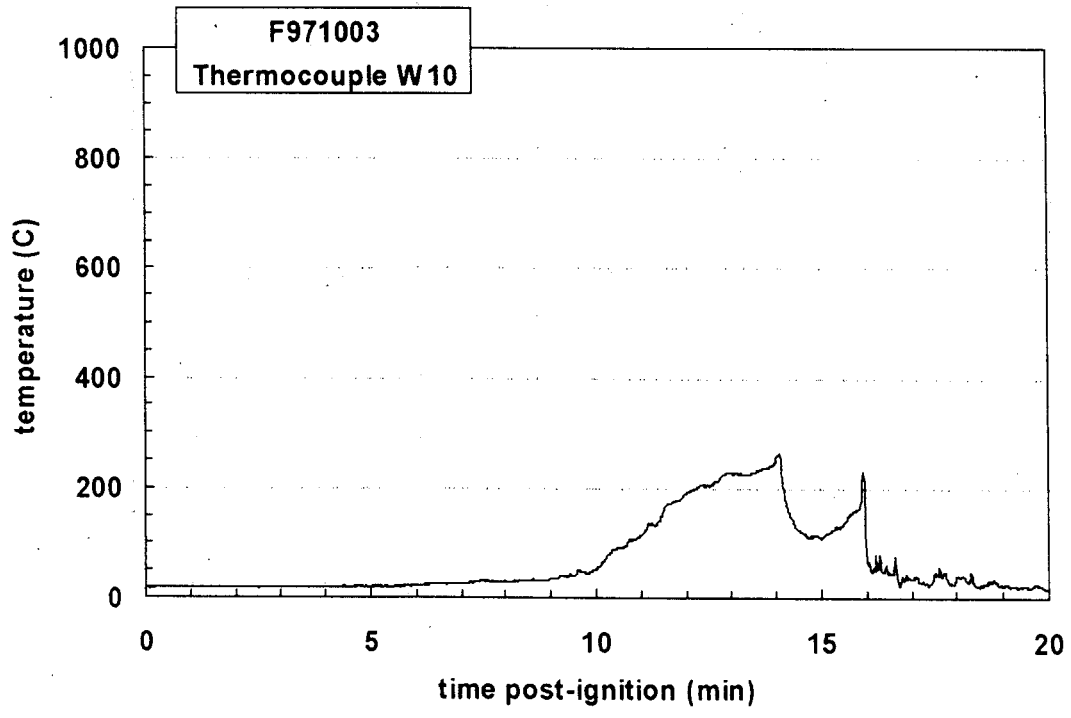

Plot C100. Fire Test F971003. Data plot from Thermocouple W10.

APPENDIX D
ASPIRATED THERMOCOUPLE DATA

An aspirated thermocouple assembly (Medtherm Corporation) was installed in the test vehicle and used to measure air temperature at six elevations in the passenger compartment of the test vehicle during this test (Fig. D1). The aspirated thermocouple assembly was fabricated from Inconel 600 tubing. Each assembly consisted of a vertical manifold (o.d. = 0.375 in. (9.5 mm), i.d. = 0.25 in. (6.4 mm), length = 16 in. (406 mm)) with six horizontal radiation shields (o.d. = 0.25 in. (6.4 mm), i.d. = 0.19 in. (4.8 mm), length = 1.00 in. (25.4 mm)). The vertical spacing between the radiation shields along the manifold was 3 in. (75 mm). Three radial holes were drilled near the tip of each radiation shield. The holes were sized to approximately balance the airflow-rates over each thermocouple. A Type-N thermocouple inserted into each radiation shield so that the thermocouple junction was positioned approximately 0.2 in. (5.1 mm) down-stream from the inlet holes.

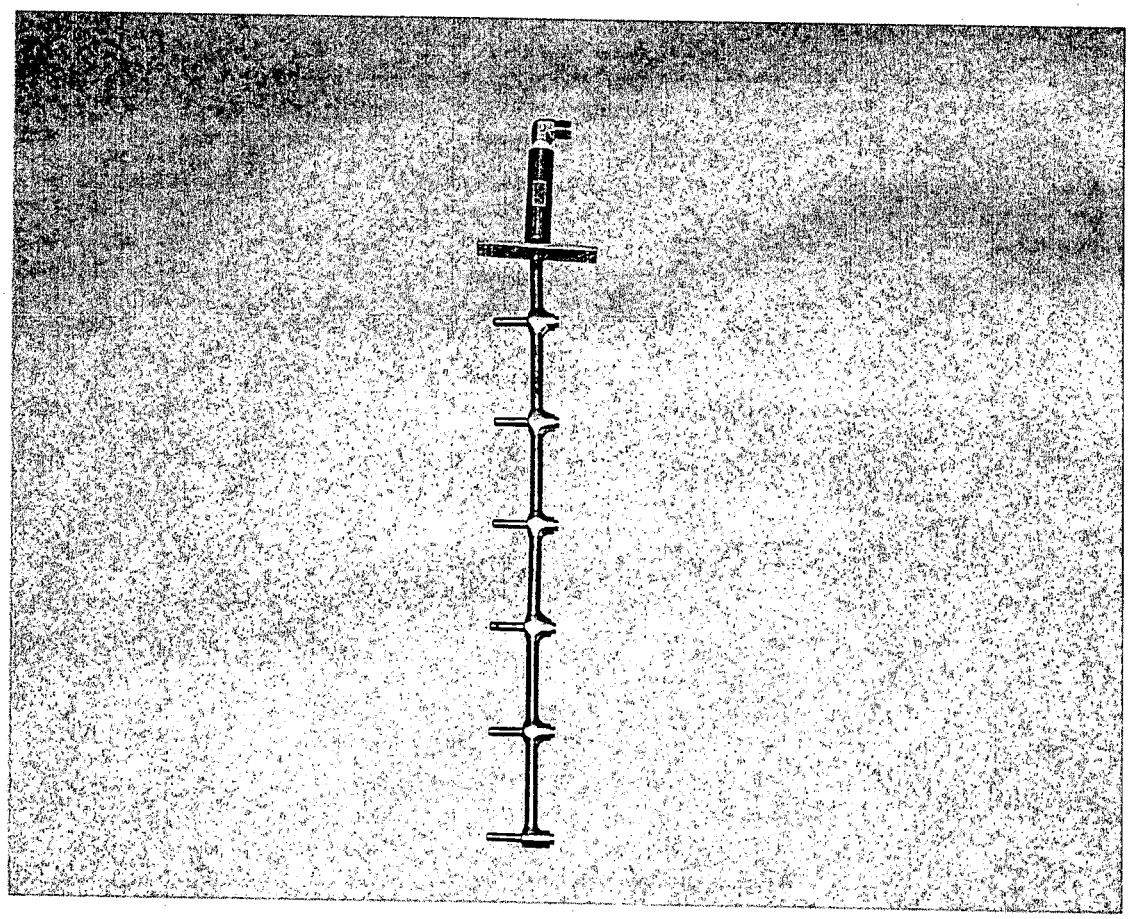

Figure D1. Fire Test F971003. Photograph of the aspirated thermocouple assembly used in the passenger compartment of the test vehicle.

The mounting flange of the aspirated thermocouple probe assembly was attached to the roof of the vehicle. The probe extended into the passenger compartment through a hole in the roof so that all 6 thermocouples were located below the headliner. The probe was vertical and located along the longitudinal mid-line of the vehicle approximately equidistant from the driver and passenger seats. The upper-most aspirated thermocouple was approximately 0.5 in. (12 mm) below the lower surface of the headliner. The manifold was connected to a rotary-vane pump with flexible copper tubing (o.d. = 0.5 in. (12 mm), length = 15 ft. (4.6 m)). The capacity of the pump was 50 L/min at atmospheric pressure.

Figures D2 and D3 show the approximate location of the aspirated thermocouple probe assembly in the test vehicle for this test.

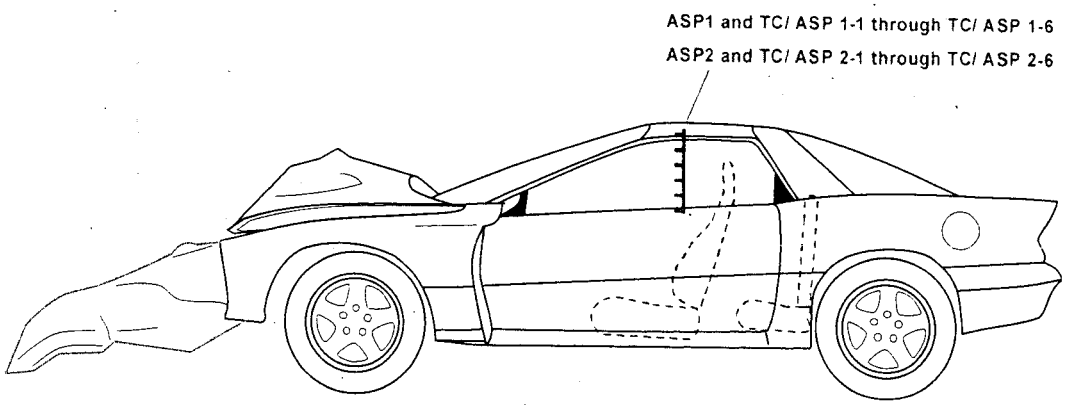

Figure D2. Fire Test F971003. Side view of the test vehicle showing the approximate location of the aspirated thermocouple probe assembly in the passenger compartment.

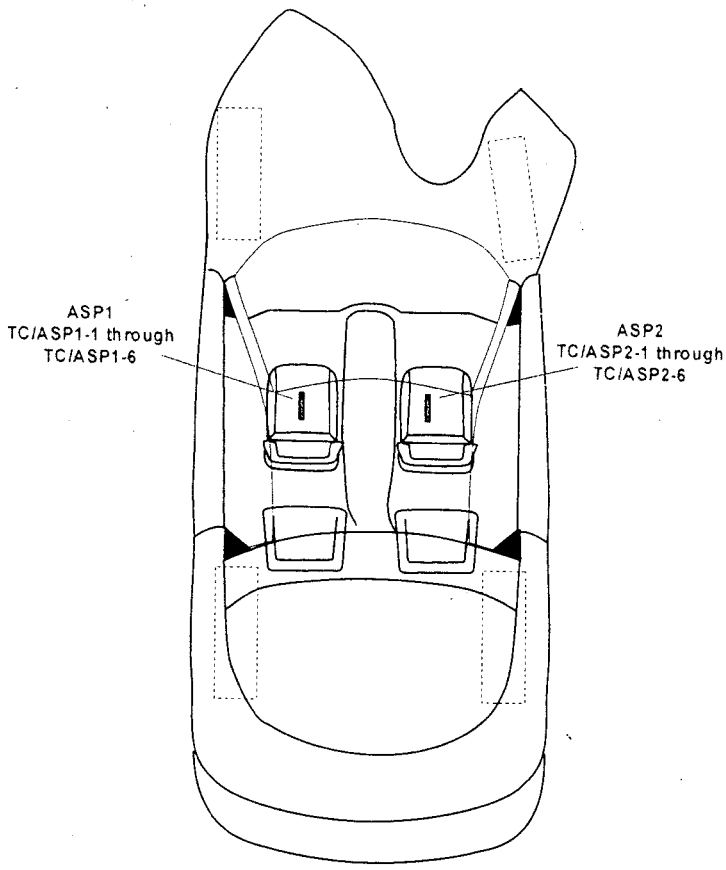

Figure D3. Fire Test F971003. Top view of the test vehicle showing the approximate location of the aspirated thermocouple probe assembly in the passenger compartment.

REFERENCES

D1. J. S. Newman and P. A. Croce. A simple aspirated thermocouple for use in fires. *J. Fire Flamm.* **10**:326-336 (1979).

D2. N. R. Keltner and K. A. Strom. Thermal Measurement Uncertainty and Compensation. Paper in preparation.

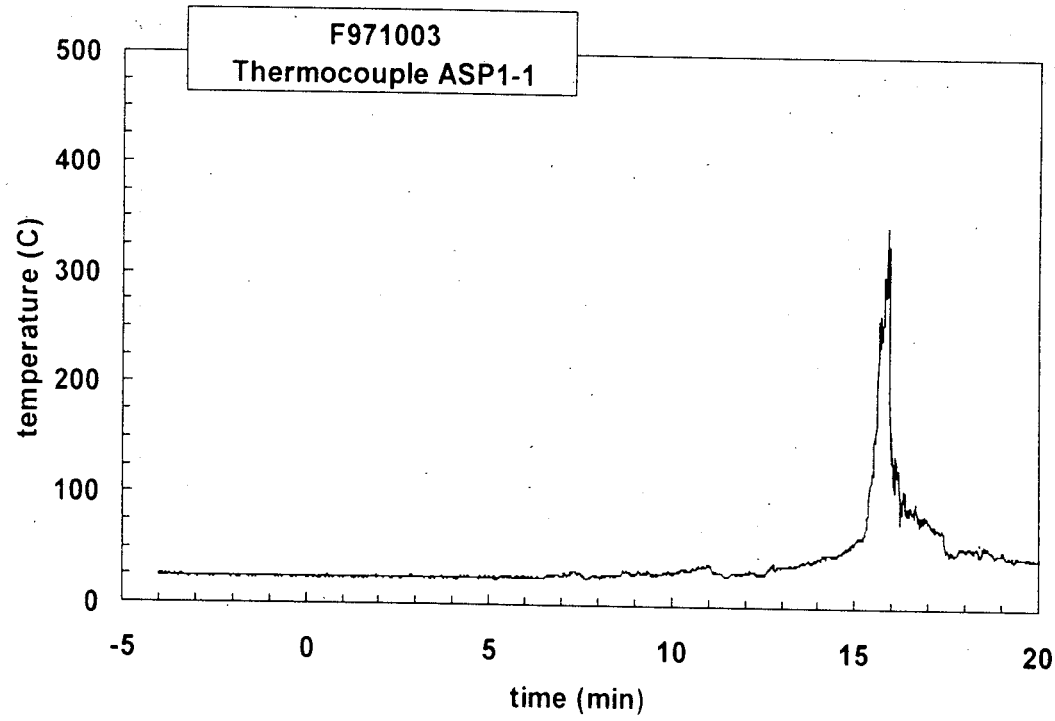

Plot D1. Fire Test F971003. Data plot from thermocouple ASP1-1.

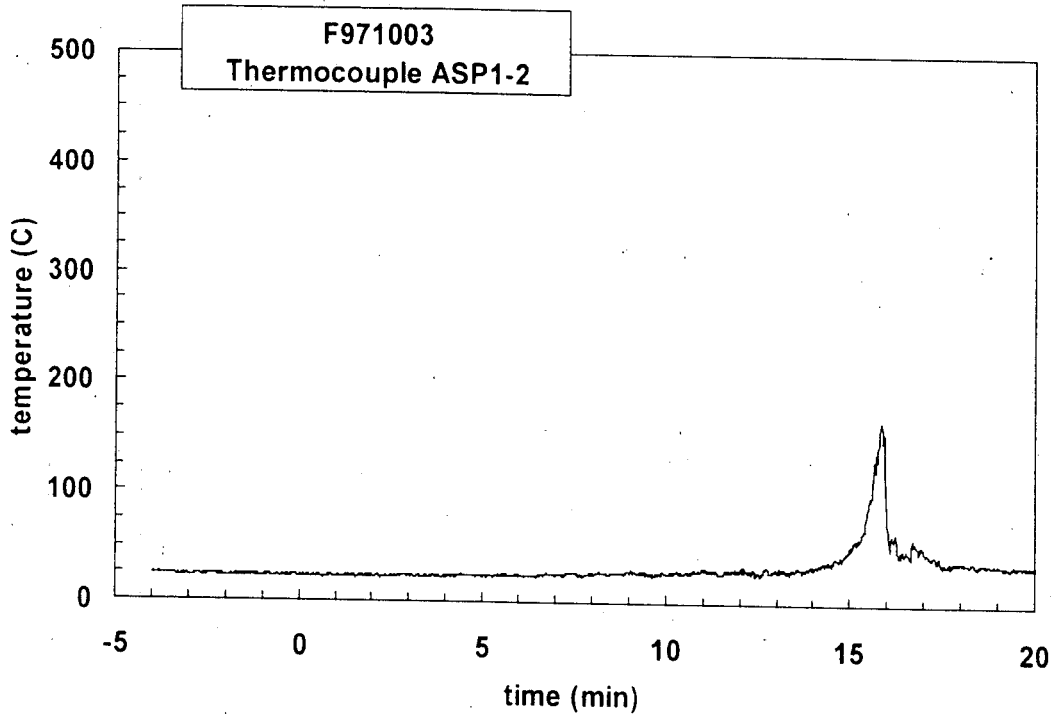

Plot D2. Fire Test F971003. Data plot from thermocouple ASP1-2.

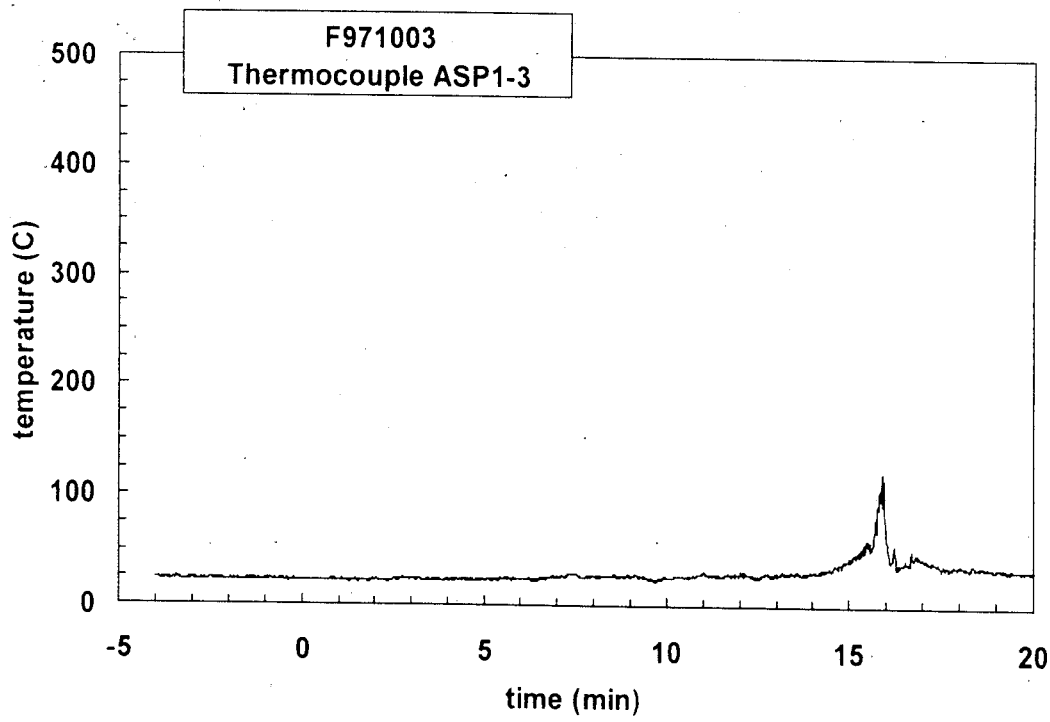

Plot D3. Fire Test F971003. Data plot from thermocouple ASP1-3.

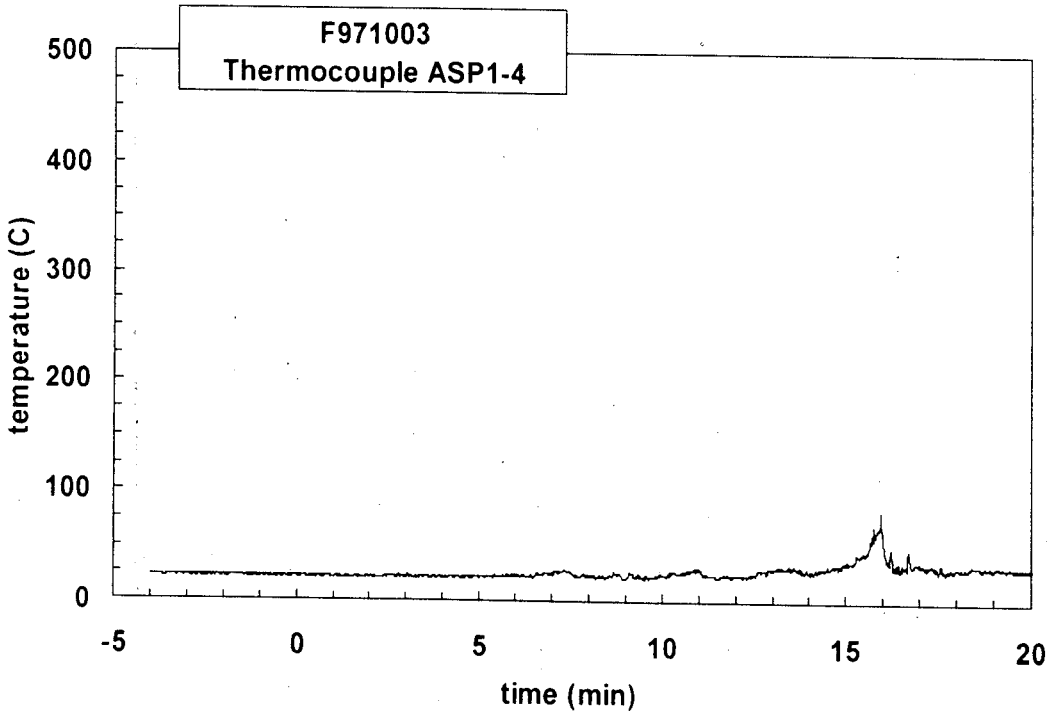

Plot D4. Fire Test F971003. Data plot from thermocouple ASP1-4.

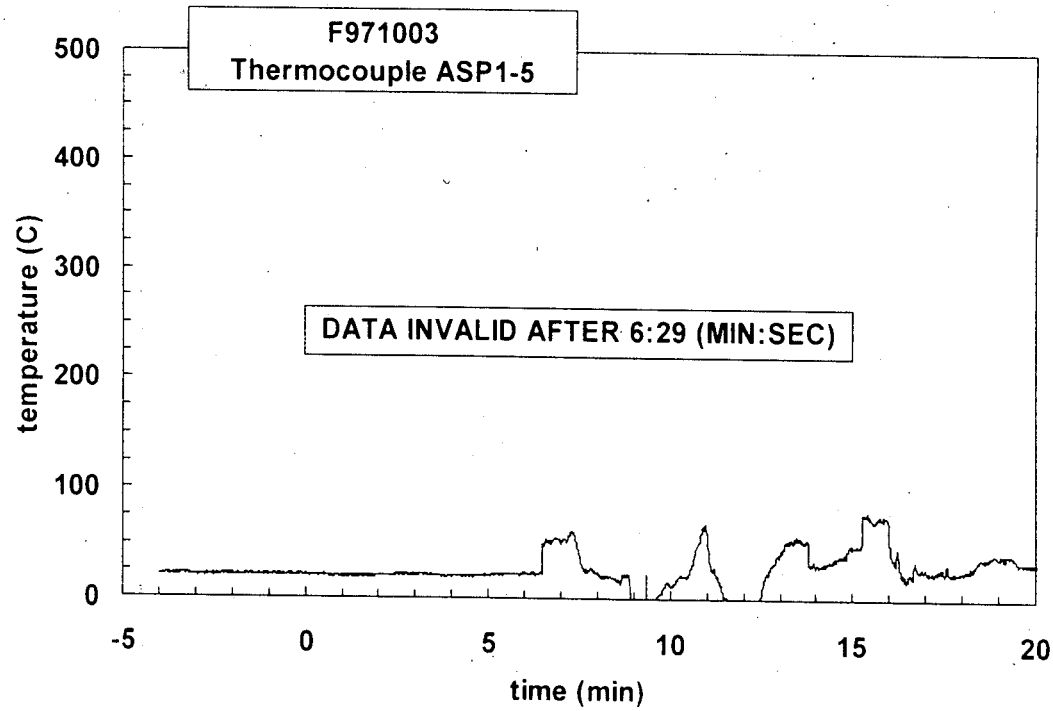

Plot D5. Fire Test F971003. Data plot from thermocouple ASP1-5. Thermocouple ASP 1-5 malfunctioned beginning at approximately 6:29 (min:sec) .

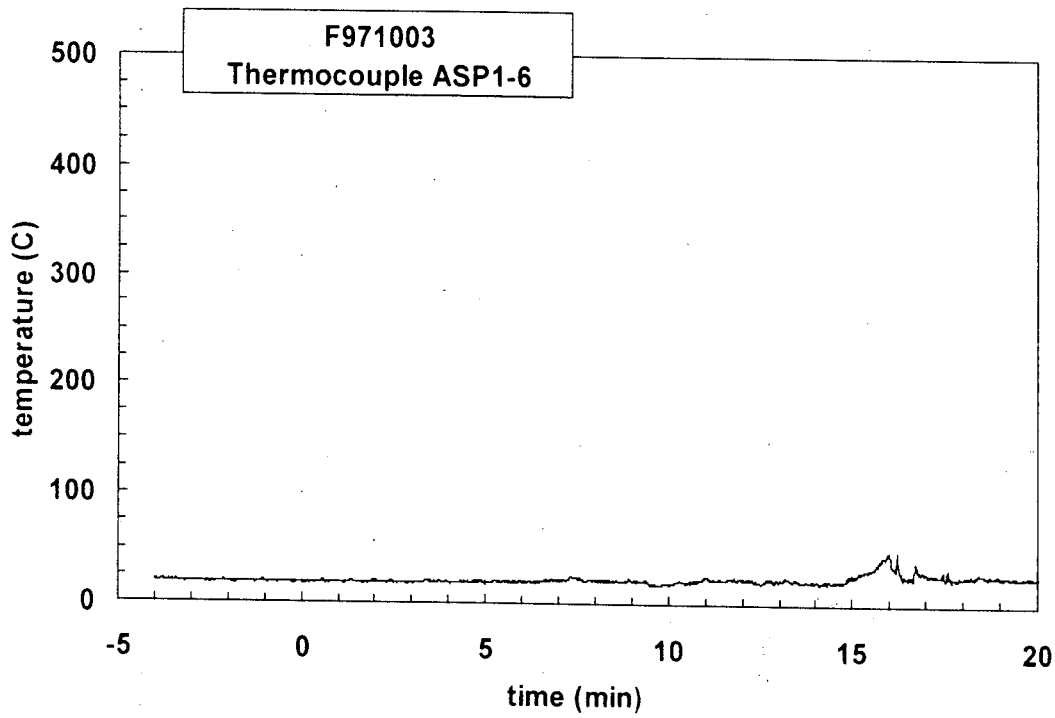

Plot D6. Fire Test F971003. Data plot from thermocouple ASP1-6.

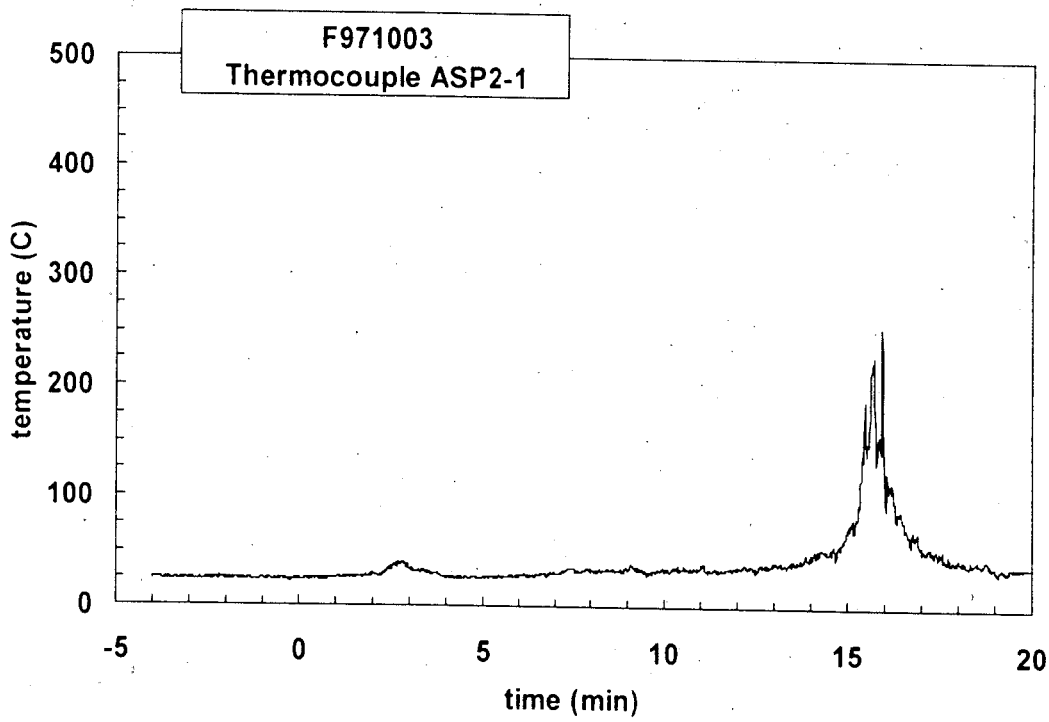

Plot D7. Fire Test F971003. Data plot from thermocouple ASP2-1.

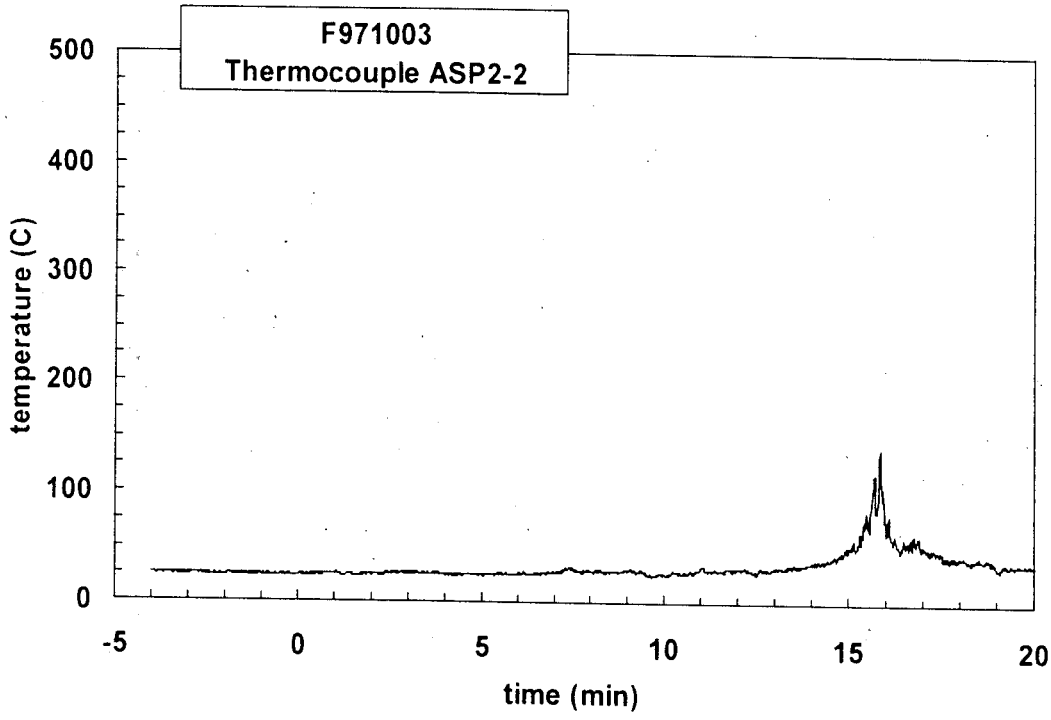

Plot D8. Fire Test F971003. Data plot from thermocouple ASP2-2.

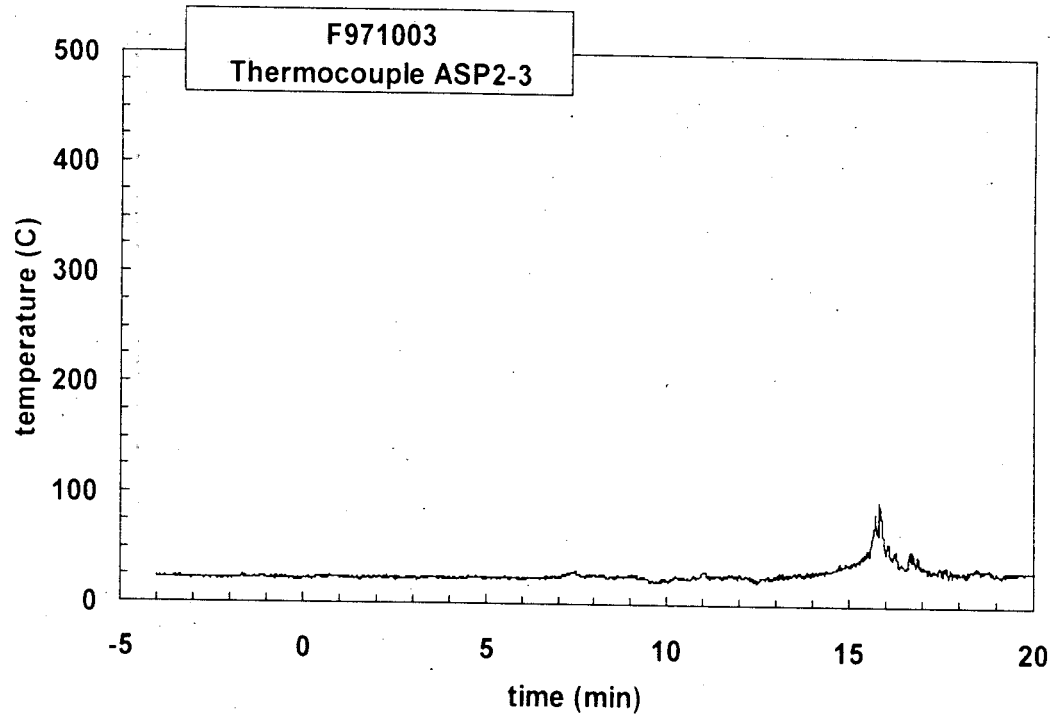

Plot D9. Fire Test F971003. Data plot from thermocouple ASP2-3.

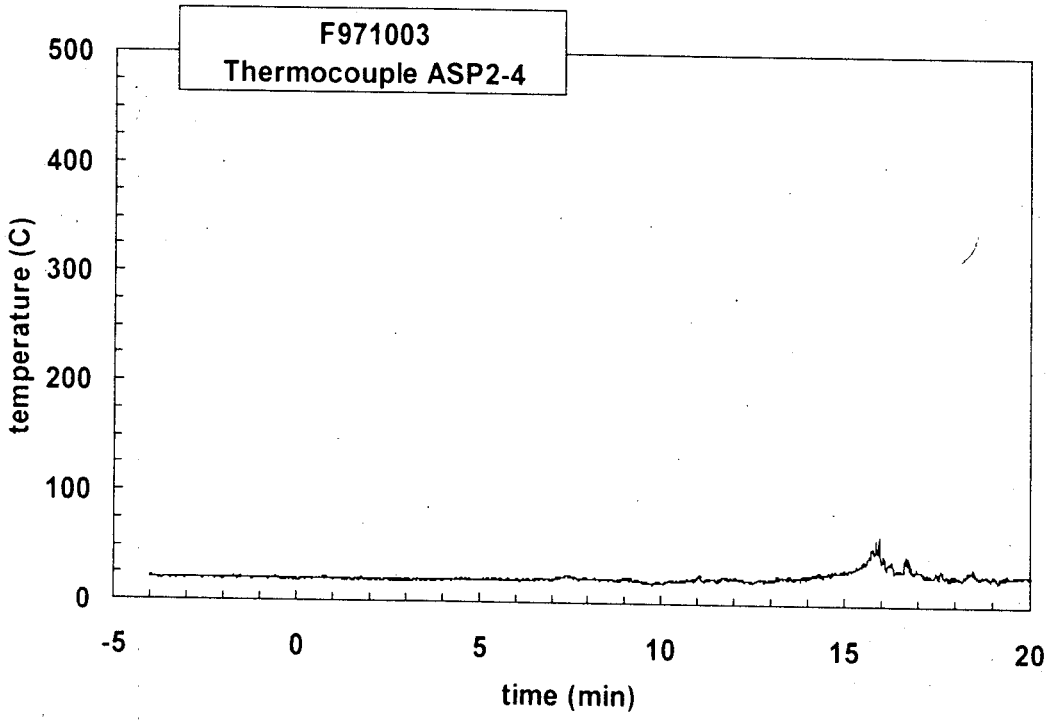

Plot D10. Fire Test F971003. Data plot from thermocouple ASP2-4.

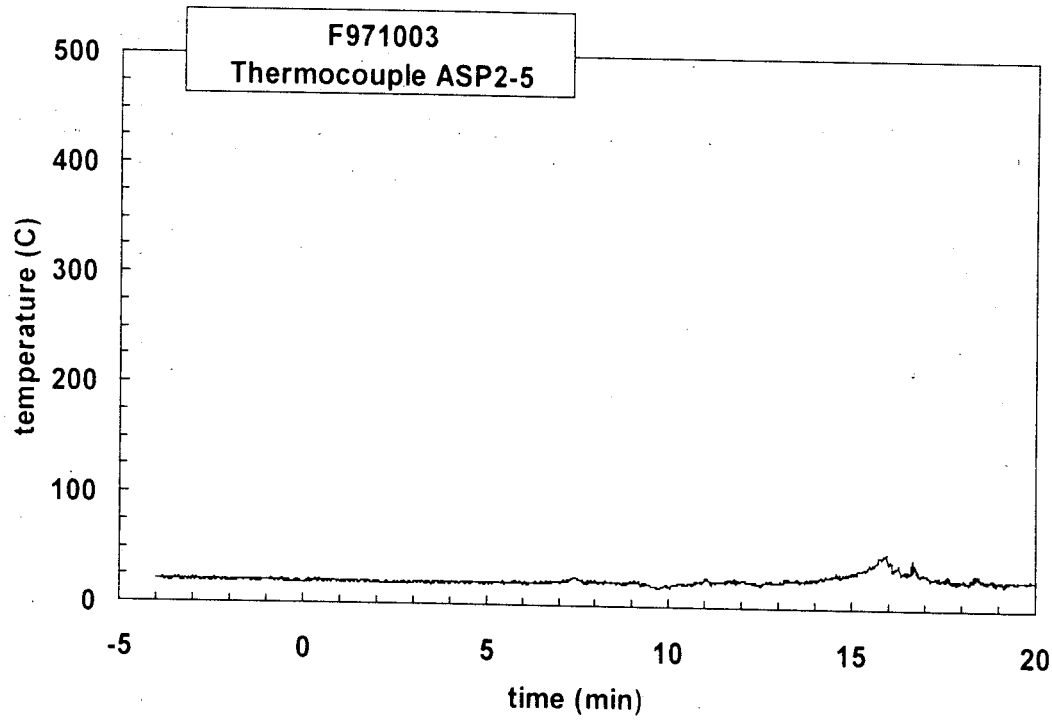

Plot D11. Fire Test F971003. Data plot from thermocouple ASP2-5.

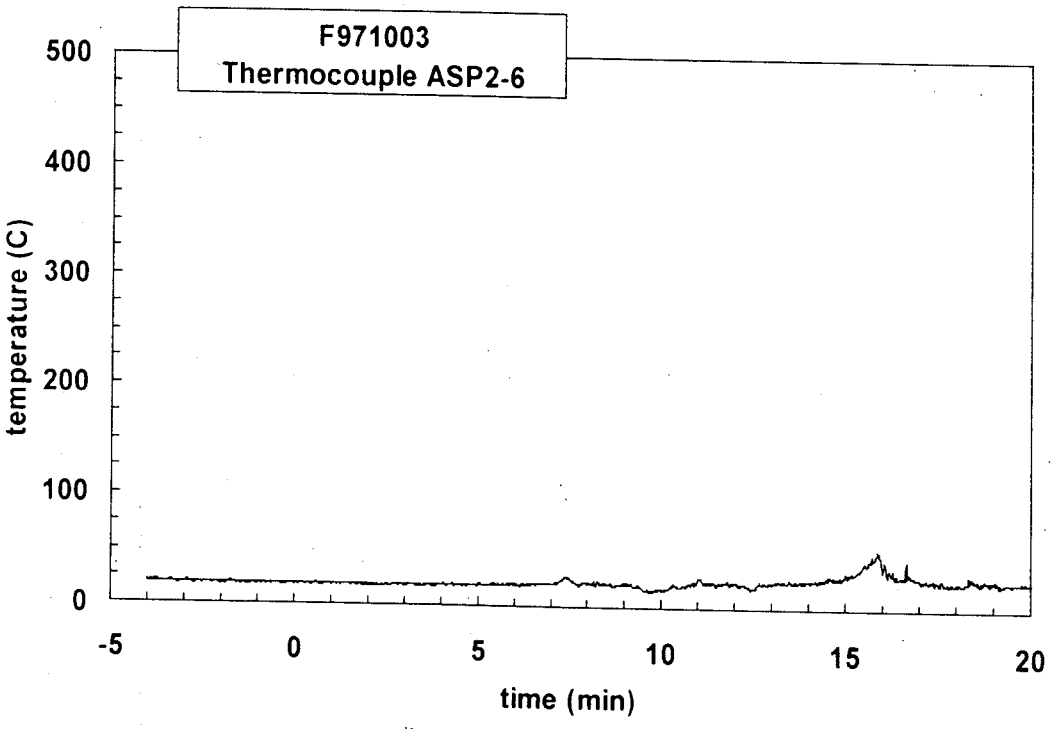

Plot D12. Fire Test F971003. Data plot from thermocouple ASP2-6.

APPENDIX E
HEAT FLUX TRANSDUCER/RADIOMETER DATA

Heat-flux transducer/radiometer assemblies (64 Series, Medtherm Corporation) were used to measure convective and radiative heat transfer to selected objects in the vehicle. Each assembly contained two Schmidt-Boelter thermopiles in a water-cooled copper body (diameter = 1 in. (25.4 mm), length = 1 in. (25.4 mm)). The faces of the heat flux transducers were coated with high-temperature optical black paint. The radiometers had permanent sapphire windows (view-angle = 150°; optical transmittance range 0.4 to 4.2 μm). Both transducers were calibrated to 100 kW/m^2 at a reference temperature of 25°C.

The PC-based data system used to acquire data from the thermocouples (**APPENDIX C**) also was used to acquire data from the heat flux transducers and radiometers. The electrical signal wires from these transducers terminated in a 5-pin circular connector (165 Series, Amphenol). Each connector was plugged into a panel-mounted jack, which was hard wired to an analog-input multiplex expansion card (DBK-12, IOTech, Inc., Cleveland, OH). As with the thermocouples, the electrical shields on the signal cables were connected to the electronic chassis grounds on the analog-input expansion cards. The data acquisition software (DASYLab) was configured to sample each channel at a rate of 10 Hz and store the data in 10-point block averages.

Figures E1 through E4 show the approximate locations of heat flux transducer/radiometer assemblies in the test vehicle. HFT/RAD1, HFT/RAD2, and HFT/RAD3 were mounted to the test vehicle in the locations shown in Figures E1 and E2. A threaded rod (diameter = ½ in.) was inserted through a hole in the roof above each of the front seats of the test vehicle. The lower end of each rod was wired to one of the seat cushion to stabilize the transducers during the test. HFT/RAD5, HFT/RAD6, and HFT/RAD7 were mounted to the threaded rod above the drivers' seat. HFT/RAD8, HFT/RAD9, and HFT/RAD10 were mounted to the threaded rod above the front passengers' seat.

One of the two fluid ports on each transducer was connected to the outlet manifold of a thermostated recirculating water bath, and the other fluid port was connected to the return manifold of the water bath using copper tubing (o.d. = 0.25 in.). The water in the water bath was equilibrated to 60°C before the test. Te flow rate of water through each body was approximately 100 mL/min during this test.

Data recorded from these transducers is shown in Plots E1 through E18.

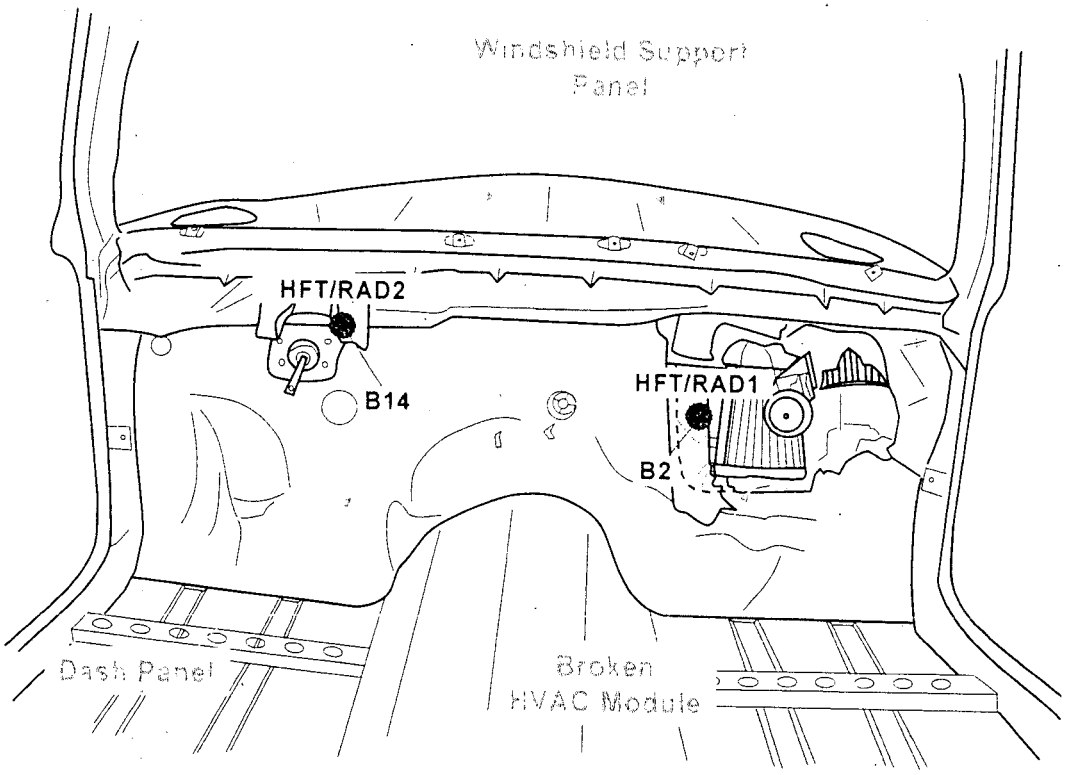

Figure E1. Fire Test F971003. Diagram showing the approximate locations of heat flux transducer/radiometer (HFT/RAD) assemblies on the dash panel of the test vehicle. HFT/RAD1 was mounted on a bracket and located in the pass-through for the HVAC module facing forward. HFT/RAD2 was inserted through a clearance hole drilled in the dash panel and facing forward. Thermocouple B2 was attached to the rear surface of HAF/RAD1 with thermally conducting ceramic cement. Thermocouple B14 was attached to the rear surface of HFT/RAD2 with thermally conducting ceramic cement.

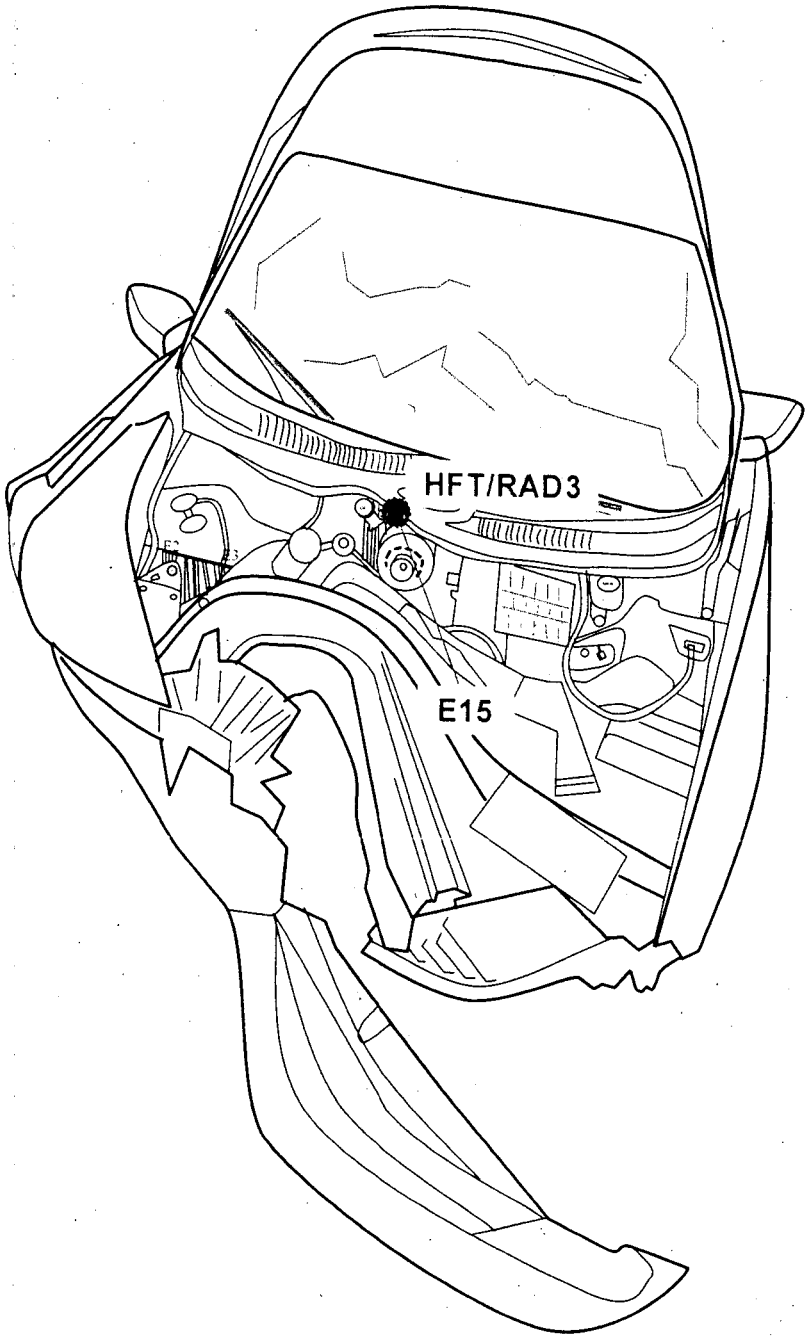

Figure E2. Fire Test F971003. Diagram showing the approximate location of an HFT/RAD (HFT/RAD) assembly in the engine compartment of the test vehicle.

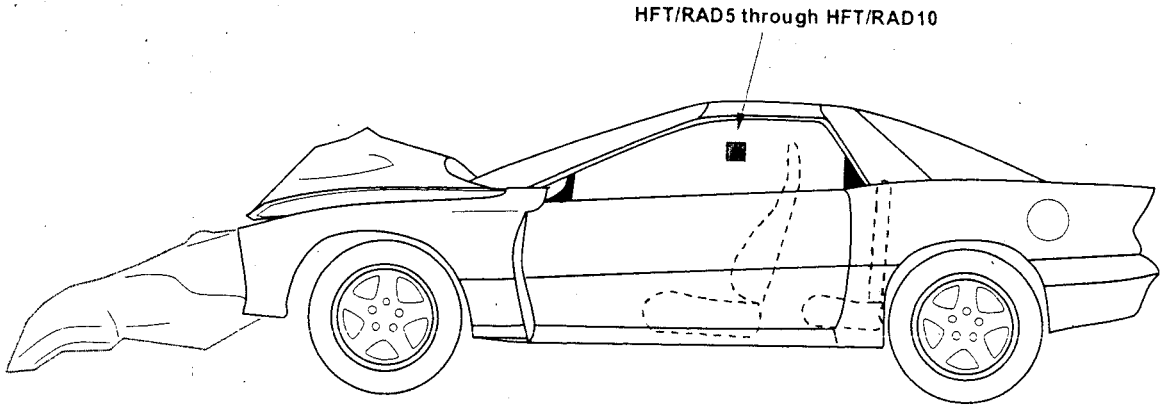

Figure E3. Fire Test F971003. Side view of the test vehicle showing the approximate locations of heat flux transducer/radiometer (HFT/RAD) assemblies located above the front seats of the test vehicle. HFT/RAD5, was approximately 80 cm above driver's seat cushion facing upward. HFT/RAD6 was approximately 80 cm above the driver's seat cushion facing forward. HFT/RAD7 was approximately 80 cm above the driver's seat cushion facing right side of the instrument panel top cover. HFT/RAD8 was approximately 80 cm above the front passenger's seat cushion facing upward. HFT/RAD9 was approximately 80 cm above the front passenger's seat cushion fading forward. HTF/RAD10 was approximately 80 cm above the front passenger's seat cushion facing the right side of the instrument panel top cover.

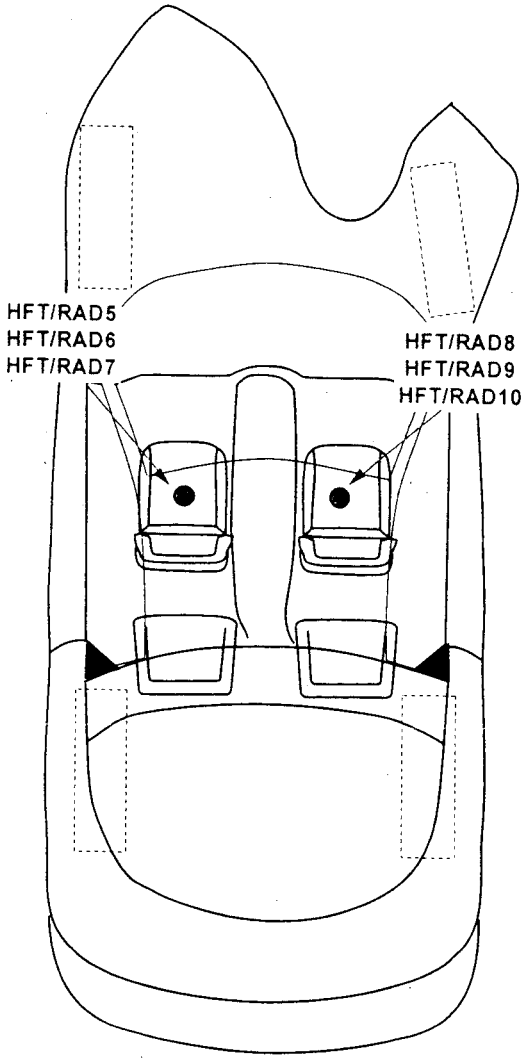

Figure E4. Fire Test F971003. Top view of the test vehicle showing the approximate locations of heat flux transducer/radiometer (HFT/RAD) assemblies located above the front seats of the test vehicle. See the caption to Figure E3 for a description of the locations of HFT/RAD5 through HFT/RAD10.

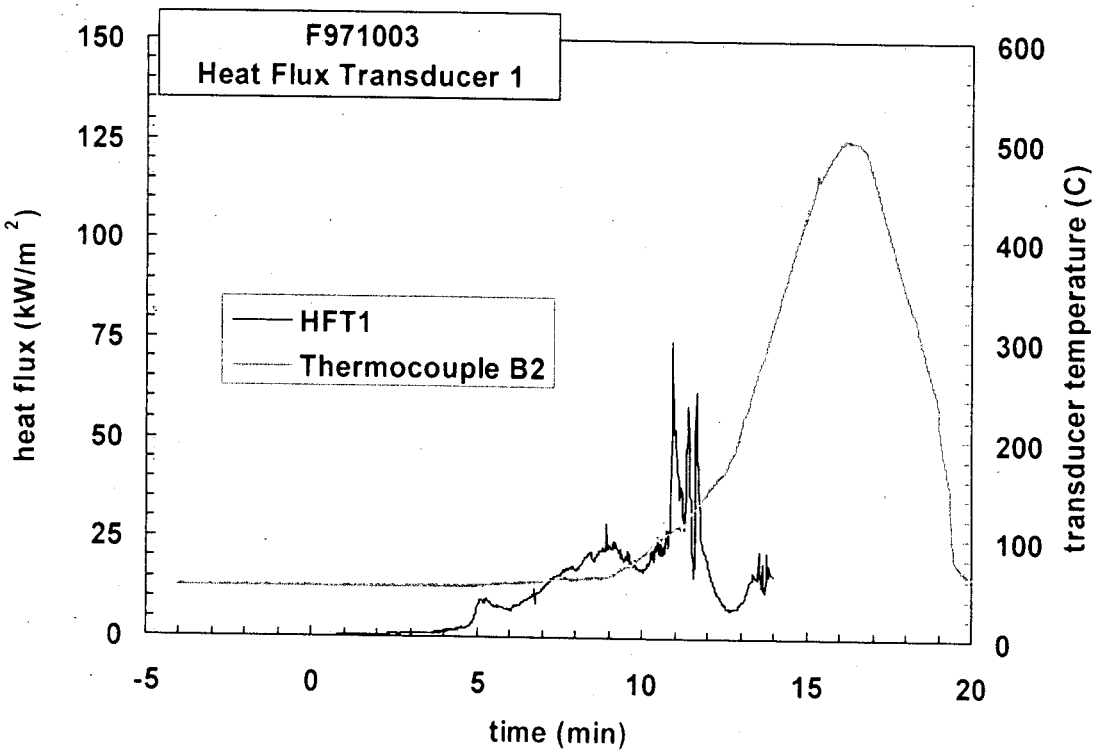

Plot E1. Fire Test F971003. Data plot from HFT1. The transducer temperature limit was exceeded at 13:98 (min:sec) post-ignition.

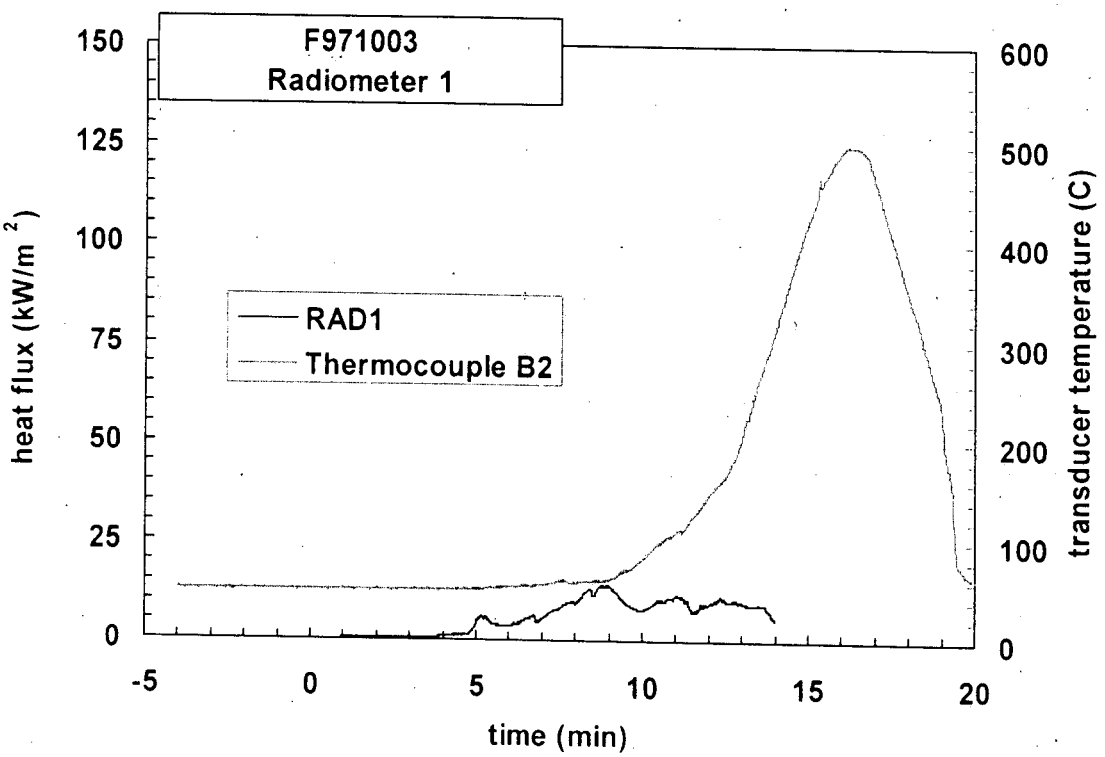

Plot E2. Fire Test F971003. Data plot from RAD1. The transducer temperature limit was exceeded at 13:98 (min:sec) post-ignition.

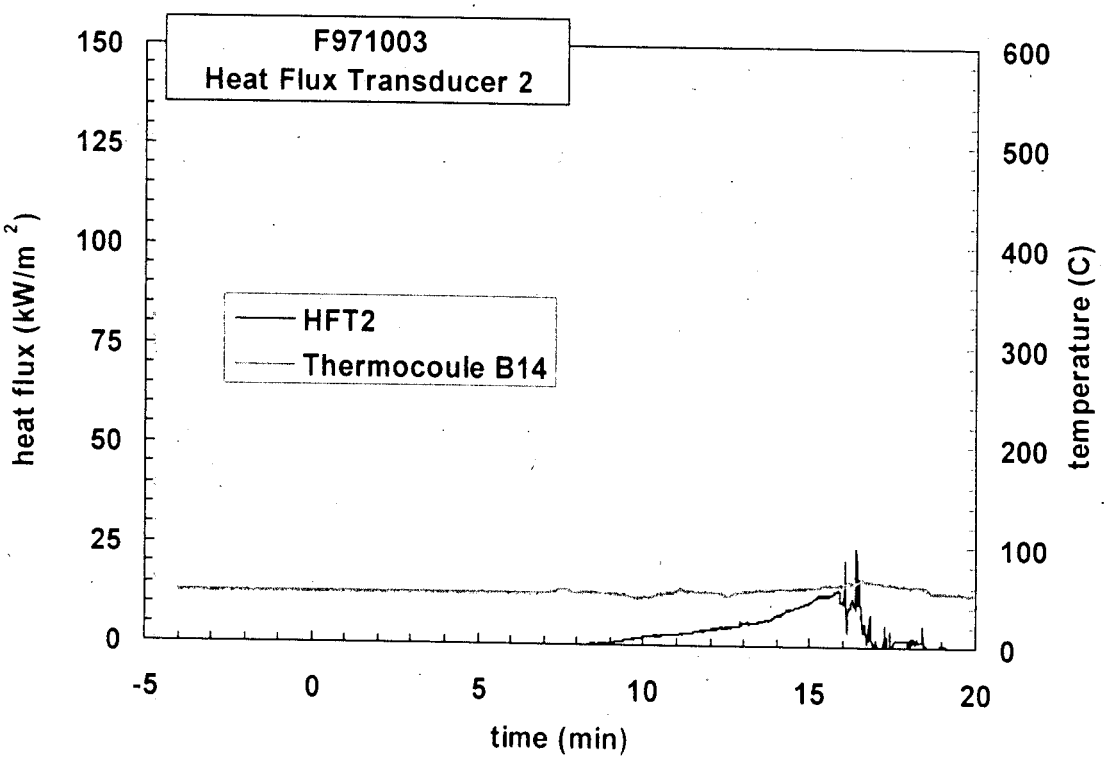

Plot E3. Fire Test F971003. Data plot from HFT2.

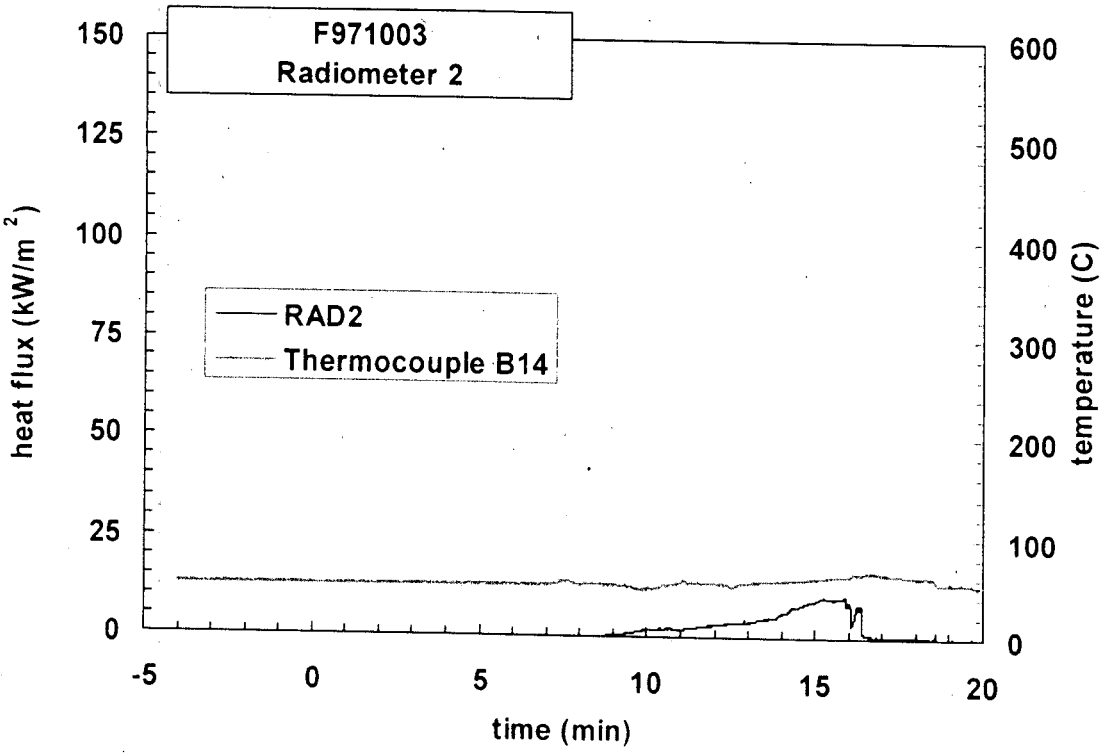

Plot E4. Fire Test F971003. Data plot from RAD2.

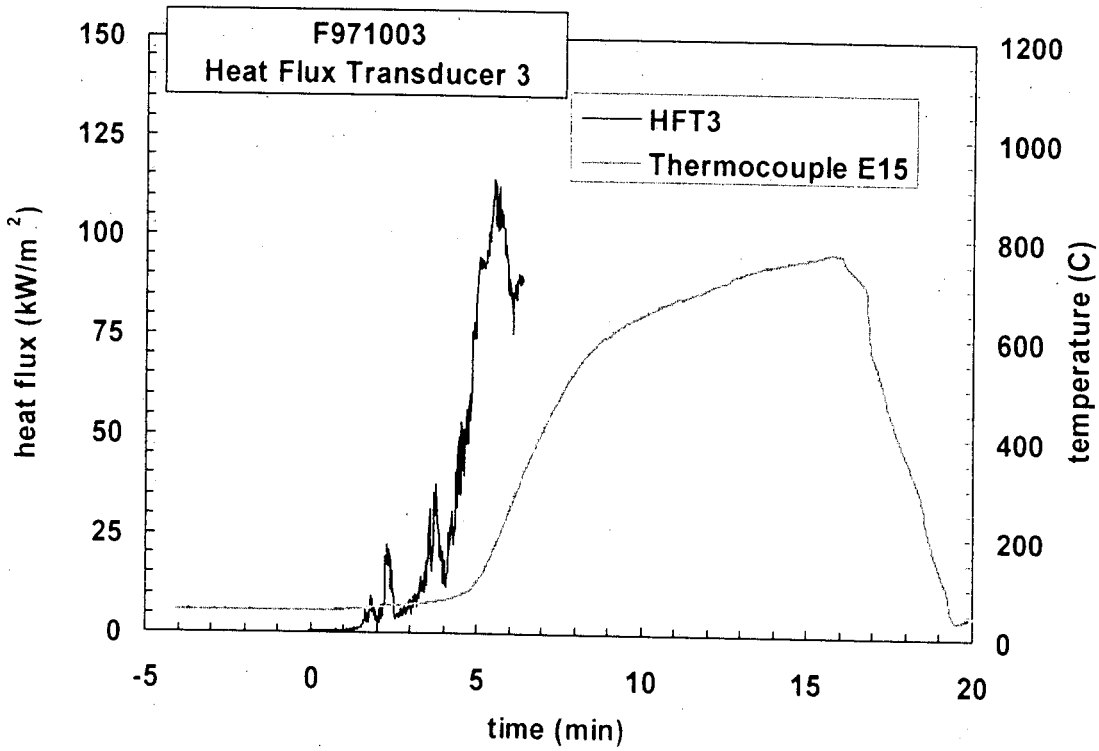

Plot E5. Fire Test F971003. Data plot from HFT3. The transducer temperature limit was exceeded at 06:37 (min:sec) post-ignition.

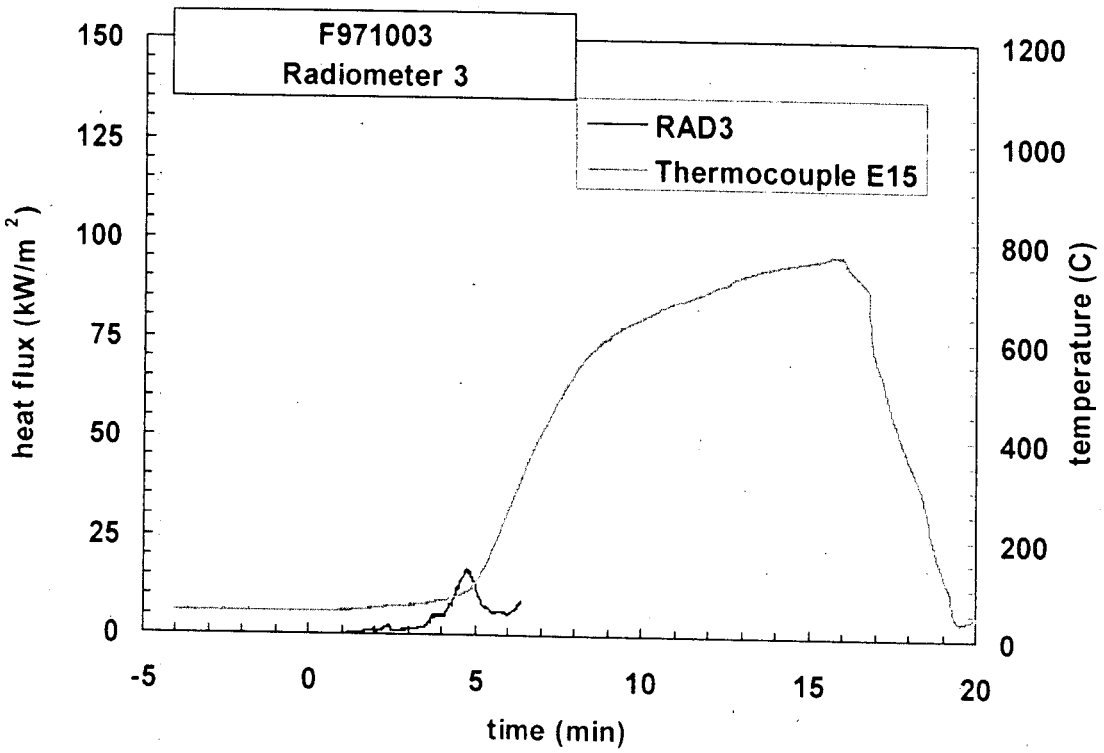

Plot E6. Fire Test F971003. Data plot fromRAD3. The transducer temperature limit was exceeded at 06:37 (min:sec) post-ignition.

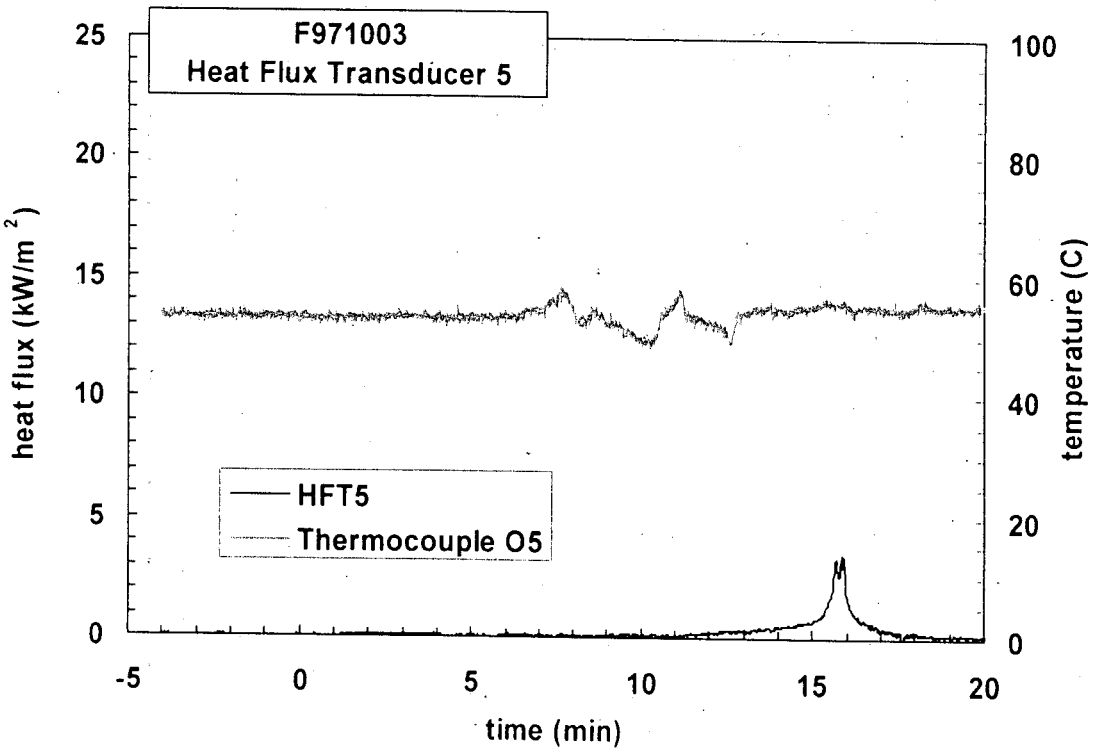

Plot E7. Fire Test F971003. Data plot from HFT5.

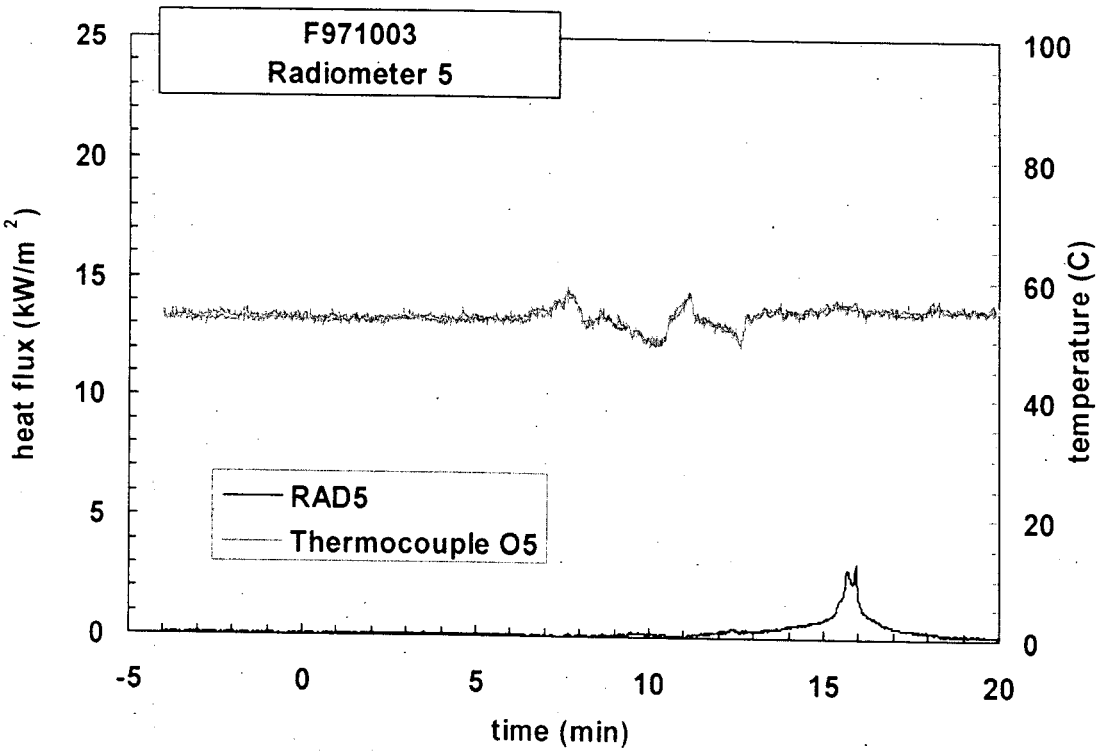

Plot E8. Fire Test F971003. Data plot from RAD5.

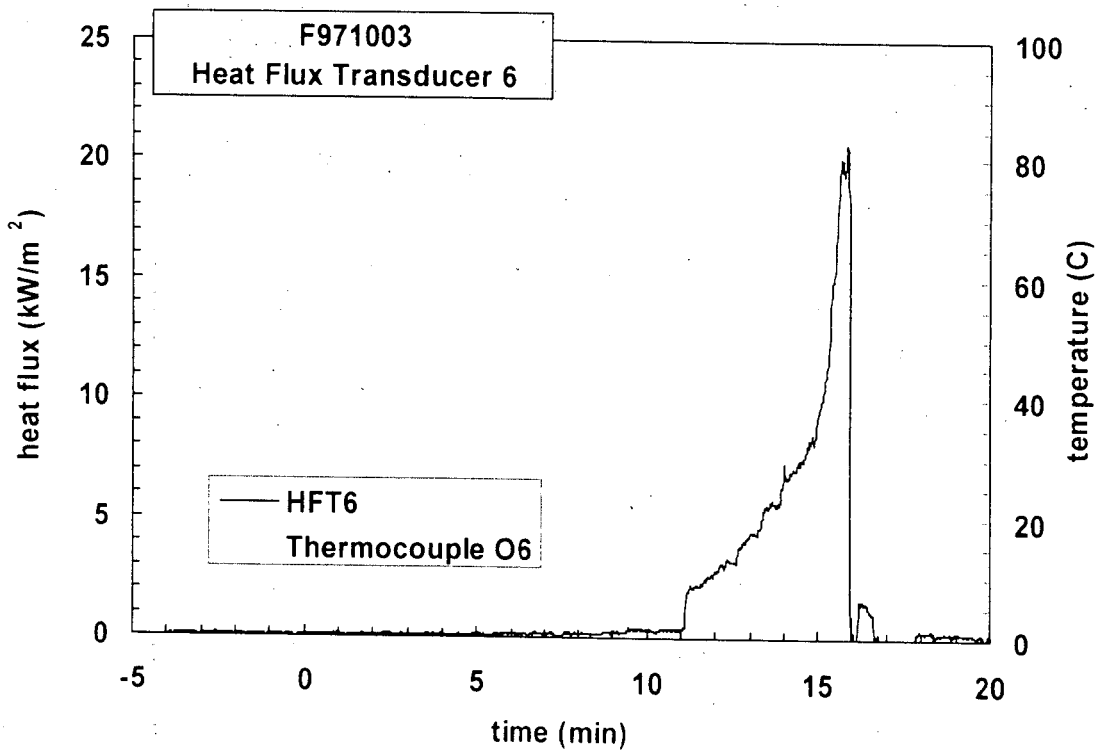

Plot E9. Fire Test F971003. Data plot from HFT6.

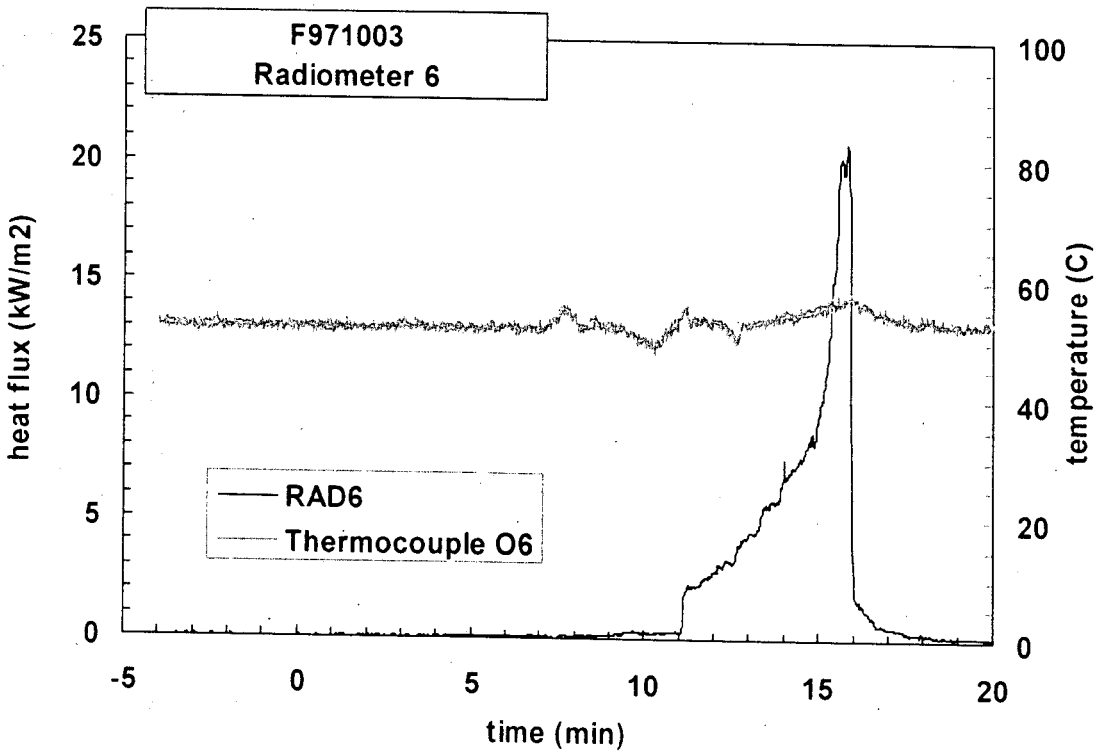

Plot E10. Fire Test F971003. Data plot fromRAD6.

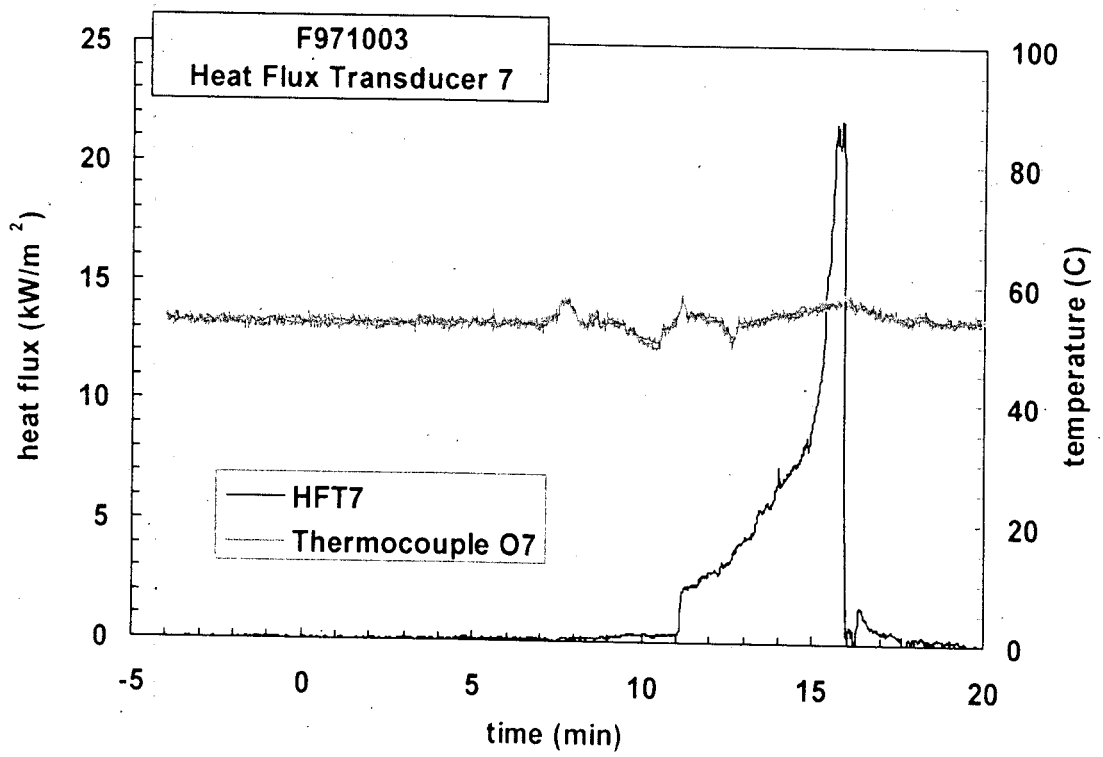

Plot E11. Fire Test F971003. Data plot from HFT7.

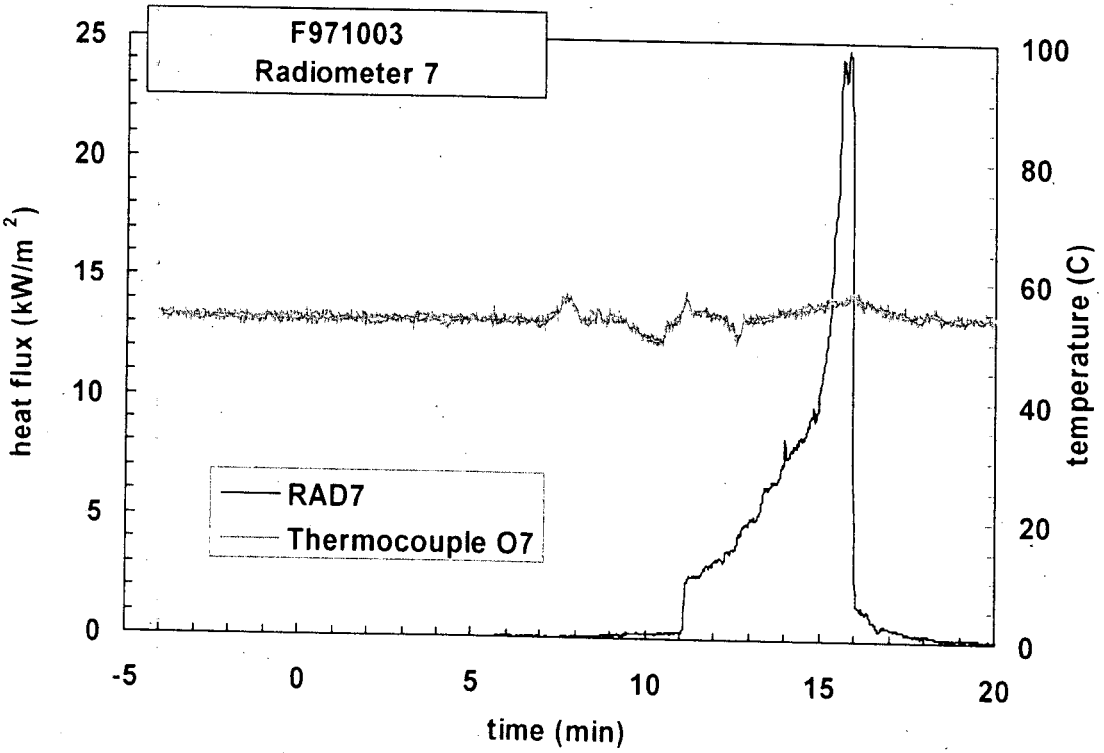

Plot E12. Fire Test F971003. Data plot from RAD7.

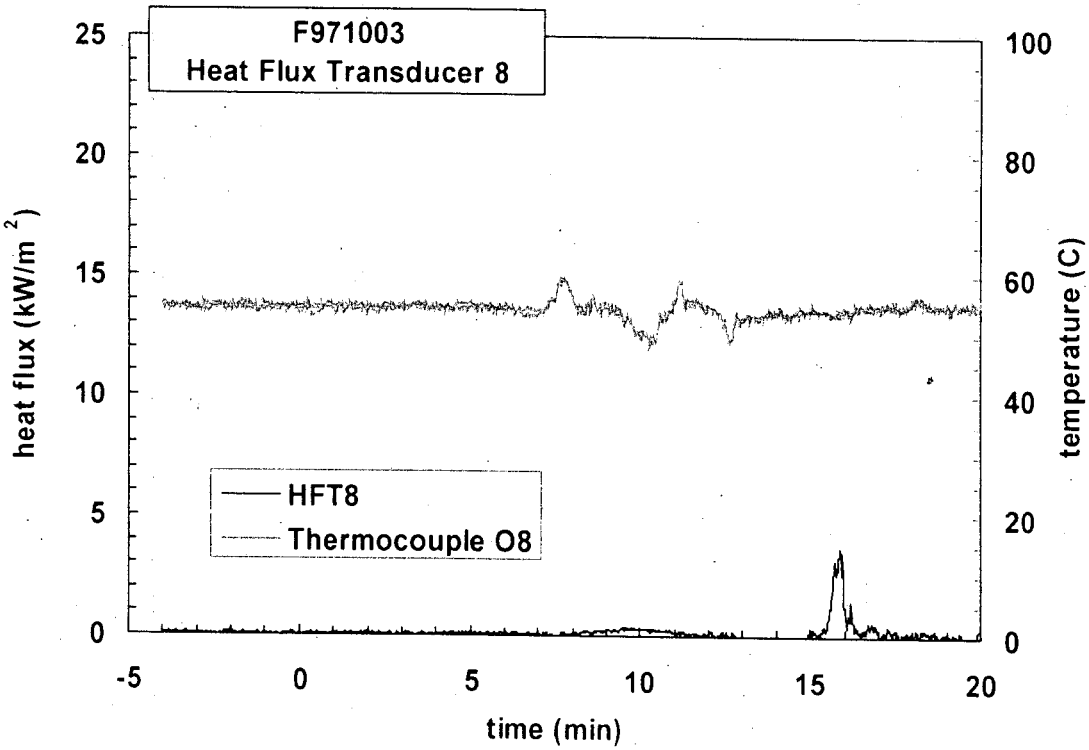

Plot E13. Fire Test F971003. Data plot from HFT8.

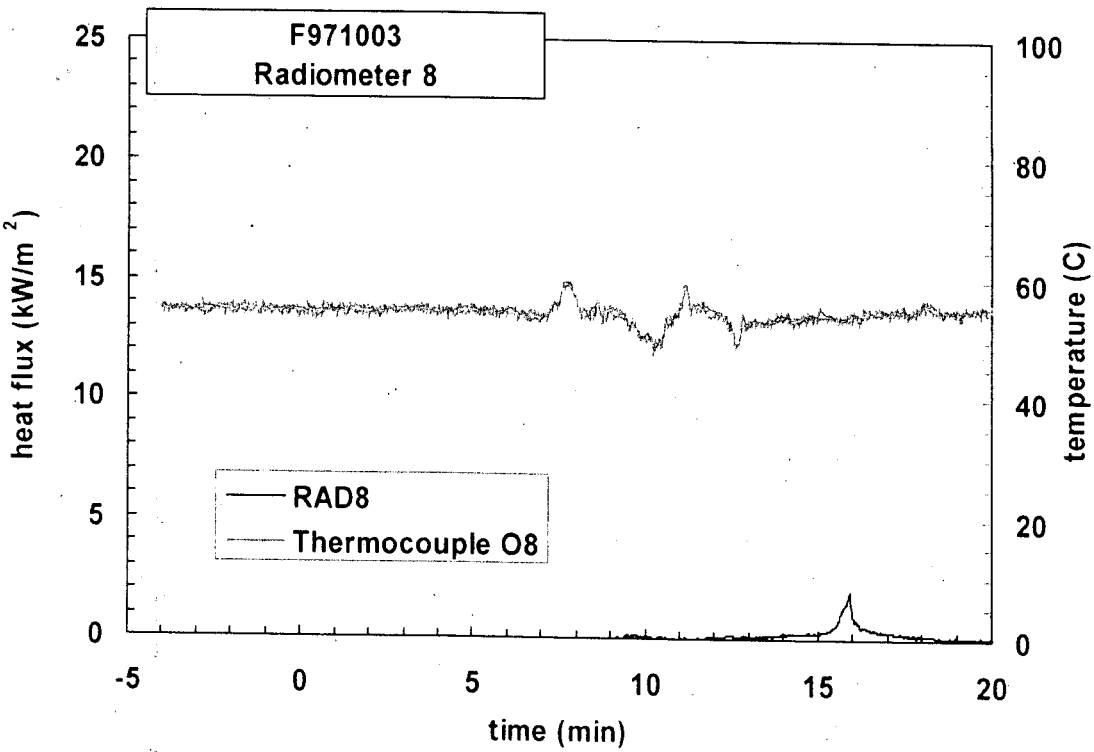

Plot E14. Fire Test F971003. Data plot from RAD8.

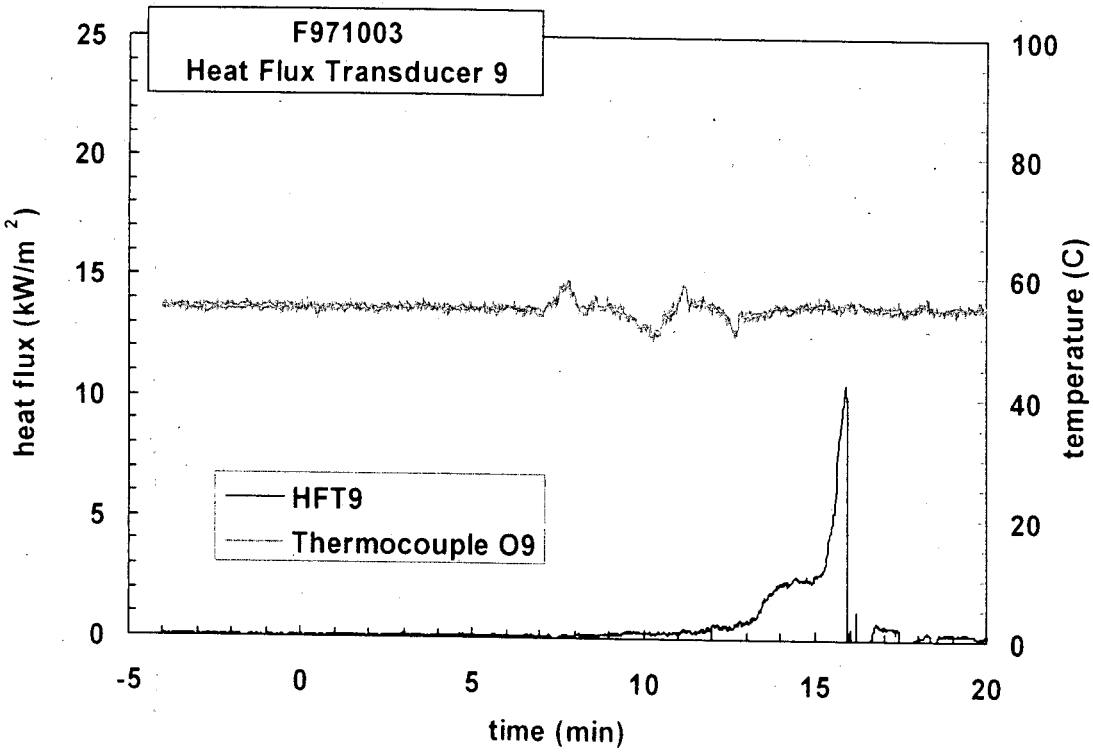

Plot E15. Fire Test F971003. Data plot from HFT9.

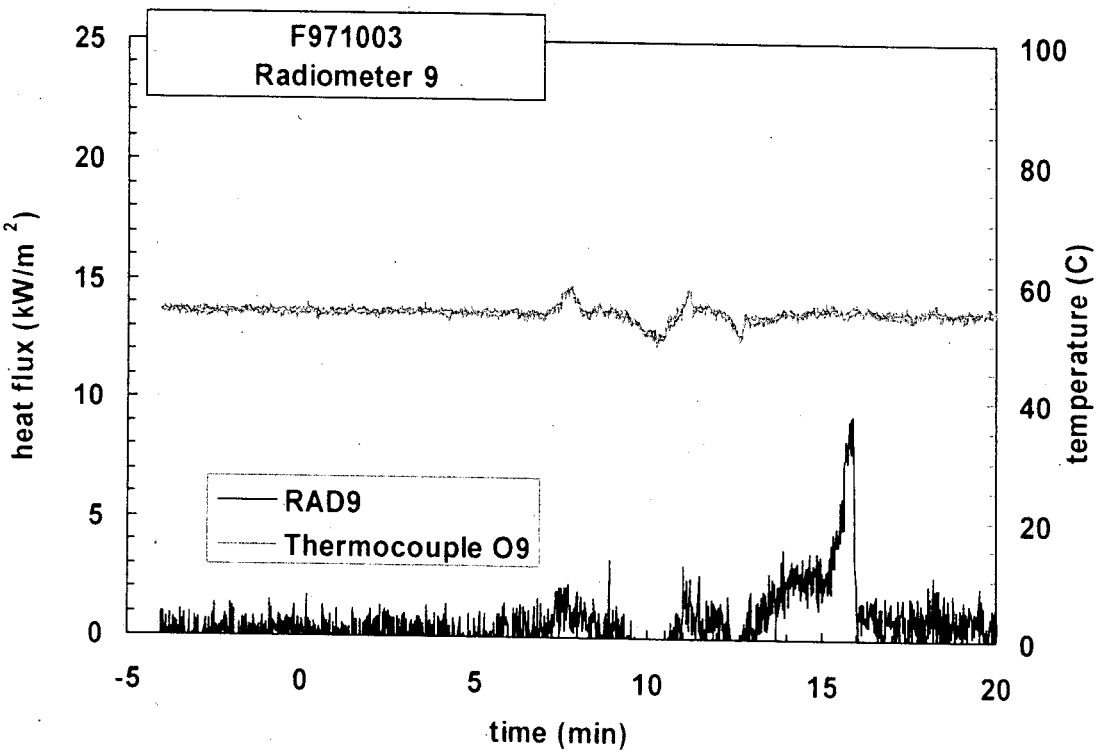

Plot E16. Fire Test F971003. Data plot from RAD9.

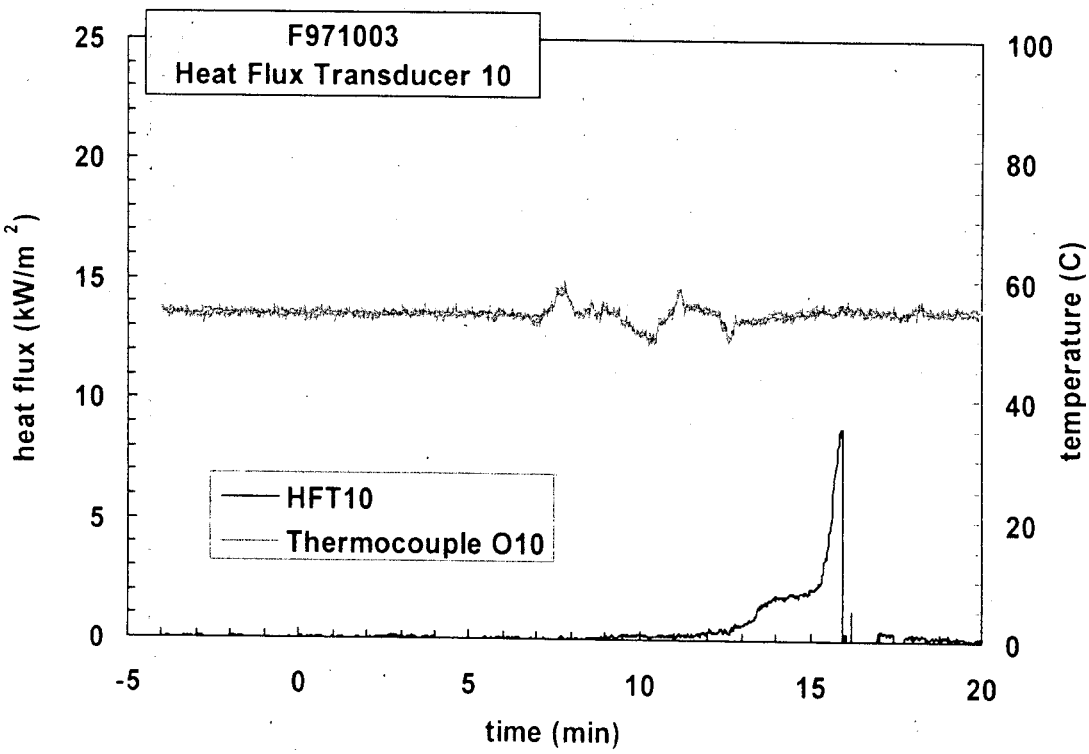

Plot E17. Fire Test F971003. Data plot from HFT10.

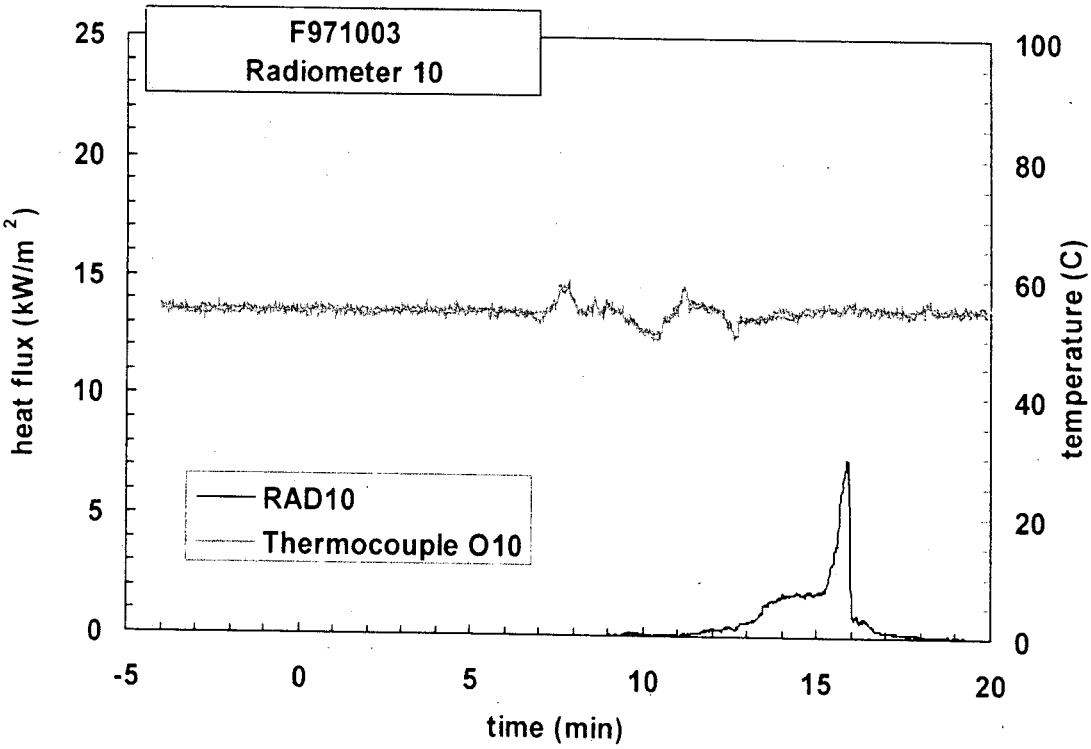

Plot E18. Fire Test F971003. Data plot from RAD10.

APPENDIX F
PRESSURE AND AIRFLOW MEASUREMENTS

Figures F1 and F2 show the approximate locations of the pressure taps and bi-directional flow probe in the test vehicle.

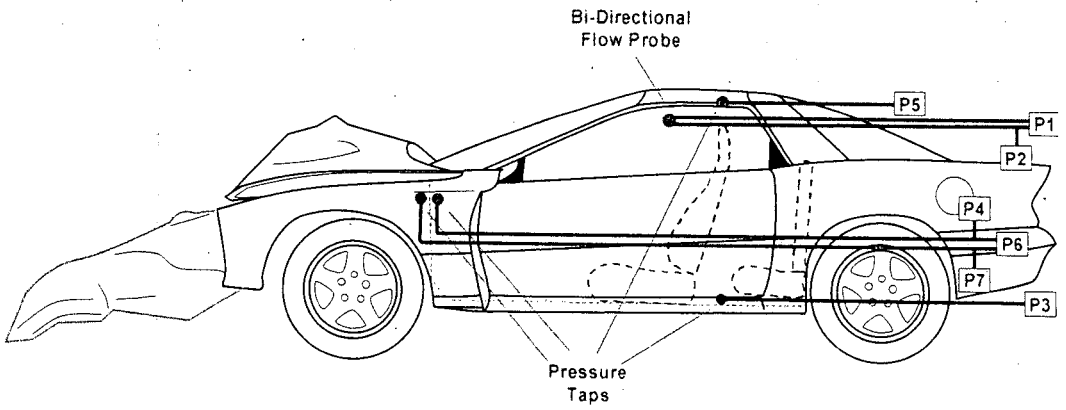

Figure F1. Fire Test F971003. Side view showing the approximate locations of the pressure taps and bi-directional flow probe in the test vehicle.

Four pressure taps were installed in the test vehicle in the following locations: above the carpet in the foot area in front of the rear right seat; in front of the rear seat back, centered horizontally and approximately 10 cm below the upper edge of the sear back; rearward of the rear bulkhead in a space above the fuel tank; below the headlining above the foot area in front of the rear right seat.

Each pressure tap was constructed from a piece of stainless steel tubing (o.d. = 0.250 in.), ending in a union-T fitting with compression-type couplings (Parker). Two of the three positions in the union-T fitting were left open. The other end of tubing was connected to a pressure gauge with solvent-resistant flexible tubing (Tygon Masterflex® 6049; i.d. = 0.250 in.; o.d. = 0.438 in.). The total length of each pressure sampling line was approximately 10 m.

A bi-directional flow probe was located in the upper rear quadrant of the right door window opening (the glass was broken in the crash test) approximately 10 cm below the upper edge of the opening. This probe was used to determine the velocity and direction of airflow through the window opening during the test. The stainless steel tubes leading from the flow probe were connected to pressure gauges with solvent-resistant resistant flexible tubing (Tygon Masterflex® 6049; i.d. = 0.250 in.; o.d. = 0.438 in.). The total length of tubing was approximately 10 m.

The velocity of gas flow through the window opening in the driver's door was calculated from the pressure difference measured across the bi-directional probe using the following relationship:

$$V = 0.070\sqrt{T\Delta p} \qquad \text{(F1)}$$

where V is the gas velocity in m/s, T is the gas temperature in degrees Kelvin, and Δp is the pressure difference in Pascals (N/m^2) [F1 and F2].

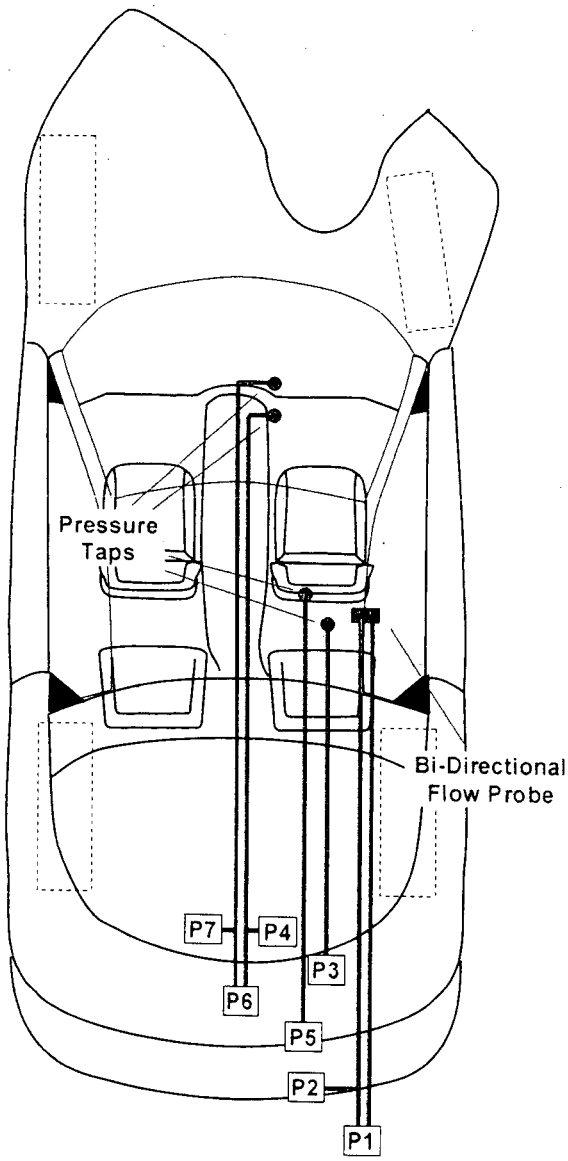

Figure F2. Fire Test F971003. Top view showing the approximate locations of pressure taps the bi-directional probe in the test vehicle.

Pressure gauges (Model C-264, Setra Systems, Acton, MA) with two pressure ranges were used for this test: - 0.5 to 0.5 (± 0.0013) in. W.C. (-124.5 to 124.5 Pascal) and -0.1 to 0.1 (± 0.0003) in. W.C. (-24.9 to 24.9 Pascal). Both gauges were accurate to 0.25% full scale. The gages were powered with a 24 volt non-regulated power supply (Setra Systems). Pressure Gauge P1 was connected to both ports on the bi-directional flow probe. The high-pressure inlet of Pressure Gauge P2 was connected to the inboard port of the bi-directional probe, and its low-pressure inlet was left open to atmosphere. The high-pressure inlet of Pressure Gauge P3 was connected to the pressure tap located above the carpet in the foot area in front of the left rear seat, and its reference was left open to atmosphere. The high-pressure inlet of Pressure Gauge P4 was connected to the pressure tap located in front of the rear seat back, and its low-pressure inlet was left open to atmosphere. The high-pressure inlet of Pressure Gauge P5 was connected to the pressure tap located below the headlining, and its low-pressure inlet was left open to atmosphere. The high-pressure inlet of Pressure Gauge P6 was connected to the pressure tap located behind of the rear bulkhead, and its low-pressure inlet was connected to the pressure tap located in front of the rear seat back. The high-pressure inlet of Pressure Gauge P7 was connected to the pressure tap located behind the rear bulkhead, and in front of the rear seat back.

The PC-based data acquisition system described in **APPENDIX C** also was used to record the electronic signals from the pressure gauges during the test. The signal leads from the pressure gauges were plugged into panel-mounted connectors, which were hard-wired to a low-gain analog-input multiplex expansion card (DBK12, IOTech). The analog-input expansion card was interfaced to the main A/D card in the PC. The signal from each pressure gauge was sampled at a rate of 100 Hz. The analog data was stored to a data file in 100-point block-averages so that the effective sampling rate during the test was 1 Hz.

Plots of the pressures recorded with Pressure Gauges P1 through P7 are shown in Plots F1 through F7. Steam generated from the water used to extinguish the flames caused fluctuations in the recorded pressure after about 16 minutes post-ignition observed in Figures F1 through F7.

REFERENCERS

F1. N. R. Keltner and J. L. Moya. Defining the thermal environment in fire tests. *Fire and Materials* **14**: 133-138, 1989.

F2. B. J. McCaffrey and G. A. Heskestad. Robust bidirectional low-velocity probe for flame and fire application. *Combustion and Flame* **26**: 125-127, 1976.

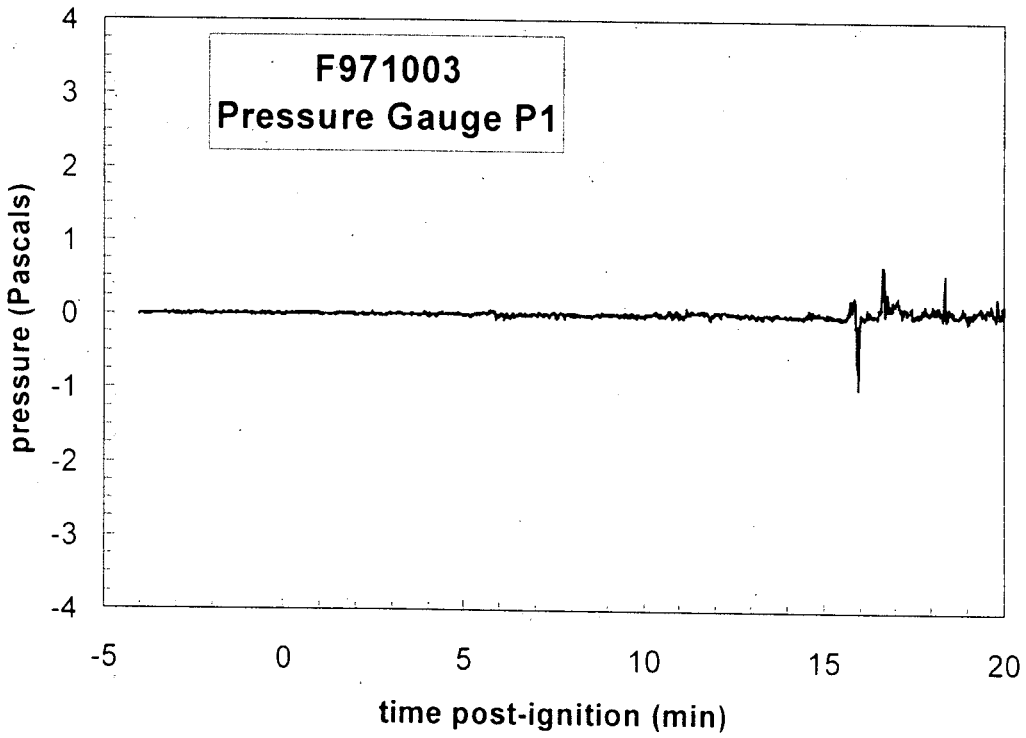

Plot F1. Fire Test F971003. Differential pressure across the bi-direction flow probe measured with P1.

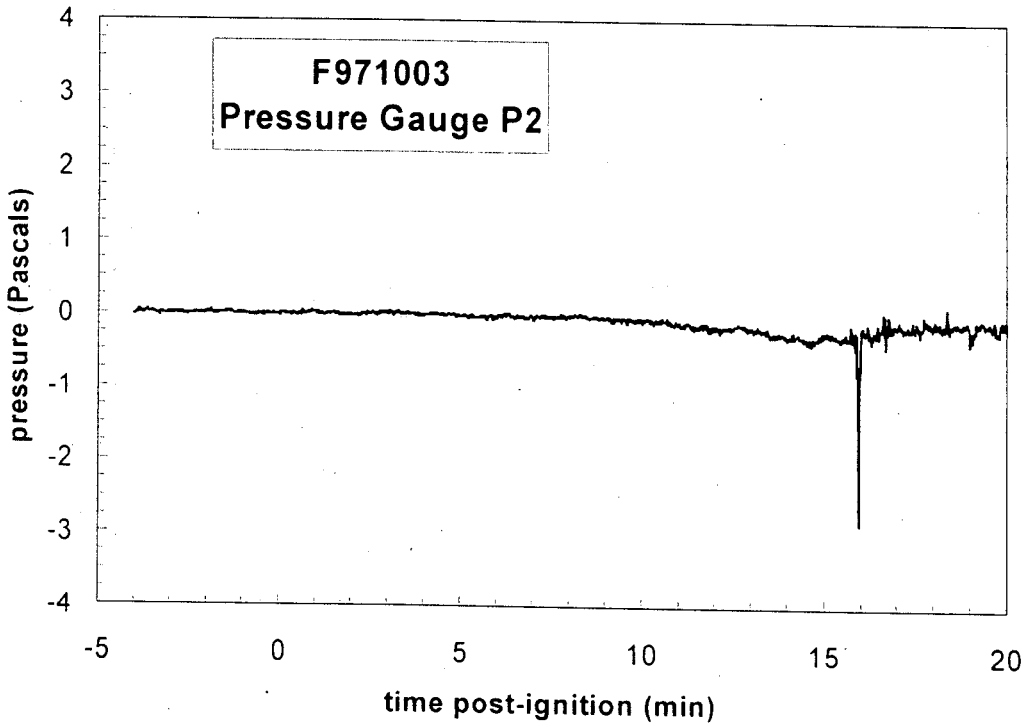

Plot F2. Fire Test F971003. Pressure at the inboard side of the bi-directional flow probe relative to atmospheric pressure measured with P2.

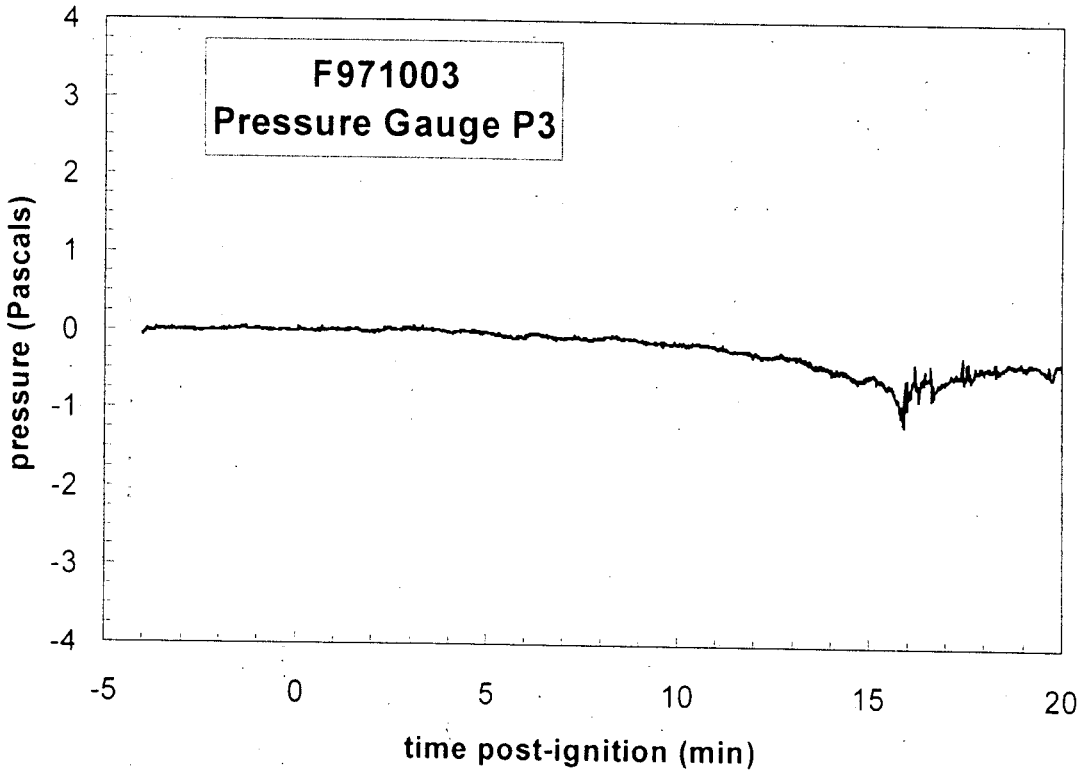

Plot F3. Fire Test F971003. Pressure above the carpet in the rear left foot area relative to atmospheric pressure measured with P3.

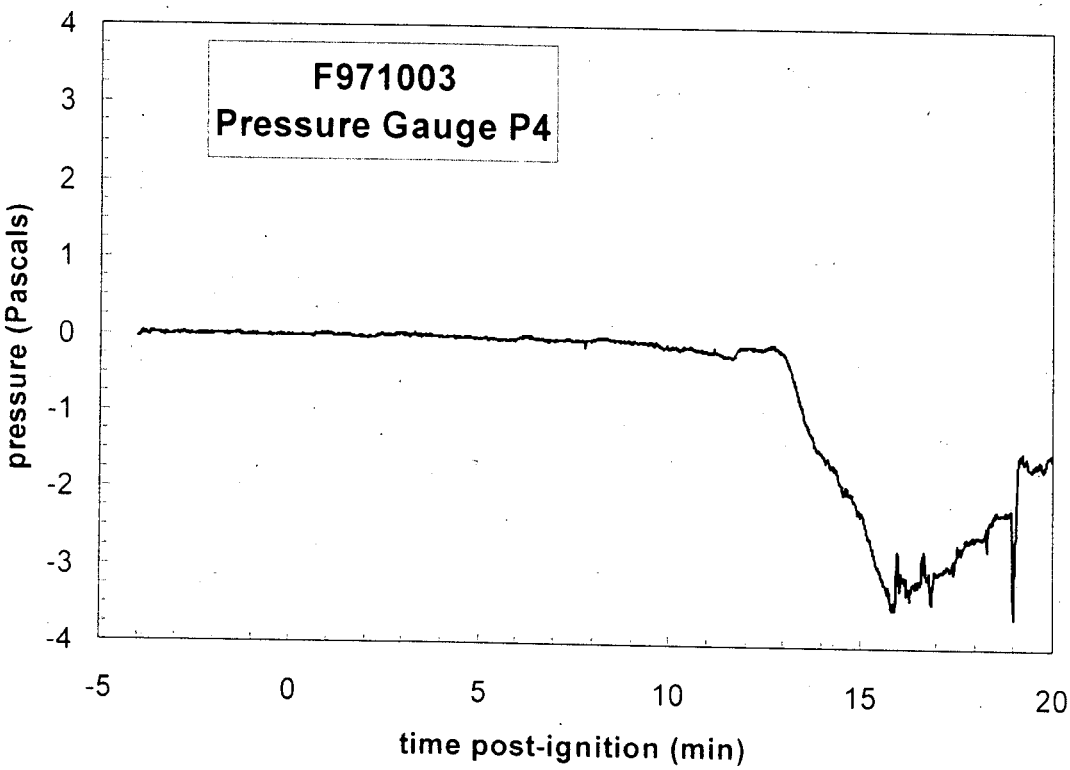

Plot F4. Fire Test F71003. Pressure in front of the rear seat back relative to atmospheric pressure measured with P4.

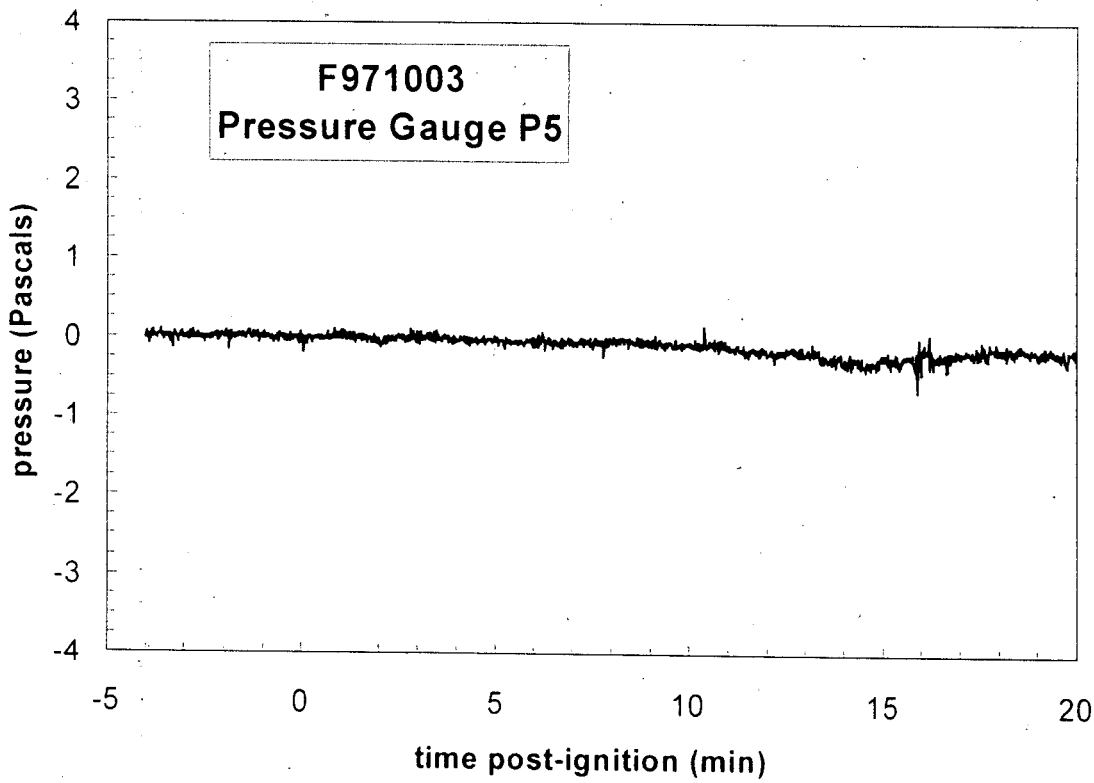

Plot F5. Fire Test F971003. Pressure below the headlining relative to atmospheric pressure measured with P5.

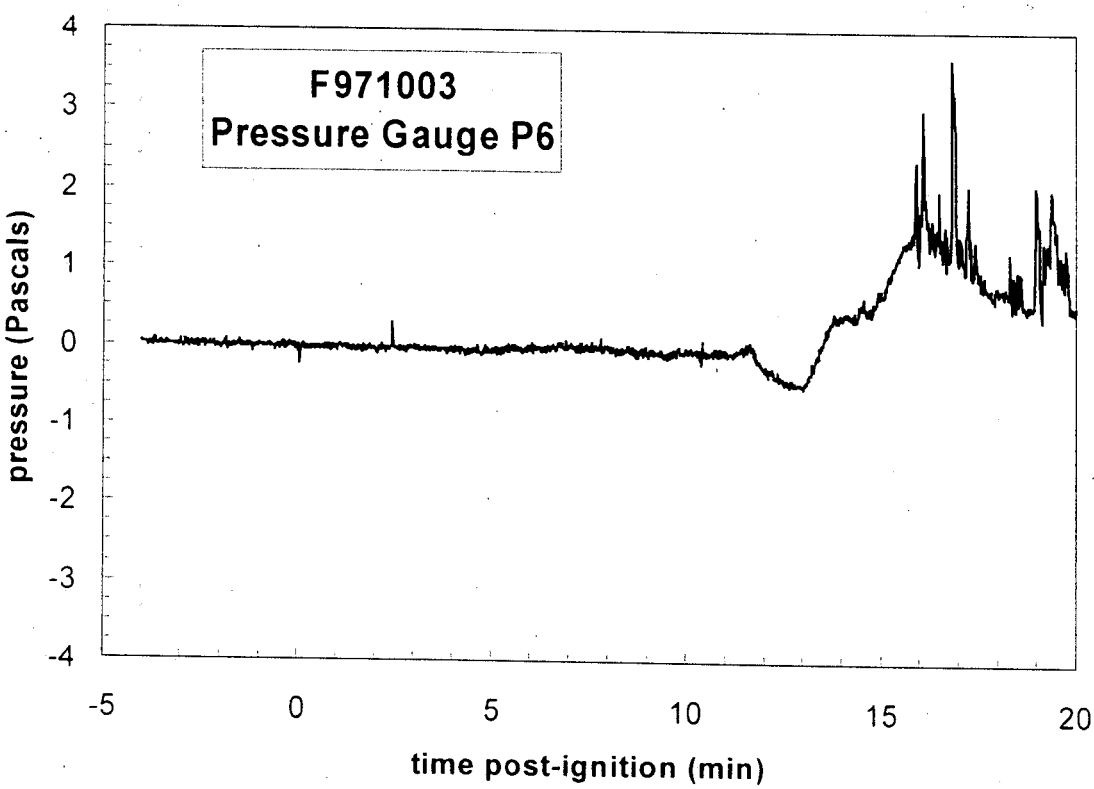

Plot F6. Fire Test F971003. Differential pressure across the rear bulkhead measured with P6.

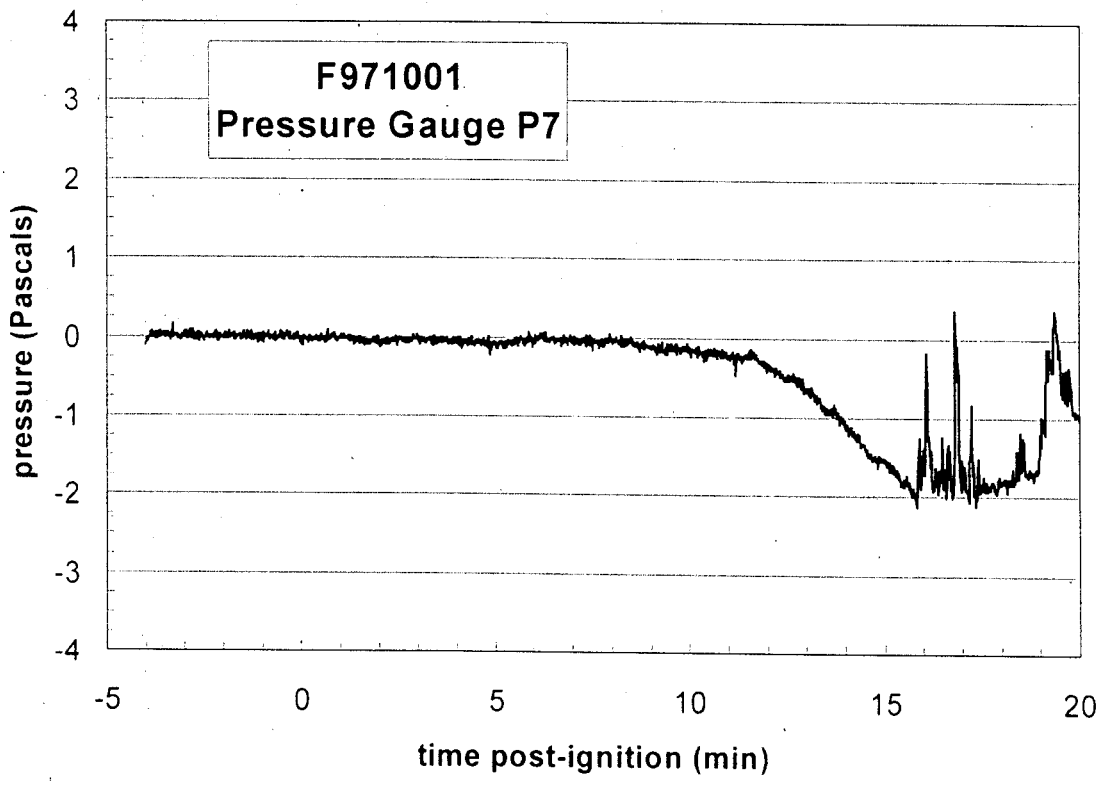

Plot F7. Fire Test F971003. Pressure behind the rear bulkhead relative to atmosphere measured with P7.

APPENDIX G
EXPERIMENTAL FIRE DETECTOR DATA

Figures G1 shows the approximate location of these experimental fire detectors in the test vehicle for this test. Both the experimental linear fire detector and the experimental pneumatic fire detector were supplied by Santa Barbara Dual Spectrum (Goleta, CA). Both of these experimental fire detectors were attached to the underside of the deformed hood, below the hood insulation compartment, along the bend in the hood from the crash test. Both of these experimental fire detectors spanned the width of the engine.

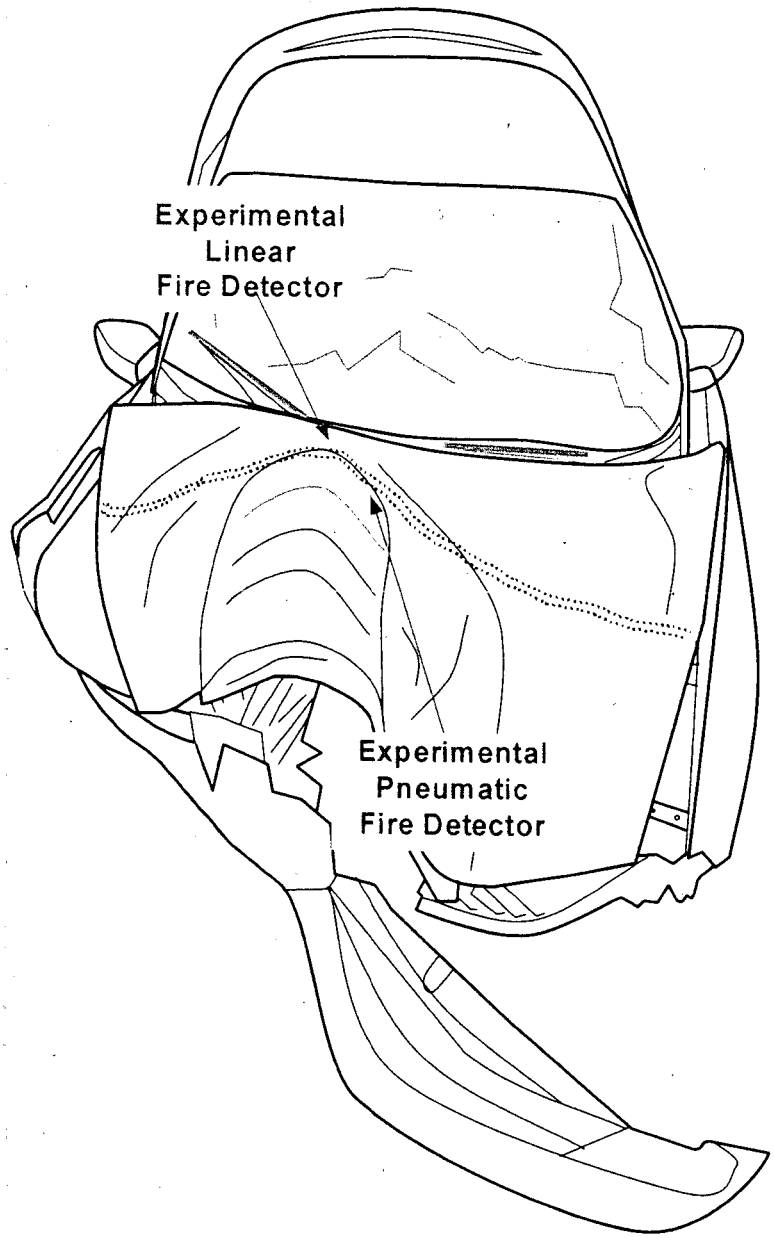

Figure G1. Fire Test F971003. Side view of the test vehicle showing the approximate location of the aspirated thermocouple probe assembly in the passenger compartment.

The experimental linear fire detector contained a signal circuit, which was normally open and closed to indicate fire detection. The experimental pneumatic fire detector contained a signal circuit to indicate detection of fire and a fault circuit to indicate a malfunction of the detector. The signal circuit in the experimental pneumatic fire detector was normally open and closed to indicate fire detection. The fault circuit in the experimental pneumatic fire detector was normally closed and opened to indicate a fault in the detector.

A schematic diagram of the electrical circuit used to test these experimental fire detectors in this test is shown in Figure G2.

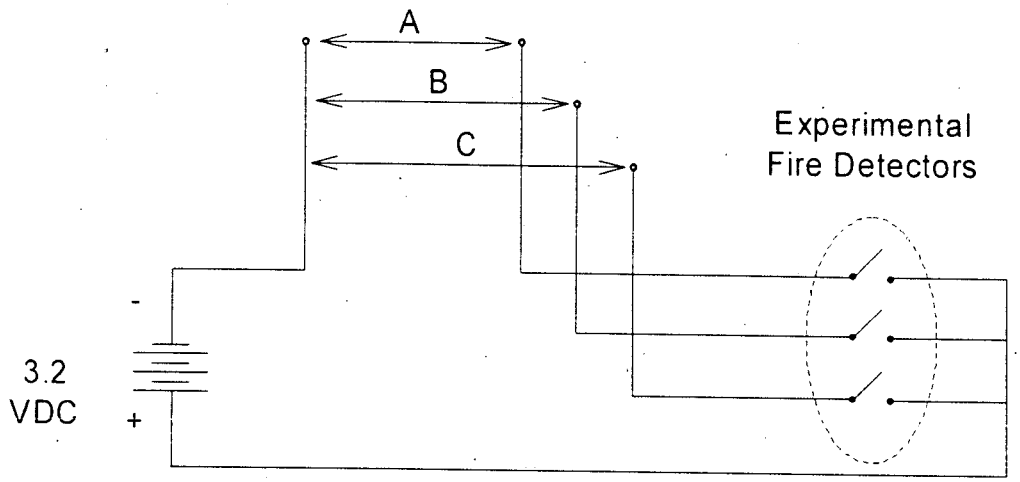

Figure G2. Fire Test F971003. Schematic diagram of the electrical circuit used to test the experimental linear and pneumatic fire detectors in this test. Two AA batteries were used to supply 3.2 VDC to the experimental fire detectors. A was the signal circuit in the experimental linear fire detector. B was the signal circuit in the experimental pneumatic fire detector signal. C was the fault circuit in the experimental pneumatic fire detector.

Shielded, twisted-pair signal cables were used to connect the experimental fire detectors to analog input channels of the channels of the data acquisition system described in Appendix B. Voltages on the signal circuit in the experimental linear fire detector and the signal and fault circuits in the experimental pneumatic fire detector were recorded from –4 minutes 1 second to 21 minutes 21 seconds post-ignition.

Plots of the data recorded from the experimental fire detectors in this test are shown in Plots G1 through G3. The voltage on the signal circuit in the experimental linear fire detector changed from 0 to +3.2 VDC at 4 minutes 14 seconds post-ignition, and from +3.2 to -0.4 VDC at 5 minutes 36 seconds post-ignition. The voltage on the signal from the experimental pneumatic fire detector changes from 0 to approximately +2.1 VDC at 4 minutes 14 seconds post-ignition, from approximately +2.1 to +3.2 VDC at 5 minutes 3 seconds, and from +3.2 to -1.48 VDC at 5 minutes 36 seconds post-ignition. The voltage on the fault circuit in the experimental pneumatic fire detector changed from +3.2 to –3.8 VDC at 5 minutes 36 seconds post-ignition.

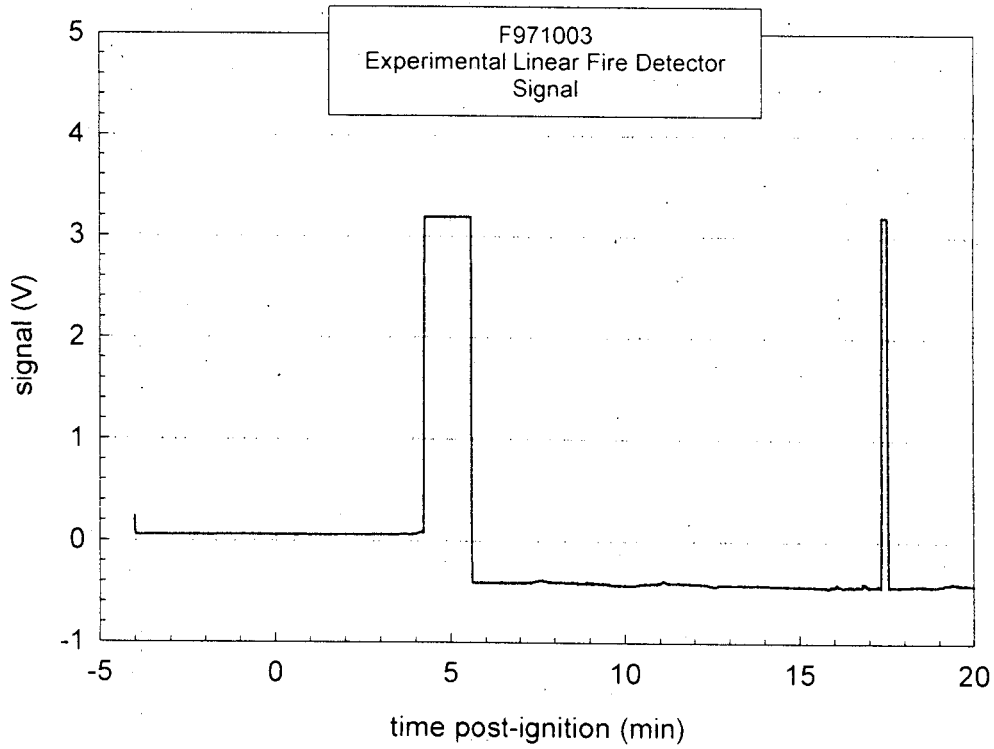

Plot G1. Fire Test F971003. Data plot of signal from the experimental linear fire detector.

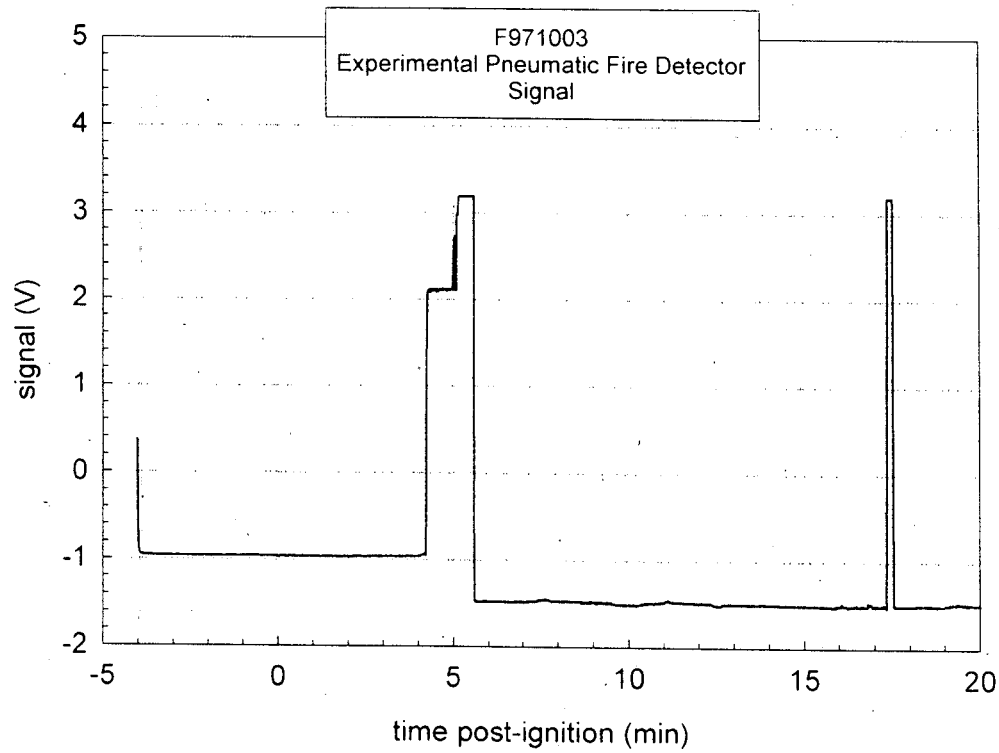

Plot G2. Fire Test F971003. Data plot of the sense-signal from the experimental pneumatic fire detector.

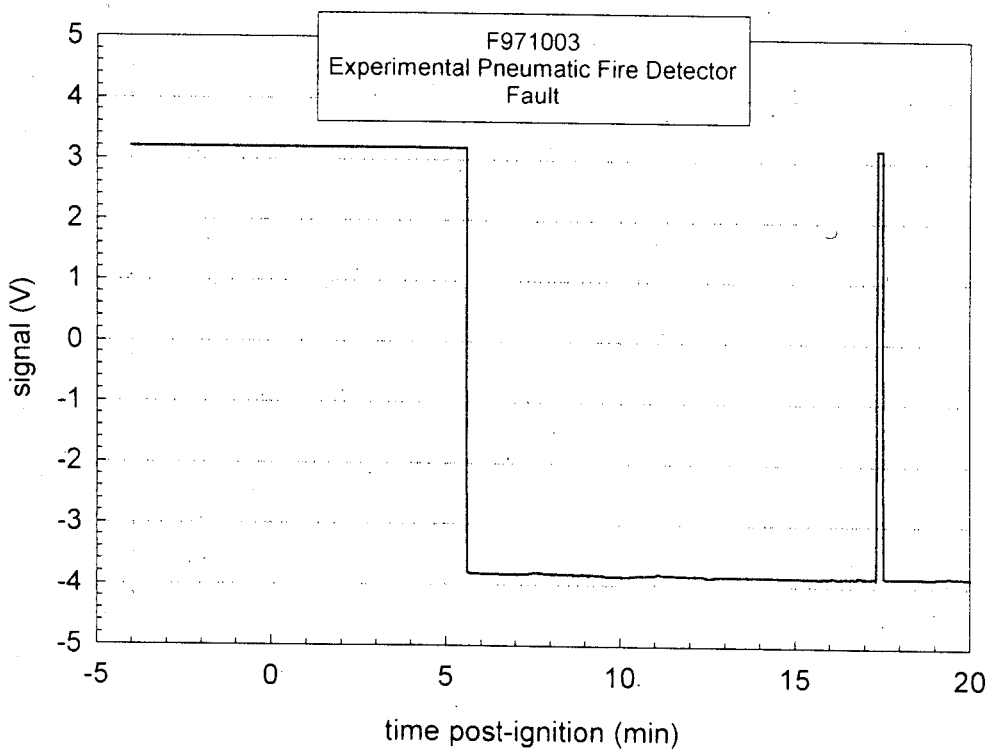

Plot G3. Fire Test F971003. Data plot of the fault-signal from experimental pneumatic fire detector.

APPENDIX H
FIRE PRODUCTS COLLECTOR DATA

Scientific and technical personnel from Factory Mutual Research Corporation were primarily responsible for obtaining and analyzing data from the Fire Products Collector (FPC) at the Factory Mutual Test Center.

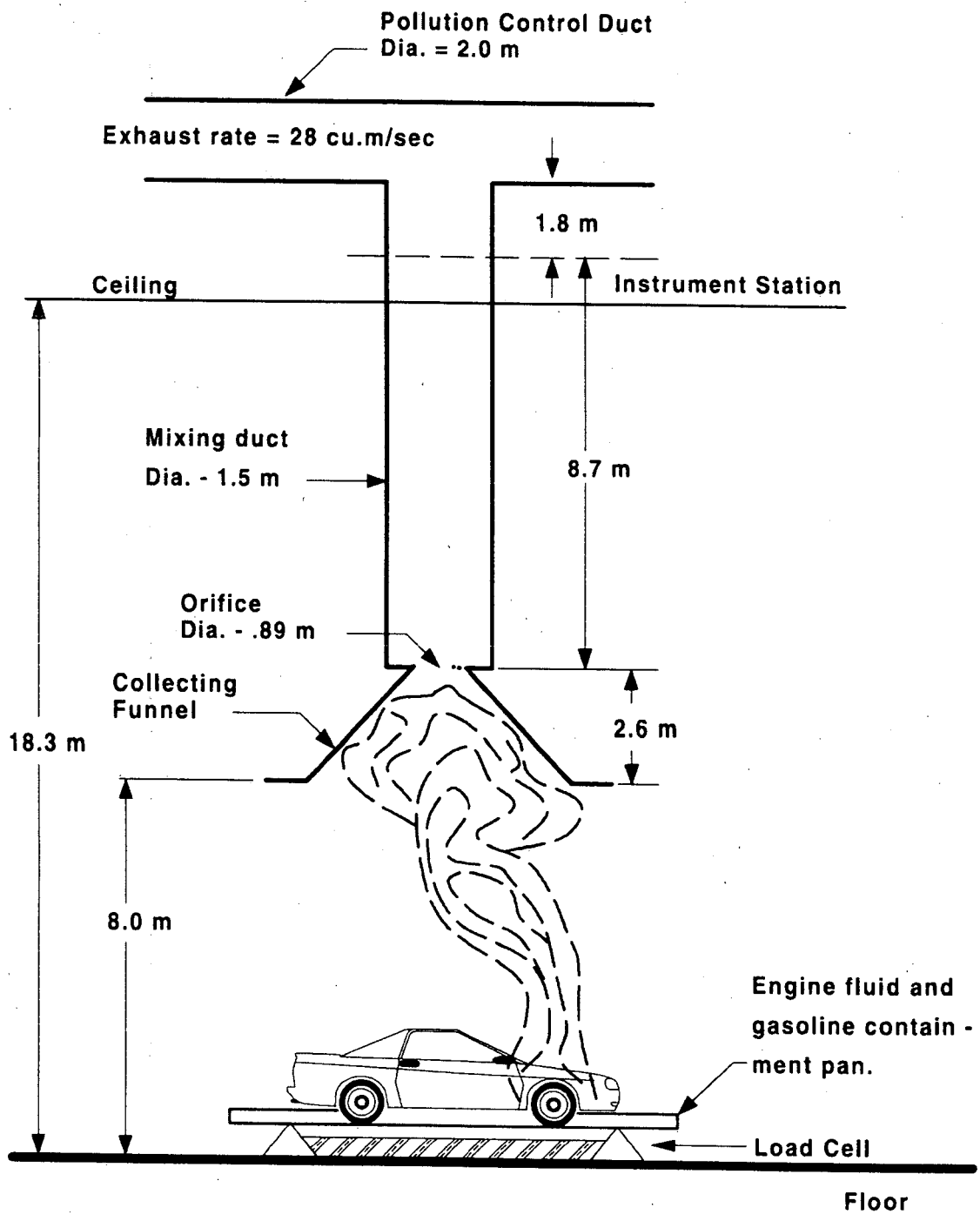

Figure H1. Fire Test F971003. Diagram of the test vehicle under the fire products collector at the Factory Mutual Test Center.

A fire products collector was used to measure heat and combustion gases generated by the burning vehicle during this test (Fig. H1). The FPC consisted of a collection funnel (diameter = 6.1 m), an orifice plate (hole = 0.9 m), and a vertical stainless steel sampling duct (diameter = 1.5 m). The sampling duct was connected to the air pollution control system of the Test Center. The blower of the air pollution control system induces gas flow through the sampling duct. Air enters the sampling duct via the orifice plate. The temperature, linear velocity, optical transmission, and chemical composition of the entrained gas were measured in the center of the sampling duct 8.66 m (5.7 duct diameters) downstream from the orifice plate, ensuring a flat velocity profile at the sampling location. The data acquisition system consisted of a Hewlett Packard 2313B analog-to-digital conversion sub-system interfaced to a Hewlett Packard 1000 computer.

Gas temperature in the sampling duct was measured with two Type-K thermocouples (30 gage) with exposed bead-type junctions. The thermocouple leads were housed in stainless steel tubes (o.d. = 6.4 mm). Ambient air temperature in the facility was measured by five Type-K thermocouples attached to the external surface of the duct at 2.44, 5.49, 9.14, 12.8, and 15.9 m above the floor. These thermocouples were shielded from radiation from the fire.

The linear velocity of the gas entrained in the sampling duct was measured with a Pitot ring consisting of four Pitot tubes. A static pressure tap was mounted on the inside wall of the sampling duct. The pressure difference between the Pitot ring and the static wall tap was measured with an electronic manometer (Barocel Model 1173, CGS Scientific Corporation).

The particulate concentration in the entrained air was determined from the optical transmission across the duct measured at 0.4579 μm (blue), 0.6328 μm (red), and 1.06 μm (infrared). The optical path length across the duct was 1.524 m. Gas was withdrawn from the sampling duct through a stainless steel tube (o.d. = 3.9 mm) at a flow rate of 0.17×10^{-3} m^3/s for chemical analysis. The gas flowed through a particulate filter, a water condenser, and a drying agent before entering the analyzers. Carbon dioxide (CO_2) and carbon monoxide (CO) were measured with two dedicated non-disperse infrared analyzers (Beckman Model 864 Infrared Analyzers). Oxygen (O_2) was measured with a paramagnetic oxygen analyzer (Beckman Model 755 Paramagnetic Oxygen Analyzer). Total gaseous hydrocarbons were measured with a flame ionization analyzer (Beckman Model 400 Flame Ionization Analyzer).

The rate of product release was calculated using the following relationship:

$$\left(\frac{dR_j}{dt}\right) = f_j\left(\frac{dV}{dt}\right)\rho_j = f_j\left(\frac{dW}{dt}\right)\left(\frac{\rho_j}{\rho_g}\right) \qquad \text{(H1)}$$

where $d(R_j)/dt$ is the mass release rate of product j in kg/s; f_j is the volume fraction of product j; dV/dt is the total volume flow rate of the gas entrained in the sampling duct in m^3/s; dW/dt is the total mass flow rate of the gas entrained in the sampling duct in kg/s; ρ_j is the density of product j in g/m^3; and ρ_g is the density of the gas entrained in the concentration measurements. The rate of oxygen consumption was calculated using equation (A1), where the volume fraction of oxygen consumed was substituted for f_j.

The volume fraction of smoke particulate was calculated from the following relationship:

$$f_s = \frac{D\lambda \times 10^{-6}}{\Omega} \qquad \text{(H2)}$$

where f_s is the volume fraction of smoke, λ is the wavelength of the light source, Ω is the extinction coefficient of particulate (a value of 0.7 was used in these calculations), and D is the optical density at each of the three wavelengths at which measurements were made:

$$D = \frac{\ln\left(I_0/I\right)}{L} \qquad \text{(H3)}$$

where I_0 is the intensity of light transmitted through clean air, I is the intensity of light transmitted through air containing smoke particulate, and L is the optical pathlength, which was equal to 1.524 m. A value of 1.1×10^6 g/m^3 was used for the density of smoke particulate (ρ_j) in equation (H1).

The convective heat release rate was calculated using the following relationship:

$$\left(\frac{dE_{conv}}{dt}\right) = \left(\frac{dW}{dt}\right) \times c_p \times \left(T_g - T_a\right) \qquad \text{(H4)}$$

where $d(E_{conv})/dt$ is the convective heat release rate in kW; dW/dt is the mass flow rate of the gas entrained in the sampling duct in kg/s; c_p is the heat capacity of the gas entrained in the sampling

duct at the gas temperature in kJ/(kg×K); T_g is the temperature of the gas entrained in the sampling duct in K; and T_a is the ambient air temperature in K.

The chemical heat release rate was calculated from the release rates of carbon dioxide and carbon monoxide as follows:

$$\left(\frac{dE_{ch}}{dt}\right) = \Delta H^{\bullet}_{CO_2} \times \left(\frac{dR_{CO_2}}{dt}\right) + \Delta H^{\bullet}_{CO} \times \left(\frac{dR_{CO}}{dt}\right) \qquad \text{(H5)}$$

where $d(E_{ch})/dt$ is the chemical heat release rate in kW; ΔH^* is the net heat of complete combustion per unit mass of carbon dioxide or carbon monoxide released in the fire in kJ/g; and dR/dt is the mass release rate of carbon dioxide or carbon monoxide in kg/s. Values of ΔH^* for carbon dioxide and carbon monoxide were obtained from the literature [H1 and H2].

The chemical heat release rate also was calculated from the oxygen consumption rate as follows:

$$\left(\frac{dE_{ch}}{dt}\right) = \Delta H^{\bullet}_{O}\left(\frac{dC_O}{dt}\right) \qquad \text{(H6)}$$

where $d(E_{ch})/dt$ is the chemical heat release rate in kW; ΔH^*_O is the net heat of complete combustion per unit mass of O_2 consumed in kJ/g; and $d(C_O)/dt$ is the consumption rate of oxygen in kg/s. The value for ΔH^*_O was obtained from the literature [H1 and H2].

The radiative heat release rate was the difference between the chemical heat release rate and the convective heat release rate:

$$\left(\frac{dE_{rad}}{dt}\right) = \left(\frac{dE_{ch}}{dt}\right) - \left(\frac{dE_{conv}}{dt}\right) \qquad \text{(H7)}$$

where $d(E_{rad})/dt$ is the radiative heat release rate; and $d(E_{ch})/dt$ is the average chemical heat release rate calculated using equations (H5) and (H6).

The vehicle was placed in a rectangular steel pan (length = 25 ft., width = 15 ft., height = 4 in.) to prevent spilled and leaking automotive fluids from spreading in the test facility. This fluid containment pan was fabricated from two sheets of carbon steel. Angle-braces were welded to

the under-side of the pan to keep it from flexing under the weight of the vehicle. The corners of the support frame rested on load cells. Mass loss was determined from data acquired from the load cells during the test.

The fluid containment pan was lined with a layer of fiberglass-reinforced cement construction board (DuraRock, USG Corporation). A thin layer of sand was used to level the concrete board so that the grade of the surface measured from the center to the edges along the major and minor axes was no greater than 1%. The joints between boards were sealed with latex caulking.

Mass loss from the burning vehicle and any burning fluids retained by the containment pan was measured with a load cell weigh-module system. The fluid containment pan was supported by an I-beam frame a load cell weight-module (KIS Series, BLH Electronics, Inc.) at each corner. These weight-modules contain cylindrical, double cantilever strain gauge transducers that are not generally affected by changes in mass distribution. The weight-module system wsa calibrated before this test by placing a series of standard weights on the fluid containment pan.

Data from the fire-products collector and load cell weight-module system are shown in Plots H1 through H5. The Fire Products Collector did not detect a fire plume until approximately 15 seconds after the gasoline was ignited. After the initial increase (approximately 15 to 25 seconds post-ignition), the heat release rate increased exponentially until the fire was extinguished (Plot H1). The heat release rate reached a maximum of approximately 1200 kW at 230 seconds post-ignition. The carbon dioxide release rate curve (Plot H2) was similar to the heat release rate curve. After initially increasing between 15 and 25 seconds post-ignition, the carbon monoxide release rate curve approached a value of 1.6 to 1.7 g/s asymptotically, and decreased when the fire was extinguished (Plot H3). The smoke release rate curve was similar, approaching a value of 0.5 to 0.6 mg/s before the fire was extinguished (Plot H4). Mass loss curve indicated that the vehicle lost between 2 and 3 kg as a result of material burning during this test (Plot H5). The resolution of the load cell system used to make the weight measurement was between 0.3 and 0.4 kg (between 10 to 15% of the total mass loss during the test), and was responsible for the high degree of scatter in the mass loss curve (Plot H5).

REFERENCES

H1. G. Heskestad. A Fire Products Collector for Calorimetry into the MW Range, Technical Report J.I. OC2E1.RA. Factory Mutual Research Corporation, Norwood, MA. June, 1981.

H2. Archibald Tewarson. "Generation of Heat and Chemical Compounds in Fires" Section 3/Chapter 4, SFPE Handbook of Fire Protection Engineering, 2nd Edition, 1995, pp. 3:53-124.

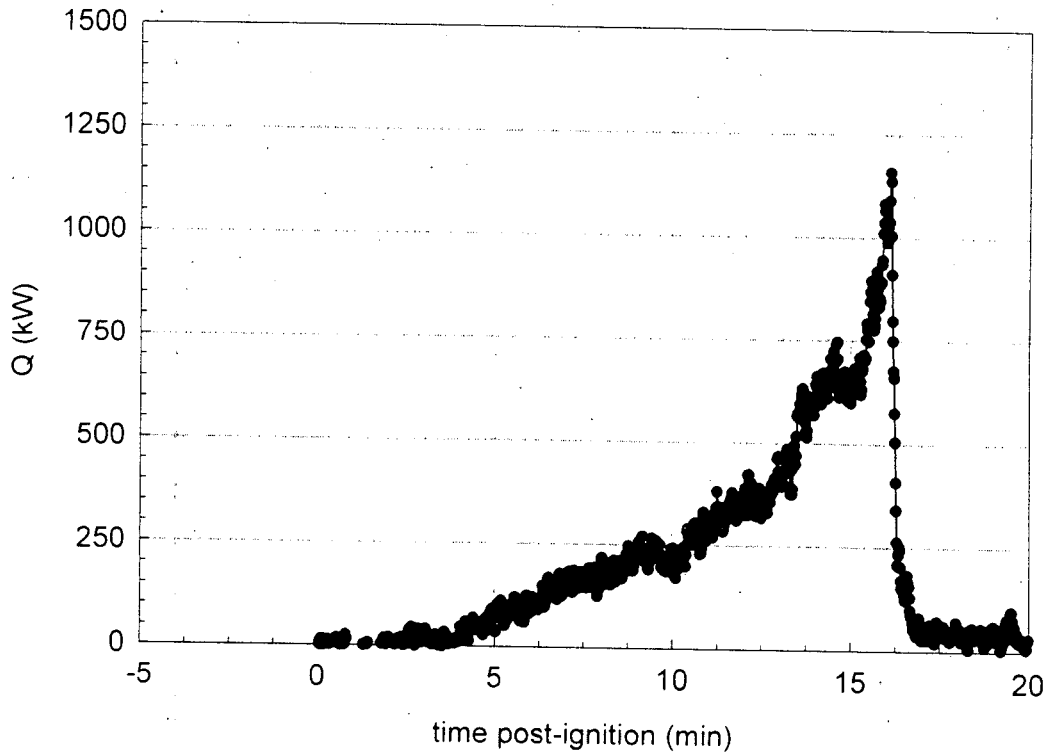

Plot H1. Fire Test F971003. Heat release rate measured using the Fire Products Collector.

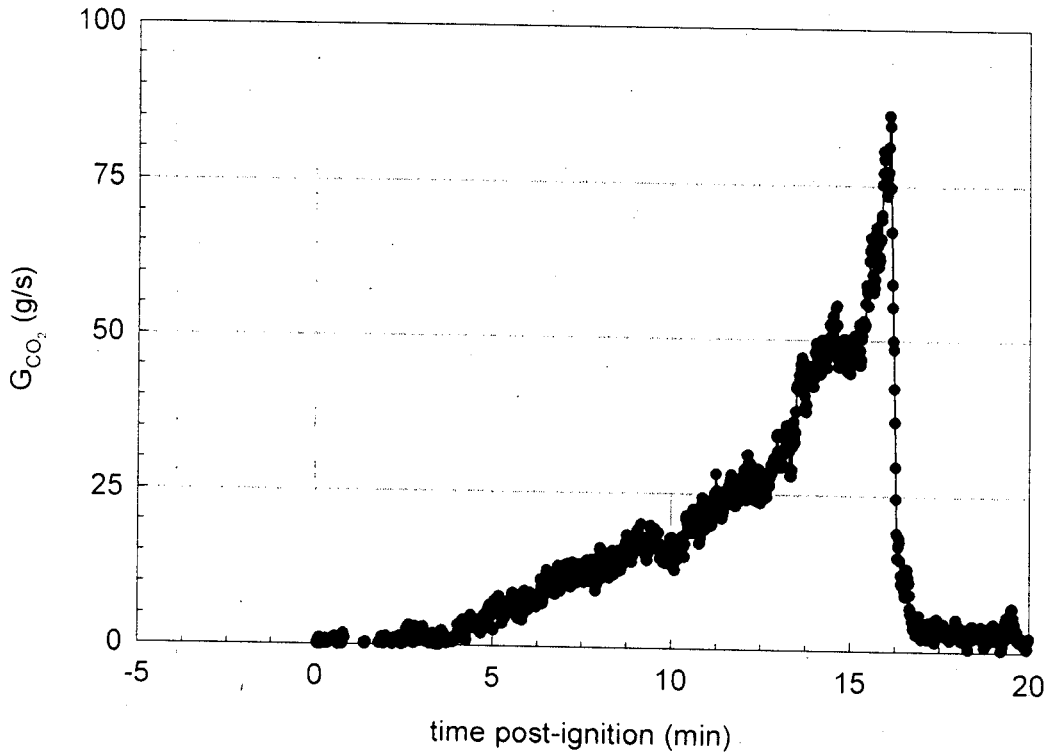

Plot H2. Fire Test F971003. Carbon dioxide release rate measured using the Fire Products Collector.

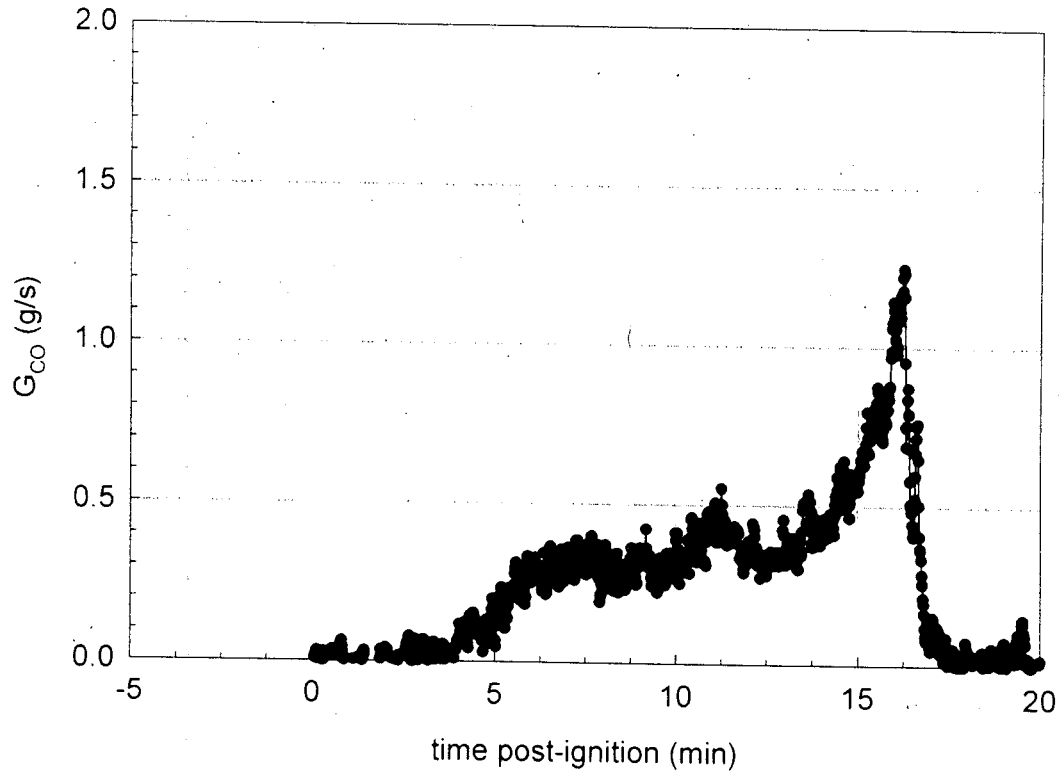

Plot H3. Fire Test F71003. Carbon monoxide release rate measured using the Fire Products Collector.

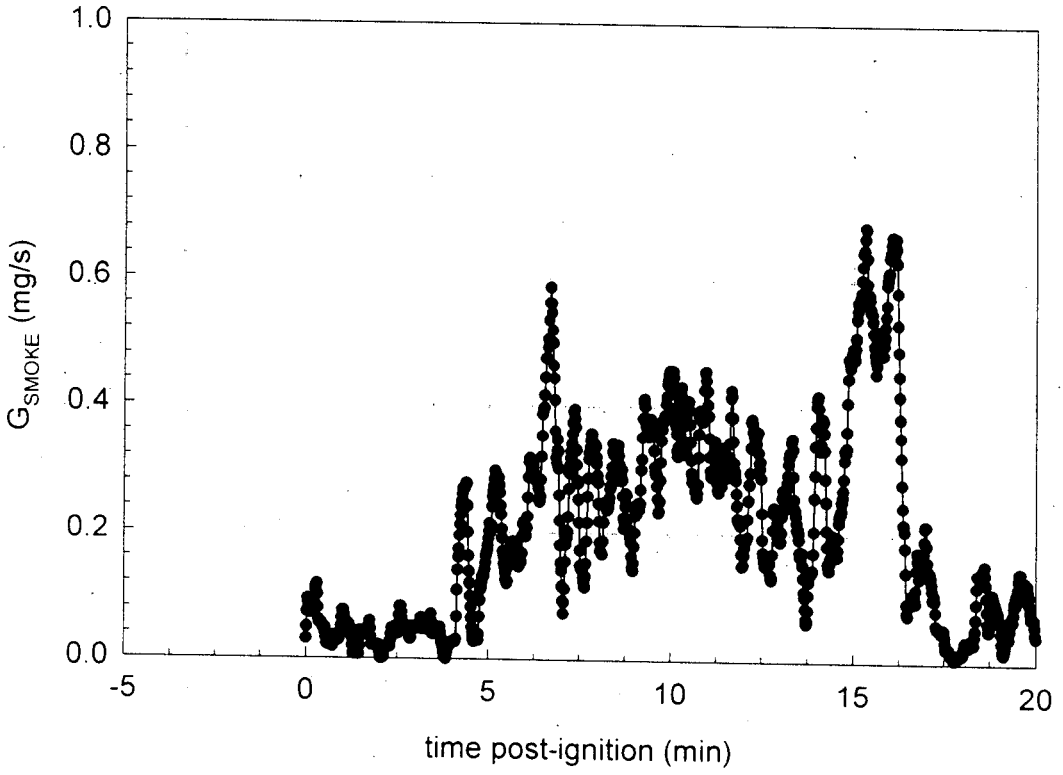

Plot H4. Fire Test F971003. Smoke release rate measured using the Fire Products Collector.

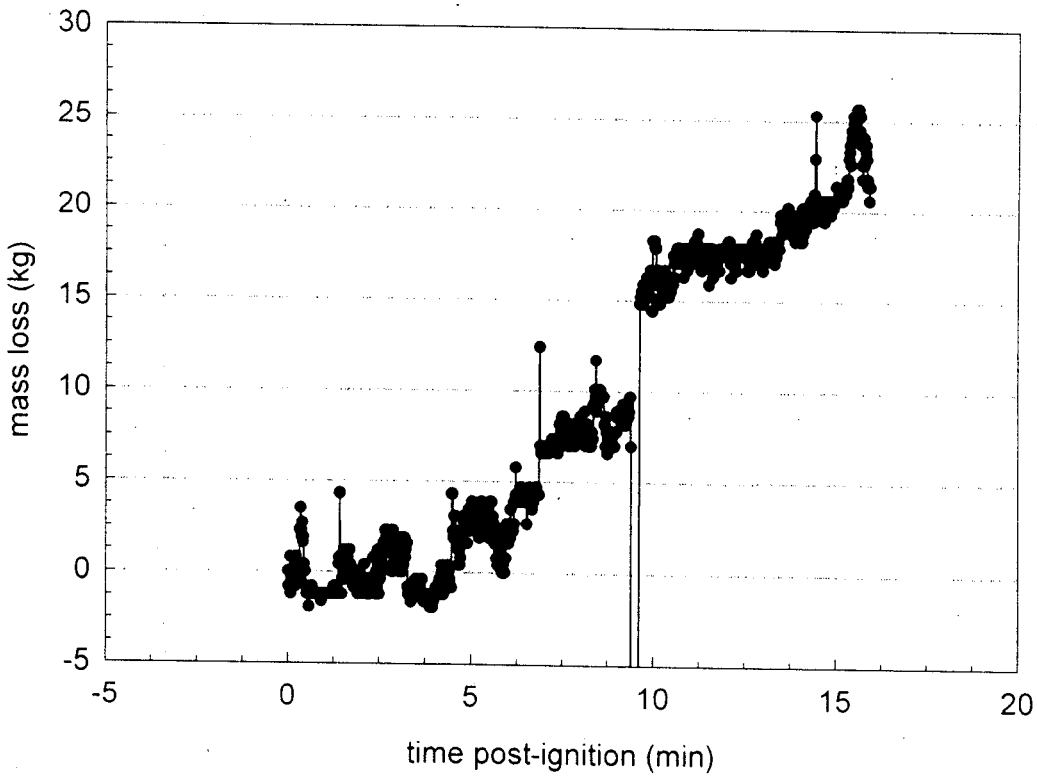

Plot H5. Fire Test F971003. Mass Loss from the test vehicle during the fire test.

APPENDIX I
PASSENGER COMPARTMENT COMBUSTION GAS DATA
FOURIER TRANSFORM INFRARED SPECTROSCOPY
AND
OXYGEN SENSOR

The sampling-line for FTIR analysis consisted of a stainless-steel tube (o.d. = 0.250 in. (6.4 mm), i.d. = 0.125 in. (3.2 mm), l = 20 ft (6.1 m)) inserted through the roof between the front seats along the longitudinal midline of the test vehicle (Fig.'s I1 and I2). The inlet of the sample-tube extended approximately 10 in. below the headlining (Fig.'s I1 and I2). The tube was not heated. The outlet of the sample tube was connected to a heated Teflon® transfer-line (o.d. = 0.250 in. (6.4 mm), i.d. = 0.125 in. (3.2 mm), l = 75 ft. (23 m)), which was connected to the gas cell of the FTIR spectrometer. The transfer-line was heated to 105°C during the test to prevent condensation of water and water-soluble gases (*e.g.*, HCl, HCN, NO, and NO_2). An in-line stainless steel filter holder containing a quartz fiber filter (o.d. = 47 mm) was placed between the sample-tube and the transfer-line to prevent smoke particles from contaminating analytical instrumentation.

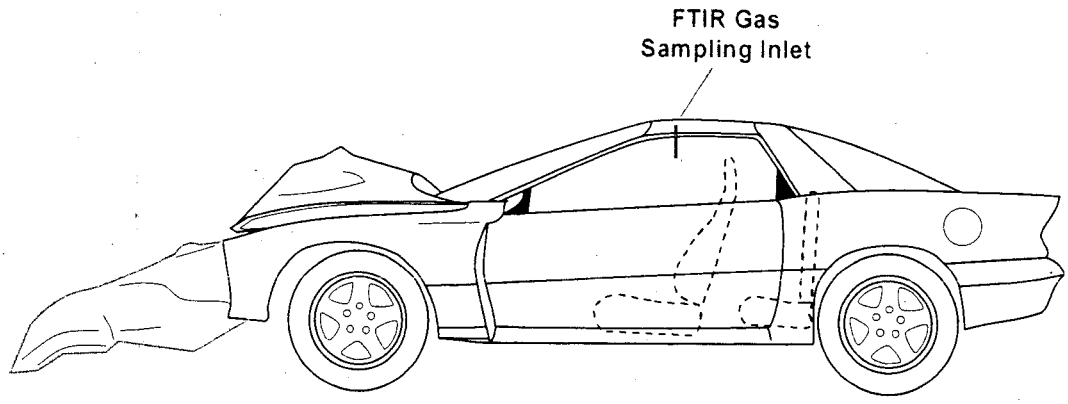

Figure I1. Fire Test F971003. Side-view of the test vehicle show the approximate location of the FTIR gas sampling inlet in the passenger compartment.

The FTIR spectrometer was a Model I-1000 Series FTIR Spectrometer (MIDAC Corporation, Riverside, California), with a KBr beam-splitter; a liquid nitrogen-cooled Mercury-Cadmium-Telluride detector; and gold-surfaced aluminum optics. This instrument was fitted with a stainless steel, multiple-reflectance gas cell (path length = 10 m) with zinc selenide windows. The gas cell was heated to 105°C. The optical bench was filled with clean, dry argon and hermetically sealed. The usable spectral range of this instrument was approximately 7400-700 cm^{-1}. Pressure in the gas cell during the fire tests was measured with a Baratron pressure gauge (MKS Instruments, Burlington, MA). The spectrometer was operated at a spectral resolution of 0.5 cm^{-1}.

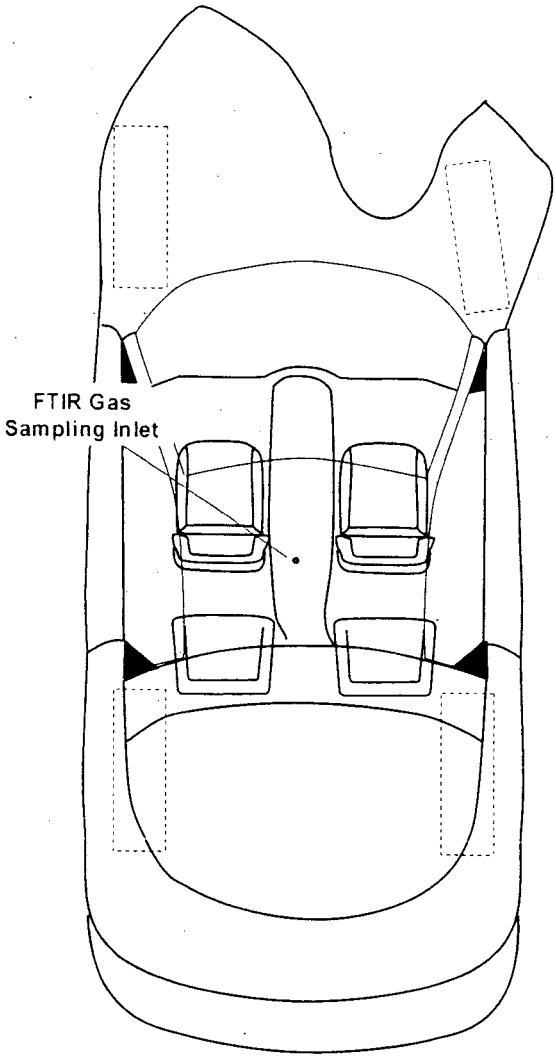

Figure I2. Fire Test F971003. Top view of the test vehicle showing the approximate location of the FTIR gas sampling inlet in the passenger compartment.

The sampling line and gas cell were equilibrated to 105°C for at least 60 minutes before sample acquisition. A reference spectrum was acquired while the gas cell was evacuated. During the fire tests, the gas cell was purged continuously with air withdrawn from the passenger compartment at a flow rate of 7 L/min. Single-scan absorbance spectra were acquired and stored to disk at intervals of 10 s. After the test, the stored spectra were analyzed using the quantitative analysis software provided by the instrument manufacturer (AutoQuant, MIDAC). This software uses a Classical Least Squares algorithm to determine gas concentrations. The method developed for analysis of combustion gases was calibrated with gas standards (Scott Specialty

Gases, Inc., Troy, MI). The standards were either NIST-traceable or produced by a gravimetric blending process.

An electrochemical oxygen sensor (Model SE-25, FIGARO USA, Inc.) was placed in the FTIR sampling line just before the FTIR gas cell. The signal from the oxygen sensor was recorded by the data acquisition system described in **APPENDIX C**. The oxygen sensor was calibrated before this test by recording its responses when purged with room air (21% O_2) and with pure nitrogen (0% O_2).

Gases in the passenger compartment measured by FTIR during this test included carbon dioxide, carbon monoxide, methane, ethylene, acetylene, hydrogen cyanide, nitric oxide, and hydrogen chloride (Plots I1 through I8). Except for carbon dioxide, which has a background concentration in air of approximately 0.05 %, the concentrations of all of these gases were less than their respective lower limits of detection at the start of this test.

The Infrared spectra acquired during this test also contained a broad absorbance band between 2800 and 3200 cm^{-1}, indicating the presence of a mixture of aliphatic hydrocarbons in the air samples from the passenger compartment. The intensity of this absorbance band generally followed the same time-course as that of methane (Plot I3), ethylene (Plot I4), and acetylene (Plot I5). This broad band appeared to contain absorbances from ethane, propane, and butane. However, all of the gaseous species contributing to this absorbance band could not be identified. Therefore, none of these species could quantified accurately.

The concentration profiles of carbon dioxide (Plot I1), carbon monoxide (Plot I2), methane (Plot I3), ethylene (Plot I4), acetylene (Plot I5), hydrogen cyanide (Plot I7) and nitric oxide (Plot I8) show peaks at 3 to 4 minutes post-ignition, 10 to 11 minutes post-ignition, and at about 16 minutes post-ignition.

The concentration profile of hydrogen chloride (HCl) during this test (Plot I6) was erratic, and close to the lower limit of detection of this gas under the conditions of this test. These results suggest that hydrogen chloride was not detected in the gas stream withdrawn from the passenger compartment during this test. The data in Plot I7 does not represent the true concentration of hydrogen chloride in the withdrawn gas stream, but is an artifact of the quantitative analysis procedure caused by high and variable concentrations of water vapor over the region of spectral absorption of hydrogen chloride.

The concentration of oxygen in the passenger compartment decrease from approximately 21% at the start of the test to 20% when the test was ended at about 16 minutes post-ignition (Plot I9).

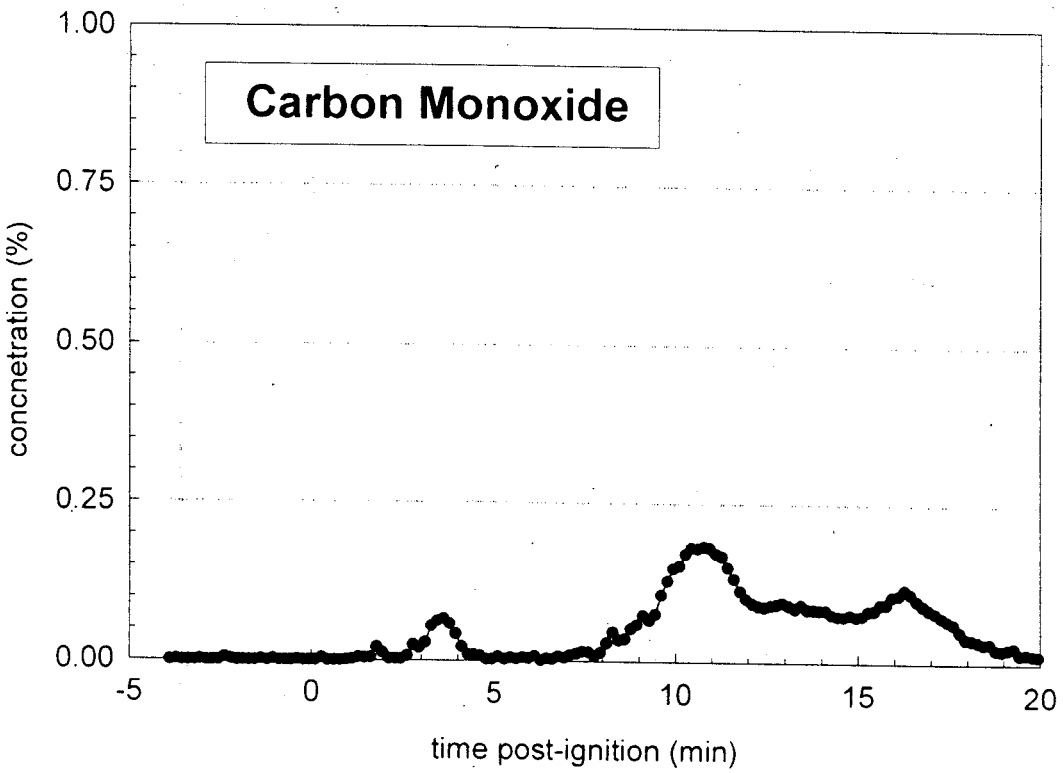

Plot I1. Fire Test F971003. Concentration of carbon monoxide (CO) in the passenger compartment determined by FTIR analysis.

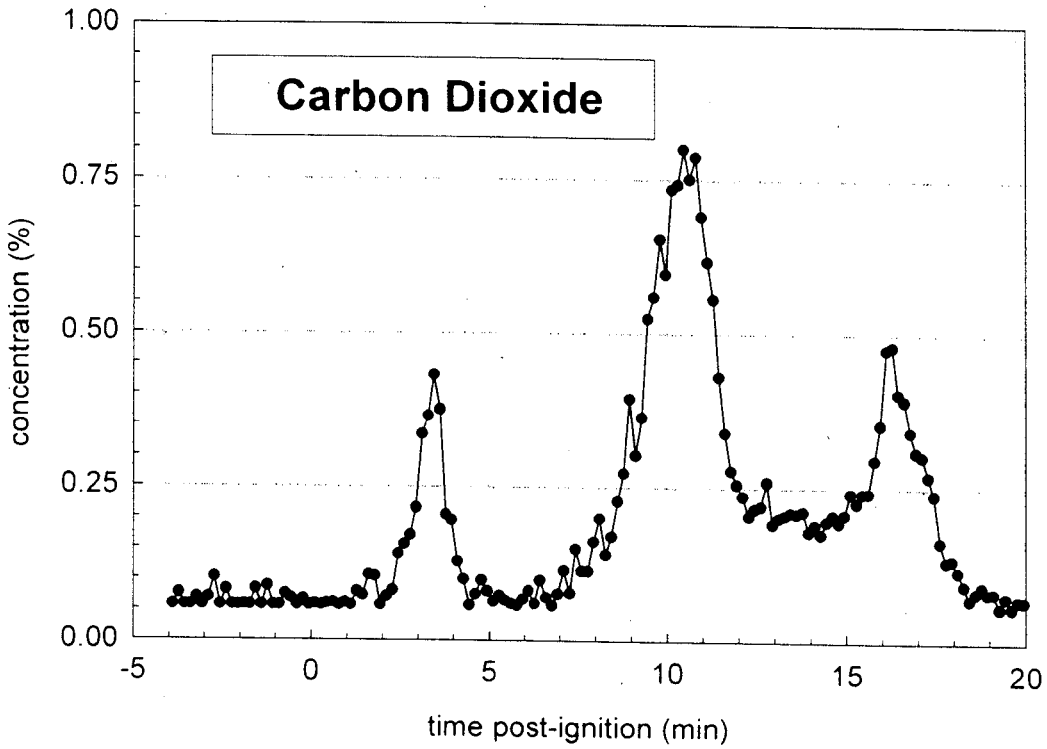

Plot I2. Fire Test F971003. Concentration of carbon dioxide (CO_2) in the passenger compartment determined by FTIR analysis.

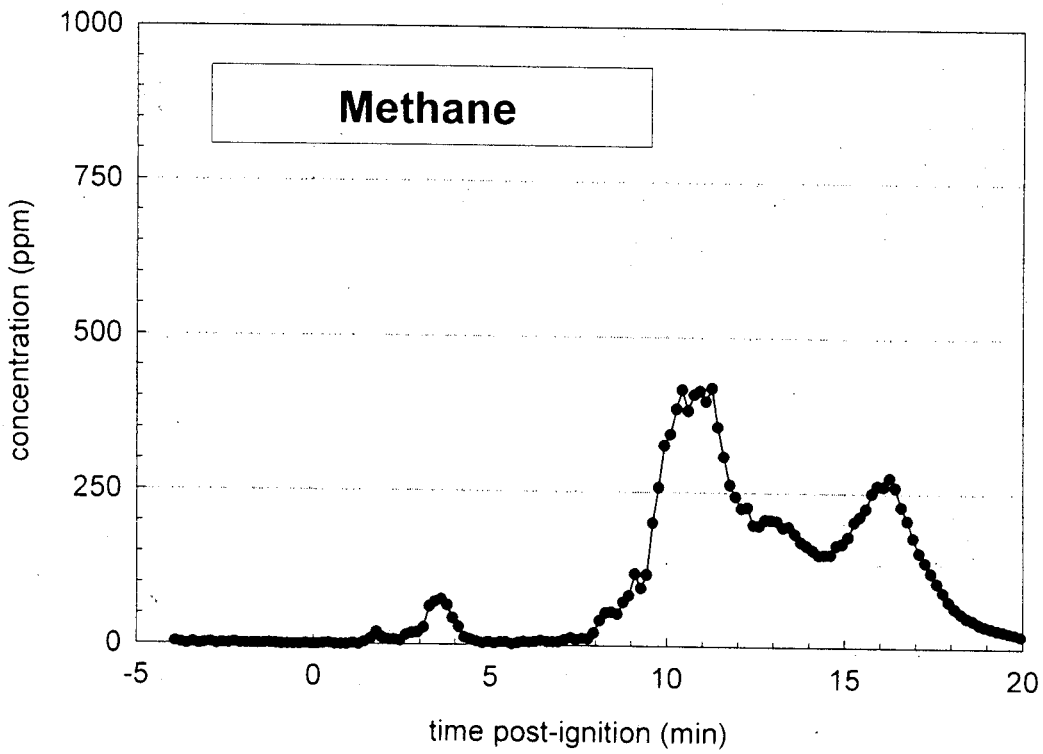

Plot I3. Fire Test F971003. Concentration of methane (CH_4) in the passenger compartment determined by FTIR analysis.

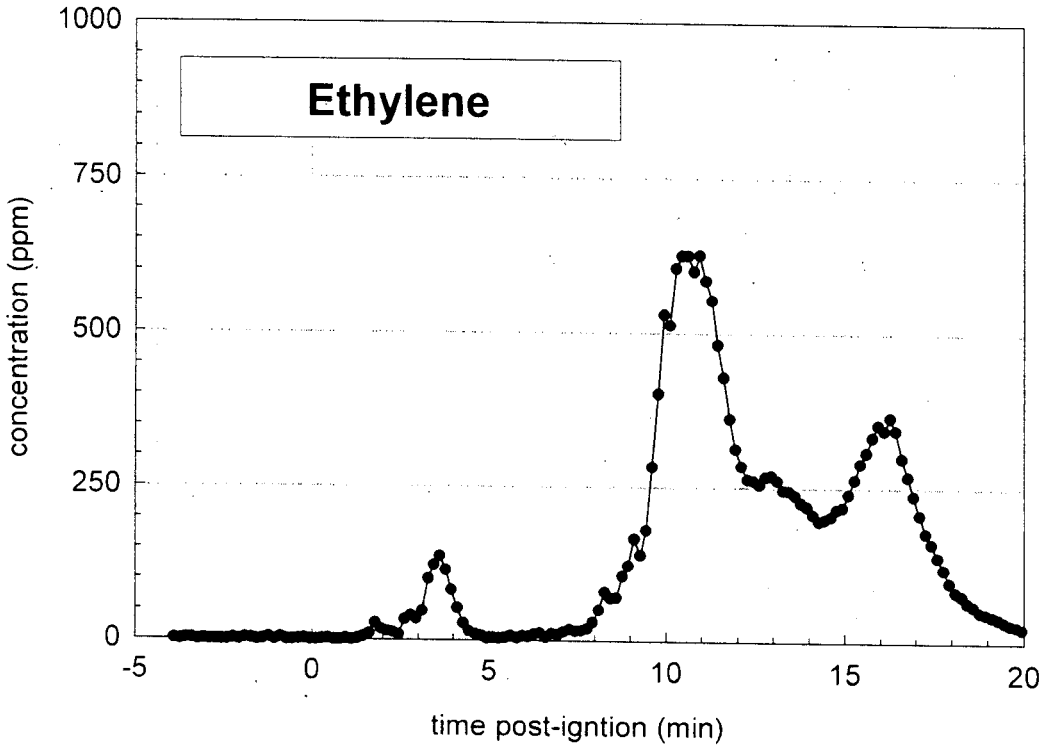

Plot I4. Fire Test F971003. Concentration of ethylene (C_2H_4) in the passenger compartment determined by FTIR analysis.

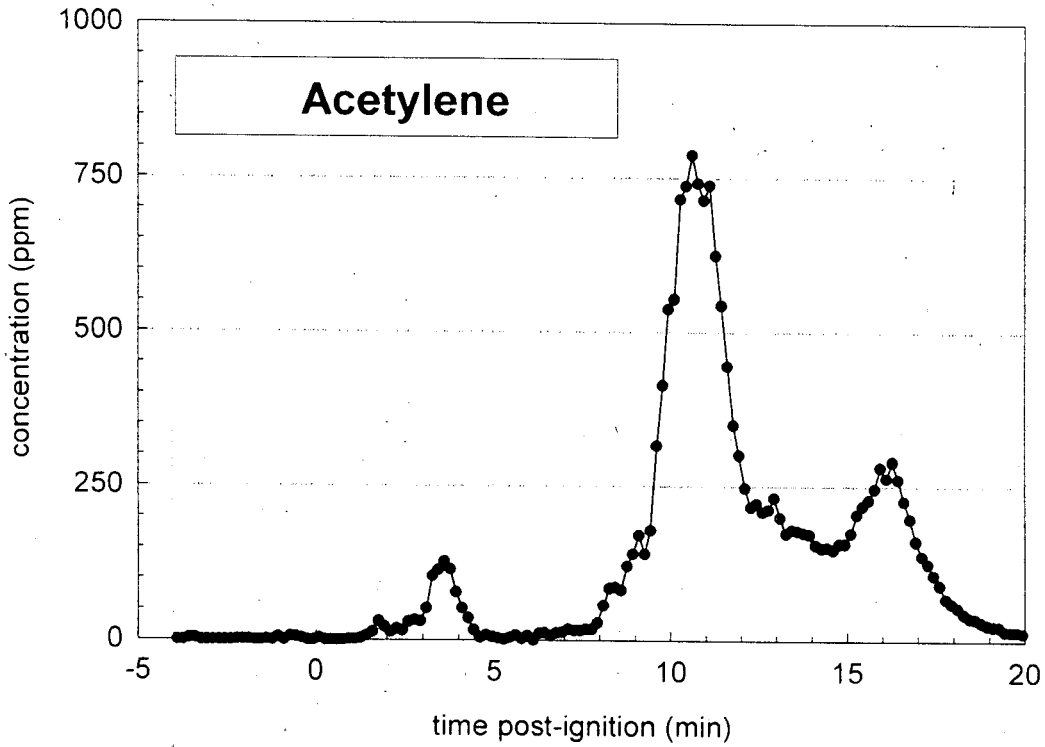

Plot I5. Fire Test F971003. Concentration of acetylene (C_2H_2) in the passenger compartment determined by FTIR analysis.

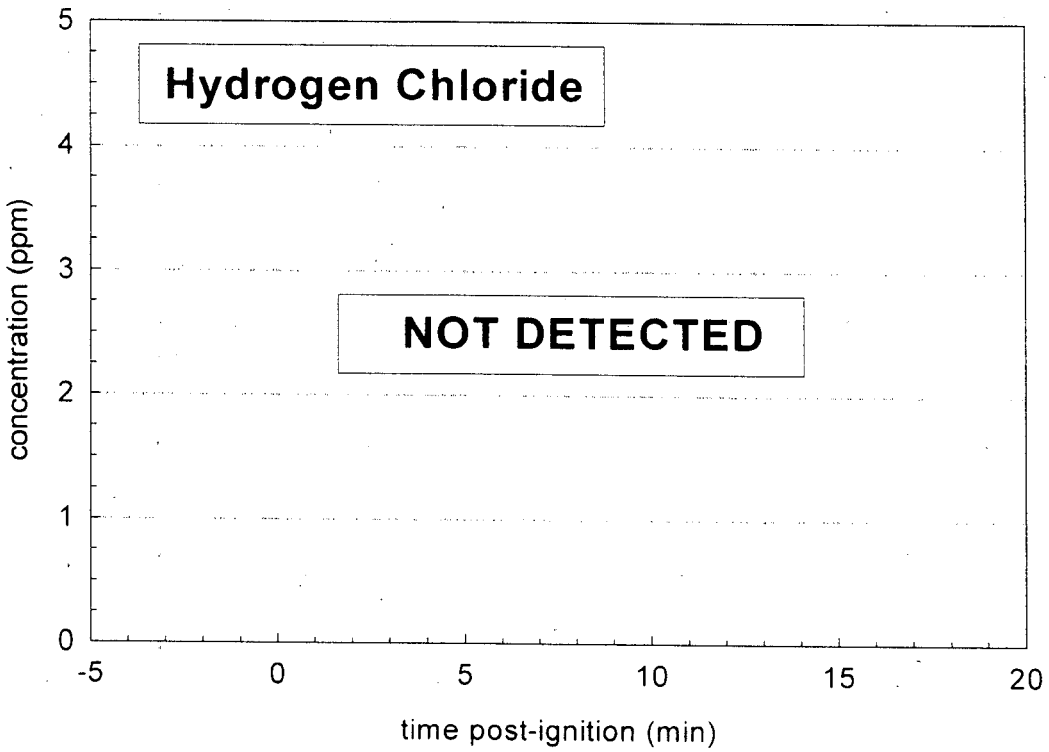

Plot I6. Fire Test F971003. Concentration of hydrogen chloride (HCl) in the passenger compartment determined by FTIR analysis.

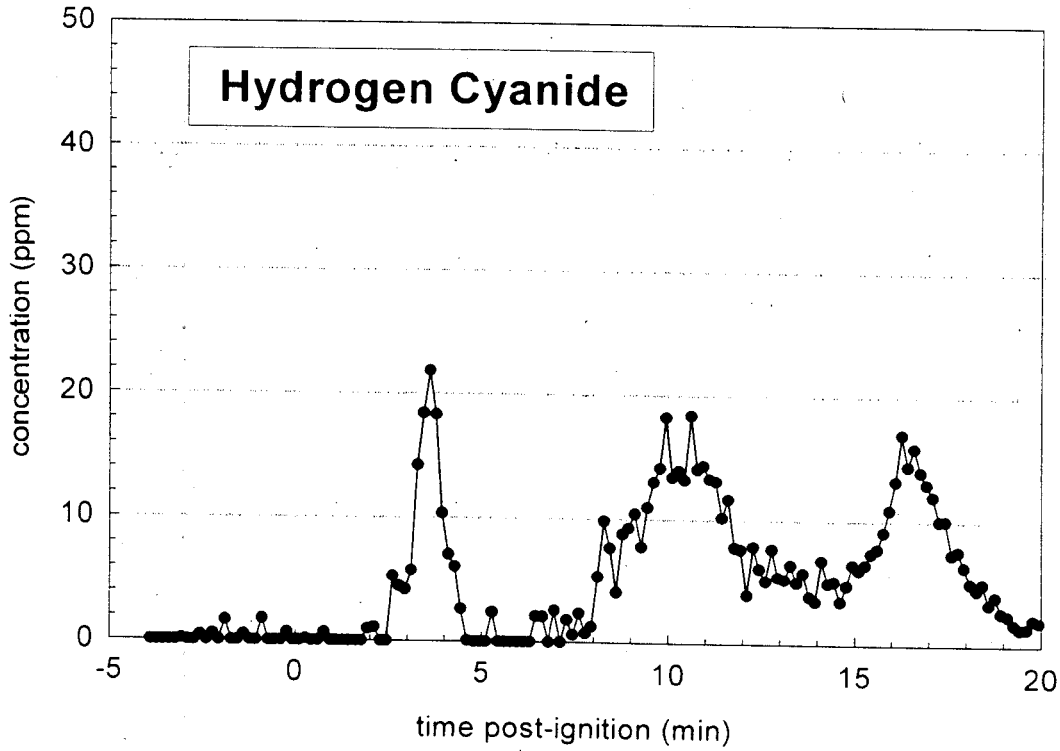

Plot I7. Fire Test F971003. Concentration of hydrogen cyanide (HCN) in the passenger compartment determined by FTIR analysis.

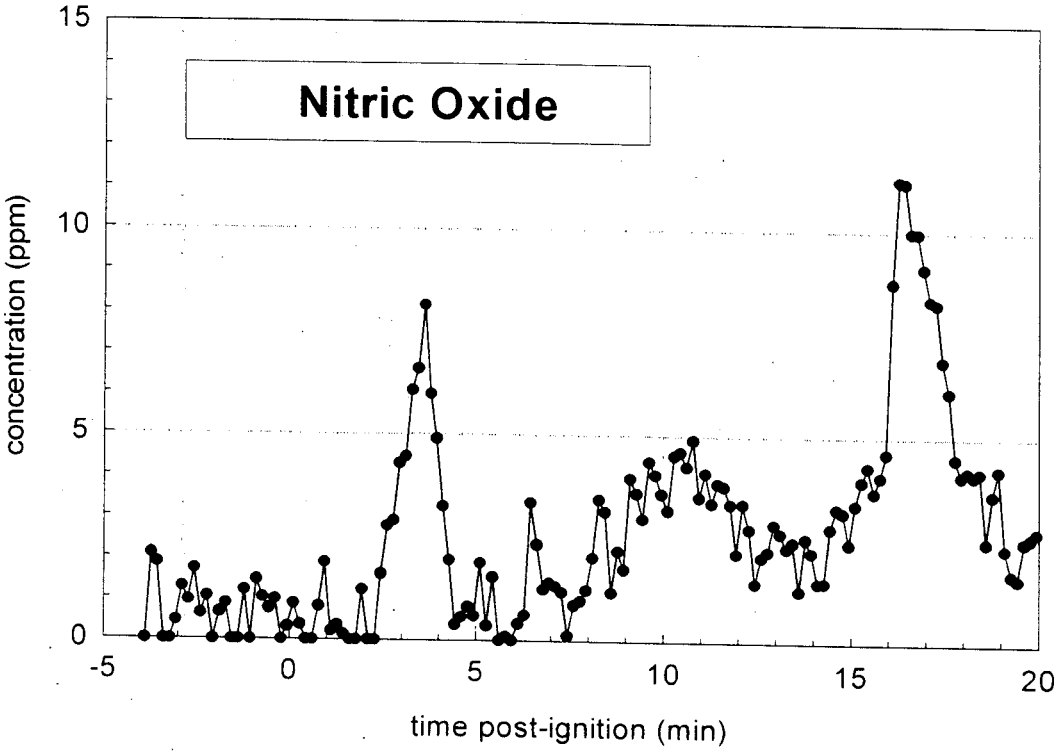

Plot I8. Fire Test F971003. Concentration of nitric oxide (NO) in the passenger compartment determined by FTIR analysis.

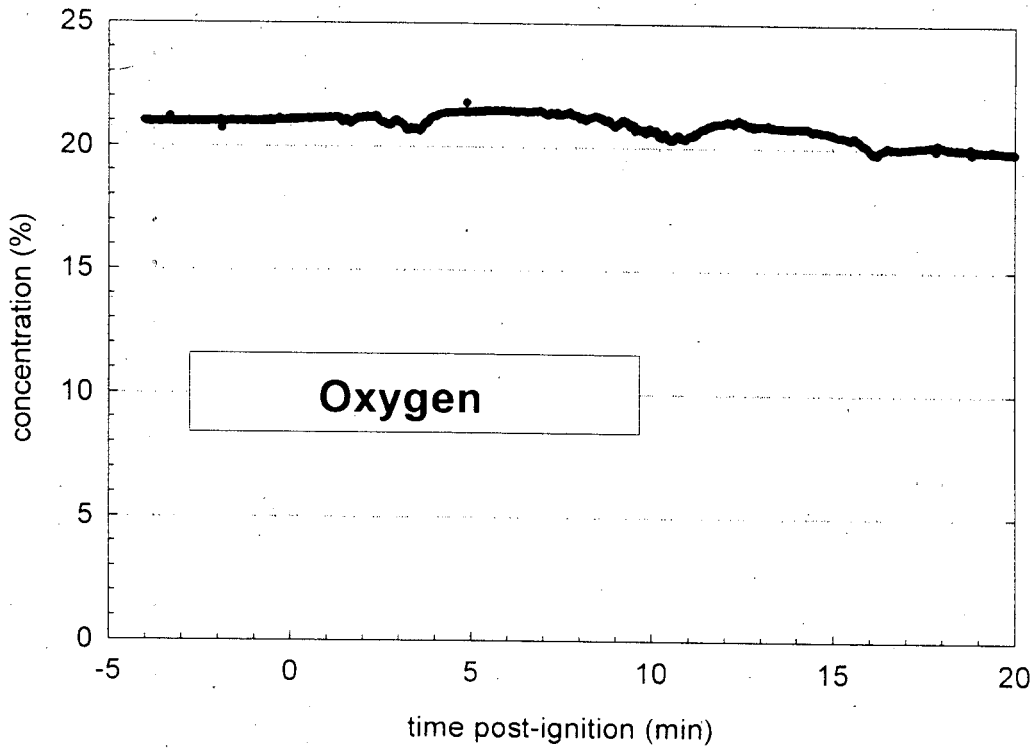

Plot I9. Fire Test F971003. Concentration of oxygen (O_2) in the passenger compartment measured with an electrochemical oxygen sensor.

APPENDIX J
PASSENGER COMPARTMENT COMBUSTION GAS DATA
GAS CHROMATOGRAPHY/MASS SPECTROSCOPY GAS ANALYSIS

The sampling-line for GC/MS samples consisted of a stainless-steel tube (o.d. = 0.250 in. (6.4 mm), i.d. = 0.125 in. (3.2 mm), l = 20 ft (6.1 m)) inserted through the roof between the front seats along the longitudinal midline of the test vehicle (Fig.'s J1 and J2). The inlet of the sample-tube extended approximately 10 in. below the headlining. The outlet of the sample tube was connected to sampling manifold by a length of stainless steel sampling tube (o.d. = ¼ in., length = 25 ft.). The sampling manifold contained five sample cartridges in parallel. Airflow was directed sequentially through the sample cartridges a solenoid-actuated gas-switching manifold. The airflow rate through the cartridges during sampling was adjusted 250 cm^3/min with a rotometer. None of the components of the GC/MS sampling line were heated.

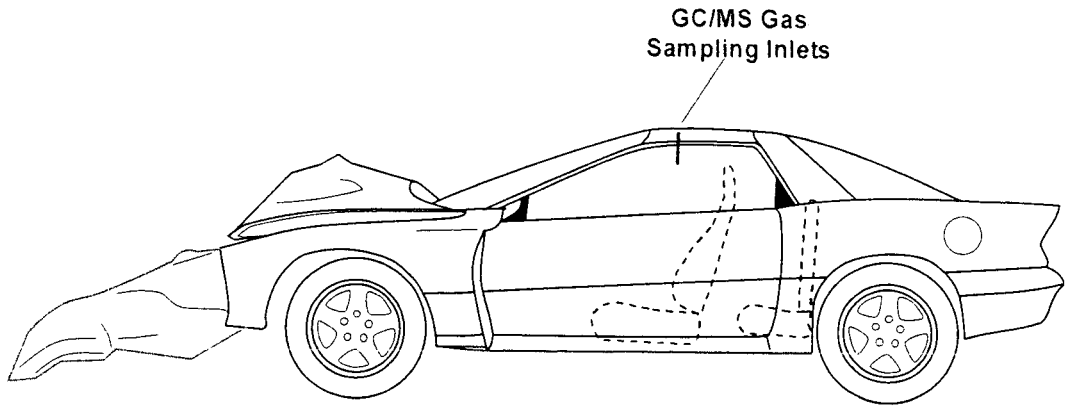

Figure I1. Fire Test F971003. Side-view of the test vehicle show the approximate locations of the FTIR gas sampling inlet and the particulate sampling inlets in the passenger compartment.

Each cartridge was a glass-lined stainless steel tube (i.d. = 4 mm; length = 10 cm; Scientific Instrument Services, Inc, Ringoes, NJ) packed with 25 mg of Carbotrap™ C Graphitized Carbon Black (Supelco, Inc.; Bellefonte, PA) in series with 15 mg of Carbotrap™ Graphitized Carbon Black (Supelco).

After the test, the sample cartridges were analyzed by thermal desorption/gas chromatography/mass spectrometry. Deuterated standards dissolved in deuterated methanol were added to each sorbent cartridge to monitor sample recovery. A modified purge-and-trap concentrator was used for thermal desorption (Model 600 Purge-and-Trap Concentrator, CDS Analytical, Oxford, PA). The gas chromatograph was a Model 5890 Series II Plus Gas Chromatograph (Hewlet Packard, Palo Alto, CA). The mass spectrometer was a Hewlet Packard Model 5989B Mass Spectrometer (Hewlett Packard). The thermal desorption unit was interfaced directly to the split/splitless injector of the gas chromatograph through a cryo-focusing unit. The

injector was operated in the split mode with a split of approximately 10 mL/min. The chromatographic column was a fused silica capillary column coated with 100% methyl silicone (HP-1 ; length = 30 m; i.d. = 0.25 mm; film thickness = 0.25 μm).

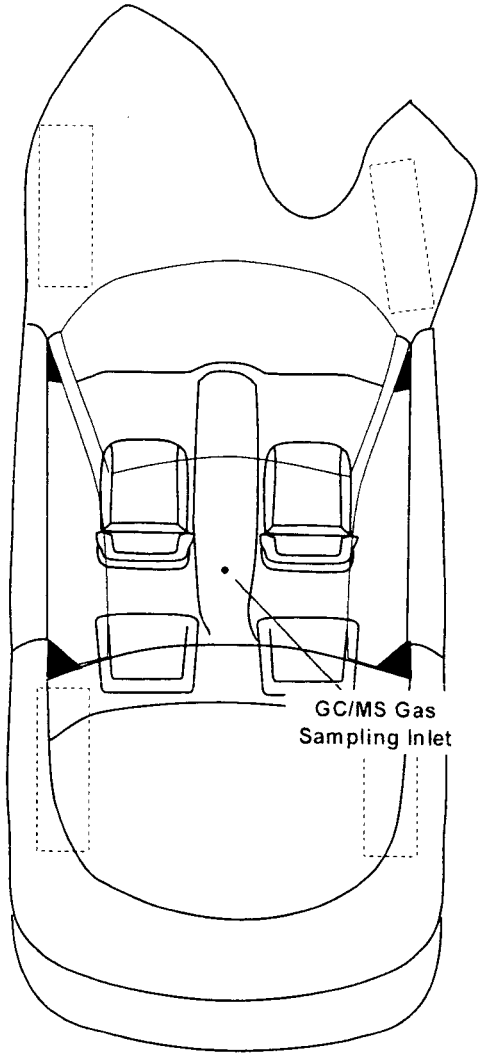

Figure J2. Fire Test F971003. Top view of the test vehicle showing the approximate locations of the GC/MS gas sampling inlet and the particulate sampling inlets in the passenger compartment.

The sample was desorbed at 320°C for 10 min, and cryofocused onto the head of the chromatographic column -80°C. The temperature of the analytical column was maintained at 0°C while the sample was desorbed and cryo-focused. To start the chromatographic analysis, the cryo-focusing unit was heated bullistically to a temperature of 320°C. The column temperature

was programmed from 0 to 325°C at a rate of 5°C/min. Mass spectra were obtained by scanning from m/z 40 to 600 at a rate of 1.2 scan/s.

Plots J1 through J6 show the mass chromatograms of the blank and samples acquired during this test. The sampling intervals in the figure captions were corrected for the time-delay for airflow through the sample-line, which was estimated to have been approximately 25 seconds.

Table JI lists components tentatively identified from analysis of the mass chromatograms of these samples. The components are listed in order of chromatographic retention time. Identifications were based on the results of a spectral search a commercial mass spectral library (Wiley 275K Mass Spectral Library). Some components were identified by interpretation of their mass spectra. The identities of all compounds listed in Table JI were confirmed by analysis of authentic standards or comparison to thermal decomposition products from standard polymer samples.

Sample 3 through 5 contained a mixture of aliphatic and aromatic hydrocarbons apparently produced by thermal decomposition of the polymeric materials in the test vehicle. For example, Samples 3 through 5 contain 2,4-dimethyl-1-hexene and 2,4-dimethyl-1-heptene. These compounds typically are produced by thermal decomposition of poly(propylene) or propylene containing polymers [J1]. Samples 3 through 5 also contain a homologous series of normal alkanes, normal terminal alkenes, and normal terminal dienes typically produced by thermal decomposition of poly(ethylene) or polymers containing poly(ethylene) blocks. Thermal decomposition of poly(styrene) or styrene containing polymers may produce a mixture of aromatic hydrocarbons containing benzene, methylbenzene, ethylbenznene, ethenylbenzene, ethynylbenzene, and n-propylbenzene (Samples 3 through 5). These compounds also are components of soot produced during incomplete combustion of many organic materials. The presence of naphthalene, indene, 1-methylnaphthalene and 2-methylnaphthalene in Samples 3 through 5 indicate that these samples also contained soot.

REFERENCES

J1. S.L. Madorsky, *Thermal Degradation of Organic Polymers*, Wiley-Interscience, New York, 1964, p. 93.

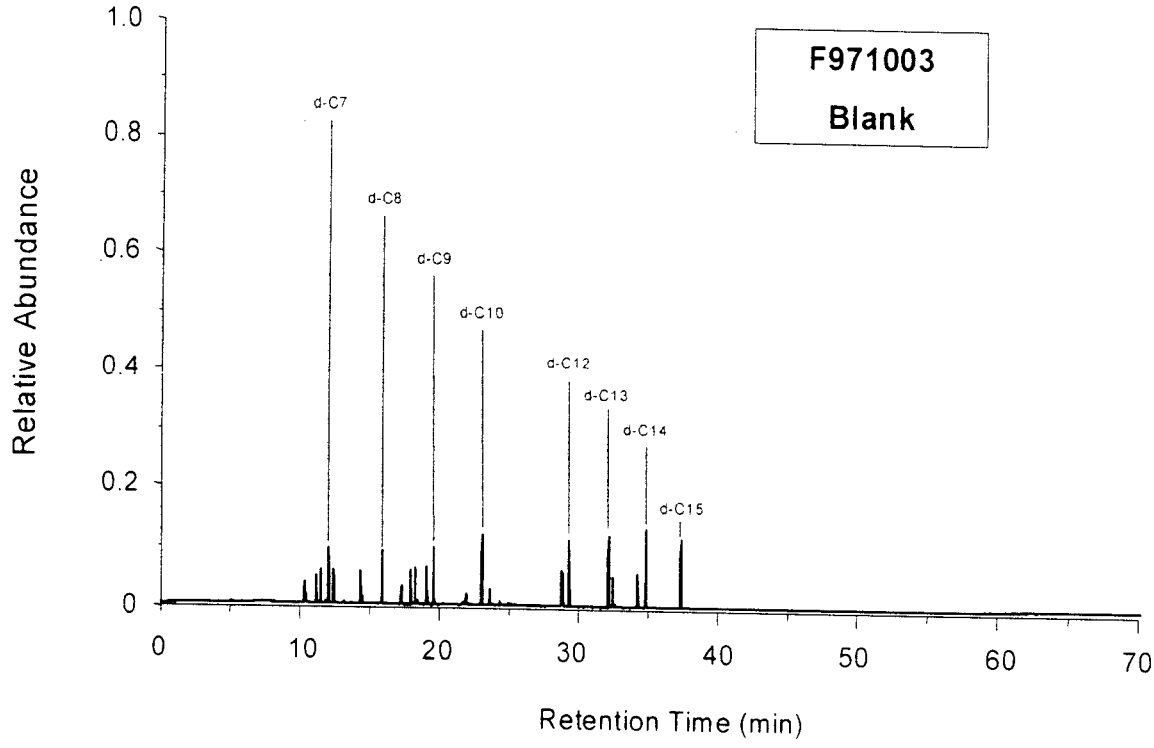

Plot J1. Fire Test F971003. Mass chromatogram from GC/MS analysis of a blank acquired for 10 minutes before the start of the test.

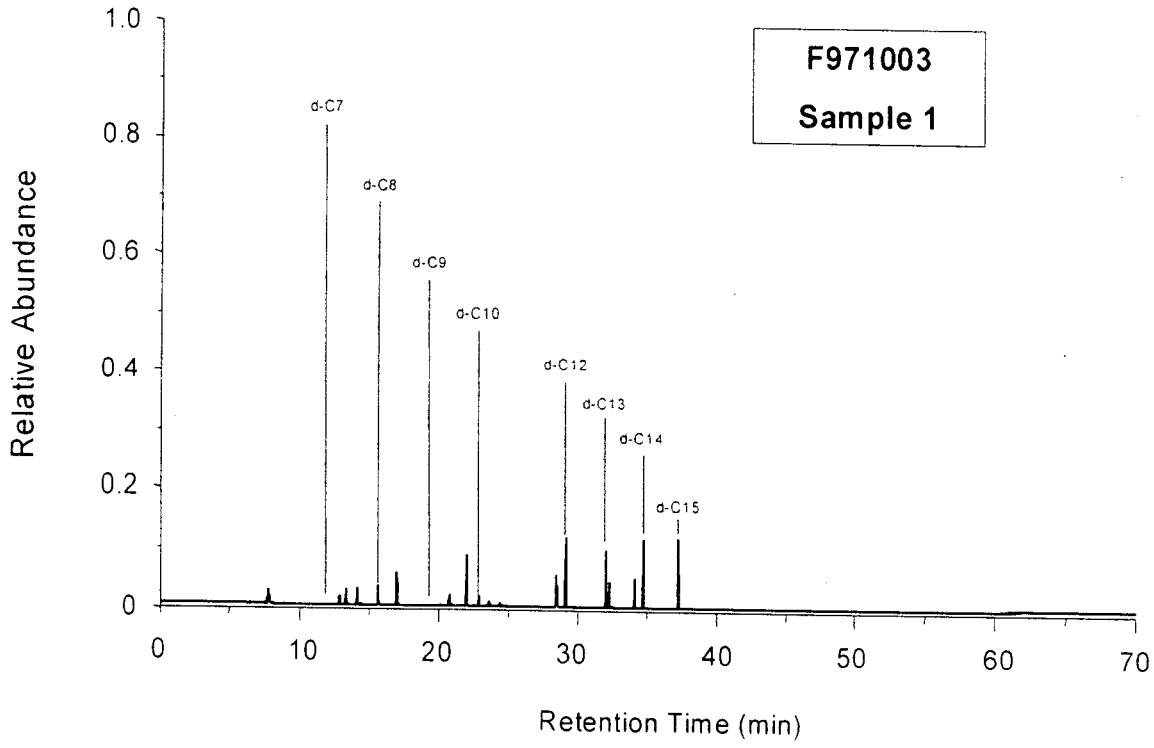

Plot J2. Fire Test F971003. Mass Chromatogram of Sample 1 acquired from 0 to 4.8 minutes post-ignition.

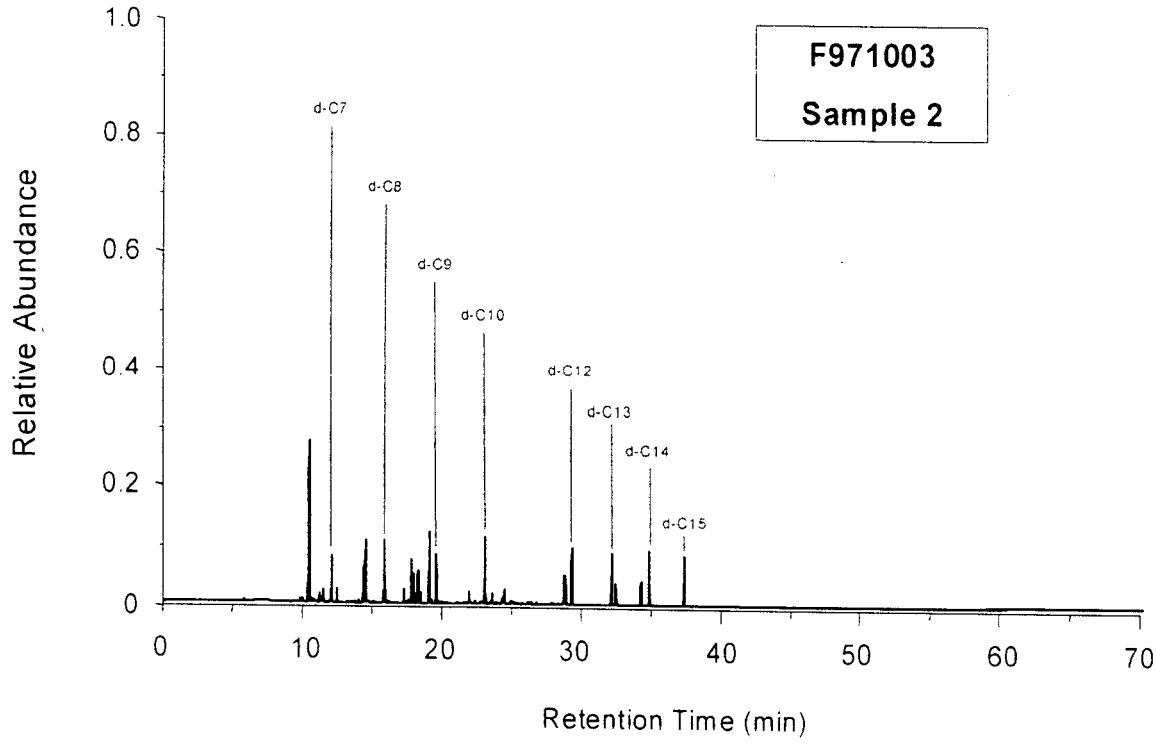

Plot J3. Fire Test F971003. Mass Chromatogram of Sample 2 acquired from 4.8 to 8.3 minutes post-ignition.

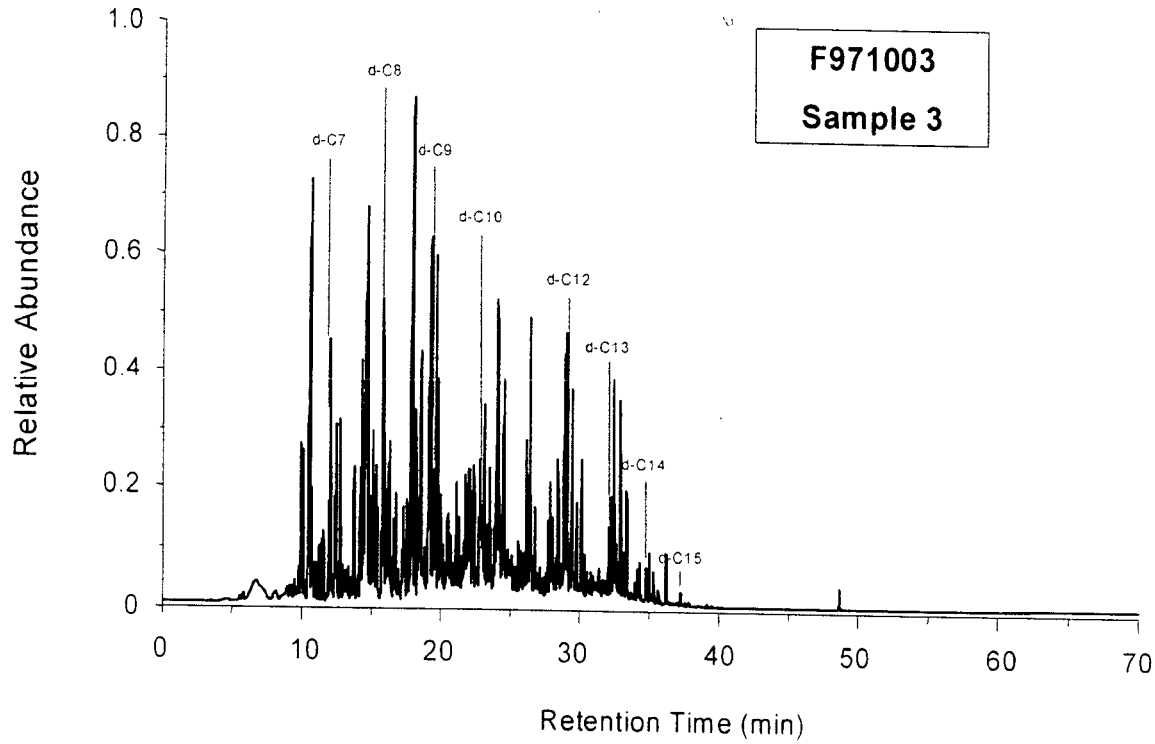

Plot J4. Fire Test F971003. Mass Chromatogram of Sample 3 acquired from 8.3 to 11.7 minutes post-ignition.

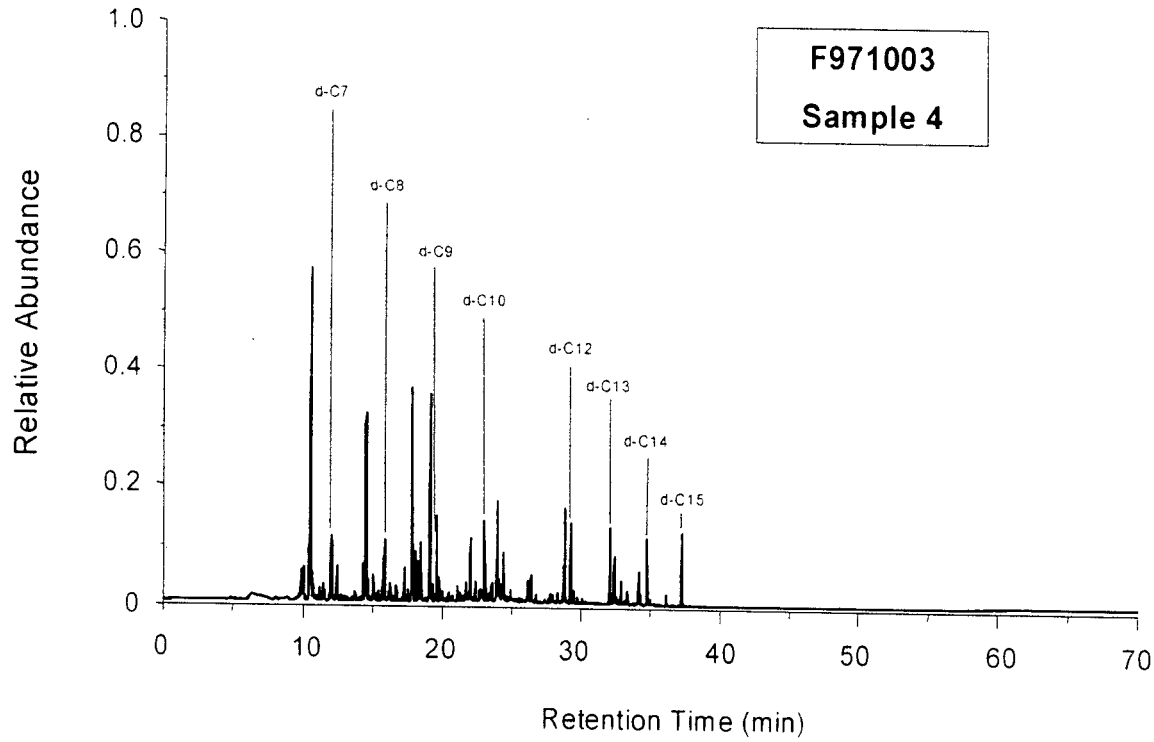

Plot J5. Fire Test F971003. Mass Chromatogram of Sample 4 acquired from 11.7 to 17.2 minutes post-ignition.

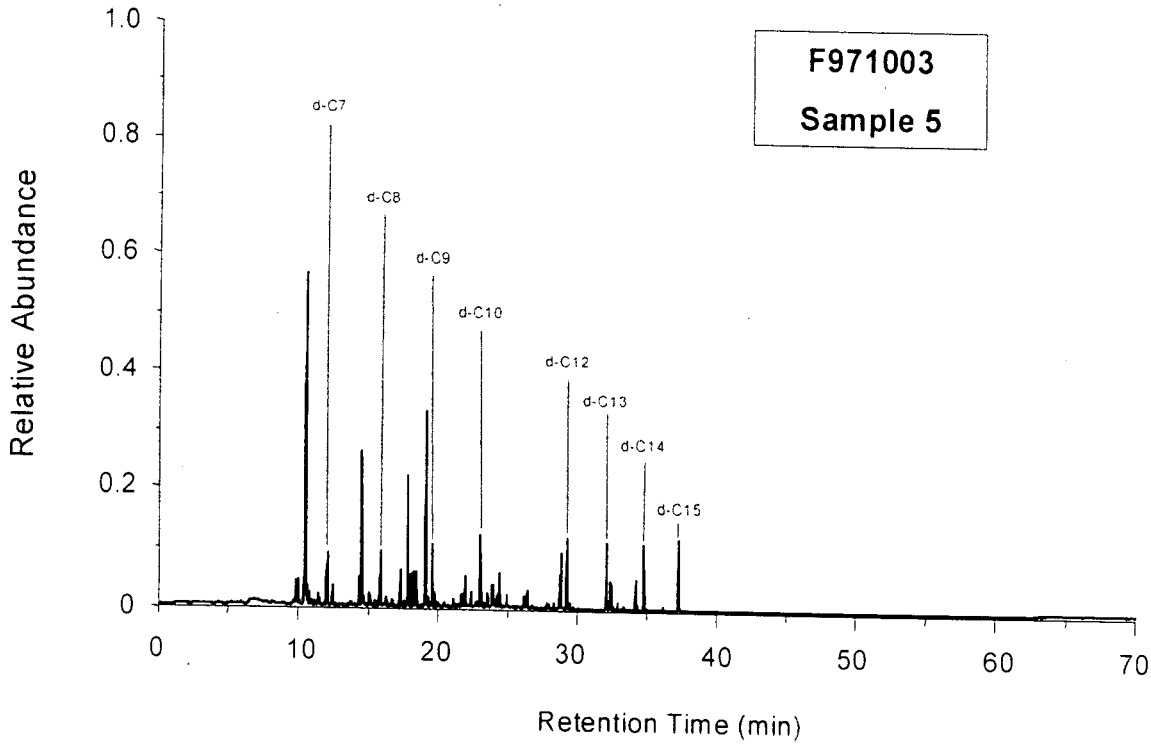

Plot J6. Fire Test F971003. Mass Chromatogram of Sample 5 acquired from 17.2 to 20.5 minutes post-ignition.

Table J1
GC/MS Peak Identification

t_R	Compound	CAS	Relative Abundance[2]					
			Blank	Sample 1	Sample 2	Sample 3	Sample 4	Sample 5
9.90	methylcyclopentadiene isomers and cyclohexadiene isomer	n/a			•	•••	••	••
10.10	methylcyclopentadiene isomer and cyclohexadiene isomer	n/a			•	••	••	••
10.43	d_6-benzene	001076-43-3	••		••	••	••	••
10.54	benzene	000071-43-2	•		•••	••••	••••	••••
11.26	2-methylhexane	000591-76-4	•			•	•	
11.44	cyclohexene	000110-83-8				••	•	•
11.53	3-methylhexane	000589-34-4	•			••	•	•
11.93	2,4-dimethyl-1-pentene	002213-32-3				••	•	
12.05	1-heptene	000592-76-7				•••	••	•
12.17	d_{16}-n-heptane (d-C_7)	33838-52-7	••	••	••	••	••	••
12.46	n-heptane	000142-82-5	•			••	•	•
14.36	2-ethyl-1-butanol	000097-95-0						
14.40	d_8-methylbenzene	002037-26-5	••	••	••	••	••	••
14.83	methylbenzene	002037-26-5				••••	•••	•••
15.88	d_{18}-n-octane (d-C_8)	017252-77-6	••	••	••	••	••	••

Table J1, continued
GC/MS Peak Identification

t_R	Compound	CAS	Relative Abundance[2]					
			Blank	Sample 1	Sample 2	Sample 3	Sample 4	Sample 5
15.89	1-octene	000111-66-0				•••	•	•
16.31	n-octane	000111-65-9				•••	•	•
17.28	hexamethylcyclotrisiloxane	000541-05-9	•	•		••	•	•
17.87	2,4-dimethyl-1-heptene	019549-87-2				••••	•••	•••
17.94	d_{10}-ethylbenzene	025837-05-2	••	••	••	••	••	••
18.14	ethylbenzene	000100-41-4				•••	••	••
18.28	d_{10}-1,4-dimethylbenzene	041051-88-1	••	••	••	••	••	••
18.47	1,4-dimethylbenzene and 1,3-dimethylbenzene	000106-42-3 000108-38-3				•••	••	•
18.64	ethynylbenzene	000536-74-3				•••	••	••
19.07	d_{10}-1,2-dimethylbenzene	056004-61-6	••	••	••	••	••	••
19.22	ethenylbenzene	000100-42-5				•••••	•••	•••
19.41	1,2-diemthylbenzene	000095-47-6				••	•	•
19.60	d_{20}-n-nonane (d-C_9)	121578-11-8	••	••	••	••	••	••
19.65	1-nonene	000124-11-8				•••	••	•
20.01	n-nonane	000111-84-2				••	•	•
20.52	1-methylethylbenzene	000098-82-8		•		•••	•	

Table J1, continued
GC/MS Peak Identification

t_R	Compound	CAS	Relative Abundance[2]					
			Blank	Sample 1	Sample 2	Sample 3	Sample 4	Sample 5
21.44	benzaldehyde	000100-52-7		••		•••	•	•
21.53	benzonitrile	000100-47-0		•••		•••	•	•
21.50	n-propylbenzene	000103-65-1		••••		•	•	•
21.83	1-ethyl-3-methylbenzene	000620-14-4				•	•	
21.89	1-ethyl-4-methylbenzene	000622-96-8				•	•	
21.92	d_6-phenol	013127-88-3	••	••	••	••	••	••
22.10	phenol	000108-65-2				•••	••	••
22.39	1-methylethenylbenzene	000098-83-9				•••	•	•
22.98	1-ethyl-2-methylbenzene	000611-14-3				•	•	•
23.06	d_{22}-n-decane (d-C_{10})	016416-29-8	••	••	••	••	••	••
23.19	1-decene	000872-05-9				•••	•	•
23.53	n-decane	000124-18-5				••	•	•
23.59	octamethylcyclotetrasiloxane		•	•		••	•	•
24.60	indene	000095-13-6				•••	••	••
24.93	d_8-methylphenol	000095-13-6	••	••	••	••	••	••
26.42	1-undecene	000821-95-4				•••	•	•
26.76	n-undecane	001120-21-4				•••	•	•

Table J1, continued
GC/MS Peak Identification

t_R	Compound	CAS	Relative Abundance[2]					
			Blank	Sample 1	Sample 2	Sample 3	Sample 4	Sample 5
28.79	d_8-naphthalene	001146-65-2	••	••	••	••	••	••
28.99	naphthalene	000091-20-3	•			••••	••	••
29.30	d_{26}-n-dodecane (d-C_{12})	121578-12-9	••	••	••	••	••	••
29.47	1-dodecene	000112-41-4				•••	•	•
29.80	n-dodecane	000112-40-3				••	•	
31.15	2-propenoic acid, 2-ethylhexyl ester	000103-11-7				•••	•	
32.12	d_{28}-n-tridecane (d-C_{13})	121578-12-9	••	••	••	••	••	••
32.16	2-methylnaphthalene	000091-57-6				•	•	
32.35	1-tridecene	002437-56-1				••	•	•
32.43	d_{10}-1-methylnaphthlene	038072-94-5	••	••	••	••	••	••
32.48	2-methyl-2-propenoic acid, 2-ethylhexyl ester	000688-84-6				•••		
32.56	1-methylnaphthalene	000090-12-0				••	•	•
33.04	n-tridecane	000629-50-5	••	••	••	••	••	••
34.20	d_{10}-biphenyl	001486-01-7	••	••	••	••	••	••
34.42	biphenyl	000092-52-4				••	•	
34.78	d_{30}-n-tetradecane (d-C_{14})		••	••	••	••	••	••

Table J1, continued
GC/MS Peak Identification

t_R	Compound	CAS	Relative Abundance[1]					
			Blank	Sample 1	Sample 2	Sample 3	Sample 4	Sample 5
35.31	n-tetradecane	000629-59-4				••		
36.33	acenaphthalene	000083-32-9				••	•	
37.28	d_{32}-n-pentadecane (d-C_{15})	036340-20-2	••	••	••	••	••	••

[1] The approximate abundance of each component in the blank and the five samples relative to the average peak area (A_{avg}) of the deuterated n-alkane internal standards in each sample: • = 5 to 50% A_{avg}; •• = 51 to 150% A_{avg}; ••• = 151 to 1,000% A_{avg}; •••• = 1,001 to 10,000% A_{avg}; ••••• = > 10,000% A_{avg}.

APPENDIX K
PASSENGER COMPARTMENT
AIRBORNE PARTICULATE ANALYSIS

Five samples of airborne particulate were samples from the passenger compartment during this test. The approximate locations of the inlets particulate samplers are shown in Figures K1 and K2.

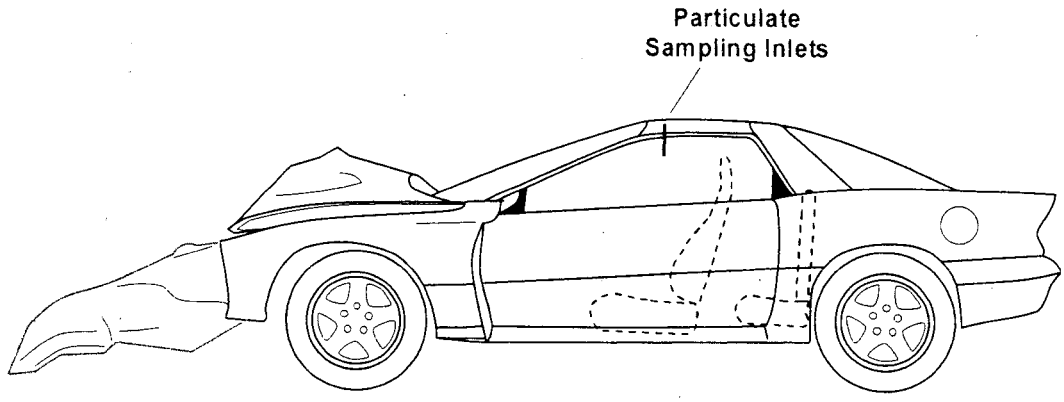

Figure K1. Fire Test F971003. Side-view of the test vehicle showing the approximate locations of the particulate sampling inlets in the passenger compartment.

Each particulate sampling apparatus consisted of an in-line stainless steel filter holder (filter diameter = 47 mm, Gelman Scientific). The inlet of each filter holder was fitted with a straight length of stainless steel tubing (o.d. = ¼ in., o.d. = $^{5}/_{16}$ in., length = 12 in.) using a compression fitting (¼ in., Swagelok). The inlet tube was inserted through the roof of the test vehicle so that it extended below the headlining approximately 10 in.. The outlet of each filer holder was connected to a vacuum manifold using flexible copper tubing (o.d. = $^{5}/_{16}$ in., length = 25 ft.). The vacuum manifold was connected to a pumping system configured to maintain constant flow through the filter holder as the pressure drop across the filter increased due to particulate loading. Qartz-fiber filters were used to collect particulate from the passenger compartment. The filters were placed in an electric furnace at 650°C in air overnight and pre-weighed. The pumping system was adjusted to maintain a volume flow rate of 30 L/min. through a single filter holder. This produced a linear velocity of approximately 29 cm/sec. of airflow perpendicular the face of the filter.

Two blanks were collected for 10 minutes before the test. Samples were collected during the test. In-line solenoid valves fitted to each port of the vacuum manifold and were actuated manually during the test to direct flow through the filter holders sequentially. The time intervals for sample acquisition were the same as those for acquiring GC/MS samples.

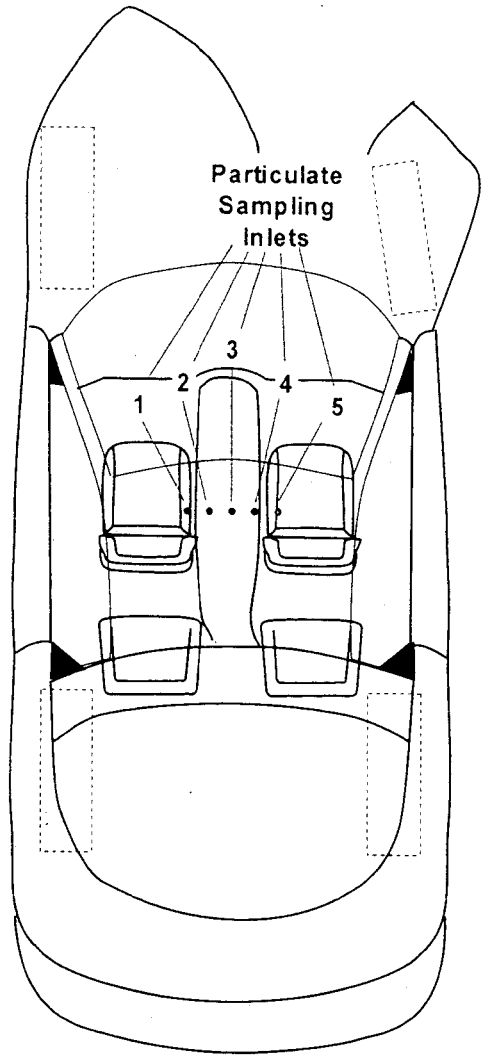

Figure K2. Fire Test F971003. Top-view of the test vehicle showing the approximate locations of the particulate sampling inlets in the passenger compartment.

After the test, the filters placed in a dissector cabinet overnight to remove water absorbed by the filter media and particulate. The weight of each filter was recorded only after constant weight was achieved. The average concentrations of airborne particulate during each sample interval ware determined from the mass of particulate collected, the volume flow rate, and the elapsed time.

A quarter was cut from each filter, weighted, and extracted for quantitative ion chromatographic analysis. The extracting solution was the mobile phase buffer. The chromatography column was an IC-Pak A HC column (Waters, Milford, MA). The mobile phase was a sodium borate/gluconate buffer at a flow rate of 1.8 mL/min [K1]. The chromatographic system consisted of a Model 616 Pump, a Model 717 Autosampler, and a Model 431 Conductivity Detector

(Waters). The following anions were measured in the ion chromatographic analysis: fluoride (F^-), bicarbonate (HCO_3^-), chloride (Cl^-), nitrite (NO_2^-), bromide (Br^-), hypochlorite ($HClO_3^-$), nitrate (NO_3^-), phosphate (HPO_4^-), sulfate (SO_4^-), and oxalate ($C_2O_4^-$).

Table KI shows the concentration of airborne particulate in the passenger compartment during this test.

Table KI
Average Airborne Particulate Concentration

Sample	Sampling Interval (min)	Sampling Time (min.)	Airborne Concentration (mg/m^3)
Blank	n/a	10	0
Sample 1	0 to 4.8	4.8	0
Sample 2	4.8 to 8.3	3.5	67
Sample 3	8.3 to 11.7	3.4	601
Sample 4	11.7 to 17.2	5.5	67
Sample 5	17.2 to 20.5	3.3	22

Table K2 shows the results of the average anion concentration in the airborne particulate. The results shown in Table KII were corrected for small amounts of bicarbonate, nitrate, phosphate, sulfate, and oxalate detected in the blanks. All samples contained chloride and bromide. Sample 4 also contained fluoride and hypochlorite.

Table KII

Average Anion Concentration in the Airborne Particulate

Sample	Anion Concentration in Airborne Particulate (μg/mg)[1]									
	F^-	HCO_3^-	Cl^-	NO_2^-	Br^-	$HClO_3^-$	NO_3^-	HPO_4^-	SO_4^-	$C_2O_4^-$
Sample 1	n/a	n/a	n/a	n/a	n/a	n/a	n/a	n/a	n/a	n/a
Sample 2	n/d	n/d	73	n/d	n/d	n/d	2	11	n/d	n/d
Sample 3	n/d	n/d	26	n/d	<1	n/d	<1	n/d	n/d	n/d
Sample 4	2	n/d	37	<1	9	n/d	n/d	n/d	n/d	n/d
Sample 5	n/d	n/d	82	n/d	22	n/d	n/d	n/d	n/d	n/d

[1] n/a = not applicable, n/d = not detected.

REFERENCES FOR APPENDIX K

K1. Method A-102, Waters Innovative Methods for Ion Analysis, Manual Number 22340, Waters Corporation, Milford, MA.